

# **Steering biogas performance by implementation of bioelectrochemical cell (BEC) technology**

Zur Erlangung des akademischen Grades eines  
DOKTORS DER NATURWISSENSCHAFTEN

(Dr. rer. nat.)

der KIT-Fakultät für Chemie und Biowissenschaften  
des Karlsruher Instituts für Technologie (KIT)

genehmigte  
DISSERTATION  
von

**Anna Prokhorova**

aus  
Jarzewo

KIT-Dekan: Prof. Dr. Willem Klopper

Referent: Prof. Dr. Johannes Gescher

Korreferent: Prof. Dr. Tilman Lamparter

Tag der mündlichen Prüfung: 22.07.2016

## **Erklärung an Eides statt**

Hiermit erkläre ich, dass ich die Dissertation mit dem Titel „Kontrolle der Biogasreaktor Performance durch Implementierung bioelektrochemischer Zelle (BEZ) Technologie“ selbstständig angefertigt habe und nur die von mir angegebenen Hilfsmittel benutzt habe. Alle Teile, die wörtlich oder dem Sinn nach anderen Werken entnommen sind, sind von mir durch Angabe der Quelle als Entlehnung gekennzeichnet. Weiterhin habe ich beim Anfertigen dieser Arbeit die Regeln zur Sicherung der guten wissenschaftlichen Praxis des KITs beachtet und alle Primärdaten gemäß Abs. A (6) am Institut archiviert. Des Weiteren versichere ich, dass die elektronische mit der schriftlichen Form dieser Arbeit übereinstimmt.

---

Ort, Datum

---

Anna Prokhorova

## Acknowledgements

First and foremost, I would like to express my sincere gratitude to my supervisor Prof. Dr. Johannes Gescher for the continuous support throughout my Ph.D research, for his patience, motivation, enthusiasm, helpful discussions during the retreat time and immense knowledge. His guidance helped me all the time of my research and writing of this thesis. And I am very thankful for the opportunity to attend the conferences and the course he sent me to, that gives me an access to the greater scientific community and not only expand my professional knowledge, but also boosted my communication skills. I could not have imagined having a better advisor and mentor for my Ph.D study.

Also I would like to thank all my cooperation partners for the efficient work and support, especially Dr. Sven Kerzenmacher, Dr. Andreas Dötsch and Marc Gauert.

I would like to thank all my fellow lab-mates in the AG Gescher Group for the friendly and easygoing atmosphere in the lab and for all the fun that we have had in the last four years. In particular, Mimi and Gunnar for the friendly and helpful advices during my integration time into German culture. Also big thanks to Sibylle and Kerstin for the nice introduction into the lab life and stimulating discussions during my study. Special Grazie to France, for the sports accompany, music concerts and all the fun that we have had together. I would like to thank Fredi for the technical support throughout my study and for the interesting conversations and useful discussions.

A very big thank you to любимый мой, Антошикус, who was walking side by side with me throughout my Ph.D study.

Last but not least, I would like to thank my family for the great support over my life, for understanding, trust and patience during my study. Thank you that you always believe in me!

## Table of contents

<b>Erklärung an Eides statt</b> .....	II
<b>Acknowledgements</b> .....	III
<b>Table of contents</b> .....	IV
<b>Abbreviations</b> .....	VIII
<b>Abstract</b> .....	1
<b>Zusammenfassung</b> .....	3
<b>Introduction</b> .....	5
1. Biogas production.....	5
1.1 General scheme of biogas performance.....	6
1.2 Limiting factors in technology.....	8
1.3 Advantages of biogas technology .....	9
2. Bioelectrochemical cell (BEC) .....	10
2.1 Principal function of BECs .....	10
2.2 Limiting factors .....	12
2.3 Application of BECs .....	14
3. Exoelectrogenic bacteria .....	16
3.1 Diversity of microorganisms .....	16
3.2 Mechanism of iron-reduction .....	17
3.3 Electron transfer mechanisms of <i>Geobacter spp.</i> .....	18
3.4 Electron transfer mechanisms of <i>S. oneidensis</i> .....	20
3.5 Interactions between bacteria and anode .....	22
4. Biofilms in BEC .....	24
5. Objectives of the research .....	25
<b>Materials and methods</b> .....	27
1. Microorganisms and chemicals .....	27
1.1 Bacterial strains .....	27
1.2 Biomass .....	27
1.3 Primers .....	28
1.4 Probes .....	29
1.5 Plasmid .....	30
1.6 Chemicals, enzymes and kits .....	31

2. Bacterial growth conditions .....	32
2.1 Aerobic growth medium and conditions for <i>S. oneidensis</i> and <i>E. coli</i> .....	32
2.2 Anaerobic growth medium and conditions for <i>S. oneidensis</i> .....	33
2.3 Anaerobic growth medium and conditions for <i>Geobacter spp.</i> .....	36
2.4 Medium for BECs .....	37
2.5 Medium for enrichment of exoelectrogenic bacteria .....	38
2.6 Storage technique of strains .....	39
3. Molecular biological methods .....	39
3.1. DNA extraction .....	39
3.2 RNA extraction .....	40
3.3 Polymerase chain reaction (PCR) .....	40
3.4 Quantitative PCR (qPCR, real time PCR) .....	42
3.5 Cloning .....	44
3.6 Colony PCR .....	45
3.7 Restriction fragment length polymorphism (RFLP) .....	46
3.8 DNA sequencing .....	47
3.9 RNA sequencing data analysis .....	47
4. Electrophoretic methods .....	47
5. Fluorescence <i>in situ</i> hybridization (FISH) .....	48
5.1 Fixation .....	50
5.2 Immobilisation .....	51
5.3 Permeabilisation of the cell membrane .....	51
5.4 Hybridization .....	51
5.5 Washing .....	52
5.6 Nonspecific staining of DNA – DAPI .....	53
5.7 Embedding and microscopy .....	53
5.8 FISH for the anodes .....	54
6. Analytical methods .....	54
6.1 Chromatographic methods .....	54
6.2 Photometric analysis .....	55
6.3 DNA and RNA concentration .....	55
6.4 Total organic carbon (TOC) determination .....	55
6.5 Coulombic efficiency .....	56
7. Electrochemical methods .....	56

7.1 Preparation and operation of BECs .....	56
7.2 Electroanalytical methods .....	59
8. Gas measurement .....	59
<b>Results</b> .....	60
1. Model exoelectrogenic biofilm .....	60
1.1 Dynamics of a model multi-species anode biofilm formation .....	60
1.2 Characterization of the biofilm stability under different electrochemical conditions .....	62
1.3 Steering metabolic activity via working electrode potentials .....	63
1.4 Transcriptome analysis .....	64
1.4.1 Transcriptome profiling of <i>G. sulfurreducens</i> gene expression .....	65
1.4.2 Transcriptome profiling of <i>G. metallireducens</i> gene expression .....	67
1.4.3 Transcriptome profiling of <i>S. oneidensis</i> gene expression .....	68
2. Natural exoelectrogenic community .....	70
2.1 Electrochemical performance and stability .....	70
2.2 Metabolite comparison between closed and open circuit in BECs .....	71
2.3 Influence of applied potentials on methane yield .....	72
2.4 Microbial diversity in the BECs with biomass .....	73
2.4.1 Archaeal community .....	74
2.4.2 Bacterial community .....	77
3. Electrical biogas system .....	82
3.1 Assessment of process characteristics: electrochemical stability and methane production .....	82
3.2 Substrate analysis .....	84
3.3 Stability of exoelectrogenic model biofilm on the anodes .....	86
<b>Discussion</b> .....	88
1. Model exoelectrogenic biofilm .....	88
1.1 Characterization the developmental growth of a model multi-species anode biofilm . .....	89
1.2 Influence of different redox potentials on current generation and stability of the biofilm on the anode surface .....	90
1.3 Variations of the central metabolism as a result of co-cultivation .....	92
2. Coupling bioelectrochemical system and anaerobic digestion .....	95

2.1 Evaluation of the electrical biogas system in terms of methane production and current generation .....	95
2.2 Methane yield and electron balances .....	98
2.3 Analysis of microbial community structure .....	99
2.3.1 Archaeal community .....	99
2.3.2 Bacterial community .....	100
2.4 Perspectives .....	101
<b>References</b> .....	103
<b>Appendix</b> .....	119
1. Transcriptome data .....	119
1.1 <i>G. sulfurreducens</i> gene expression .....	119
1.2 <i>G. metallireducens</i> gene expression .....	148
1.3 <i>S. oneidensis</i> gene expression .....	149
2. Publications and Manuscripts .....	167

**Abbreviations list**

<b>Abbreviation</b>	<b>Description</b>
AD	Anaerobic digestion
BEC	Bioelectrochemical cell
NHE	Normal hydrogen electrode
SCE	Saturated calomel electrode
DAPI	4',6-diamidino-2-phenylindole
FA	Formamide
OD	Optical density
RT	Room temperature
DMSO	Dimethyl sulfoxide
FISH	Fluorescence <i>in situ</i> hybridization
TOC	Total organic carbon
CE	Coulombic efficiency
qPCR	Quantitative PCR
EDTA	Ethylene diamine tetra acetate
LSV	Linear sweep voltammetry
OCP	Open circuit potential
VFA	Volatile fatty acids
PEM	Proton exchange membrane

## Abstract

Nowadays global energy crisis requires a multifaceted solution. Bioenergy is an important part of this strategy. To ensure an efficient biogas performance, in many cases it would be advisable to steer microbial degradation of the substrate. A new concept for integrating conventional anaerobic digester (AD) with bioelectrochemical cell (BEC) technology was investigated in the current study. The BEC technology stands out as an attractive potential technology in bioenergy, since it can convert energy stored in organic matter directly into bioelectricity. Coupling AD with BEC could be a profitable approach that could lead to overcoming limiting factors in AD, such as hydrogen partial pressure and accumulation of volatile fatty acids, inhibiting the methanogenesis.

In the first part of the current study the dynamics of a model exoelectrogenic biofilm, consisting of the three well-known exoelectrogenic microorganisms *Shewanella oneidensis*, *Geobacter sulfurreducens*, and *Geobacter metallireducens*, was analyzed at different stages of growth. The metabolic network of the community and their potential synergistic interactions within the biofilm were characterized through the systematic integration of electrochemical and transcriptome analyses. The conducted experiments revealed that the microorganisms build a stable biofilm on an electrode surface that is rather resilient to changes in the redox potential of the anode. The community operated at maximum electron transfer rates at electrode potentials that were higher than 0.04 V versus normal hydrogen electrode. Current densities decreased gradually with lower potentials and reached half-maximal values at -0.08 V. Transcriptomic results point towards a positive interaction of the individual strains. At least *S. oneidensis* and *G. sulfurreducens* show an upregulation of their central metabolism as a response to cultivation under mixed-species conditions. Interestingly, *G. sulfurreducens* was detected in the planktonic phase of the bioelectrochemical reactors only in mixed-culture experiments but not when it was grown in the absence of the other two organisms. It is possible that *G. sulfurreducens* cells used flavins which were released by *S. oneidensis* cells as electron shuttles. This would allow the organism to broaden its environmental niche.

In the second part of the present research a potential effect of BECs on biogas performance and carbon degradation rate was investigated using a linear sweep voltammetry (LSV) experiment in comparison with a parallel experiment under open circuit potential (OCP) mode. Microbial diversity was characterized throughout the experiments with a specific focus on the abundance of methanogenic species. The obtained results demonstrated a suppressive influence of applied potentials on methanogenic population, consequently on methane

formation. The natural exoelectrogenic community was able to generate current outputs of  $0.91 \mu\text{A cm}^{-2}$ , which is more than 480-fold lower in comparison with the current produced by the model biofilm pre-incubated on the anode surface. Methane yield efficiency was accounted as 86.4% and 63% for OCP and LSV mode, respectively. Interestingly, carbon sources were utilized actively in BECs under applied potentials, until exoelectrogenic microorganism were able to produce electrons, but under potentials below -0.15 V carbon degradation was slowed down.

In the third part of the present thesis an effect from the implementation of coupled BECs with AD was boosted by using anodes that were pre-incubated with the model multi-species biofilm. A very stable level of generated current was detected throughout the experimental time course. The model biofilm was still capable to produce half of its maximum current values under these conditions. In comparison with the OCP experiment, methane efficiency was lowered to 44%, but at the same time Coulombic efficiency was very high (64%).

## Zusammenfassung

Die globale Energiekrise erfordert neue und facettenreiche Lösungsansätze. Hierbei ist die Bioenergie ein wichtiger Bestandteil dieser Strategien. Um eine effiziente Biogasleistung sicherzustellen, kann es in vielen Fällen ratsam sein den mikrobiellen Abbau des Substrats zu steuern. In dieser Arbeit wurde ein neues Konzept zur Integration von bioelektrochemischen Zellen (BEZ) in konventionelle Vergärungsanlagen (VA) untersucht. Die BEZ-Technologie gilt als vielversprechende Technologie im Bereich der Bioenergie, da sie Energie, die in organischer Substanz gespeichert ist direkt in Strom umwandeln kann. Die Integration von BEZ in VA könnte ein profitablerer Ansatz, um bisher limitierende Faktoren zu überwinden. Diese Leistungs-begrenzenden Faktoren sind z.B. hoher Wasserstoff-Partialdruck und die Anhäufung von flüchtigen Fettsäuren und führen zur Hemmung der Methanogenese.

Hierzu sollte im ersten Teil dieser Arbeit zunächst die Dynamik eines exoelektrogenen Biofilm-Modells untersucht werden. Der Biofilm bestand aus den drei bekannten exoelektrogenen Mikroorganismen *Shewanella oneidensis*, *Geobacter sulfurreducens* und *Geobacter metallireducens* und wurde während verschiedenen Stadien des Wachstums analysiert. Das metabolische Netzwerk der mikrobiellen Gemeinschaft und mögliche synergistische Interaktionen innerhalb des Biofilms wurden durch die systematische Integration von elektrochemischen und transkriptionellen Analysen charakterisiert. Die durchgeführten Experimente zeigten, dass die Mikroorganismen einen stabilen Biofilm auf einer Elektrodenoberfläche aufzubauen, der relativ unbeeinflusst von Änderungen des Redoxpotentials der Anode ist. Das Verhalten des exoelektrogenen Konsortiums wurde sowohl bei optimalen als auch bei limitierenden Elektrodenpotentialen untersucht. Dabei zeigte sich, dass sich die Stromdichten mit sinkenden Potentialen verringerten und halb-maximale Werte bei -0,08 V erreichten. Die Ergebnisse der Transkriptom-Daten weisen auf eine positive Wechselwirkung der einzelnen Stämme untereinander hin. Zumindest *S. oneidensis* und *G. sulfurreducens* zeigen eine Hochregulation ihres zentralen Stoffwechsels als Antwort auf die Kultivierung unter Bedingungen als gemischte Spezies. Interessanterweise konnte *G. sulfurreducens* in Mischkulturexperimenten nur in der planktonischen Phase der bioelektrochemischen Reaktoren detektiert werden, wohingegen die Zellen in Abwesenheit der anderen beiden Organismen sowohl planktonisch als auch sessil vorkamen. Es scheint möglich, dass *G. sulfurreducens* Zellen Flavine verwendet, die zuvor durch *S. oneidensis* Zellen als Elektronenshuttles sekretiert wurden. Dies würde es dem Organismus ermöglichen, seine ökologische Nische zu erweitern.

Im zweiten Teil der vorliegenden Thesis wurde der Einfluss von BEZs auf die Leistung von Biogasanlagen untersucht. Hierzu wurde die Geschwindigkeit des Kohlenstoffabbaus in Leerlaufpotential (LLP)-Modus mit einem linearer Sweep Voltammetrie (LSV) Experiment verglichen. Die mikrobielle Diversität wurde während der Versuche mit besonderem Fokus auf die Vielfalt von methanogenen Spezies charakterisiert. Die Ergebnisse zeigen einen inhibierenden Einfluss der angelegten Potentiale auf das methanogene Konsortium und auf die Methanbildung. Die Methanertragseffizienz wurde mit 86,4% und 63% für LLP und LSV-Modus ermittelt. Interessanterweise wurden die Kohlenstoffquellen in BEZs unter angelegtem Potenzial abgebaut, bis die exoelektrogenen Mikroorganismen der Lage waren, Elektronen zu erzeugen, jedoch war der Kohlenstoff Abbau bei Potentialen unter -0,15 V verlangsamt.

Im dritten Teil der vorliegenden Arbeit konnte die Wirkung Integration von BEZ in VA unter Verwendung von vorinkubierten Anoden verstärkt werden. Ein sehr stabiles Niveau von erzeugtem Strom wurde während des gesamten Versuchszeitverlaufs erfasst. Der Modell-Biofilm war in der Lage die Hälfte seiner maximalen Stromwerte unter diesen Bedingungen zu erzeugen. Im Vergleich mit dem LLP Experiment wurde Methanertragseffizienz auf 44% gesenkt, aber zugleich war Coulomb-Effizienz sehr hoch (64%).

## Introduction

Energy has been universally recognized as one of the most important inputs for economic growth and human development (Stern *et al.*, 2004). The use of fossil fuels, especially oil and gas, for all human needs in recent years has accelerated and this triggers the global energy crisis. That is why there is an international interest in developing low carbon renewable energy technologies. Moreover a renewable bioenergy is viewed also as one of the ways to decrease the current global warming crisis. Another important environmental problem of today's society is the continuously increasing production of organic wastes. Meanwhile it is also known that biomass is a sustainable energy source that is utilized throughout the world. The use of organic biomass is environmentally friendly and provided approximately 14% of world's energy needs. Thus the conversion of the global energy industry to renewable energy sources is one of the major challenges of this century.

It is well known that fuels, such as ethanol, butanol, methane and hydrogen can be produced by microorganisms. In this view biogas technology, that generated a combustible gas from anaerobic biomass digestion, is a well-known and established technology. There are already millions of biogas plants in operation throughout the world. In Germany and other industrialized countries, power generation is the main purpose of biogas plants. Conversion of biogas to electricity has become a standard technology.

### 1. Biogas production

Production of biogas through anaerobic digestion (AD) of animal manure and digestible organic waste streams converts these substrates into renewable energy and offers a natural fertiliser for agriculture (Weiland, 2010). In the same time, it removes the organic components from the overall waste streams, thus increasing the efficiency of energy conversion by incineration of the remaining wastes. This technology nowadays has the potential to become a key technology to treat organic waste streams and generate heat and electricity for the refinery (Verstraete *et al.*, 2005). AD is a microbiological process of decomposition of organic matter under anoxic conditions, which is ordinary to many natural environments. Highly diverse microbial communities are involved in the anaerobic process which has two main end products: biogas and digestate. Biogas is a combustible gas consisting of methane and carbon dioxide in the approximate ratio 3:1 and small amounts of

other gases with trace elements. Digestate is the decomposed substrate, rich in macro- and micro nutrients and therefore suitable to be used as plant fertilizer (Al Seadi, 2008).

### 1.1. General scheme of biogas performance

Formation of a biogas is a result of several associated process steps, in which the initial material is continuously converted into smaller particles. The biochemical conversion of biomass into biogas is a complex procedure that requires a wide range of microorganisms. General stages of the AD process are shown in Figure 1.1.

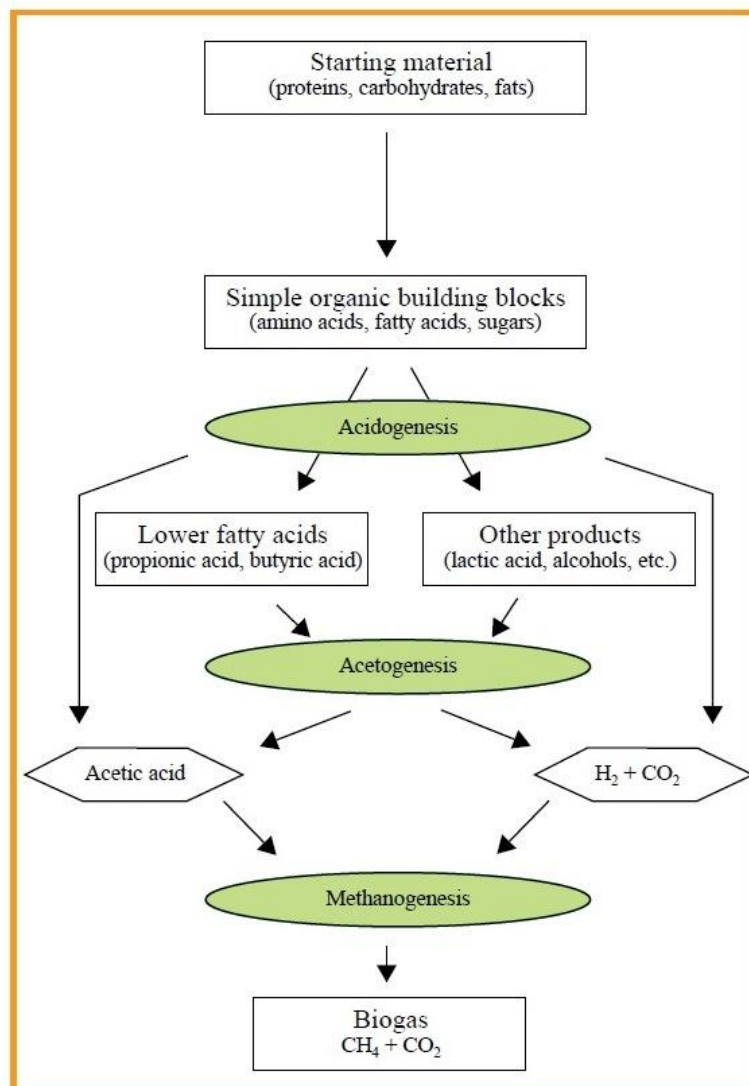


**Figure 1.1.** Schematic representation of anaerobic decomposition during the biogas production (Gülzow, 2010).

First, biomass is hydrolyzed to the mono- and oligomers. Hydrolysis is the essential step, because biomass is normally comprised of very large organic polymers, which are otherwise unusable. During hydrolysis, polymers like carbohydrates, lipids, nucleic acids and proteins

are converted into glucose, glycerol, purines and pyridines. Hydrolytic microorganisms excrete hydrolytic enzymes, which convert biopolymers into simpler and soluble compounds. The intermediate products resulting from hydrolysis are further fermented by acidogenic (fermentative) bacteria into methanogenic substrates (acetic, propionic and butyric acid) along with carbon dioxide and hydrogen in acidogenesis stage. These fermentative bacteria produce an acidic environment in the digester while creating simple sugars, amino acids and fatty acids.

The main point of the acetogenesis stage is the formation of acetate, a derivative of acetic acid, from carbon and energy sources by acetogens. These microorganisms catabolize many of the products formed during acidogenesis into acetic acid, CO<sub>2</sub> and H<sub>2</sub>. The hydrogen partial pressure is particularly important in this connection. Excessively high hydrogen content prevents the conversion of the intermediate products of acidogenesis, for energy-related reasons. As a consequence, organic acids, such as propionic acid, isobutyric acid, isovaleric acid and hexanoic acid, accumulate and inhibit the formation of methane. For this reason, the acetogenic bacteria (hydrogen-forming bacteria) must co-exist in a close biotic community with the hydrogen-consuming methanogenic archaea, which consume hydrogen together with carbon dioxide during the formation of methane (interspecies hydrogen transfer), thus ensuring an acceptable environment for the acetogenic bacteria (Wandrey *et al.*, 1983). Thus, acetogenesis and methanogenesis usually run parallel, as symbiosis of two groups of organisms.

Methanogenesis constitutes the final stage of anaerobic digestion in which methanogens create methane from the final products of acetogenesis as well as from some of the intermediate products from hydrolysis and acidogenesis. The hydrogenotrophic methanogens produce methane from hydrogen and carbon dioxide, whereas the acetoclastic methane-forming bacteria produce methane by acetic acid cleavage. Under the conditions prevailing in agricultural biogas plants, at higher organic loading rates methane is formed primarily via the reaction pathway utilising hydrogen, while it is only at relatively low organic loading rates that methane is formed via the reaction pathway involving the cleavage of acetic acid (Lebuhn *et al.*, 2008). It is known from sewage sludge digestion that 70% of the methane originates from acetic acid cleavage and only 30% from hydrogen utilization (Gülsow, 2010). However, in an agricultural biogas plant this is true at best of high-capacity digesters with very short retention times (Bauer *et al.*, 2008). Recent research confirms that interspecies hydrogen transfer is plainly what determines the rate of methane formation (Demirel *et al.*, 2008). Thus,

methanogenesis is a critical stage in the entire anaerobic digestion process, because it is the slowest biochemical reaction of the process.

Essentially, the four phases of anaerobic degradation take place simultaneously in a single-stage process. But due to the fact, that the methanogenic microorganisms are the weakest contributor in a biocenosis according their low rate of growth and their sensitivity to disturbances, the environmental conditions have to be adapted to the requirements of the methanogens.

## **1.2. Limiting factors in technology**

The stability of the AD process is reflected by the concentration of intermediate products like the volatile fatty acids (VFA). The VFA are intermediate compounds, such as acetate, propionate, butyrate and lactate, produced during acidogenesis. In most cases, AD process instability will lead to accumulation of VFA inside the digester, which can lead furthermore to a drop of pH-value. If too much organic matter is fed into the process within too short a period of time, the acid metabolic products of acidogenesis will accumulate, by that methanogenesis will be inhibited. The pH value of the AD substrate influences the growth of methanogenic microorganisms and affects the dissociation of some compounds of importance for the AD process. Acidogenic microorganisms usually have lower optimum pH values. The optimum pH range for mesophilic digestion is between 6.5 and 8.0 and the process is severely inhibited if the pH-value decreases below 6.0 or rises above 8.3. Recent research revealed that methane formation takes place within a relatively narrow pH range, from about 5.5 to 8.5, with an optimum interval between 7.0 and 8.0 for most methanogens (Nalinga and Legonda, 2015). Consequently, if the fermentation process takes place in one single digester, this pH range must be maintained. Regardless of whether the process is single-stage or multi-stage, the pH value is established automatically within the system by the alkaline and acid metabolic products formed in the course of anaerobic decomposition (Kaltschmitt and Hartmann, 2001). On the other hand, the pH value is supposed to rise if ammonia is released as a result of the breakdown of organic nitrogen compounds. The inhibitory effect of ammonia consequently increases.

The production of hydrogen during the acetogenesis and acidogenesis stages increases the hydrogen partial pressure. This can inhibit the metabolism of the acetogenic bacteria. Another inhibiting product of the digestion process is hydrogen sulphide ( $H_2S$ ), which in dissolved form can inhibit the decomposition process as a cytotoxin at concentrations as low as  $50 \text{ mg L}^{-1}$ . As the pH value drops the proportion of free  $H_2S$  rises, increasing the risk of inhibition.

One possible way of reducing the H<sub>2</sub>S concentration is by precipitation as sulphides with the aid of iron ions (Braun, 1982).

Methanogenesis is severely influenced by operation conditions. Composition of feedstock, feeding rate, temperature, and pH are examples of factors influencing the methanogenesis process. Digester overloading, temperature changes or large entry of oxygen can result in termination of methane production.

### **1.3. Advantages of biogas technology**

The main advantage of such technology is an environmental aspect, as energy and gas are produced out of renewable resources that would otherwise require being disposal. Moreover, the production of biogas in urban areas could be a valid alternative for the correct management of solid wastes disposed in a landfill. So usage of biogas is saving fossil fuel. Furthermore there is no additional carbon dioxide (CO<sub>2</sub>) emission produced. Of course CO<sub>2</sub> is produced during the biological process and by the use of biogas fuel. But there is a significant difference: the CO<sub>2</sub> emission that originates from the use of biogas matches the amount that was fixed by the production of biomass. No additional CO<sub>2</sub>, which is considered to be harmful to the climate, is produced. So it could be considered as a non-polluting technology in nature. The production of biogas does not require oxygen, which means that resources are conserved by not using any further fuel.

Moreover biogas could be produced everywhere: no matter if the biogas plant is located in an industrial or rural area. Also this technology is independent of sunlight. The use of bacteria to produce high-quality fuel is a big economical advantage that not just attracts big industrial nations, but also small and emerging countries. Biogas technology is easy to set up and require little capital investment on a small scale basis. In fact, many farms can become self-sufficient by utilizing biogas plants and the waste material produced by their livestock each day. A single cow can provide enough waste material within a day to power a light bulb the entire day.

Not only gas, electrical power and heat are produced by a biogas plant. Compressed Natural Gas (CNG) is biogas that has been compressed and can be used as a fuel for vehicles. Another benefit is the production of a high-quality fertilizer, because nitrate, phosphor and potassium remain nearly untouched during the biological process.

In Germany, more than 7,000 biogas plants were installed in 2012 (Agency for Renewable Resources, 2013). An annual electricity production of up to 17.5 billion kWh makes biogas the mainstay of bioenergy.

## 2. Bioelectrochemical cell (BEC)

Recently a new technology, generating electricity from renewable resources without a net CO<sub>2</sub> emission, was presented (Lovley, 2006; Davis and Higson, 2007). Producing electricity from organic matter with bioelectrochemical cells (BEC) is a concept that arguably dates back almost 100 years. The earliest BEC concept was demonstrated by Potter in 1910 (Ieropoulos *et al.*, 2005). Electrical energy was produced from living cultures of *Escherichia coli* and *Saccharomyces* by using platinum electrodes (Potter, 1911). But this discovery did not make a big interest until the 1980s, when it was discovered that current density and the power output could be greatly enhanced by the addition of electron mediators. The outer layers of many microbial species are composed of non-conductive lipid membrane, peptidoglycans and lipopolysaccharides that prevent the direct electron transfer to the anode. Electron mediators accelerate the transfer (Davis and Higson *et al.*, 2007). Thus this technology became more attractive and in recent years the number of journal publications dealing with BEC technology increased rapidly. BECs push forward the possibility of harvesting electricity from organic waste and renewable biomass. Moreover such technology offer the possibility of extracting over 90% of the electrons from organic compounds, and can be self-sustaining and renewing when populated with microorganisms that conserve energy from electron transfer to electrodes (Lovely *et al.*, 2006).

### 2.1. Principal function of BECs

Bioelectrochemical cells (BECs) are devices that convert organic waste streams to an energy form (electricity or hydrogen) using microorganisms as catalysts. Generally bacteria are used in BECs to generate electricity while accomplishing the biodegradation of organic matters or wastes (Park *et al.*, 2000; Wilkinson *et al.*, 2000). Figure 1.2 shows a schematic diagram of a typical BEC for producing electricity.

An electrochemical cell is a galvanic cell in which chemical energy is directly converted into electrical energy. In a BEC microorganisms serve as catalysts and oxidize organic substrates to CO<sub>2</sub>, protons and electrons. The typical BEC consists of an anodic and a cathodic chamber partitioned by a proton exchange membrane (PEM) (Kim *et al.*, 2003). The anode compartment is typically maintained under anoxic conditions, whereas the cathode is often localized in an oxic environment (flushed with air). Microbes in the anodic chamber of an BEC oxidize substrate and generate electrons and protons in the process (Rabaey and Verstraete, 2005).

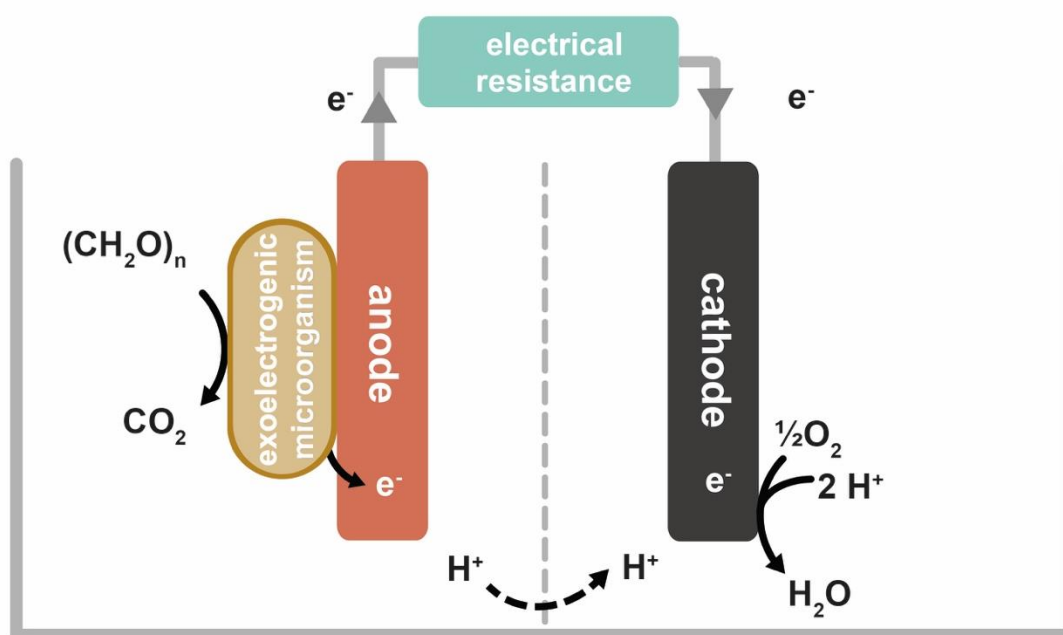
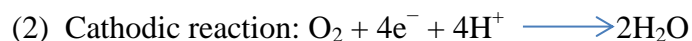
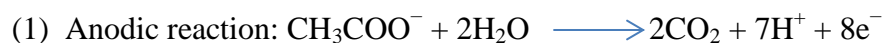


**Figure 1.2.** Schematic diagram of a typical two-chamber bioelectrochemical cell.

Electrons flow from the anode to the cathode through an external electrical connection that typically includes a resistor, a battery to be charged or some other electrical device. Carbon dioxide is produced as an oxidation product. However, there is no net carbon emission because the carbon dioxide in the renewable biomass originally comes from the atmosphere in the photosynthesis process. Unlike in a direct combustion process, the electrons are absorbed by the anode and are transported to the cathode through an external circuit. The protons enter the cathodic chamber by crossing a PEM, where they combine with oxygen to form water. Typical electrode reactions are shown below using acetate as an example substrate:



The overall reaction is the oxidation of the substrate to carbon dioxide and water with a concomitant production of electricity as a by-product. Based on the electrode reaction pair presented above, a BEC bioreactor can generate electricity from the electron flow from the anode to the cathode in an external circuit.

Effective anaerobic oxidation of complex organic matter requires the fermentation products from the metabolism of sugars, amino acids and related compounds, in addition to other

constituents, such as aromatic compounds and long chain fatty acids, to be oxidized with electron transfer to an electron acceptor. The closest analogues to electrodes for microbial metabolism in natural environments are  $\text{Fe}^{3+}$  oxides, because both electrodes and  $\text{Fe}^{3+}$  oxides are insoluble and extracellular electron acceptors. The oxidation of organic matter, coupled to the reduction of  $\text{Fe}^{3+}$  oxides in sedimentary environments, requires the cooperation of a consortium of fermentative microorganisms and  $\text{Fe}^{3+}$ -reducing microorganisms.  $\text{Fe}^{3+}$ -reducing microorganisms metabolize the fermentation products and the organic compounds that fermentative microorganisms do not readily metabolize, oxidizing them to carbon dioxide, with  $\text{Fe}^{3+}$  oxides serving as the electron acceptor (Lovley *et al.*, 1989). In BECs microorganisms use an anode as an electron acceptor. Due to its inert structure theoretically this acceptor can't be consumed. From a biotechnological perspective this is a very promising aspect.

## 2.2. Limiting factors

So far, performances of laboratory BECs are still much lower than the ideal performance. There may be several possible reasons. Power generation of a BEC is affected by many factors including microbe type, fuel biomass type and concentration, ionic strength, pH, temperature, and reactor configuration (Liu *et al.*, 2005a). The following operating parameters can be regulated to decrease the polarizations in order to enhance the performance of a BEC. Generally, it is difficult to compare the performance of BECs with a literature data due to an absence of standard routine or procedure of performing electrochemical experiments. Thus experimental conditions, such as anode material, electrochemical setup, medium and substrate are often varying from time to time (Logan, 2009).

**Electrode material.** The type of material used in electrode preparation will show a vital effect on BECs efficiency. The usage of better performing electrode materials will always improve the performance of BEC because different anode materials result in different activation polarization losses. Platinum and Platinum-black electrodes are superior to graphite, graphite felt and carbon-cloth electrodes for both anode and cathode constructions, but their costs are much higher.

In previous study (Schroder *et al.*, 2003) an increase of the power from 100 to 600  $\text{mW m}^{-2}$  were achieved with platinumized carbon-cloth anode in an agitated anaerobic culture of *E. coli* using a standard glucose medium at 0.55  $\text{mmol L}^{-1}$ . Platinum also has a higher catalytic activity with regard to oxygen than graphite materials. BECs with Platinum or Platinum-

coated cathodes yielded higher power densities than those with graphite or graphite felt cathodes (Moon *et al.*, 2005).

**pH buffer and electrolyte.** If no buffer solution is used in a working BEC, there will be an obvious pH difference between the anodic and cathodic chambers, though theoretically there will be no pH shift when the reaction rate of protons, electrons and oxygen at the cathode equals the production rate of protons at the anode. The PEM causes a transport barrier to the cross membrane diffusion of the protons, hence BEC operation can lead to a pH difference between anode and cathode compartment (Gil *et al.*, 2003). However, the pH difference increases the driving force of the proton diffusion from the anode to the cathode chamber and finally a dynamic equilibrium can form. Some protons generated with the biodegradation of the organic substrate transferred to the cathodic chamber are able to react with the dissolved oxygen, while some protons are accumulated in the anodic chamber when they do not transfer across the PEM quickly enough to the cathodic chamber. Increasing ionic strength by adding NaCl to BECs also improved the power output (Jang *et al.*, 2004) possibly due to the fact that NaCl enhanced the conductivity of both by anolyte and the catholyte.

**Proton exchange system.** Proton exchange systems can affect an BEC system's internal resistance and concentration polarization loss and they in turn influence the power output of the BEC. Nafion (DuPont, Wilmington, Delaware) is a most popular membrane material, because of its highly selective permeability of protons. However, the transport of other cations is unavoidable during the BEC operation with Nafion. Hence, Nafion as well as other PEMs used in the BECs are not a necessarily proton specific membranes but actually cation specific membranes. The ratio of PEM surface area to system volume is important for the power output. The BEC internal resistance decreases with the increase of PEM surface area over a relatively large range (Oh *et al.*, 2005).

**Operating conditions in the anodic chamber.** Substrate type, concentration and feed rate are important factors that impact the performance of BECs. Power density varies greatly with different substrates. Electricity generation is dependent on substrate concentration both in batch and continuous-flow mode BECs. Usually a higher substrate concentration yields a higher power output in a wide concentration range. Park and Zeikus (2003) reported that current increased with the lactet concentration up to a concentration of 200 mM in a single compartment BEC inoculated with *S. putrefaciens*. Gil *et al.* (2003) found that the maximum

current was related to the amount of added fuel with a lower concentration up to 50 mg L<sup>-1</sup> COD. Moon *et al.* (2006) investigated the effects of substrate concentration on the performance of an MFC and showed that the power density increased with the increase in substrate concentration. Interestingly, the electricity generation in a BEC is often higher at a relatively low level of feed rate before heading downward. This may be because a high feed rate promoted the growth of fermentative bacteria faster than those of the electrochemically active bacteria in a mixed culture (Rabaey *et al.*, 2004). However, if microbes are growing around the electrodes as biofilms, the increased feed rate is unlikely to affect the flora. Another possible reason is that the high feed rate brings in other alternate electron acceptors competing with the anode to lower the output.

**Operating conditions in the cathodic chamber.** Oxygen is the most commonly used electron acceptor in BECs for the cathodic reaction. Power output of an BEC strongly depends on the concentration level of electron acceptors. Several studies (Moon *et al.*, 2006) indicated that dissolved oxygen (DO) was a major limiting factor when it remained below the air-saturated level. Surprisingly, a catholyte sparged with pure oxygen that gave 38 mg/L DO did not further increase the power output compared to that of the air-saturated water (at 7.9 mg/L DO) (Oh *et al.*, 2004). The rate of oxygen diffusion toward the anode chamber goes up with the DO concentration. Power output is much greater using ferricyanide as the electron acceptor in the cathodic chamber. So far, reported cases with very high power outputs such as 7200 mW m<sup>-2</sup>, 4310 mW m<sup>-2</sup> and 3600 mW m<sup>-2</sup> all used ferricyanide in the cathodic chamber (Oh *et al.*, 2004; Schroder *et al.*, 2003), while less than 1000 mW m<sup>-2</sup> was reported in studies using DO regardless of the electrode material. This is likely due to the greater mass transfer rate and lower activation energy for the cathodic reaction offered by ferricyanide. Using hydrogen peroxide solution as the final electron acceptor in the cathodic chamber increased power output and current density according to (Tartakovsky *et al.*, 2006).

### 2.3. Application of BECs

Over the past 40 years researchers have suggested many applications for microbial fuel cells, including household electrical generators and power generators for small portable electronic devices, boats, automobiles, electronics in space and self-feeding robots (Sisler *et al.*, 1962; Shukla *et al.*, 2004; Wilkinson *et al.*, 2000). Chaudhury and Lovley (2003) reported that *R. ferrireducens* could generate electricity with an electron yield as high as 80%. An extremely high coulombic efficiency (CE) of 97% was reported during the oxidation of formate with the catalysis of Pt black (Rosenbaum *et al.*, 2006). Applications of BECs in a spaceship are also

possible since they can supply electricity while degrading wastes generated onboard. Some scientists envision that in the future a miniature BEC can be implanted in a human body to power an implantable medical device with the nutrients supplied by the human body (Chiao *et al.*, 2002).

Moreover BECs can be used to produce hydrogen instead of electricity. Under normal operating conditions, protons released by the anodic reaction migrate to the cathode to combine with oxygen to form water. Hydrogen generation from the protons and the electrons produced by the metabolism of microbes in a BEC is thermodynamically unfavorable. Liu *et al.* (2005b) applied an external potential to increase the cathode potential in a BEC circuit and thus overcame the thermodynamic barrier. In this mode, protons and electrons produced by the anodic reaction are combined at the cathode to form hydrogen. In biohydrogen production by using BECs, oxygen is no longer needed in the cathodic chamber. Thus, BEC efficiencies will be improved because there will be no leakage of oxygen into the anodic chamber.

Another interesting area is developing large-scale microbial electrochemical cells for the conversion of sewage and other organic waste to electricity and the bioremediation of contaminated environments (Rabaey and Verstraete, 2005; Angenent *et al.*, 2004; Mohanakrishna *et al.*, 2010). BECs using certain microbes have a special ability to remove sulfides as required in wastewater treatment (Rabaey *et al.*, 2006). Sanitary wastes, food processing wastewater, swine wastewater and corn stover are all great biomass sources for BECs because they are rich in organic matters (Suzuki *et al.*, 1978; Liu *et al.*, 2004; Oh and Logan, 2005; Min *et al.*, 2005; Zuo *et al.*, 2006). Up to 80% of the COD can be removed in some cases (Liu *et al.*, 2004; Min *et al.*, 2005) and a coulombic efficiency as high as 80% has been reported (Kim *et al.*, 2005). However, none of these applications is yet practical. At present, microbial fuel cells can produce enough current to power small electronic devices for short periods or to trickle-charge capacitors for applications with higher power demands. However, the size of these BECs precludes their incorporation into the electronic devices where they can supply power.

Apart from the aforementioned applications, another potential application of the BEC technology is to use it as a sensor for pollutant analysis and *in situ* process monitoring and control (Chang *et al.*, 2004, 2005). The proportional correlation between the coulombic yield of BECs and the strength of the wastewater make BECs possible biological oxygen demand (BOD) sensors (Kim *et al.*, 2003). A number of works (Chang *et al.*, 2004; Kim *et al.*, 2003) showed a good linear relationship between the coulombic yield and the strength of the wastewater in a quite wide BOD concentration range. A BEC-type BOD sensor constructed

with the microbes enriched with BEC can be kept operational for over 5 years without extra maintenance (Kim *et al.*, 2003), far longer in service life span than other types of BOD sensors reported in the literature.

### 3. Exoelectrogenic bacteria

#### 3.1. Diversity of microorganisms

Many microorganisms possess the ability to transfer the electrons derived from the metabolism of organic matter to the cell surface and thus reduce extracellular acceptors such as metals, minerals or an anode. Electrochemically active bacteria transfer electrons to the electrode through an electron transport system that either consists of a series of components in the bacterial extracellular matrix or together with electron shuttles dissolved in the bulk solution. The longer the process of microbial metal reduction is explored, the more is known about their diversity. Marine sediment, soil, wastewater, fresh water sediment and activated sludge are all rich sources for these microorganisms. A number of recent publications discussed the screening and identification of microbes and the construction of a chromosome library for microorganisms that are able to generate electricity from degrading organic matter (Logan *et al.*, 2008; Logan 2006; Niessen *et al.*, 2004).

Electrochemically active microorganisms have great importance in the natural environment, especially in metal oxidation and reduction and the associated effects on mineral dissolution, the carbon cycle, and the sorption and complexation of phosphorus and heavy metals (Kim *et al.*, 2007). There are model organisms such as *Shewanella oneidensis* or *Geobacter sulfurreducens* that were intensively investigated in the past, but these organisms are just a grain of sand in the desert in terms of the phylogenetic (and probably biochemical) diversity.

*S. oneidensis* MR-1 is a member of the  $\gamma$ -Proteobacteria and is a model organism for extracellular electron transfer. It was named after Dr. James H. Shewan and the place where it was isolated, the sediment of Lake Oneida in New York, USA (Venkateswaran *et al.*, 1999). It is a facultative anaerobic rod with a polar flagellum (Hau and Gralnick, 2007). The optimum growth temperature is 30°C (Venkateswaran *et al.*, 1999), but it can also grow at 4°C (Hau and Gralnick, 2007). *S. oneidensis* can use up to 20 different electron acceptors, including soluble compounds such as nitrate, nitrite, fumarate, sulfur, thiosulfate, DMSO and TMAO, but also insoluble minerals such as iron or manganese (Schwalb *et al.*, 2002; Schwalb *et al.*, 2003; Hau and Gralnick, 2006; Cruz-Garcia *et al.*, 2007; Shirodkar *et al.*, 2010). The electron donor spectrum, however, is rather small. Aerobically, *S. oneidensis* oxidizes lactate,

acetate, pyruvate, glucose, propionate, N-acetylglucosamin, ethanol, formate and some amino acids to CO<sub>2</sub>. Under anoxic conditions lactate is the preferred substrate and acetate and formate are excreted as final products (Scott and Neelson, 1994).

*G. sulfurreducens* PCA belongs to the  $\delta$ -proteobacteria. It was isolated from the sediment of a hydrocarbon polluted stream in Norman, Oklahoma, USA. It is a non-mobile rod with a growth optimum between 30-35°C (Caccavo *et al.*, 1994). As electron donor it can use hydrogen, acetate (Caccavo *et al.*, 1994) and lactate (Aklujkar *et al.*, 2009) while iron, sulfur, fumarate and malate can serve as electron acceptors (Caccavo *et al.*, 1994). Initially, it was assumed that *G. sulfurreducens* is a strict anaerobic bacterium, but later it was shown that *G. sulfurreducens* is aero-tolerant and can use up to 10% of oxygen as an electron acceptor (Lin *et al.*, 2004).

*G. metallireducens* GS-15 is phylogenetically closely related to *G. sulfurreducens*. It was isolated from the sediment of the Potomac River in Maryland, United States. *G. metallireducens* is a strictly anaerobic rod with an optimum growth temperature between 30-35°C (Lovley *et al.*, 1993). It can utilize a huge variety of different carbon compounds as electron donors. In addition to simple organic acids such as acetate, more complex and aromatic compounds such as phenol, toluene and alcohols can be metabolized by this strain. Nitrate or iron can be used as electron acceptors (Aklujkar *et al.*, 2009). Feist *et al.* (2014) could further show that *G. metallireducens* also is capable to fix CO<sub>2</sub> by using a reductive citric acid cycle.

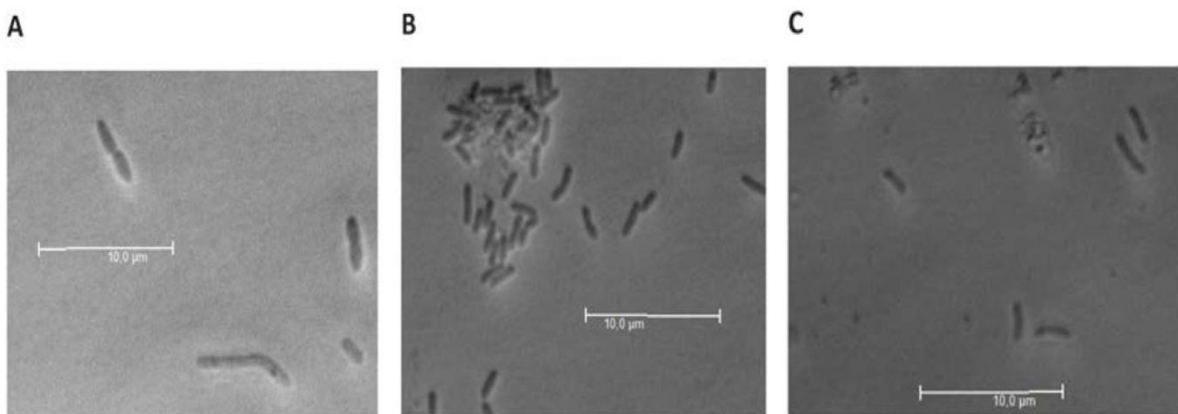


**Figure 1.3.** Light microscope images of exoelectrogenic microorganisms: A) *S. oneidensis* MR-1, B) *G. sulfurreducens* PCA, C) *G. metallireducens* GS-15

### 3.2. Mechanism of iron-reduction

Bacteria, which gain energy through oxidation of Fe<sup>2+</sup> (ferrous iron) or the reduction of Fe<sup>3+</sup> (ferric iron) have a strong influence on the global iron cycle (Kraemer *et al.*, 2005). Iron is the

fourth most abundant metal on Earth (Schlegel, 2007) and the most frequently utilized transition metal in the biosphere (Kappler and Straub, 2005). Thus, iron redox reactions have the potential to support a significant amount of microbial biomass. Since the 1980s it has been known that  $\text{Fe}^{3+}$  is able to serve as an electron acceptor for the anaerobic oxidation of organic carbon sources (Lovley, 1991; Thamdrup et al., 2000). Also  $\text{Fe}^{3+}$  could be reduced during anaerobic growth of some microorganisms, these microorganisms had a primarily fermentative metabolism and the formation of  $\text{Fe}^{2+}$  was considered to be due to side reactions (or co-metabolism) in their central metabolism (Lovley and Phillips, 1987). Evidence that  $\text{Fe}^{3+}$  reduction is linked to energy conservation was missing and it was often considered that  $\text{Fe}^{3+}$  was reduced by non-enzymatic reactions in the culture. The ability of microorganisms to yield energy to support cell growth coupled to the reduction of  $\text{Fe}^{3+}$  as electron acceptor was first reported in the 1980s (Balashova and Zavarzin, 1979). Until 1998 it was not recognized that hyperthermophiles could use  $\text{Fe}^{3+}$  as final electron acceptor (Vargas *et al.*, 1998). Remarkably, it is known today that most hyperthermophiles can reduce  $\text{Fe}^{3+}$  (Lovley *et al.*, 2004). This ferric iron can be used as electron acceptor using hydrogen gas as electron donor (Russell, 2002). Since other electron acceptors for hydrogen oxidation were sparse at the beginning of life on our planet, ferric iron and sulfat are supposed to be the first electron acceptors that were used on earth (Lovley *et al.*, 2004). Additionally, photolithotrophs might have utilized reduced iron as electron donor. Those photolithotrophes were discovered only shortly after the isolation of the first dissimilatory metal reducing bacterium (DMRB) (Straub *et al.*, 2001; Jiao and Newman, 2007). Their activity might have promoted growth of iron reducing bacteria even before substantial amounts of molecular oxygen were present in the atmosphere. Hence, ferric iron respiration indeed could be considered, next to sulfur respiration, as one of the first forms of energy conservation. Today, it is well established that reduction of ferric iron accounts for significant turnover of organic carbon in many environments (Nealson *et al.*, 2002). Although there are  $\text{Fe}^{3+}$ -reducing microorganisms which can couple the reduction of ferric iron to the oxidation of complex organic matter, they do not appear to be competitive with fermentative microorganisms in the same habitats (Lovley and Phillips, 1989).

### **3.3. Electron transfer mechanisms of *Geobacter* spp.**

Much of the research on extracellular electron exchange in exoelectrogenic species has been conducted with *G. sulfurreducens*. *G. sulfurreducens* has served as the species of choice up

until now because it was the first to have a genome sequence (Méthé *et al.*, 2003) and methods for genetic manipulation (Coppi *et al.*, 2001).

*G. sulfurreducens* belongs to dissimilatory metal reducing microorganisms, which gain energy in the form of ATP during the dissimilatory reduction of metal oxides under anaerobic conditions in soils and sediments. The electrons are transferred to the final electron acceptor such as  $\text{Fe}_2\text{O}_3$  mainly by a direct contact with the mineral oxides (Lovley *et al.*, 2004; Vargas *et al.*, 1998). Figure 1.3 illustrates the chemical compounds proposed to be involved in the electron transport to a solid-state final electron acceptor (anode) in *G. sulfurreducens* (Lovley *et al.*, 2004; Vargas *et al.*, 1998; Holmes *et al.*, 2004).

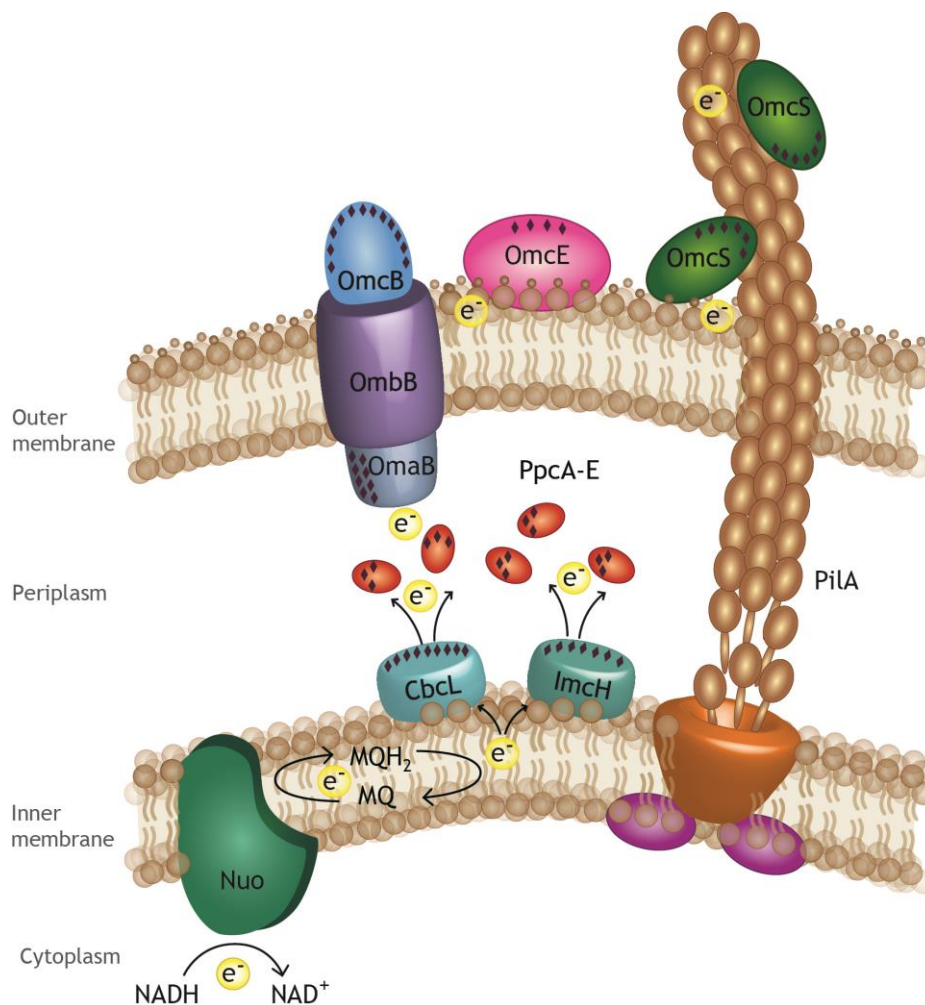


**Figure 1.3.** Summary of components proposed to be involved in the electron transport from cells to the anode in BECs using metal reducing *Geobacter* species (Lovley, 2006; Santos *et al.*, 2015). The oxidation of organic molecules releases electrons to the menaquinone (MQ) pool via NADH dehydrogenase. Thereafter *c*-type cytochromes are responsible for the electron transfer from the MQH<sub>2</sub> pool to the extracellular acceptor (ImcH, CbcL, PpcA, OmcB, OmcE, OmcS). According to a recent study by Zacharoff (2016), there are two electron

transfer pathways out of the inner membrane: ImcH is used for respiration to extracellular electron acceptors with redox potentials greater than -0.1 V, while CbcL is required at the lowest anode potentials.

89 putative *c*-type cytochromes were found in the genome of *G. sulfurreducens* PCA. 78 proteins of them have more than one heme group) and one may have up to 27 heme groups (Methé *et al.*, 2003). The high number complicates the resolution of the electron transport pathway. So far it is known, that the oxidoreductase is anchored in the cytoplasmic membrane and that respiratory electrons are transferred into the menaquinol pool. After that the electrons are transferred via two electron transfer pathways: with redox potentials greater than -0.1 V vs. SHE the multiheme *c*-type cytochrome ImcH is used and under lower potentials the multiheme *c*-type cytochrome CbcL is required (Zacharoff *et al.*, 2016). The periplasmic cytochrome A (PpcA) was suggested to be a major player for the transfer of electrons through the periplasm of the organism. There are a large number of *c*-type cytochromes that can be found in the outer membrane, however, the exact function of the individual proteins is not known. However two membrane complexes were found similarly to the MtrABC complex in *S. oneidensis*. One consists of OmbB-OmbA-OmcB and the other of OmbC-OmaC-OmcC (outer membrane - Om) (Liu *et al.*, 2014). These complexes are very important not only for the reduction of fumarate, but also for the reduction of Fe<sup>3+</sup>, where the electrons are further transported to OmcS. OmcS is a cytochrome that is directly associated with pili formed by *G. sulfurreducens*, which are composed of PilA, and are also necessary for the reduction of Fe<sup>3+</sup> (Leang *et al.*, 2010). Mehta *et al.* (2005) presented results, that both genes, OmcS and OmcE, are involved in electron transfer to Fe<sup>3+</sup> oxides in *G. sulfurreducens*.

76 putative *c*-type cytochromes were identified in the genome of *G. metallireducens*, 66 of them have more than one heme binding group (Butler *et al.*, 2010). The PilA protein of *G. metallireducens* shows 76% of homology to the protein sequence of PilA of *G. sulfurreducens* (Smith *et al.*, 2014). Also here, these pili are essential for the iron reduction in *G. metallireducens*. Moreover, it was shown in the same study, that reduction of iron oxide by *G. metallireducens* is catalyzed 17 times faster, than by *G. sulfurreducens* (Tremblay *et al.*, 2011).

### **3.4. Electron transfer mechanisms of *S. oneidensis***

There are 41 putative *c*-type cytochrome encoding genes present in the genome of *S. oneidensis*. Figure 1.4 shows the compounds proposed to be involved in the electron transfer in *S. oneidensis*. The oxidoreductase is anchored in the cytoplasmic membrane that transfers

electrons to the menachinol pool (Q). Thereafter, the electrons are transported to the tetraheme cytochrome CymA (cytoplasmic membrane protein A), that plays an important role as a distributor and transfers electrons to various periplasmic c-type cytochromes. There is a network of c-type cytochromes in periplasm, which function is possibly not only to pass the electrons to terminal reductases, but also to act as a capacitor whenever there is a lack of a usable electron acceptor (Schütz *et al.*, 2009). Then the electrons are transferred to a complex of metal reducing proteins (Mtr ABC), anchored into the outer membrane. While MtrB and MtrC are both decaheme cytochromes, MtrA is a  $\beta$ -barrel protein that forms a pore through the outer membrane.

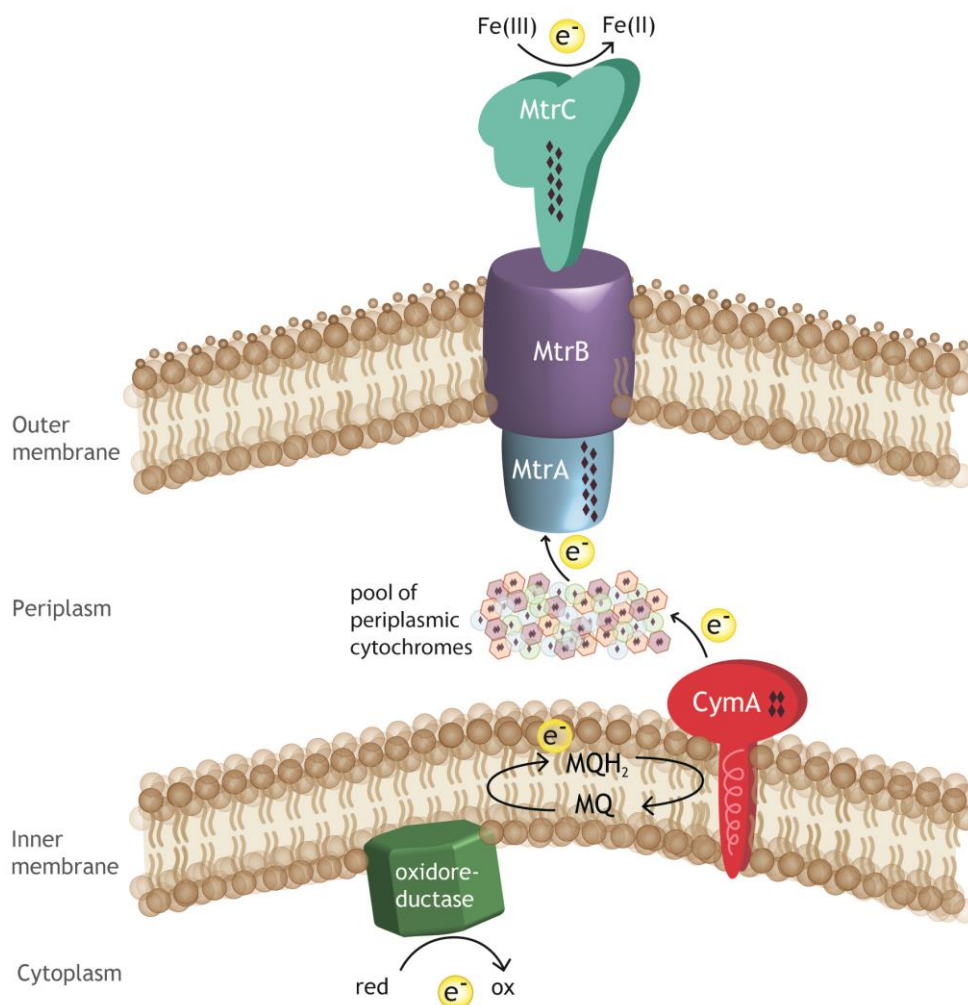


**Figure 1.4.** Summary of components proposed to be involved in the extracellular electron transfer in *S. oneidensis* (Paquete and Louro, 2010; Fonseca *et al.*, 2013; Breuer *et al.*, 2015). The oxidation of organic molecules releases electrons to the menaquinone (MQ) pool via oxidoreductase. From this point, a network of c-type cytochromes is responsible for the long-range electron transfer from the MQH<sub>2</sub> pool to extracellular acceptors. CymA is proposed to accept electrons from the MQH<sub>2</sub> pool, which are then delivered to multiheme periplasmic cytochromes, which establish the interface between the cytoplasmic and the OM associated electron

transfer components. Thereafter *c*-type cytochromes are responsible for the electron transfer from the MQH2 pool to the extracellular acceptor (CymA, MtrABC).

### 3.5. Interactions between bacteria and anode

In BECs the electrons liberated from the organic matter are transferred to electrodes. This is a key step that needs to be understood for the efficient conversion of waste to electricity. There are three primary mechanisms proposed to be used by microorganisms to transfer electrons to electrodes (Figure 1.5).

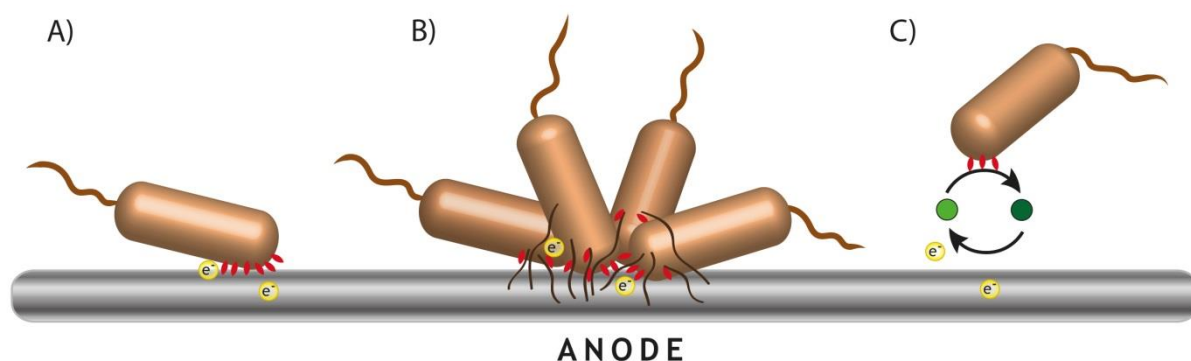


**Figure 1.5.** Mechanisms of electron transfer in exoelectrogenic microorganisms on the anode. The figure shows three different strategies to transfer electrons to an anode. A) Direct transfer of electrons to the acceptor via cytochromes (red ovals) on the cell surface. B) Transfer through microbial nanowires. Conductive Pili and soluble cytochromes allow formation of a biofilm of several cell layers with a conductive network to the anode surface. C) First electrons are transferred from the cell surface to a soluble shuttle component (reduced form; dark green). After that, the shuttle is reoxidized at the anode and can diffuse back to the microbial cells (light green). The shuttle can be both endogenous and exogenous in origin.

Direct electron transfer requires physical contact between extracellular components of the bacteria involved in the transport of electrons and the anode surface (Figure 1.5 A). It was proposed that electrons might be directly transferred from the cell to the electrode through outer-membrane *c*-type cytochromes, and in some studies it was shown that outer-membrane cytochromes are important for electron shuttle reduction (Nevin *et al.*, 2002). In the cytochrome proteins heme cofactors serve as electron-transferring catalytic centers. Direct transfer requires a distance of less than 15 Å between the heme group of a cytochrome and the insoluble acceptor (Kerisit *et al.*, 2007). Nevertheless, it was shown that biofilms of exoelectrogenic cells can be conductive. Hence, multiple layers of cells can form as a biofilm on the anode surface.

Figure 1.5 B shows the second possibility of using nanowires, which are very small conductive cell appendages. For *S. oneidensis* it was postulated that these nanowires are protuberances of the outer membrane filled with periplasm and thus constitute a cell surface extension (Pirbadian *et al.*, 2014).

The third possibility is to use a shuttle-molecule. In this mechanism electrons are transported by artificial mediators, sometimes referred to as electron shuttles. Shuttles are soluble redox-active molecules, which are reduced at the cell surface and diffused away from the cell, where they reduce extracellular substrates. The literature shows the application of several synthetic and natural exogenous electron shuttles like methylene blue, thionine, anthraquinone-2,6-disulphonate (AQDS), 2-hydroxy-1,4-naphthoquinone and neutral red or the bacteria are able to produce their own mediators such as riboflavin and flavin mononucleotide (FMN) (Figure 1.5 C). These electron shuttles are sometimes capable to cross cell membranes and to accept electrons from one or more electron carriers within the cell (Lovley, 2006; Shukla *et al.*, 2004). Mediators are important in BECs which use microorganisms such as *Escherichia coli*, *Pseudomonas*, *Proteus*, and *Bacillus species* that are unable to effectively transfer electrons derived from central metabolism to the outside of the cell (Davis *et al.*, 2007). Detailed investigations on the action of neutral red, which seems to be one of the most effective mediators, have demonstrated that it can accept electrons from NADH and can be enzymatically reduced by a hydrogenase, and possibly formate dehydrogenase (Park *et al.*, 2000; Holmes *et al.*, 2004). The mediators should possess the following characters for efficient electron transportation (1) able to cross the cell membrane easily; (2) able to grab electrons from the electron carries of the electron transport chains; (3) possess a high electrode reaction rate; (4) having a good solubility in the anolyte; (5) non-biodegradable and non-toxic to microbes; (6) low cost. In some studies it was proposed that *S. oneidensis* cells produce their own electron shuttles as a mechanism to facilitate electron transfer to  $\text{Fe}^{3+}$  (Park *et al.*, 2003). Biosynthesis of an electron shuttle is energetically expensive and therefore an electron shuttle must be recycled many times in order to recoup this energy investment. For this reason, microorganisms that produce electron shuttles are expected to have a competitive disadvantage in open environments in which the shuttle will rapidly be lost from the site of release. This might explain why species from the *Geobacteraceae* predominate over other species under  $\text{Fe}^{3+}$ -reducing conditions in many sedimentary environments (Rosso *et al.*, 2003). Electron shuttles were produced in BECs that were sequentially fed glucose over time, but without substantial medium replacement (Lies *et al.*, 2005). Significant limiting factor in

electricity production by several microorganisms that produce an electron shuttle is that they only incompletely oxidize their organic fuels.

#### **4. Biofilms in BEC**

An anode biofilm is a crucial component in BECs for electrogenesis. Better knowledge about the biofilm development process on electrode surfaces is believed to improve BEC performance. The term biofilm has been proposed for a structured community of microorganisms that adheres irreversibly to surfaces (biotic or abiotic) and is enclosed in a self-developed polymeric matrix of a primarily polysaccharide containing material (Donlan *et al.*, 2002). The formation of biofilms on an anode is one of several ways to ensure electron transfer (Figure 1.5 B). However, the exact mechanism of the electron transfer through the biofilm is not yet fully understood. On the anodes, which serve as an electron acceptor, *Shewanella spp.* form thin biofilms (McLean *et al.*, 2010). In contrast *Geobacter spp.* form thicker aggregates, in which electron transfer occurs over several cell lengths (Reguera *et al.*, 2006). The mechanisms of electron transfer in biofilms with exoelectrogenic microorganisms are an intensively researched and debated area. *G. sulfurreducens* nanowires are known as conductive or structuring elements of the biofilm (Reguera *et al.*, 2007; Malvankar *et al.*, 2011; Strycharz-Glaven *et al.*, 2011). In addition, the outer membrane cytochrome OmcZ seems to play an important role, because deletion of this gene significantly reduced power production (Schechter *et al.*, 2014). In thin (ca. 10  $\mu\text{m}$ ) wild type biofilms, genes for OmcS and OmcE are more highly expressed than in planktonic cells grown with a soluble electron acceptor such as Fe(III) citrate (Holmes *et al.*, 2006). Pili were found in the cell's supernatant of *Geobacter* cultures and scientists postulated a conductivity comparable to those of synthetic metallic nanostructures, which is still controversial (Malvankar *et al.*, 2011).

#### **5. Objectives of the research**

In the past decades, AD has steadily gained importance. However, the technology is not regarded as a top priority in science policy and in industrial development at present. In order for AD to further develop, it is crucial that AD profits from the current fuel issues emerging in the international arena. AD can provide low-cost treatment of sewage and solid domestic wastes, which represents a vast application potential that should be promoted in the developing world.

In order to increase the efficiency of the biogas performance, it is necessary to identify all limiting factors in the fermentation process and to overcome them. According to the fact, that conversion of biomass into biogas is a complex procedure that requires a large range of microorganisms, here comes the first and one of the most critical bottlenecks of biogas technology. Such complexity of the symbiosis excludes any control of the fermentation process. Moreover, hydrogen plays an important role in the above-mentioned processes. Acetogenic bacteria and methanogens need to live in a tight, syntrophic community, in which the hydrogen partial pressure is low enough. If this is not possible because the methanogenesis does not proceed fast enough, lower fatty acids accumulate in the reactor, which leads to a drop in pH. This in turn inhibits methanogens and consequently reduces the biogas yield. It is therefore crucial for proper fermentation processes that the entire process of biogas production remains in a stable equilibrium.

To solve these problems a new approach was investigated in this study in which we regard conventional AD and bioelectrochemical cell (BEC) technologies as complementary. For this purpose electrodes were installed directly into the biogas fermenter (Figure 1.6).

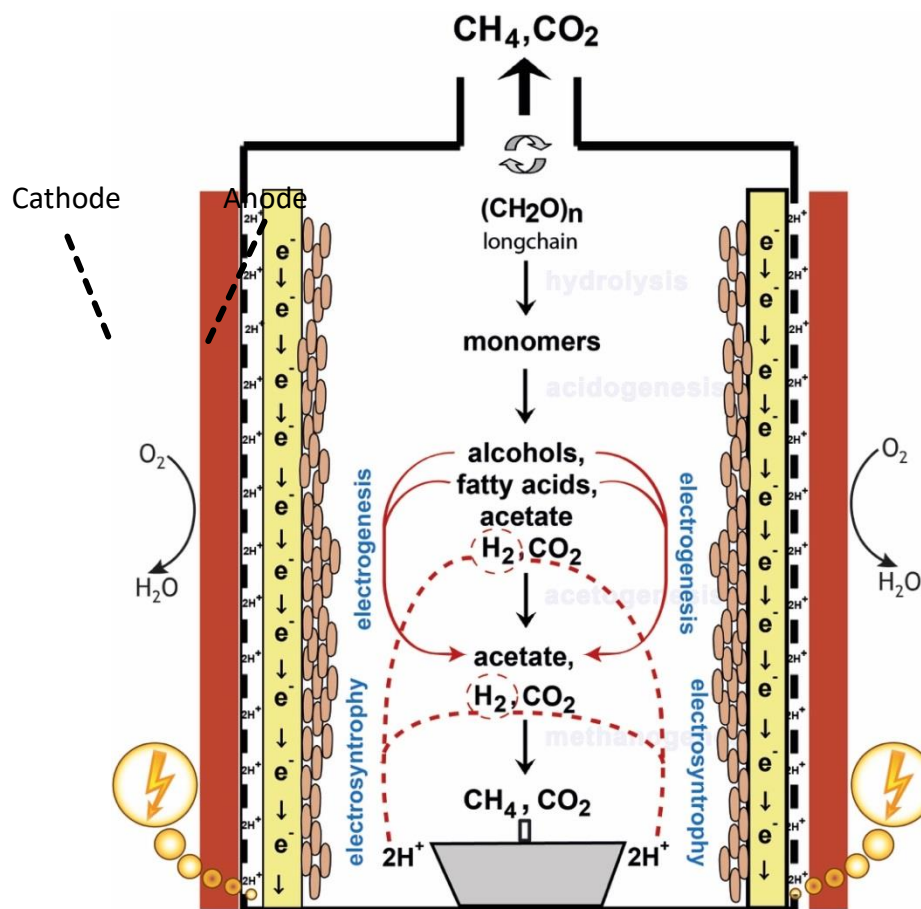


**Figure 1.6.** Schematic structure of an electric biogas plant.

Thus the object of the current study represents an innovative biogas digester with installed electrodes. The anode of the BEC is attached to the inner part of the biogas-reactor and colonized with exoelectrogenic microorganisms, whereas the cathode is attached to the outside part of the biogas-reactor and flushed with air. The cathode compartment is electrically connected to the anode and separated from the anode by an ion-permeable separator. Electrochemically active microorganisms will consume VFA thus supporting the acetogenesis stage and pH value and also lower the hydrogen partial pressures through the electrosynergy that will support the acetogenesis and methanogenesis stages. Moreover, the whole fermentation process will be accelerated. By controlling the exoelectrogenic activity of microorganisms, it could be possible to steer the fermentation process and moreover simultaneously produce electric energy.

The main aim of the current research was to identify and investigate the possibility to steer the exoelectrogenic activity as exemplified by the model multi-species community on the anode surface. That gives us a possibility to control the electrogenesis and electrosynergy, hence to regulate VFA depletion. For better understanding of cell interactions within the model community, synergistic behavior should be characterized through the transcriptome approach. Afterwards the coupling technology of AD and BEC should be characterized in terms of methane yield efficiency, electrical outputs and the microbial diversity under different electrochemical conditions. Moreover the electric biogas reactor with the anodes, which were previously pre-incubated with the model multi-species biofilm, should be evaluated in comparison with the conventional AD and non-pre-incubated electric biogas reactors.

## Materials and methods

### 1 Microorganisms and chemicals

#### 1.1. Bacterial strains

All strains that were used in this study are listed in Table 2.1.

**Table 2.1.** Bacterial strains used in this study.

Species (strain number)	Relevant genotype	Reference
<i>S. oneidensis</i> MR-1 (JG493)	synthetic sequence; 71982::Barcode	Dolch <i>et al.</i> , 2016
<i>G. sulfurreducens</i> PCA (JG 543)	synthetic sequence; 453226::kan Barcode	Dolch <i>et al.</i> , 2016
<i>G. metallireducens</i> GS-15 (JG 850)	synthetic sequence; 254254::kan Barcode pk18mob	Dolch <i>et al.</i> , 2016
$\alpha$ -Select Chemically Competent Cells (Gold Efficiency)	F <sup>-</sup> deoR endA1 recA1 relA1 gyrA96 hsdR17(rk <sup>-</sup> , mk <sup>+</sup> ) supE44 <i>thi</i> -1 phoA $\Delta$ (lacZYA-argF)U169 $\Phi$ 80lacZ $\Delta$ M15 $\lambda$ <sup>-</sup>	Bioline

#### 1.2. Biomass

The biomass used for the experiments in this study presented by a mixture of 60% sludge from a biogas reactor and 40% of a freshly prepared silage mixture listed in Table 2.2. All components were mixed at high speed in a food blender for 5 minutes.

**Table 2.2.** Composition of a silage mixture.

Component	Amount
Corn silage	8 g (about 2.64 oDM)
Na <sub>2</sub> CO <sub>3</sub> (100 mM)	25 mL

Trace element solution SL-10 (see Table 3)	100 µL
Aqua dest.	75 mL

**Table 2.3.** Composition of trace element solution SL-10 used for preparing a silage mixture.

Component	Amount
HCl (25%; 7.7 M)	10.00 ml
FeCl <sub>2</sub> x 4 H <sub>2</sub> O	1.50 g
ZnCl <sub>2</sub>	70.00 mg
MnCl <sub>2</sub> x 4 H <sub>2</sub> O	100.00 mg
H <sub>3</sub> BO <sub>3</sub>	6.00 mg
CoCl <sub>2</sub> x 6 H <sub>2</sub> O	190.00 mg
CuCl <sub>2</sub> x 2 H <sub>2</sub> O	2.00 mg
NiCl <sub>2</sub> x 6 H <sub>2</sub> O	24.00 mg
Na <sub>2</sub> MoO <sub>4</sub> x 2 H <sub>2</sub> O	36.00 mg
Aqua dest.	990.00 ml

### 1.3. Primers

All primers used in this study are listed in Table 2.4

**Table 2.4.** All primers that was used in this study.

Number	Primer name	Sequence (5' – 3')	Function/Reference
1	<i>S. oneidensis</i> barcode for	GACTGTACTTGGCATTG G	qPCR forward primer for <i>S. oneidensis</i> (Dolch <i>et al.</i> , 2016)
2	<i>S. oneidensis</i> barcode rev	GATCCATTAGCACAGAC TTA	qPCR reverse primer for <i>S. oneidensis</i> (Dolch <i>et al.</i> , 2016)
3	<i>G. sulfurreducens</i> barcode for	CGGTTCTATCGACCTAC C	qPCR forward primer for <i>G. sulfurreducens</i> (Dolch <i>et al.</i> , 2016)
4	<i>G. sulfurreducens</i> barcode rev	CTGCTTGATGAACGAGA G	qPCR reverse primer for <i>G. sulfurreducens</i> (Dolch <i>et al.</i> , 2016)

5	<i>G. metallireducens</i> barcode for	CCGTGCTCTGTATGATA C	qPCR forward primer for <i>G. metallireducens</i> (Dolch <i>et al.</i> , 2016)
6	<i>G. metallireducens</i> barcode rev	CAGGATTTCTCGAATTT CTC	qPCR reverse primer for <i>G. metallireducens</i> (Dolch <i>et al.</i> , 2016)
7	Bact 27F	GAGTTTGATCCTGGCTC A	General forward primer for 16S rDNA detection of bacteria (Rainey <i>et al.</i> , 1992)
8	U 1492R	GGTTACCTTGTTACGAC TT	Universal 16S rDNA reverse primer (Lane, 1991)
9	Arch 915F	AGGAATTGGCGGGGGA G	Forward primer for 16S rDNA detection of archaea (Ziegler <i>et al.</i> , 2013)
10	Arch 349F	YCCGGCGTTGAMTCCA ATT	Forward qPCR primer for archaea (Swan <i>et al.</i> , 2010)
11	Arch 806R	GGACTACVSGGGTATCT AAT	Reverse qPCR primer for archaea (Swan <i>et al.</i> , 2010)
12	T3 TOPO F	ATTAACCCTCACTAAAG GGA	Forward primer for vector pCR <sup>TM</sup> 4-TOPO (Life Technologies)
13	T7 TOPO R	TAATACGACTCACTATA GGG	Reverse primer for vector pCR <sup>TM</sup> 4-TOPO (Life Technologies)

#### 1.4. Probes

Special fluorescently labeled oligonucleotide probes and helper oligonucleotides that were used for fluorescence *in situ* hybridization (FISH) experiments are listed in Table 2.5.

**Table 2.5.** Fluorescently labeled oligonucleotide probes and helper oligonucleotides for FISH experiment. The used formamid concentration is shown as FA.

Probe	Sequence	Specification	Reference	FA [%]
SHEW227	AGCTAATCCCACCTAGGT WCATC	<i>Shewanella spp.</i>	Hugget et al. (2008)	40
GEO 1	AGAATCCAAGGACTCCG T	<i>G. metallireducens</i>	Summers et al. (2010)	20
HGEO1-1	GAAGGTCCCCCCTTTTC CCGC	Helpers for GEO1	Dolch et al., 2016	
HGEO1-2	GGGCTTATCCGGTATTAG CACC	Helpers for GEO1	Dolch et al., 2016	
GEO 2	AGAATCCAAGGACTCCG T	<i>G. sulfurreducens</i>	Richter et al. (2007)	20
HGEO2-1	GTCCCCCCTTTTCCCGC AAGA	Helpers for GEO2	Dolch et al., 2016	
HGEO2-2	CTAATGGTACGCGGACTC ATCC	Helpers for GEO2	Dolch et al., 2016	
ARCH915	GTGCTCCCCGCCAATTC CT	Archaea domain	(Amann et al., 1990a)	20
EUB338-I	GCTGCCTCCCGTAGGAGT	Eubacteria domain	(Amann et al., 1990a)	0 - 35

### 1.5. Plasmid

Taq polymerase-amplified PCR product was directly ligated into the plasmid vector pCR<sup>TM</sup>4-TOPO<sup>®</sup> (Fig. 2.1) and afterwards cloned into the  $\alpha$ -select cells. The vector contains the *ccdB* gene fused to the C-terminus of the LacZ $\alpha$  fragment. Insertion of a PCR product disrupts expression of the *lacZ $\alpha$ -ccdB* gene fusion permitting growth of only positive recombinants upon transformation in TOP10 cells. The vector contains a single 3' thymidine (T) overlap and a covalently bounded topoisomerase.

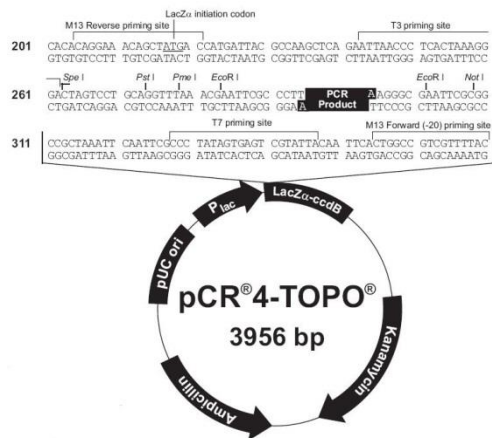


Fig. 2.1. pCR<sup>TM</sup>4-TOPO<sup>®</sup> vector.

## 1.6. Chemicals, enzymes and kits

Chemicals and biochemicals were obtained from Allichem (Darmstadt, Germany), Carl Roth GmbH & Co. KG (Karlsruhe, Germany), Sigma-Aldrich (Munich, Germany), Bioline (Luckenwalde, Germany), New England Biolabs (Frankfurt am Main, Germany), Fluka Chemie GmbH (Steinheim, Germany) and Thermo Scientific (Karlsruhe, Germany). Enzymes and kits used in this study are listed in Table 2.6.

Table 2.6. Enzymes and kits used in this study.

Product	Manufacturer
innuPREP Stool DNA Kit	Analytic Jena (Jena, Deutschland)
Wizard <sup>®</sup> Genomic DNA Purification Kit	Promega (Mannheim)
Wizard <sup>®</sup> SV Gel and PCR Clean-Up system	Promega (Mannheim)
MangoMix	Bioline (Luckenwalde)
iProof High-Fidelity Polymerase	Biorad (Munich)
MidoriGreen	Biozym (Hessisch Oldendorf)
1 kb DNA Ladder	New England BioLabs (Frankfurt/Main)
100 bp DNA Ladder	New England BioLabs (Frankfurt/Main)
6x DNA Loading Dye Solution	Fermentas (St. Leon-Rot)
DyNAmo ColorFlash SYBR Green qPCR Kit	Biozym (Hessisch Oldendorf)
4',6-diamidino-2-phenylindole (DAPI)	Appllichem (Darmstadt)
TOPO <sup>®</sup> TA Cloning Kit	Life Technologies (Darmstadt)

RNeasy Mini kit	Qiagen (Hilden, Germany)
Perfectly blunt <sup>®</sup> cloning Kit	Life Technologies (Darmstadt)
BfuCI	New England BioLabs (Frankfurt/Main)
Sau3AI	New England BioLabs (Frankfurt/Main)

## 2. Bacterial growth conditions

All media and buffers were prepared using deionized water and subsequently autoclaved. Heat-labile solutions were filtrated using a sterile filter (0.2 µm pore size).

### 2.1. Aerobic growth medium and conditions for *S. oneidensis* and *E. coli*

*S. oneidensis* cells were routinely cultured aerobically in tubes or Erlenmeyer flasks with LB-medium (lysogeny broth) at 30°C in a shaking incubator at 180 rpm (innova<sup>®</sup>44, Eppendorf, Hamburg, Germany).

**Table 2.7.** Composition of LB-medium used for aerobic growth of *S. oneidensis*.

Component	Amount [g/l]	End concentration
Tryptone	10	1%
Yeast extract	5	0.5%
NaCl	5	85 mM

*S. oneidensis* and *E. coli* were also grown on the LB-agar plates described in Table 2.8 in temperature controlled incubators with 30°C and 37°C, respectively. Kanamycin was used as a selection marker in a concentration of 50µg/ml

**Table 2.8.** Composition of LB-agar medium used for growth on plates for *S. oneidensis* and *E.coli*.

Component	Amount [g/l]	End concentration
Tryptone	10	1%
Yeast extract	5	0.5%
NaCl	5	85 mM
Agar	20	2%

For the transformation of chemically competent cells, *E. coli* was first cultured in SOB medium (super optimal broth) that is described in Table 2.9 and further in SOC medium (super optimal broth with catabolite repression) that is described in Table 2.10.

**Table 2.9.** Composition of SOB medium.

Component	Amount [g/l]	End concentration
Tryptone	20	1 %
Yeast extract	5	0.5 %
NaCl	0.58	10 mM
KCl [1M]	2.5 ml/l	2.5 mM

**Table 2.10.** Composition of SOC medium.

Component	Amount [g/l]	End concentration
SOB	944 ml/l	-
MgCl <sub>2</sub> x 6H <sub>2</sub> O [1 M]	20 ml/l	20 mM
Glucose [10%]	36 ml/l	0.36%

## 2.2. Anaerobic growth medium and conditions for *S. oneidensis*

Standard anaerobic techniques were used throughout the study (Balch et al. (1976)). First, aerobically pre-grown cells were cultured in PBS medium (phosphate-buffered saline) that is described in Table 2.11. Afterwards, cells were inoculated in the special anaerobic carbonate buffered medium (Table 2.12) that contained sodium lactate [12.5 mM] as electron donor and carbon source and Fe (III) citrate [50 mM] as electron acceptor.

All components for PBS media were mixed together and thereafter the pH was adjusted to 7.4. Bottles were sealed with a butyl rubber stopper and then connected to an anaerobic gas system that allows flushing the medium with 99% of nitrogen and degassing with vacuum in a continuous mode. One cycle usually includes 1-2 minutes with a gas phase and further 1-2 minutes with a vacuum. About 15 cycles were used for a complete degasing. Thereafter, the medium was autoclaved.

**Table 2.11.** Composition of PBS medium.

Component	Amount [g/l]	End concentration [mM]
NaCl	8	137
KCl	0.2	2.7
Na <sub>2</sub> HPO <sub>4</sub> x 2 H <sub>2</sub> O	1.78	10
KH <sub>2</sub> PO <sub>4</sub>	0.24	1.76
(NH <sub>4</sub> ) <sub>2</sub> SO <sub>4</sub>	1.18	8.9
Fumaric acid	11.6	100
NaOH	8	200
Sodium Lactate [50% (w/w)]	11.2	50
Casein hydrolysate	1	0.1%
Trace elements solution [100x] (Table 13)	10 ml/l	-
MgSO <sub>4</sub> x 7H <sub>2</sub> O [1 M]	1 ml/l	1
CaCl <sub>2</sub> x 2H <sub>2</sub> O [100 mM]	1 ml/l	0.1
pH with NaOH [1 M] adjust to 7.4		

Anaerobic carbonate buffered medium was prepared in bottles capped with butyl rubber stoppers. Electron donor and electron acceptor were added before autoclaving. To remove oxygen, media was boiled for 10 minutes and afterwards flushed with a mixture of N<sub>2</sub> and CO<sub>2</sub> (80:20) for 30 min. After that, the medium was autoclaved. Thereafter, the medium was complemented and the pH was adjusted to 7.2. Yeast extract and cysteine solutions were sterile filtrated and then connected through the sterile filters to the anaerobic system for 15 cycles. After that, they were stored at room temperature. Sodium ascorbat, calcium chloride and magnesium chloride were prepared in anaerobic flasks, connected to an anaerobic system for 15 cycles and afterwards autoclaved.

**Table 2.12.** Composition of carbonate buffered medium.

Component	Amount [g/l]	End concentration [mM]
KH <sub>2</sub> PO <sub>4</sub>	0.42	30
K <sub>2</sub> HPO <sub>4</sub>	0.22	10
NH <sub>4</sub> Cl	0.20	40
KCl	0.38	50
NaCl	0.36	60

NaHCO <sub>3</sub>	1.8	21
Na <sub>2</sub> CO <sub>3</sub>	0.5	5
Trace elements (Table 13)	10 ml/l	-
Selenite-tungstate (Table 14)	1 ml/l	-
Aqua dest.	Ad 980 ml	
Cook, cool down, flush with a gas and autoclave		
Vitamin solution (Table 15)		-
Yeast extract [20% (w/v)]	10 ml/l	0.2% (w/v)
Cystein [0.5 M]	5 ml/l	1
Sodium ascorbate [200 mM]	1 ml/l	0.2
Casitone [20%]	10 ml/l	0.2% (w/v)
CaCl <sub>2</sub> x 2 H <sub>2</sub> O [0.85 M]	1 ml/l	0.85
MgCl <sub>2</sub> x 6 H <sub>2</sub> O [1 M]	1 ml/l	1
pH with NaOH [1 M] adjust to 7.2		

For preparing NB trace elements solution, nitrilotriacetic acid was titrated in deionized water using KOH [1 M] to pH 6.5. Afterwards, all other components were added gradually. After autoclaving NB-solutions were stored at 4°C.

**Table 2.13.** Composition of NB trace elements solution.

Component	Amount [g/l]	End concentration [mM]
Nitrilotriacetic acid	2.14	11.2
Titrated to pH 6.5 using KOH [1 M]		
MnCl <sub>2</sub> x 4 H <sub>2</sub> O	0.1	0.5
FeSO <sub>4</sub> x 7 H <sub>2</sub> O	0.3	1.1
CoCl <sub>2</sub> x 6 H <sub>2</sub> O	0.17	0.7
ZnSO <sub>4</sub> x 7 H <sub>2</sub> O	0.2	0.7
CuCl <sub>2</sub> x 2 H <sub>2</sub> O	0.3	1.8
AlK(SO <sub>4</sub> ) <sub>2</sub> x 12 H <sub>2</sub> O	0.005	10.5 µM
H <sub>3</sub> BO <sub>3</sub>	0.005	80.9 µM
Na <sub>2</sub> MoO <sub>4</sub> x 2 H <sub>2</sub> O	0.11	0.5
NiSO <sub>4</sub> x 6 H <sub>2</sub> O	0.11	0.4
Na <sub>2</sub> WO <sub>4</sub> x 2H <sub>2</sub> O	0.2	0.6

Aqua dest.	Ad 11	
------------	-------	--

**Table 2.14.** Composition of selenite-tungstate solution.

Component	Amount [g/l]	End concentration [mM]
NaOH	0.5	13
Na <sub>2</sub> SeO <sub>3</sub>	3 mg/l	17 μM
Na <sub>2</sub> WO <sub>4</sub> x 2H <sub>2</sub> O	4 mg/l	12 μM
Aqua dest.	Ad 11	

The vitamin solution was sterile filtrated, then flushed with sterile nitrogen using the anaerobic system and stored in the dark at 4°C.

**Table 2.15.** Composition of NB trace elements solution.

Component	Amount [mg/l]	End concentration [μM]
Biotin	2	8.1
Folic acid	2	4.5
Pyridoxine-HCl	10	48.6
Thiamin-HCl	5	14.8
Riboflavin (vitamin B2)	5	13.3
Niacin (vitamin B3)	5	40.6
DL calcium pantothenate	5	10.5
Vitamin B12	0.1	0.07
4-Aminobenzoic acid	5	36.5
Lipoic acid	5	24.2
Aqua dest.	Ad 11	

### 2.3. Anaerobic growth medium and conditions for *Geobacter* species

*Geobacter* species have been previously considered as strictly anaerobes (Lovley *et al.*, 1993; Caccavo *et al.*, 1994). Both *Geobacter* strains were cultured in a carbonate buffered medium, described above (Table 2.12) that was additionally supplemented with the appropriate electron donors and electron acceptors for each strain. For *G. sulfurreducens* sodium acetate [10 mM] was used as electron donor and sodium fumarate [40 mM] as electron acceptor. For

*G. metallireducens* sodium acetate [10 mM] was also used as electron donor and sodium nitrate [10 mM] as electron acceptor. Cells were cultured in anaerobically closed tubes or Schott flasks at 30°C.

#### 2.4. Medium for BECs

For simultaneous growth of all three strains together in BECs, a special anode medium was designed. Components for this medium are listed in Table 2.16. Medium was prepared anaerobically as carbonate buffered medium described above.

**Table 2.16.** Composition of anode medium for BEC.

Component	Amount [g/l]	End concentration [mM]
KH <sub>2</sub> PO <sub>4</sub>	0.42	30
K <sub>2</sub> HPO <sub>4</sub>	0.22	10
NH <sub>4</sub> Cl	0.20	40
KCl	0.38	50
NaCl	0.36	60
NaHCO <sub>3</sub>	1.8	21
Na <sub>2</sub> CO <sub>3</sub>	0.5	5
Sodium lactate [50% (w/w)]	2.8	12.5
Propionic acid	0.48	5
Trace elements (Table 13)	10 ml/l	-
Selenite-tungstate (Table 14)	1 ml/l	-
Aqua dest.	Ad 980 ml	
Cook, cool down, flush with a gas and autoclave		
Vitamin solution (Table 15)		-
Yeast extract [20% (w/v)]	10 ml/l	0.2% (w/v)
Cystein [0.5 M]	5 ml/l	1
Sodium ascorbate [200 mM]	1 ml/l	0.2
Casitone [20%]	10 ml/l	0.2% (w/v)
CaCl <sub>2</sub> x 2 H <sub>2</sub> O [0.85 M]	1 ml/l	0.85
MgCl <sub>2</sub> x 6 H <sub>2</sub> O [1 M]	1 ml/l	1
pH with NaOH [1 M] adjust to 7.2		

Cathode medium was prepared aerobically and without a carbon source. All components are listed in Table 2.17.

**Table 2.17.** Composition of cathode medium for BEC.

Component	Amount [g/l]	End concentration [mM]
KH <sub>2</sub> PO <sub>4</sub>	0.42	30
K <sub>2</sub> HPO <sub>4</sub>	0.22	10
NH <sub>4</sub> Cl	0.20	40
KCl	0.38	50
NaCl	2.6	433
MgCl <sub>2</sub> x 6 H <sub>2</sub> O	0.21	27
Trace elements (Table 13)	10 ml/l	-
Selenite-tungstate (Table 14)	1 ml/l	-
Sodium ascorbate [200 mM]	1 ml/l	0.2
Aqua dest.	Ad 990 ml	

Prior to all MFC experiments, the cells were washed twice in an anaerobic buffer (Table 2.18) and were thereafter resuspended to an OD<sub>655</sub> of 1.0 in the same buffer. The initial cell density in the MFCs was set to an OD<sub>655</sub> of 0.1. The optical density during anaerobic growth on ferric citrate was measured at a wavelength of 655 nm to avoid scattering caused by ferric iron.

**Table 2.18.** Composition of washing buffer.

Component	Amount [g/l]	End concentration [mM]
KH <sub>2</sub> PO <sub>4</sub>	0.42	30
K <sub>2</sub> HPO <sub>4</sub>	0.22	10
NH <sub>4</sub> Cl	0.20	40
KCl	0.38	50
Aqua dest.	Ad 1000 ml	

## 2.5. Medium for enrichment of exoelectrogenic bacteria

In order to identify exoelectrogenic bacteria that naturally occur in biogas plants, an enrichment experiment was performed on a slightly modified carbonate buffered medium (Table 2.12) in two different variations. The first medium was additionally supplemented with

sodium acetate [6.25 mM], sodium lactate [20 mM] and ferric citrate [50 mM]. The variation contained sodium fumarate [40 mM], sodium nitrate [10 mM], sodium acetate [10 mM] and sodium lactate [20 mM]. Prior to the complementation, each medium was additionally supplemented agar. Thereafter, Schott flasks with medium were connected to the anaerobic system for 15 cycles and autoclaved. Afterwards flasks were cooled down in the water bath at 60°C and then were complemented with the rest of the components. The agar-medium was poured into Petri dishes in a glovebox. For growing anaerobic bacteria on solid agar plates, an anaerobic jar was used with a special gas pack that consumes all oxygen inside the chamber after it is sealed.

## 2.6. Storage technique of strains

*S.oneidensis* cells were stored on LB plates at 4°C. Both *Geobacter* species were stored as cryo-stocks that were prepared anaerobically in a glovebox. 900 µl of each culture pre-grown on an appropriate medium was mixed with 100 µl of DMSO solution in cryo-tubes. Afterwards they were transferred into liquid nitrogen solution for 10 minutes and stored at -80°C.

## 3. Molecular biological methods

### 3.1. DNA extraction

Genomic DNA was extracted from the planktonic cells and the anode biofilm using the innuPREP Stool DNA Kit (Analytic Jena, Jena, Germany). Liquid samples from the planktonic phase of the MFCs were treated as suggested by the manufacturer. Prior to the extraction, 1 ml of each sample was centrifuged at 16,000 x g for 2 minutes, 800 µl of supernatant was discarded and the remaining 200 µl resuspended. Anode samples were first incubated in the lysis solution at room temperature for 10 minutes and thereafter were cut into 2 pieces as technical duplicate.

Cell quantities were obtained by using quantitative PCR (qPCR). To obtain the qPCR detection limits for each strain, a standard curve based on the threshold cycle ( $C_T$ ) for a dilution series of DNA from pure cultures (1,  $1 \times 10^{-1}$ ,  $2 \times 10^{-2}$ ,  $1 \times 10^{-2}$ ,  $2 \times 10^{-3}$  and  $1 \times 10^{-3}$  diluted with the DNase-free water) was constructed and triplicate qPCR was conducted. The negative control samples contained DNase-free water instead of template DNA. To determine the initial concentration, cells were counted using a Neubauer hemocytometer with a 0.01 mm depth (Marienfeld, Lauda-Knigshofen, Germany).

### 3.2. RNA extraction

RNA was extracted individually from the triplicates of 4 experimental BEC set-ups that were inoculated either with pure cultures of *Shewanella oneidensis* MR-1, *Geobacter sulfurreducens* PCA, *Geobacter metallireducens* GS-15 or a mixed culture of the three strains. Prior to the extraction, all anodes with a biofilm were additionally pre-incubated in 3 ml of Bacteria Protect solution for 10 minutes at room temperature (Qiagen RNeasy Mini kit, Hilden, Germany). Total RNA was isolated from the anode-biofilms using the RNeasy kit provided by Qiagen according to the manufacture's instruction. Residual DNA was removed with an overnight DNase I digestion at 37°C. Further purification of RNA from DNA was conducted using the Ambion DNA-free kit (Life Technologies, Carlsbad, CA, USA). Aliquots from treated samples were subjected to PCR amplification with specific primers (Table 1) to validate the absence of genomic DNA. The Ambion MICROBExpress bacterial mRNA enrichment kit (Life Technologies) was used for rRNA depletion. Strand specific cDNA libraries were prepared from 50 ng of rRNA-depleted RNA following the TruSeq v2 RNA protocol (Illumina). The libraries were prepared using multiplex primers to allow simultaneous sequencing on a single lane, which was performed on a HiSeq1500 using SBS v3 kits (Illumina) generating paired end reads of 2 x 51 nt (*G. sulfurreducens* and *S. oneidensis*) or 2 x 100 nt (mixed species and *G. metallireducens* samples). Cluster detection and base calling were performed using RTAv1.13 and quality of reads was assessed with CASAVA v1.8.1 (Illumina). Sequencing yielded between 2.3 and 37.2 million read pairs that were deposited at the GEO database under the accession number GSE79750.

### 3.3. Polymerase chain reaction (PCR)

The polymerase chain reaction (PCR) is a method that is used to rapidly amplify a specific region of a single DNA molecule in vitro to yield sufficient quantities that can be cloned, sequenced, analyzed by restriction mapping etc. This method was chosen for preparative amplification of DNA fragments for subsequent cloning experiments and for analytical control of previous cloning experiments.

The PCR reactions were performed in a thermocycler (S1000, Biorad, Munich, Germany). For analytical control the ready to use MangoMix™ was used. MangoMix is a complete ready-to-use 2x pre-optimized reaction mix containing MangoTaq™ DNA Polymerase, dNTPs, red and orange reference dyes and 3 mM MgCl. A standard reaction of 20 µl is shown in Table 2.19.

**Table 2.19.** Standard reaction components for PCR with MangoMix (20  $\mu$ l).

Component	Volume [ $\mu$ l]
MangoMix [x2]	15
Primer forward [2pmol/ $\mu$ l]	7.5
Primer reverse [2pmol/ $\mu$ l]	7.5
Template DNA [0.1-0.5 $\mu$ g/ $\mu$ l]	1

For preparative amplification of genes or DNA fragments Phusion High fidelity Polymerase was used. Phusion DNA Polymerase possesses 5'-3' polymerase activity and a 3'-5' exonuclease activity and will generate blunt-ended products. This enzyme was used when high fidelity for cloning was necessary. A standard reaction of 50  $\mu$ l is shown in Table 2.20.

**Table 2.20.** Standard reaction components for PCR with Phusion (50  $\mu$ l).

Component	Volume [ $\mu$ l]
Phusion GC Buffer [x5]	10
10mM dNTPs	1
Primer forward [2pmol/ $\mu$ l]	12.5
Primer reverse [2pmol/ $\mu$ l]	12.5
DMSO	3
Phusion DNA polymerase	1
Template DNA [0.1-0.5 $\mu$ g/ $\mu$ l]	1
ddH <sub>2</sub> O	9

The following standard program was used (Table 2.21). Steps two through four were repeated 30 times. As denaturing temperature for MangoMix 95°C and for Phusion polymerase 98°C were chosen. The annealing temperature depended on the respective primer pair. The elongation time was set according to the size of the expected DNA fragment (MangoMix (Taq polymerase): 1 kb min<sup>-1</sup>; Phusion polymerase: 2 kb min<sup>-1</sup>). A single colony could also be used as DNA template. The colony was patched on a master plate prior to addition to the reaction.

**Table 2.21.** PCR program for standard reactions. Steps 2-4 were repeated 30 times. The denaturation step was conducted at 95°C with MangoMix and at 98°C with Phusion polymerase.

Temperature	Duration	Function
95°C (98°C)	5 min	Initial denaturation
95°C (98°C)	30 sec	Denaturation
50°C - 65°C	30 sec	Annealing the primers
72°C	30 sec/kb	Elongation
72°C	5 min	Final elongation
12°C	∞	End

### 3.4. Quantitative PCR (qPCR, real time PCR)

Quantitative PCR allows not only to detect the amplified products, but also to quantify them online. This is possible by including in the reaction a fluorescent molecule that reports an increase in the amount of DNA with a proportional increase in fluorescent signal.

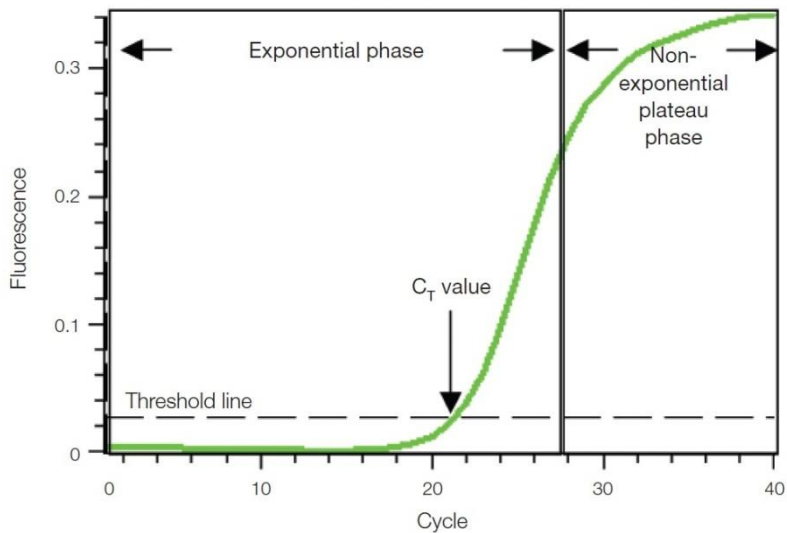


**Figure 2.3.** Amplification plot of the qPCR run.

During the exponential phase, the amount of PCR product approximately doubles in each cycle. It is obvious that at some point reaction components become limiting. Thus the reaction slows and enters the plateau phase (Figure 2.3). The cycle number at which enough product is amplified to yield a detectable fluorescent signal is called the threshold cycle ( $C_T$ ). Since the  $C_T$  value is measured in the exponential phase when reagents are not limiting, qPCR can be

used to reliably and accurately calculate the initial amount of template present in the reaction. The specialized thermal cycler CFX96 (Bio-Rad, Munich, Germany), equipped with fluorescence detection modules, was used to monitor the fluorescence during the amplification.

In the current study SYBR Green I was used as a DNA-binding dye for qPCR, which binds nonspecifically to double-stranded DNA (dsDNA). SYBR Green I exhibits little fluorescence when it is free in solution, but its fluorescence increases up to 1,000-fold when it binds dsDNA (Figure 2.4). Therefore, the overall fluorescent signal from a reaction is proportional to the amount of present dsDNA and will increase as the target is amplified.

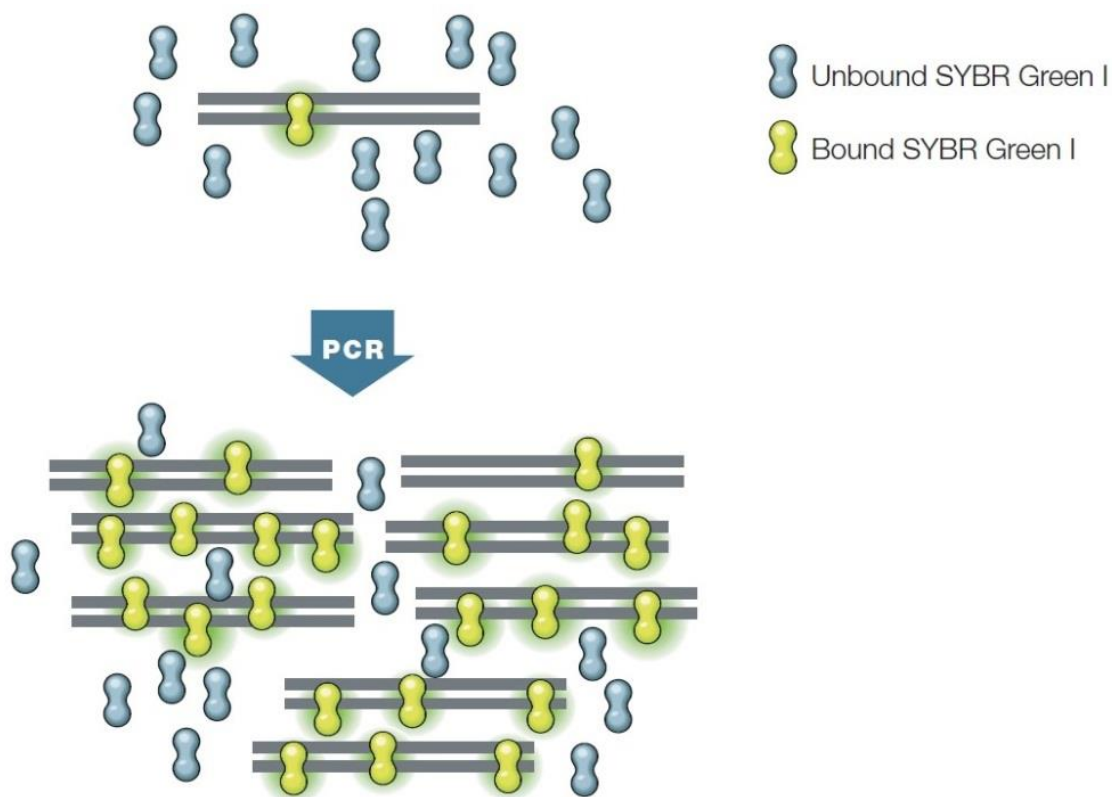


**Figure 2.4.** DNA-binding dyes in qPCR. Fluorescence increases dramatically when the dye molecules bind to dsDNA (Real-time PCR Application guide, Bio-Rad, 2006).

The amplification was carried out using the following program (Table 2.22):

**Table 2.22.** qPCR program for standard reactions. Steps 2-4 were repeated 34 times. The fluorescence was measured in each cycle after step 4.

Temperature	Duration	Function
95°C	7 min	Initial denaturation
95°C	10 sec	Denaturation

55 - 65°C	15 sec	Annealing the primers
60°C	30 sec	Elongation
Measure the fluorescence		
60°C	30 sec	Final elongation
60 - 98°C	each 5 sec	Melting curve

The optimal annealing temperature was determined in the range of 55 - 65°C by using a temperature gradient qPCR. The  $C_T$  values were automatically calculated with the Bio-Rad CFX Manager software. The standard curves were obtained by plotting the  $C_T$  value versus the logarithm of the concentration of each dilution of template DNA. According to the DyNamo Flash SYBR Green qPCR Kit manual, the amplification was carried out in a total volume of 20  $\mu$ l (Table 2.23).

**Table 2.23.** Standard reaction components for qPCR with SYBR Green I (20  $\mu$ l).

Component	Volume [ $\mu$ l]
MasterMix with blue dye	10
Primer forward [4 $\mu$ M]	2.5
Primer reverse [4 $\mu$ M]	2.5
ddH <sub>2</sub> O	4
Template DNA [0.1-0.5 $\mu$ g/ $\mu$ l]	1

Because SYBR Green binds to all dsDNA, it was necessary to check the specificity of the qPCR assay by analyzing the reaction products. For this purpose, at the end of the qPCR run a melting curve was performed as a validation step, starting from the final elongation temperature at 60°C up to 95°C. The amplification products were loaded for verification on a 2.5% agarose-gel. All primer sequences are depicted in Table 2.4.

### 3.5. Cloning

The main advantage of TOPO<sup>®</sup> Cloning is that amplified PCR products can be directly cloned using the *Taq* polymerase. This topoisomerase is covalently bound to an opened vector and enables integration of a DNA fragment from a PCR reaction without further enzymes. The PCR fragment needs to contain a recognition sequence and must be produced with a *Taq* polymerase, which is producing blunt ends. This allows PCR inserts to ligate efficiently with

the vector. The topoisomerase-reaction was performed according to manufacturer's instructions.

The TOPO<sup>®</sup> Cloning Kit pEXP5-CT/TOPO<sup>®</sup> TA Expression was used in this study. First, an amplified PCR product was ligated into the TOPO<sup>®</sup> vector. All components for such reaction are listed in Table 2.24.

**Table 2.24.** Reaction components for TOPO<sup>®</sup> cloning.

<b>Component</b>	<b>Volume [<math>\mu</math>l]</b>
PCR-product	4
Salt solution	1
TOPO <sup>®</sup> vector	1

This ligation was incubated at room temperature for 30 minutes. Afterwards it was transformed into the  $\alpha$ -competent cells that were part of the cloning kit. For the transformation, 2  $\mu$ l of the ligation-product was added to the ice cold competent cells and gently mixed. Then, the cells were incubated on ice for 30 minutes. Afterwards the cells were heat-shocked for 30 seconds at 42°C without shaking in a water bath. Next, they were immediately transferred to ice. After that, 250  $\mu$ l of room temperature SOC medium were added, tubes were tightly closed and incubated for 1 hour at 37°C (130 rpm). After this time 50  $\mu$ l of cells were spread on a pre-warmed Kan50 plate and incubated at 37°C overnight.

### 3.6. Colony PCR

Using the colony PCR it is possible to analyze bacterial clones quickly and easily (Gussow and Clackson, 1989). On the next day after cloning, 48 colonies were gridded in a 96-well format on Kan50 LB plates using sterile pipette tips that subsequently were used in a PCR reaction. The insert of the vector was amplified by PCR using the specific primers T7 and T3. These primers are specially designed for the TOPO<sup>®</sup> vector. The colony PCR was conducted, using the following components for the reaction (Table 2.25):

**Table 2.25.** Reaction components for the colony PCR.

<b>Component</b>	<b>Volume [<math>\mu</math>l]</b>
MangoMix	10
T7 Primer forward	5
T3 Primer reverse	5

TOPO <sup>®</sup> vector	1
--------------------------	---

The PCR was conducted with the following program (Table 2.26):

**Table 2.26.** Standard PCR program for the colony PCR. Steps 2-4 were repeated 30 times.

Temperature	Duration	Function
95°C	2.5 min	Initial denaturation
95°C	30 sec	Denaturation
45°C	30 sec	Annealing the primers
72°C	2 min	Elongation
72°C	7 min	Final elongation
12°C	∞	End

### 3.7. Restriction fragment length polymorphism (RFLP)

Restriction length polymorphism (RFLP) is a technique that allows to detect differences in homologous DNA sequences by digestion of the DNA samples with specific restriction endonucleases. Such enzymes cut DNA sequences from two organisms optimally at different locations. Thus, it is possible to obtain a specific restriction pattern for each organism.

In the current study this method was used as a tool to characterize mixed communities. A nearly full length 16S rRNA gene fragment of the extracted DNA from the biomass samples was amplified by PCR using the following primers: Bact 27F, Arch 915F and Universal 1492R (Table 2.4). PCR products were purified using a Wizard SV Gel and PCR clean-up system. The PCR product from the colony PCR step was then digested with the restriction enzyme BfuCI or with its Isoschizomer Sau3AI using the following procedure in Table 27 at 37°C for 2 hours. These both enzymes cut the sequence “GATC”.

**Table 2.27.** Reaction components for the RFLP.

Component	Volume [μl]
PCR Product	20
CutSmart-Buffer	2.64
BfuCI	0.5
ddH <sub>2</sub> O	0.56

Meanwhile for bacteria and archaea two different 1.5% agarose gels were prepared. The digested products were loaded on an agarose gel and run at 80V for about 80 minutes.

### 3.8. DNA sequencing

16S rDNA sequence analysis and similarity comparison were performed using the BLAST program of the National Center for Biotechnology Information (<http://www.ncbi.nlm.nih.gov>) and the Ribosomal Database Project (<http://rdp.cme.msu.edu>). The phylogenetic tree was constructed using the neighbor-joining method in the Geneious program (Saitou and Nei, 1987).

### 3.9. RNA sequencing data analysis

Sequence data were clipped if necessary to obtain a fixed length of 51 nt in all samples and mapped to a database containing the merged genomes of *Geobacter metallireducens* GS-15 (NCBI GenBank accession number NC\_002939.5), *Geobacter sulfurreducens* PCA (NC\_007517.1), *Shewanella oneidensis* MR-1 (NC\_004347.2) and its megaplasmid (NC\_004349.1) using *bowtie2* (Langmead and Salzberg, 2012). Differential expression profiles were calculated for each species individually in pure cultures versus the mixed culture by comparing the gene expression from the mapped sequences using *HTSeq* (Anders and Huber, 2010) for counting and *DESeq2* (Love *et al.*, 2014) for differential expression analysis. Genes were considered as differentially expressed if the expression differed at least 4-fold (identical to  $\log_2FC = +/-2$  which was used in the Excel files but this may be more compressible to the general audience) with an adjusted p value of less than 0.05.

## 4. Electrophoretic methods

Agarose gel electrophoresis was used to separate DNA by size (e.g. length in base pairs) for visualization and purification (Sambrook *et al.*, 1989). Electrophoresis uses an electrical field to move the negatively charged DNA toward a positive electrode through an agarose gel matrix. The gel matrix allows shorter DNA fragments to migrate more quickly than larger ones. Thus, the length of a DNA fragment can be determined by running it on an agarose gel alongside a DNA ladder. Small format gels were made by boiling 1% (w/v) dry agarose suspended in 60 ml TAE buffer (in Table 2.28 is shown 50-fold stock solution) until it became clear.

**Table 2.28.** Composition of TAE buffer (50-fold stock solution), used during the agarose gel electrophoresis as leveling agents.

Component	Amount
Tris-HCl	242 g
Adjust pH to 8 using glacial acetic acid (about 57.1 ml)	
EDTA [0.5 M]	100 ml
Aqua dist.	ad 1000 ml

The solution was cooled to 60°C and then 0.6 µg/ml Midori Green (diluted 1:5 in TAE buffer) was added before pouring. Midori Green intercalates into the DNA helix and shows then fluorescence of green color upon excitation with UV-light (312 nm). The gel chamber was filled with TAE buffer. DNA samples were mixed with 6-fold loading buffer (Table 2.29) and transferred into the holders in a gel. A constant voltage of 120 V was applied to the chamber. A DNA size marker was always included in the gel to determine relative sizes of DNA fragments.

**Table 2.29.** Composition of loading dye buffer (6-fold concentrated solution).

Component	Amount [ml]
Glycerin	6 g
50x TAE buffer	1.2
Bromophenol blue	1
Aqua dist.	2.8

## 5. Fluorescence *in situ* hybridization (FISH)

FISH was used for the simultaneous visualization, identification and localization of each strain in the multi-species community. This method uses a fluorescent oligonucleotide probe that hybridizes to the rRNA and can be designed to hybridize to specific strains or whole domains of microorganisms. Generally, these probes are presented by a small DNA fragment, comprising an attached fluorescent dye.

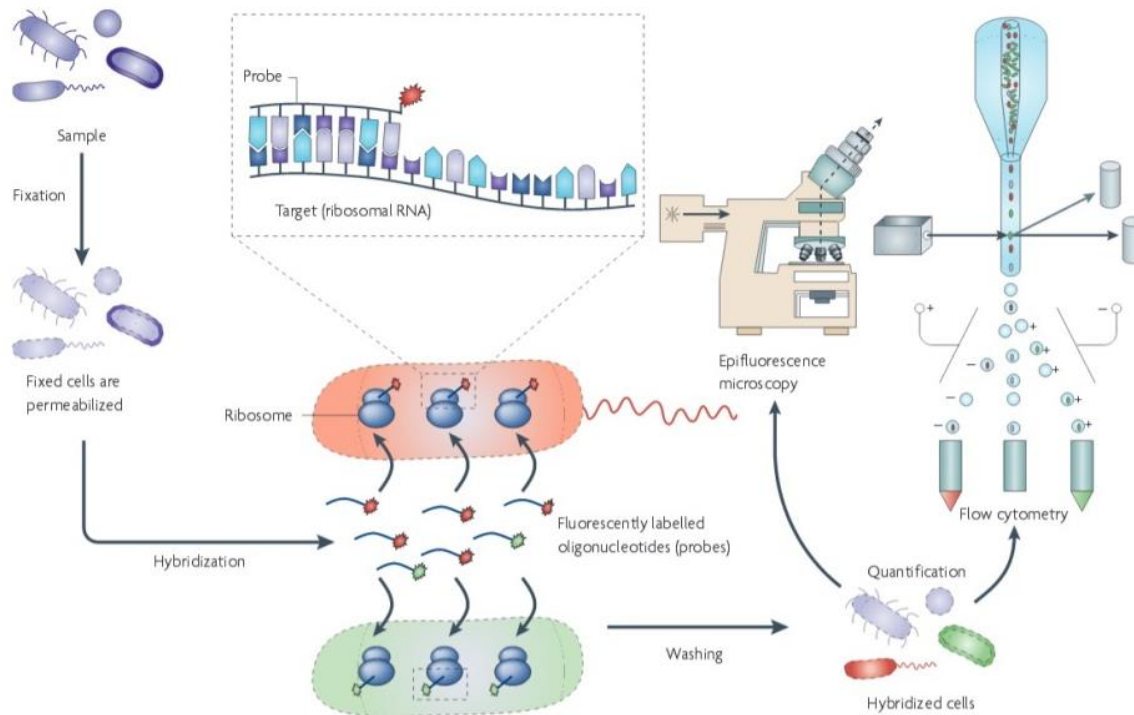


**Figure 2.6.** General scheme of FISH experiment (Amann and Fuchs, 2008). Firstly the sample is fixed with formaldehyde or ethanol to stabilize the cells and then permeabilized the cell membranes. The labelled oligonucleotide probe is then added and allowed to hybridize to its intracellular targets before the excess probe is washed away. The sample is then ready for microscopy.

In this study we analyzed samples that were taken from the planktonic phase in a BEC and directly from the anode surface at the end of the experiment. Table 2.30 shows an overview of all stages of the hybridization.

**Table 2.30.** Guidance for FISH experiment.

Component	Duration	Temperature	Function
Fixation solution	1-4 h	4°C	Fixation of cells
1x PBS	30 min	4°C	Washing
1x PBS : Ethanol [100%] = 1:1		-20°C	Storage
HCl [0.1 M]	1 min	RT	Permeabilization of cells
ddH <sub>2</sub> O	Quick dip	RT	Washing
-	-	37°C	Drying
-	-	4°C	Storage
Hybridization buffer with a Probe (extra with a helper	2 h	46°C	Hybridization

oligonucleotide)			
Washing buffer	Quick dip	48°C	Washing
Washing buffer	15 min	48°C	Washing
ddH <sub>2</sub> O	Quick dip	RT	Washing
1x SSC	10 min	RT	Washing
-	-	37°C	Drying
DAPI	5-25 min	RT	Nonspecific staining of DNA
-	-	4°C	Storage

### 5.1. Fixation

Liquid samples were fixed with 4% formaldehyde solution (Table 2.31) for 1 hour at 4°C. Thereafter, they were washed twice in PBS medium via centrifuging at 8,000 rcf for 2 minutes. The samples were then stored in a 50% (v/v) ethanol solution at 20°C.

Complete anodes were fixed with the same concentration of formaldehyde for 4 hours at 4°C. Thereafter they were washed twice in 1x PBS medium for 30 minutes and afterwards were stored in a 50% ethanol (v/v) solution at 4°C.

**Table 2.31.** Composition of 10x PBS solution for FISH.

Component	Amount [g/l]
NaCl	80
KCl	2
Na <sub>2</sub> HPO <sub>4</sub> x 2 H <sub>2</sub> O	7.64
KH <sub>2</sub> PO <sub>4</sub>	2
Adjust pH to 7.5	
Aqua dist.	ad 1L

**Table 2.32.** Composition of fixation solution for FISH.

Component	Amount [ml]
10x PBS	10
37% formaldehyde	10.8
Aqua dist.	79.2

## 5.2. Immobilisation

Fixed liquid cells were immobilized on the microscope slides coated with Teflon. Per each well 10  $\mu$ l of sample were added and dried at 37°C. Eventually 2-3 drops of 0.1% low melt agarose in 1xPBS were added to the wells and afterwards were dried at 37°C.

## 5.3. Permeabilisation of the cell membrane

The samples were incubated with the 0.1 M HCl for 1 minute in order to make the cell membrane permeable for the fluorescence probes. Afterwards they were washed with distilled water with the following desiccation at 37°C.

## 5.4. Hybridization

Depending on the selected target, an appropriate concentration of formamide was chosen (see in Table 2.5). First, the hybridization buffer was prepared in a 50 ml sterile plastic tube using the components listed in Table 2.33. Then, it was warmed at 60°C in the water bath in order to dissolve SDS solution completely and later cooled down on ice. The buffer was filtrated through sterile filters (0.2  $\mu$ m) into 2 ml reaction tubes and stored at -20°C.

**Table 2.33.** Composition of hybridization solution for FISH.

Component	20% [FA]	30% [FA]	40% [FA]
NaCl [5 M]	1.08 ml	1.08 ml	1.08 ml
Tris-HCl [1 M], pH 8.0	0.12 ml	0.12 ml	0.12 ml
ddH <sub>2</sub> O	3.6 ml	3.0 ml	2.4 ml
20% SDS	3 $\mu$ l	3 $\mu$ l	3 $\mu$ l
Formamid	1.2 ml	1.8 ml	2.4 ml

Second, a wet hybridization chamber was prepared with the appropriate concentration of formamide (Table 2.34). For such purpose a Kimtech tissue was put into the 50 ml reaction tube and then an appropriate amount of distilled water and formamide was added.

**Table 2.34.** Composition of a wet hybridization chamber for FISH.

Component	20% [FA]	30% [FA]	40% [FA]
ddH <sub>2</sub> O	1.6 ml	1.4 ml	1.2 ml
Formamid	0.4 ml	0.6 ml	0.8 ml

Prior to work with the fluorescent dye it is important to organize dark conditions in the fume hood. All working solutions of probes and helper oligonucleotides should be diluted in distilled water to a concentration of  $50 \mu\text{g ml}^{-1}$ . Probes with the same formamide concentration can be simultaneously hybridized. For each sample on the microscope slide  $14 \mu\text{l}$  of hybridization buffer and  $1 \mu\text{l}$  of probe were added (or  $13 \mu\text{l}$  of hybridization buffer with  $1 \mu\text{l}$  of probe and  $1 \mu\text{l}$  of helper oligonucleotide, where it is needed). Then this microscope slide was installed into the prepared wet hybridization chamber covered with the aluminum foil and incubated in the oven at  $46^\circ\text{C}$  for 2 hours.

### 5.5. Washing

The wash buffer for the appropriate formamide concentration were prepared as described as listed in Table 2.35 and was pre-warmed in a water bath at  $48^\circ\text{C}$ . Prior to use the 20-fold stock solution of SSC (Table 2.36) was autoclaved. The procedure of all washing steps is described in Table 30.

**Table 2.35.** Composition of a washing buffer for FISH.

Component	20% [FA]	30% [FA]	40% [FA]
NaCl [5 M]	2.15 ml	1.02 ml	0.46 ml
Tris-HCl [1 M], pH 8.0	1 ml	1 ml	1 ml
EDTA [0.5 M], pH 8.0	0.5 ml	0.5 ml	0.5 ml
20% SDS	25 $\mu\text{l}$	25 $\mu\text{l}$	25 $\mu\text{l}$
ddH <sub>2</sub> O	Ad 50 ml	Ad 50 ml	Ad 50 ml

**Table 2.36.** Composition of a SSC solution for FISH.

Component	Amount [g/l]	End concentration [M]
NaCl	175.3	3
Tri-Na-Citrate Dihydrate	88.2	0.3
Adjust pH to 6 using HCl		
ddH <sub>2</sub> O	Ad 1L	

For staining, samples with different formamide concentrations higher concentrations were hybridized before lower concentrations.

### 5.6. Nonspecific staining of DNA – DAPI

4',6-diamidino-2-phenylindole (DAPI) is a fluorescent stain that binds strongly to A-T rich regions in DNA. When bound to double-stranded DNA, DAPI has an absorption maximum at a wavelength of 358 nm (ultraviolet) and its emission maximum is at 461 nm (blue). Therefore, for fluorescence microscopy DAPI is excited with ultraviolet light and is detected through a blue/cyan filter. Working solution for staining consists of 1 µl of DAPI [1 mg ml<sup>-1</sup>] and 999µl of distilled water. 15 µl of such solution were added to each sample on the microscope slide and incubated for 5 minutes in dark conditions. Afterwards, the slide was washed twice with distilled water and quickly submerged with 100% ethanol.

### 5.7. Embedding and microscopy

The microscopy slides were protected with the coverslips. For such purpose an embedding buffer was prepared in dark conditions and after that stored at 4°C (Table 2.37). One drop of buffer was added to each sample and long (24 x 60 cm<sup>2</sup>) coverslips were placed on the microscope slide. These prepared slides can be stored at -20°C.

**Table 2.37.** Composition of an embed buffer for FISH.

Component	Amount [ml]
Citifluor	1.1
Vectashield	0.2
1x PBS	0.1

Images were analyzed with a Leica DM 5500 B microscope using a 63x immersion lens and a digital color camera DFC 300 FX (Leica, Wetzlar, Germany). In this study we used the following filter sets that are listed in Table 2.38. For image processing and creating 3D images the ImageJ software (Rasband, 1997 – 2004) was used.

**Table 2.38.** Specification of the filters for FISH experiment that were used in the Leica DM 5500 B microscope.

Filter cube	Fluor dye	Excitation range	Excitation filter	Suppression filter
A4	DAPI	UV	BP 360/40	BP 470/40
I3	FITC	Blue	BP 450/490	LP 515
Y3	CY3	Green	BP 545/30	BP 610/75

Y5	CY5	Red	BP 640/30	BP 690/50
----	-----	-----	-----------	-----------

### 5.8. FISH for the anodes

Whole anodes were placed in special plastic box, fitted to the size. Generally, anodes were stained using the same procedure as described above (2.5.3 – 2.5.7) with minor changes. An immobilization step was excluded because the anodes can be directly used for microscopy without using microscope slides. For the hybridization step, a big plastic box covered completely with an aluminum foil was used. 1.5 ml of hybridization buffer was used for each anode sample. At the washing stage instead of a quick dip step anodes were washed twice with 1 ml of washing buffer.

## 6. Analytical methods

### 6.1. Chromatographic methods

High-performance liquid chromatography (HPLC) was used to separate compounds that are dissolved in solution. HPLC instruments consist of a reservoir of a mobile phase, a pump, an injector, a separation column, and a detector. Compounds are separated by injecting a plug of the sample mixture onto the column. The different components in the mixture pass through the column at different rates due to differences in their partitioning behavior between the mobile liquid phase and the stationary phase. Solvents must be degassed to eliminate formation of bubbles. The pumps provide a steady high pressure with no pulsation, and can be programmed to vary the composition of the solvent during the course of the separation. Typical detectors rely on a change in refractive index, UV-VIS absorption, or fluorescence after excitation with a suitable wavelength.

The time taken for a particular compound to travel through the column to the detector is known as its retention time. This time is measured from the time at which the sample is injected to the point at which the display shows a maximum peak height for that compound.

Samples for HPLC measurement were prepared via centrifuging at 16,000 x g for 2 minutes and following filtration through the sterile polytetrafluoroethylene filter (0.2 µm) to a clean tube. Eventually they were stored at -20°C. For the analysis, 100 µl of sample were mixed with 10 µl of 0.5 M H<sub>2</sub>SO<sub>4</sub> in special HPLC vials. Products were separated in the column with 5 mM H<sub>2</sub>SO<sub>4</sub> as the mobile phase. For measurements the EZChrom Elite Compact Software was used.

## 6.2. Photometric analysis

Fe(II) concentrations can be measured by a photometric assay with the ferrozine reagent that forms a blue complex (Stookey, 1970). Fe(II) in the sample is easily reoxidized by molecular oxygen from the air. This can be avoided if the sample is acidified immediately after withdrawing from the culture flask. At pH values below 3.5 the oxidation of Fe(II) proceeds very slowly (Singer and Stumm, 1970). Unfortunately, the formation of the blue ferrozine complex shows only a linear dependence to Fe(II) concentration for pH values between 4 and 10 (Stookey, 1970). To resolve this problem, 0.1% (w/v) ferrozine reagent (3-(2-pyridyl)-5,6-bis(4-phenylsulfonic acid)-1,2,4-triazine) was combined with 50% (w/v) ammonium acetate to form a strongly alkaline solution which could neutralize the acidified sample. Usually, 180  $\mu$ l ferrozine solution was added to 20  $\mu$ l sample in a microtiter plate and the absorption at 562 nm was measured after 5 min. Dilutions of all samples were made with 1 M HCl. Ammonium iron (II) sulfate solution, dissolved in 1 M HCl was used as a Fe (II) standard.

## 6.3. DNA and RNA concentration

DNA and RNA concentrations were measured using the NANOdrop 2000 Spectrophotometer (Thermo Scientific, Schwerte).

## 6.4. Total organic carbon (TOC) determination

One of the important parameters for assessing the organic load of biomass is the proportion of the total organic carbon (TOC). The TOC value of a sample can be quantified by determining the present total carbon (TC) and total inorganic carbon (TIC) according the formula (1):

(1)

$$TOC = TC - TIC$$

TC of a sample is converted to CO<sub>2</sub> by means of thermal oxidation at 800°C with oxygen and platinum as the catalyst. After that the CO<sub>2</sub> concentration can be measured by using a NDIR-sensor (nondispersive infrared sensor). The TIC of a sample can be measured by the acidified sample with 10% orthophosphoric acid and thereby the TIC is released as CO<sub>2</sub>. Samples were quantified using a multi N/C 2100S and TOC-Gas-Generator TG 600 from Analytik Jena. All samples were prepared with a dilution 1:10 (ddH<sub>2</sub>O), measured in triplicate and calculated automatically.

## 6.5. Coulombic efficiency

One of the criteria for quantifying the performance of a electrochemical setup is the coulombic efficiency (CE). The Coulombic efficiency was calculated as the ratio between moles of electrons detected as current and the total electron moles released via substrate oxidation (Logan, 2008) using the following formula (2):

$$CE = \frac{\text{Coulombs recovered}}{\text{Total coulombs in substrate}} \quad (2)$$

For complex systems, such as biomass we assumed that it is more convenient to use TOC as a measure of substrate concentration. According the fact, that there are 4 electrons per 1 mol of carbon with the molar weight 12 g mol<sup>-1</sup>, the final version of formula becomes (3):

$$C_E = \frac{3 \int I dt}{(F * V_{an} * \Delta TOC)} * 100, \quad (3)$$

where I is the current (A), F represents Faraday's constant (96485 C mol<sup>-1</sup>), and V<sub>an</sub> is the cell internal volume (i.e., the volume of BECs in L). ΔTOC is equal to the difference between TOC<sub>in</sub> and TOC<sub>out</sub> (values in g L<sup>-1</sup>).

## 7. Electrochemical methods

### 7.1. Preparation and operation of BECs

All experiments were carried out in a three electrode system with the anode, cathode and saturated calomel electrode (SCE) as the working electrode, counter electrode and reference electrode, respectively. All measurements were conducted versus normal hydrogen electrode (NHE). In the current study two different types of electrochemical setups were used: two chambered and with one chamber. To study and characterize the model exoelectrogenic community, small two chambered microbioelectrochemical cells were used (Figure 2.8).

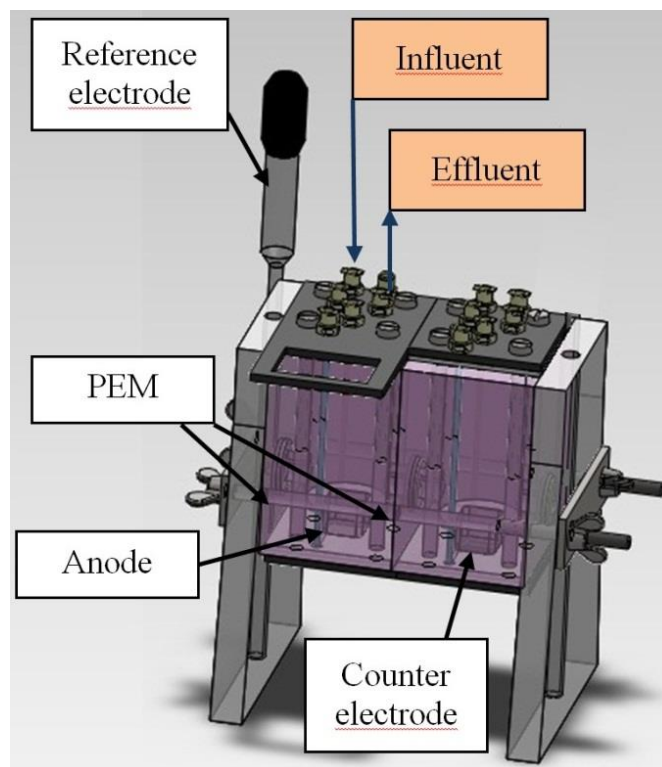


**Figure 2.8.** Two chambered BEC setup (Richter, 2014).

Before every usage, all compartments of the BEC were autoclaved to exclude contamination. The individual chambers of the BEC were separated from each other by a proton exchange membrane Fumapem F-950 (PEM). A SCE was used as the reference electrode. Two 2.25 cm<sup>2</sup> pieces of activated carbon cloth C-Tex 13 were used as anode and cathode, respectively. The titanium electrodes were connected to a potentiostat using croco clamps (Pine Instruments, Grove City, USA). These BEC experiments were carried out at 30°C.

The medium used for these experiments was composed as described above (Table 2.16). For one of the transcriptome analysis experiments, *G. sulfurreducens* was cultured alone. Hence, 5 mM sodium acetate was added to the medium additionally, since this strain cannot grow with propionate and is dependent on a point mutation in the lactate promoter to express the necessary enzymes for lactate consumption. In contrary, acetate is produced from lactate by *S. oneidensis* thereby allowing a constant acetate feed under co-culture conditions. In all experiments the anode chamber contained 22.5 ml of anode medium (Table 2.16), whereas the cathode chamber and the reference electrode compartment contained 25 ml and 5 ml, respectively of cathode medium (Table 2.17). During the whole experiment, the anode chamber was flushed with a gas mixture of 80% N<sub>2</sub>/20% CO<sub>2</sub>, while the cathode chamber was purged with compressed air to provide dissolved oxygen for the reactions.

Prior to all BEC experiments, the cells were washed twice (7,000 g for 5 minutes) in a washing buffer (Table 2.18) and were thereafter resuspended to an OD<sub>655</sub> of 1.0 in the same buffer. Cells density was determined using a spectrophotometer (Thermo Scientific GENESYS 20).

The initial cell density in the BECs was set to an OD<sub>655</sub> of 0.1. The anode chamber was connected to a peristaltic pump and after the first 24 h of the experiment fresh medium was constantly pumped through the system with a flow rate of 0.14 ml/min.

For the experiment with the biomass the second setup only with one chamber was used (Figure 2.9).

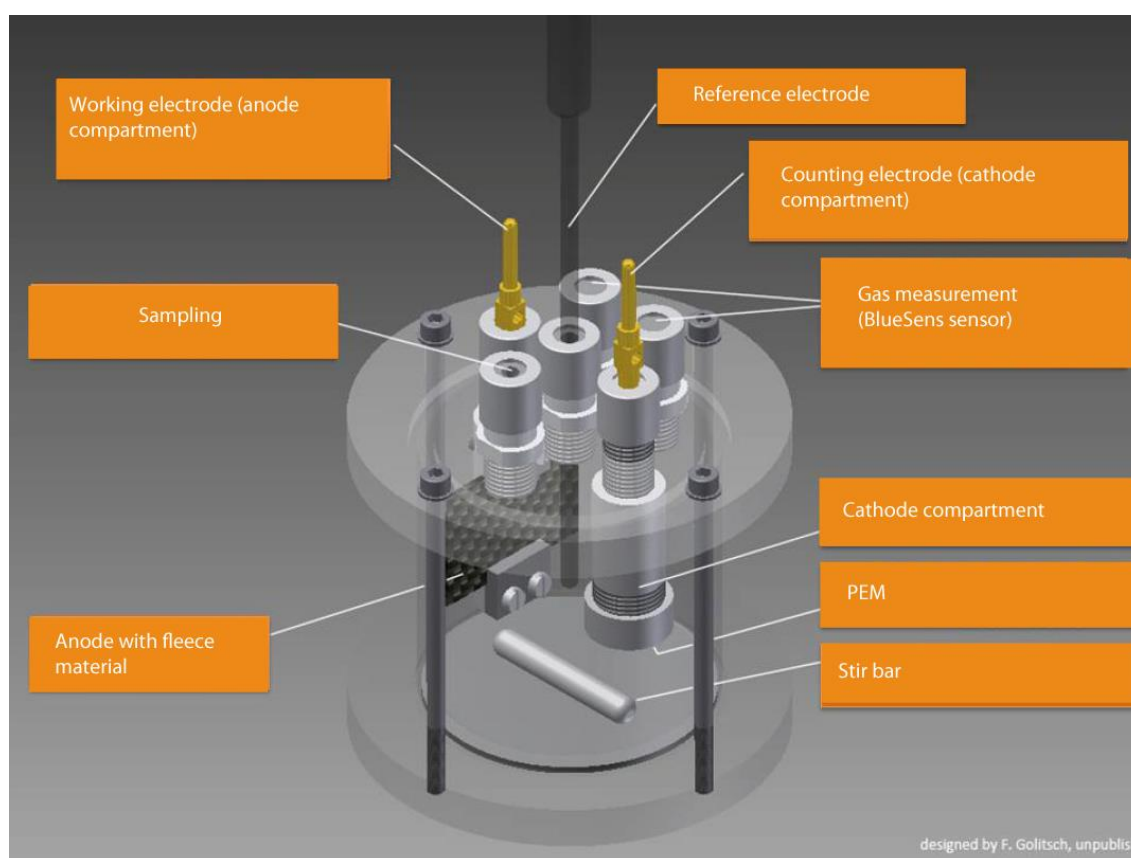


**Figure 2.9.** One chamber BEC setup (Golitsch, unpublished)

The electrochemical setup consisted of anode and cathode compartments that were localized in one glass cylinder (total volume 300 ml). The cathode section was filled with 9 ml of cathode medium (Table 2.17). A Fumapem F-950 membrane was used to separate the cathode compartment from the surrounding inoculum. The electrode in the cathode section was a platinum net connected via a platinum wire (chemPUR, Karlsruhe, Germany). The anode was made from a graphite felt (SGL Group, Carbon Company, Meitingen, Germany) with the size

6,5 x 2,5 cm<sup>2</sup> and a stainless steel needle as an electrode. A saturated calomel electrode (SCE) was placed between the anode and the cathode compartment.

All electrodes were connected to the potentiostat (Pine Instruments, Grove City, USA) via croco-clamps. Current and potential measurements for long-term experiments were collected directly from the potentiostat output every 10 minutes and data was logged with the AfterMath software (Pine Research Instrumentation, Grove City, USA). For current-potential analyses, the BECs were equilibrated in the Open Circuit Potential mode for 2 hours, until the potential stabilized. Cells for these experiments were prepared with the same procedure as described above (one chambered BEC). All experiments were carried out at 35°C in a temperature-controlled incubator.

## 7.2. Electroanalytical methods

To characterize the dynamics of the model biofilm and to investigate its stability under different electrochemical parameters, chronoamperometry mode (CA) and linear sweep voltammetry mode (LSV) were used. To investigate the influence of applied potential on methanogens in the biogas reactor additionally open circuit potential mode (OCP) was conducted.

In LSV experiments the electrode potential is varied at a constant rate throughout the scan and the resulting current is measured. All potentials are specified in relation to the reference electrode. In this study such mode was conducted to determine the minimal potential at which an exoelectrogenic multi-species biofilm or natural exoelectrogenic biofilm is still capable to transfer respiratory electrons to the working electrode. An initial applied potential of 0.04 V was linearly decreased to the value of - 0.26 V with a sweep rate of 0.25  $\mu\text{V s}^{-1}$ . Thereafter, the sweep was repeated in reverse direction until the starting potential of 0.04 V was reached. OCP is the potential in a working electrode comparative to the electrode in reference at which no current can flow in the cell.

## 8. Gas measurement

The exhaust gas analysis was performed using the biogas analyzer Yieldmaster with BCS-CH<sub>4</sub> and BCS-CO<sub>2</sub> gas sensors (BlueSens, Herten, Germany). All data were automatically documented by the software BACVis.

## Results

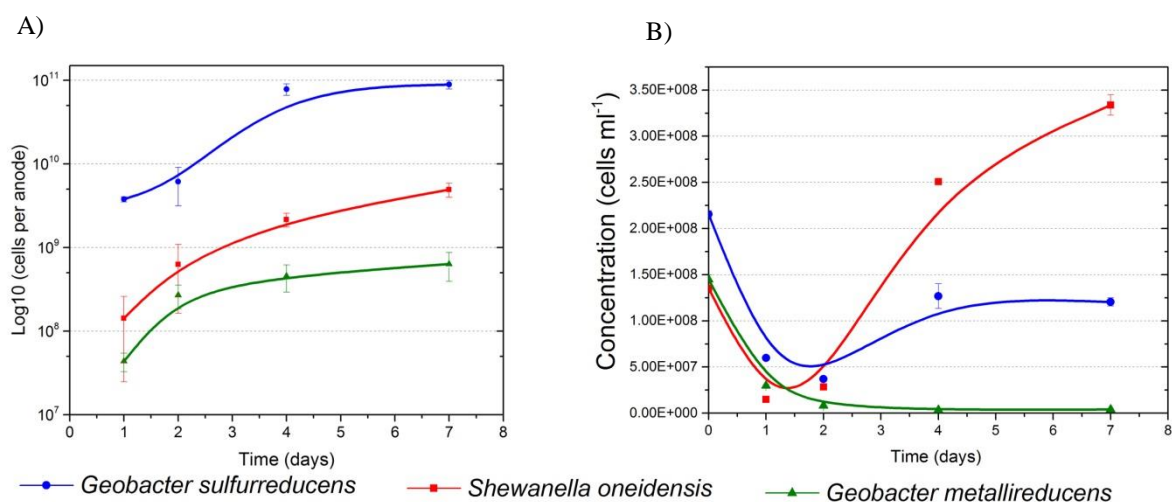
### 1. Model exoelectrogenic biofilm

As part of the current thesis microbe-microbe and microbe-electrode interactions were investigated in the microbial bioelectrochemical cells (BECs). The model biofilm was composed of the well-known and widely spread exoelectrogenic strains: *S. oneidensis* MR-1, *G. sulfurreducens* PCA and *G. metallireducens* GS-15.

#### 1.1 Dynamics of a model multi-species anode biofilm formation

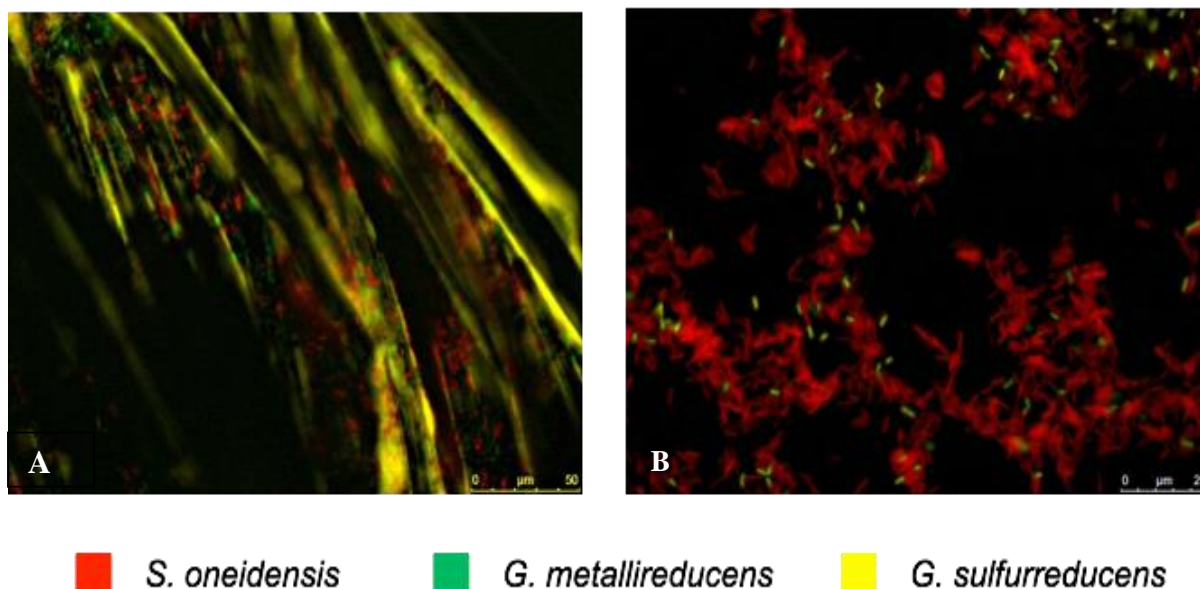
The general goal of the first research part was to analyze the dynamics of community composition as well as of metabolic processes of a controlled microbial community on the anode surface. The three model strains were added to equal OD-values to the BECs, so that the final optical density was 0.1. Of note, the OD values do not correspond to the same cell numbers for the different species, due to the differences in the cell size of these strains. The anode potential was adjusted to 0.04 V. The composition of the anode biofilms as well as the planktonic community were analyzed in triplicate after 1, 2, 4, and 7-days following inoculation using quantitative PCR (qPCR).

Figure 3.1 (A) shows the results of the anode biofilm analysis, where *G. sulfurreducens* clearly dominated the sessile community starting from the first day on and demonstrated the stable presence of around 90% during the whole experimental time. Nevertheless, neither *S. oneidensis* nor *G. metallireducens* were outcompeted from the anode surface during the time course of the experiment, but on the contrary, all strains have been growing actively. The total number of sessile cells at the end of the experiment was  $8.45 \times 10^{10} \pm 2.61 \times 10^9$ . Results from the planktonic phase display a more dynamic development of the community as compared to the anode biofilm, where *S. oneidensis* cells were the major contributor (Figure 3.1 B). The percentage of *S. oneidensis* cells increased within the first 4 days to 67% and as shown on the graph they have grown actively starting from the second day. At the same time *G. metallireducens* cells were almost eliminated from the planktonic phase. The total number of planktonic cells were accounted for  $4.58 \times 10^8 \pm 1.58 \times 10^7$ . Interestingly, planktonic *G. sulfurreducens* cells were observed in the mixed species experiment but not in reactors that were inoculated with *G. sulfurreducens* alone (see section 3.1.4).



**Figure 3.1.** Quantitative growth curve of the model exoelectrogenic biofilm: A) directly on the anode surface and B) in the planktonic phase in a time course of 7 days. The analyses were conducted at different time point following inoculation with an initial inoculum that consisted of equal fractions of the three barcoded strains. Cell numbers were quantified using a qPCR analysis.

FISH experiments corroborated the qPCR-based results (Figure 3.2). The anode biofilm is composed mainly out of *G. sulfurreducens* cells, whereas the planktonic phase consisted almost exclusively of *S. oneidensis* cells. The microscopic pictures also display the different sizes of *Shewanella* compared to *Geobacter* cells that lead to a starting composition of equal OD values but different concentrations of the individual strains.



**Figure 3.2.** Fluorescent *in situ* hybridization (FISH) pictures of the exoelectrogenic community. A) Cells on the anode surface, B) cells in the planktonic phase after 1 week of the experiment. *Geobacter sulfurreducens* was stained in yellow (Cy5), *Geobacter metallireducens* in green (FITC) and *Shewanella oneidensis* in red (Cy3).

After 2-3 days of cultivation the multi-species biofilm generated stable currents that reached values of  $0.62 \pm 0.02 \text{ mA cm}^{-2}$ .

## 1.2. Characterization of the biofilm stability under different electrochemical conditions

In a first part the biofilm community development was investigated under a constant applied potential of 0.04 V. So far independent triplicates have showed a developmental similarity. In a second set of experiments the stability of the previously described multi-species biofilm was investigated under varying electrochemical process parameters. Fifteen BECs were started at the same time under the following applied potentials: 0.44 V, 0.24 V, 0.04 V, -0.06 V and -0.16 V. Interestingly, the produced current values were highly similar during the time course of the experiment if the applied potential was in a range between 0.04 and 0.44 V (Figure 3.3). They were in the range of  $0.5\text{-}0.7 \text{ mA cm}^{-2}$ . Lower currents were observed only if the working electrodes were poised to potentials lower than 0.04 V.

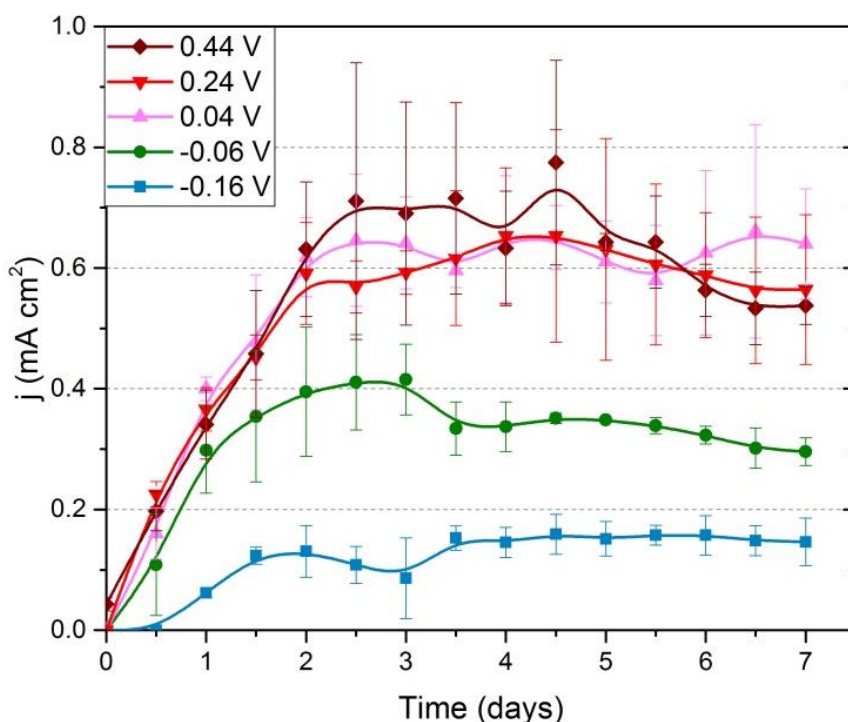


**Figure 3.3.** Stability of the model exoelectrogenic biofilm under different applied potentials. Under positive applied potentials (0.04-0.44 V) current density was roughly identical and was in the range of  $0.5\text{-}0.7 \text{ mA cm}^{-2}$ . While the negative range of applied potentials give us an opportunity to steer the activity of exoelectrogens.

The biofilm community compositions at the end of the experiments were similar under all tested conditions and comparable to the results shown in the previous section (Figure 3.4). At

the end of the 7 days incubation period, *G. sulfurreducens* accounted for  $89 \pm 5\%$  of all organisms on the anode surface. *S. oneidensis* cells were present in quantities between 5 and 12%, while *G. metallireducens* was only detectable in minor quantities.

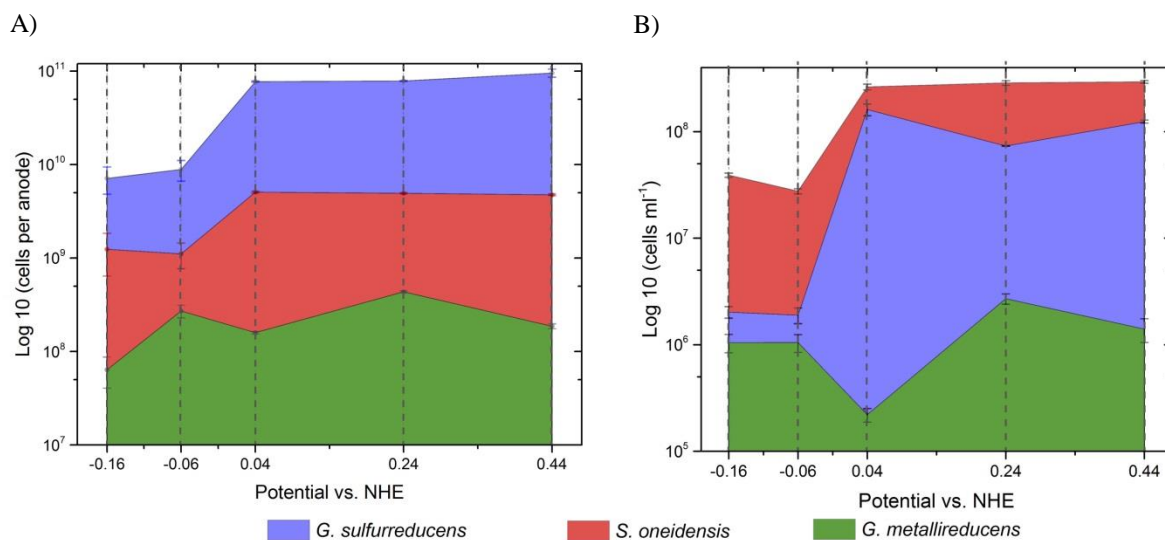


**Figure 3.4.** Quantitative analysis of the cells ratio on the anode surface (A) and in the planktonic phase (B) under different applied potentials. *G. sulfurreducens* clearly dominated in this model exoelectrogenic biofilm. Under applied negative potentials decreased amounts of cells were detected throughout all three strains.

In line with the measured current densities we could see a pronounced drop in cell density if potentials below 0.04 V were applied. Working electrodes poised to a potential of -0.06 V had more than 80% less cells compared to anodes adjusted to a potential of 0.04 V. In comparison, all anodes poised to positive values showed only minor differences in terms of overall cell number. Planktonic cells in the reactors were also quantified. Here, *S. oneidensis* (57 – 73%) and *G. sulfurreducens* (26 – 43%) comprised the majority of organisms (Figure 3.5). While *S. oneidensis* as well as *G. sulfurreducens* responded similarly to the different potentials, such a clear trend for *G. metallireducens* could not be observed.

### 1.3. Steering metabolic activity via working electrode potentials

In the previous experiment it was observed that applied potentials below 0.04 V seem to hamper electron transfer to the anode surface. Nevertheless, so far it was not possible to deduce a potential at which half-maximal rates could be achieved. Therefore, linear sweep voltammetry experiments were conducted to determine the minimal potential at which an exoelectrogenic multi-species biofilm is still capable to transfer respiratory electrons to the

working electrode. An initial applied potential of 0.04 V was linearly decreased to the value of -0.26 V with a sweep rate of  $0.75 \mu\text{V s}^{-1}$ .

Thereafter, the sweep was repeated in reverse direction until the starting potential of 0.04 V was reached. As indicated in Figure 3.5, the cells stopped to produce current if the applied potential was below approximately -0.2 V.

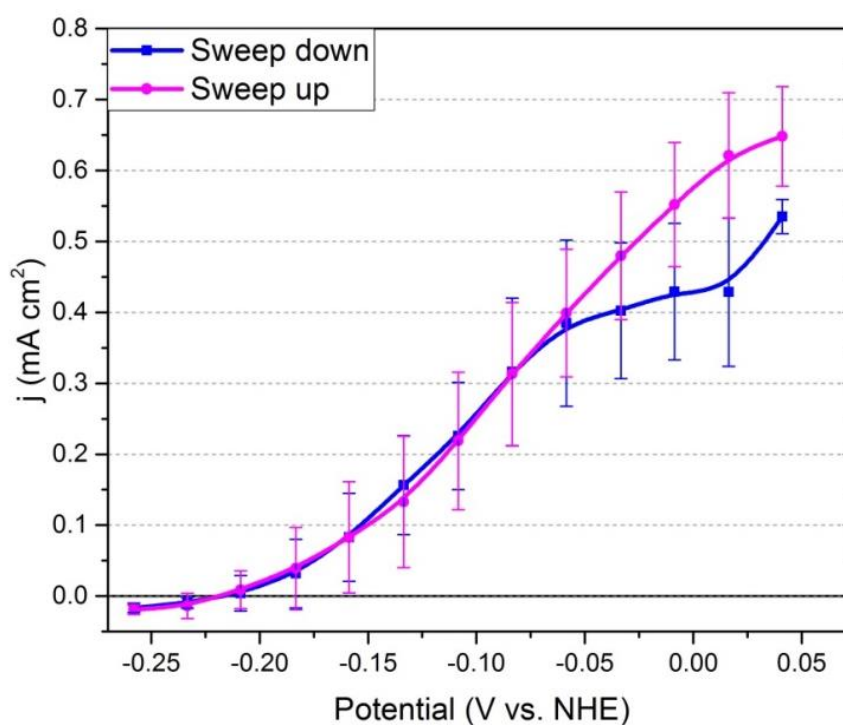


**Figure 3.5.** Stability of the model exoelectrogenic biofilm under linear sweep voltammogram mode, applying negative range of potentials forward and reverse starting from 0.05 V. The limiting potential, where cells stop to produce electrons was detected below approximately -0.2 V. Generally the exoelectrogenic consortium was not affected by applying negative potentials, since a directly following experiment in the other potential direction showed similar results.

Interestingly, the consortium stability does not seem to be highly affected by variations of electron transfer rates since an instantaneously following experiment in the other potential direction showed similar current values. This is surprising since the very low sweep rate results in an overall time course of more than 9 days for the overall sweep from 0.04 V down to 0.26 V and back up to 0.04 V.

#### 1.4. Transcriptome analysis

Transcriptomes and metatranscriptomes were analyzed to reveal metabolic changes of the individual strains as a result of the shift from solitary to multispecies growth on anodes.

Twelve BECs were started. They contained in triplicate either single cultures of *S. oneidensis*, *G. sulfurreducens* and *G. metallireducens* or a mixture of all three strains. The applied working electrode potential was in all cases 0.04 V. The experiment was conducted over a time course of seven days. The medium contained lactate and propionate as carbon and electron sources. Acetate was additionally added only in the experiments which were conducted with *G. sulfurreducens* alone. As was shown previously by Summers (2010) wild type of *G. sulfurreducens* can grow on lactate, but with a very low growth rate, that could be accelerated only by a spontaneous point mutation. Under co-culture conditions acetate will be produced by *S. oneidensis* as an end-product of lactate oxidation.

During solitary growth all strains produced less current compared to co-culture conditions (about 0.6 mA cm<sup>-2</sup>). The highest current production in solitary growth was recorded for *G. sulfurreducens* (in average 0.47 mA cm<sup>-2</sup>). Whereas *S. oneidensis* produced around 0.13 mA cm<sup>-2</sup> and *G. metallireducens* roughly 0.06 mA cm<sup>-2</sup>.

This study focuses on the central metabolic changes that are results of co-cultivation. A comparison of the transcriptomes from solitary and co-culture growth revealed that 1124 of the 3,430 protein-coding genes of *G. sulfurreducens* showed log<sub>2</sub>fold changes higher than +/- 1 with corresponding padJ values below 0.05. Of the total 4,214 genes of *S. oneidensis*, 677 followed the above-described characteristics, while in *G. metallireducens* only 23 genes could be detected as differentially expressed (Supplementary table). The reason for this rather low amount of detectable candidate genes might be due to a reduced experimental sensitivity caused by the limited growth of the *G. metallireducens* cells compared to the other two strains and its subsequently reduced representation in the mixed species transcriptomic data.

#### **1.4.1. Transcriptome profiling of *G. sulfurreducens* gene expression**

As mentioned above, there is a multitude of differentially expressed genes in *G. sulfurreducens* cells grown in the absence or presence of *S. oneidensis* and *G. metallireducens*. Generally, it seems as if the central metabolism of *G. sulfurreducens* is generally upregulated under co-culture conditions (Figure 3.6). For example, transcripts for the genes, that are associated with an acetate uptake, *aplBC* (2- and 4.8-fold, respectively) and gene for succinyl:acetate coenzyme A (CoA)-transferase *ato-1* (2.4-fold), that activate acetate for oxidation and gluconeogenesis, were upregulated in co-culture growth conditions. TCA cycle gene transcripts were also in higher abundance during co-culture growth, including transcripts for citrate synthase *gltA* (2-fold) that is required for entry of acetyl-CoA into the

TCA cycle. Moreover, two genes of gluconeogenesis were discovered to be upregulated under co-culture conditions (*eno*: 2.4-fold upregulated; *pgk*: 2.5-fold upregulated).

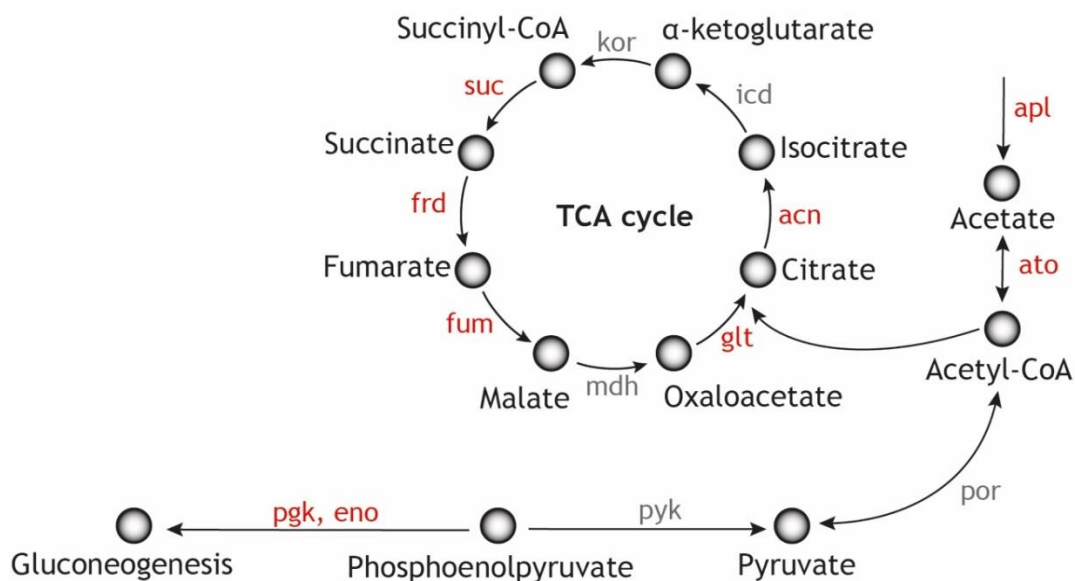


**Figure 3.6.** Central metabolism in *G. sulfurreducens*. Genes that are upregulated under co-culture conditions are highlighted in red.

The NADH dehydrogenase Nuo, which encodes the large-membrane-associated NADH dehydrogenase that transfers reducing equivalents generated in the TCA cycle to the menaquinone pool, was also upregulated during co-culture growth conditions (average upregulation of *nuo* genes: 2.65 fold).

When *G. sulfurreducens* cells oxidize acetate, they are absolutely dependent upon electron transfer to a terminal electron acceptor for energy generation. Outer membrane cytochromes in *Geobacter spp.* have been shown to have a critical role in extracellular electron transfer to minerals as well as other external electron acceptors such as the anode of a microbial fuel cell (Qian *et al.*, 2011). Transcriptome analysis has revealed a number of cytochrome genes that show induced expression, including *omcB* and *omcE*. Specifically, both cytochromes were shown to be essential for the electron transfer to the cell surface of *G. sulfurreducens* (Nevin *et al.*, 2009; Leang *et al.*, 2003). The periplasmic triheme cytochrome PpcA is one of the most abundant cytochromes in *G. sulfurreducens*. PpcA is localized in the periplasm and evidence was provided that it is involved in the transport of respiratory electrons from the cytoplasmic to the outer membrane (Lloyd *et al.*, 2003). Transcript abundance for *ppcA* (10.6-fold) and its homolog *ppcD* (7.5-fold) was upregulated in co-culture growth. In agreement with the upregulation of cytochromes is the increased transcription of pili genes, including *pilA*, which is required for high density current production (Reguera *et al.*, 2006).

The expression patterns for nitrogen fixation in *G. sulfurreducens* were presented by *nif*, *gnf* and *gln* clusters. Of note, genes necessary for nitrogen fixation show a strong decrease in transcription as a result of co-cultivation (*nif* > 19.6-fold downregulated; *gnf* > 3.8-fold downregulated; *gln* > 6.8-fold downregulated). One of the four hydrogenases in *G. sulfurreducens*, encoded by the *hyb*-genes, could yield insights into physiological function. The protein functions as a respiratory-uptake hydrogenase. Hence a high abundance of *hyb* encoding genes in the experiment with co-culture conditions (>9-fold upregulated) suggests that *G. sulfurreducens* cells also have used hydrogen as an electron donor. It is of interest to note that *cydA* and *cydB* showed a downregulation of (6.1- and 5.4-fold, respectively) as a result of co-cultivation. The encoded cytochrome bd-ubiquinol oxidase was discussed as a mechanism to cope with oxidative stress (Giuffre *et al.*, 2014).

#### 1.4.2. Transcriptome profiling of *G. metallireducens* gene expression

*G. metallireducens* showed an interesting adaptation during the growth with *G. sulfurreducens* and *S. oneidensis* which is an upregulation of the *prp*-operon (in average of 2.9-fold) (Figure 3.8). The *prp*-genes encode the necessary proteins for propionate oxidation (Aklujkar *et al.*, 2009). *G. metallireducens* can grow with acetate and propionate. Among this multi-species biofilm only *G. metallireducens* has an ability to utilize propionate as an electron donor (Lovley D. *et al.*, 1993).

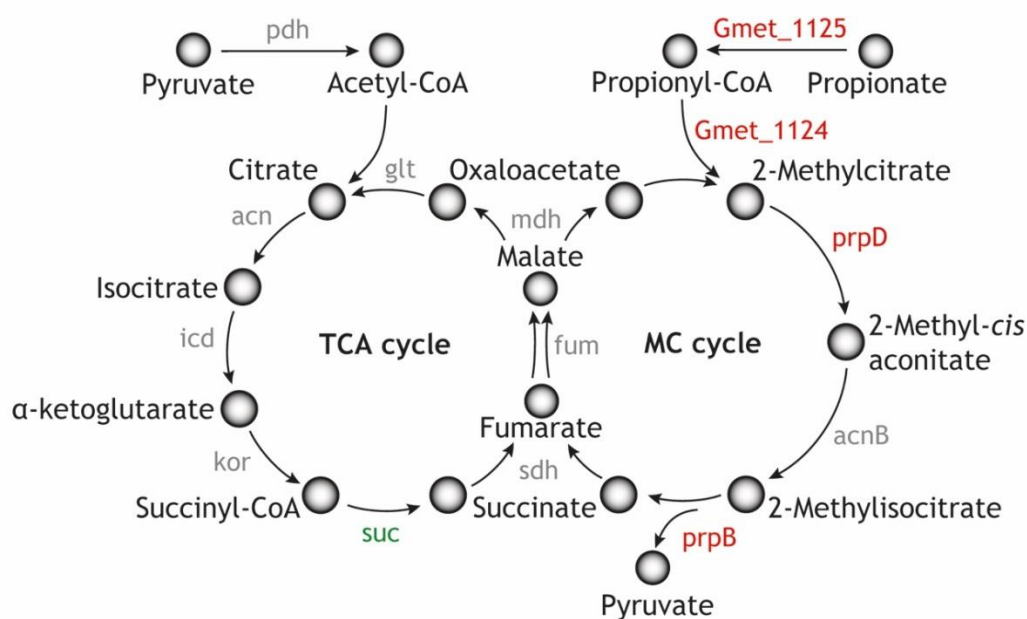


**Figure 3.8.** Central metabolism in *G. metallireducens*. Genes that are upregulated under mixed-culture conditions are highlighted in red, genes that are downregulated in green.

Gene expression of *cydA* and *cydB*, that are responsible for the oxidative stress, were also highly downregulated under co-culturing (4.6- and 3.4-fold, respectively).

### 1.4.3. Transcriptome profiling of *S. oneidensis* gene expression

In this study, mRNA expression patterns of *S. oneidensis* in batch cultures from the anode surface and planktonic phase were compared versus a mixed culture in model multi-species biofilm respectively. Such comparison revealed no significant difference in cells growing on the anode surface in comparison to cells growing in the planktonic phase, but there were some interesting points in comparison of solitary sessile growth cells versus the growth under co-culture conditions.

Protein-coding genes involved in lactate transport and oxidation were upregulated (SO\_1518 – 1522 > 3-fold) during the co-culture (Figure 3.7).

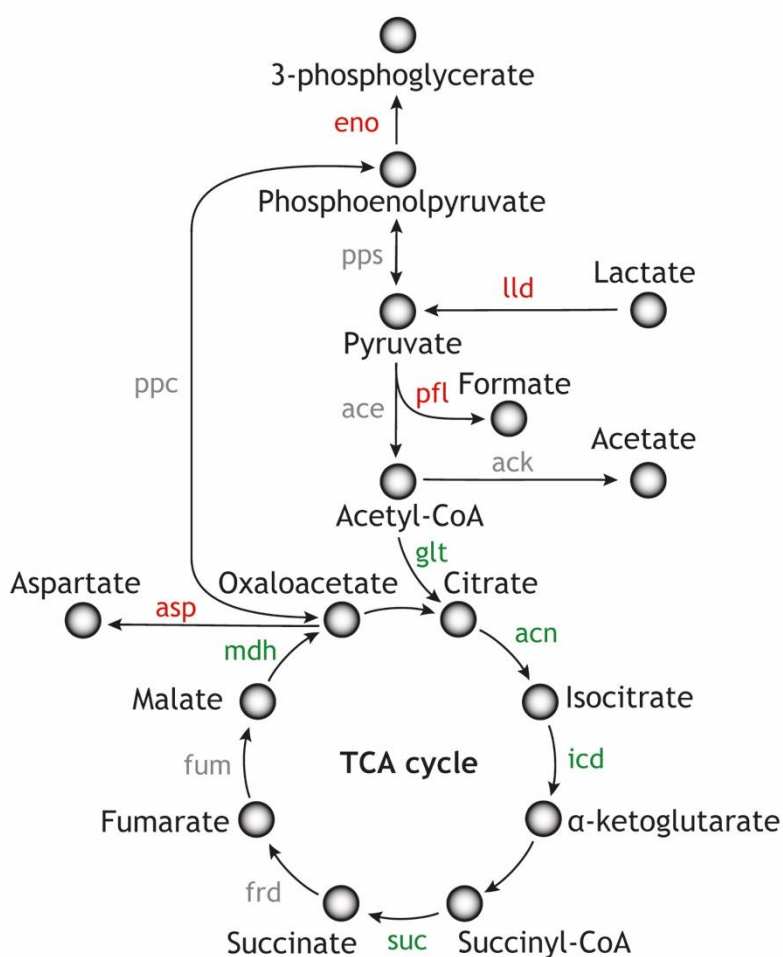


**Figure 3.7.** Central metabolism in *S. oneidensis*. Genes that are upregulated under mixed-culture conditions are highlighted in red, genes that are downregulated in green.

In contrary, TCA cycle genes expression was downregulated under co-culture conditions. The Mtr pathway, which is necessary for electron transport through the outer membrane and to an extracellular electron acceptor (*mtrABC* and *omcA* showed a 2.3-fold average upregulation), was upregulated during the growth in co-culture.

*S. oneidensis* also responded to co-cultivation with the upregulation of a hydrogenase (*hypBEF* > 2.5-fold, *hyaABCD* > 4.5-fold). Hydrogenases catalyze the reversible reduction of protons into molecular hydrogen and have a central role in the energy metabolism. Moreover genome analysis shows the presence of some genes involved in pyruvate metabolism with upregulation during the co-culturing: pyruvate-formate lyase *pflB* (2.8-fold) and its activating enzyme *pflA* (3-fold), the transcriptional repressor of pyruvate metabolism *pdhR* (3.1-fold). Also interesting to mention is a corresponding upregulation of the formate dehydrogenase *fdh* (4-fold up).

There are also a number of gene clusters that are upregulated in cells grown in the absence of *G. sulfurreducens* and *G. metallireducens*. For example, regulator *tyrR*, which supposed to be a master regulator of the degradation pathways for various amino acids, including phenylalanine *phhAB* (5.4- and 6.1-fold), tyrosine *fahA* (4.7-fold), branched chain amino acids *ldn* (4.2-fold), *liu* cluster (> 8.6-fold), *ivd* cluster (> 3.8-fold), as well as the glyoxylate shunt *aceAB* (7.8- and 8.4-fold) were downregulated during the co-cultivation.

## 2. Natural exoelectrogenic community

The general aim of the second research part was to analyze electrochemical performance and stability of natural exoelectrogenic community occurring in a biogas reactor and to investigate whether the electrodes, installed into the reactor and were poised to certain potentials, can influence methane production. Additionally, the microbial community was characterized through RFLP analysis. All experiments were made in triplicate. BECs were operated over a period of 35 days and have shown high reproducibility in methane and current production as well as a potential stability. The pH value was measured every day during the whole experiment. In all BECs these values were largely stable and varied in the range of  $\text{pH } 7.45 \pm 0.35$ .

### 2.1. Electrochemical performance and stability

In a first part of the current study the model biofilm community development was investigated under different applied potentials. It was detected, that the exoelectrogenic activity of the model organisms could be steered via a negative range of anode potentials. Thus in a second part of the experiments it was the goal to observe whether the natural exoelectrogenic community could perform the same stability and dependence on negative potentials. In parallel with the BECs under linear sweep voltammetry (LSV) mode another three BECs under open circuit potentials (OCP) were started. It was our hypothesis that a suitable applied potential should select for a natural environmental community of exoelectrogenic microorganisms on the electrode surface. Contrary, various fermentative bacteria from the biomass, instead of exoelectrogens, should be presented in abundance under open circuit mode condition (when no electrons can flow over the potentiostat to the cathode). Such microbial community differences should go along with diverse metabolites as a result of biomass degradation. This should be detectable for instance via variations in methane production (see section 3.2.2).

Figure 3.10 (A) shows the current generation under sweep potentials within a negative range. An initial applied potential of 0.04 V was linearly decreased to the value of - 0.26 V with a sweep rate of  $0.25 \mu\text{V s}^{-1}$ . As indicated in Figure 3.10 (B), under open circuit mode the microbial community established a quite stable potential in the range of -0.20 – -0.26 V within 2 days, which is near in the oxidation-reduction potential reported for other methanogenic reactors (Sasaki *et al.*, 2010). The results from the linear sweep experiment corroborated the results with the model community but on a different level. The limiting

potential was detected at the same values (below approximately -0.2 V), as for the model exoelectrogenic biofilm. The natural exoelectrogenic community generated currents densities of about  $0.91 \pm 0.16 \mu\text{A cm}^{-2}$  which is more than 600-fold lower in comparison to the value of current produced by the model exoelectrogenic biofilm. As was expected according to the data from the previous section (3.1.3), the natural exoelectrogenic community created a stable biofilm that was not influenced by constant change of the applied potential (Fig. 3.10 A).

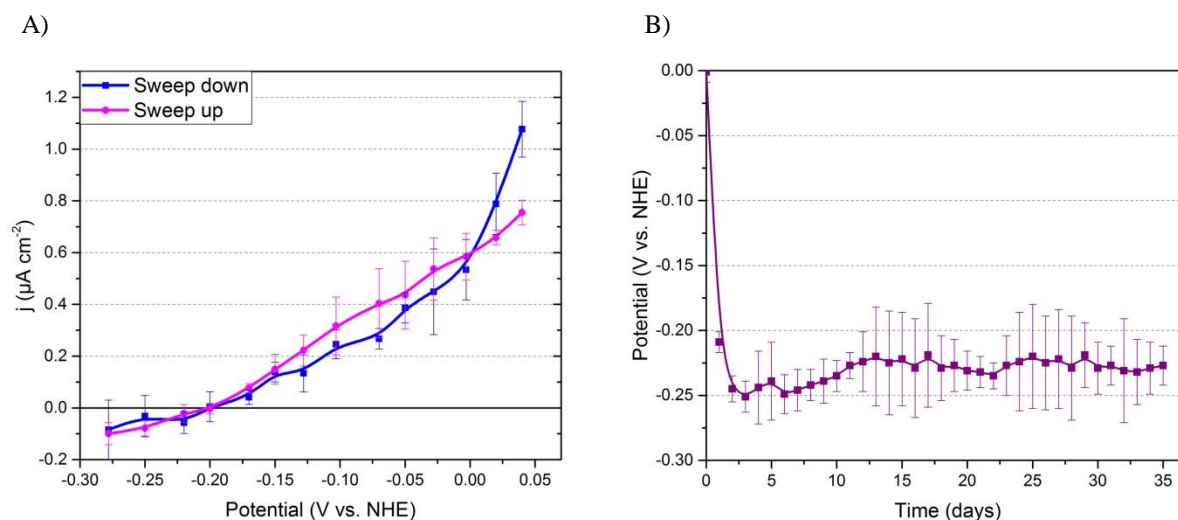


**Figure 3.10.** Electrochemical performance of the natural exoelectrogenic community under A) linear sweep voltammogram mode, applying negative range of potentials forward and reverse starting from 0.05 V, and under B) open circuit potential mode. In both cases the limiting potential, where cells stop to produce electrons was detected below approximately -0.2 V. Natural exoelectrogenic consortium in the same way as a model biofilm was not affected by applying negative potentials.

## 2.2. Metabolite comparison between closed and open circuit in BECs

Diverse metabolites were observed during the biomass degradation within both systems. Among the metabolites, acetate, propionate, succinate, lactate and formate were detected within the initial stages of the experiment, whereas only acetate and propionate persisted as dominant byproducts (Figure 3.11 A). Acetate was the most abundant VFA in all BECs with a primary concentration of  $30 \pm 4 \text{ mM}$ . After 1 day of the experimental time course, the acetate concentration increased in both systems. Starting from day 2 to day 8 in all BECs acetate was consumed gradually under identical electrochemical conditions and the concentrations reached values of  $28.8 \pm 5.2 \text{ mM}$ . Within this time frame, the propionate concentration increased in all reactors slightly from  $9.8 \pm 2.5 \text{ mM}$  to  $11.9 \pm 0.8 \text{ mM}$ . After day 8, when LSV mode was activated, acetate was degraded within 4 days in the closed system and the degradation trend of acetate corresponded to the methane production trend (Figure 3.12), that

supports the fact that acetate was successfully utilized for both processes, current and methane generation. Conversely, propionate was not degraded or consumed by exoelectrogenes under LSV mode after formation. In both systems, open and closed, propionate was presented with the same concentration and had an identical degradation rate.

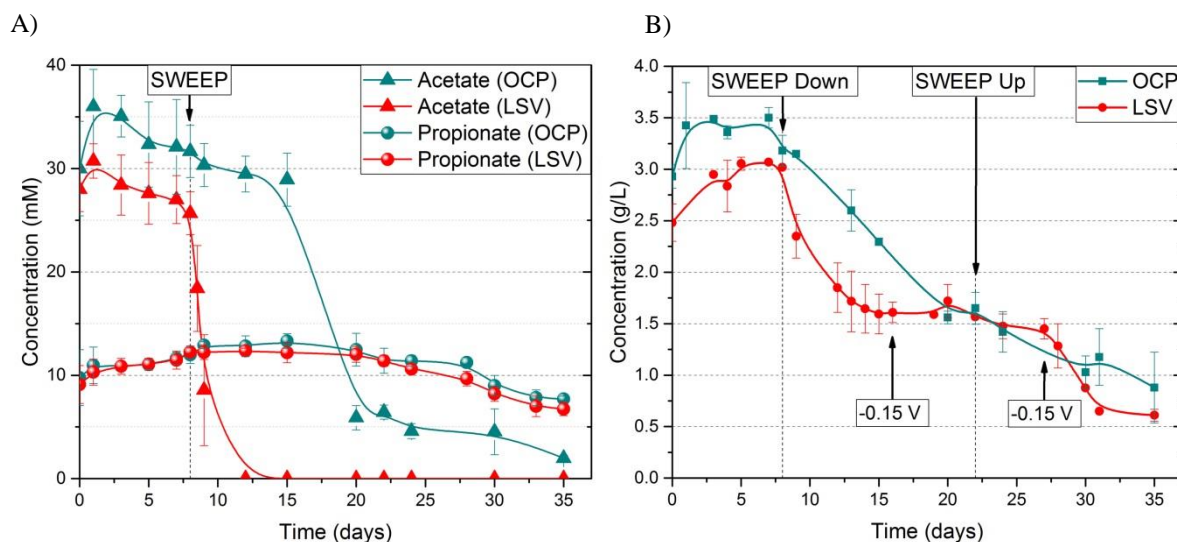


**Figure 3.11.** A) Analysis of metabolites during the LSV and OCP mode. B) TOC analysis during the LSV and OCP mode.

To investigate the ability of the biofilms to adapt to biomass as a carbon source, the amount of TOC removal was analyzed. At the end of the experiment  $75 \pm 2\%$  TOC removal was obtained in the closed systems, which was comparable with TOC removal in open system ( $70 \pm 10\%$ ). When LSV mode was applied, TOC concentration decreased sharply from 3.0 g/L to 1.6 g/L and then remained stable at these values for more than 10 days. Interestingly, this stability was observed at the time point, when applied potentials were below -0.15 V. When the sweep lead back to higher anode potentials, the TOC removal rates increased again. In BECs with open circuit, the TOC concentration was degraded gradually over the time.

### 2.3. Influence of applied potentials on methane yield

In order to investigate an effect of a poised electrode on methanogenesis, six BECs were started simultaneously. To achieve reproducible and reliable data, all BECs were started in OCP mode. At the time point, when the methane production was stable and reached values above 60%, LSV mode was applied to three of the 6 bioelectrochemical cells. Figure 3.12 shows the comparison of methane production between closed- and open- circuit in the BECs. The biogas production in both experimental setups increased steadily over time starting from the first day on, but there an obvious difference was observed after the LSV mode was

activated. After 2 days under applied potential conditions, methane production started to decrease significantly, while a substantial amount of methane was still constantly observed within the open circuit system. That clearly suggests that the oxidation of biomass via an electrode negatively affected methanogenesis most probably because of a substrate competition which is in favor to anode assisted oxidation because of higher Gibbs free energy values.

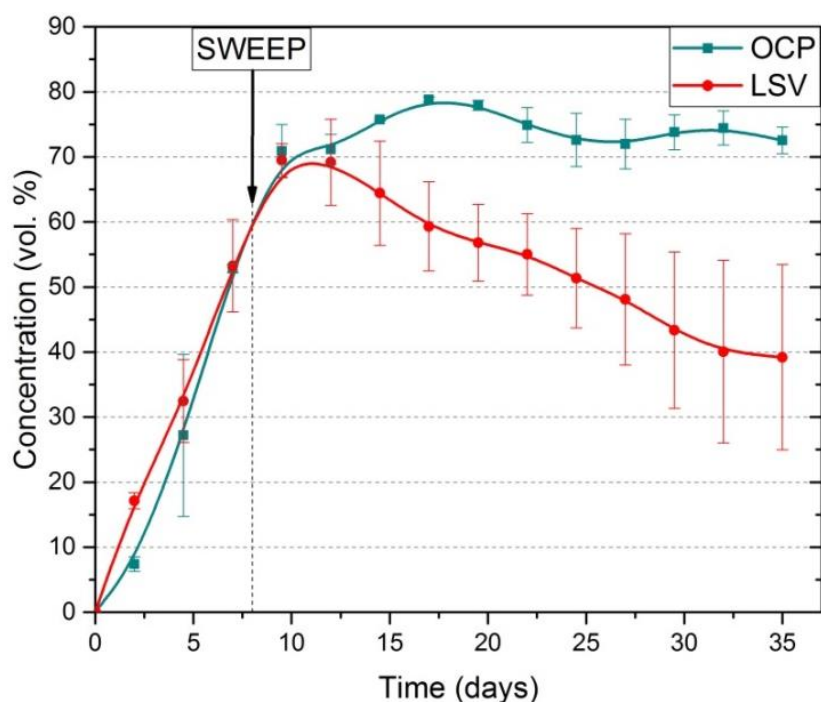


**Figure 3.12.** Comparison of methane production under LSV vs. OCP modes. Arrow indicates the time point, when LSV mode was applied (methane production has reached value of 60%).

Data obtained from metering the gas production capacity of the anaerobic processes in open systems were as follows: the overall volume reached a value of  $693 \pm 39$  ml, whereas under closed circuit conditions the total gas volume was only  $595 \pm 70$  ml.

#### 2.4. Microbial diversity in the BECs with biomass

Microbial diversity and function were analyzed using the RFLP technique. Every week DNA was isolated from samples of the BECs and further purified in order to amplify it using PCR primers targeting the 16S rDNAs. The PCR products were ligated into a TOPO-vector that was subsequently transformed. For the clone library, 48 clones were randomly picked from each sample and analyzed by colony-PCR to distinguish strains by RFLP using the pattern of the DNA sequence. An example of such a gel is shown in Figure 3.13:

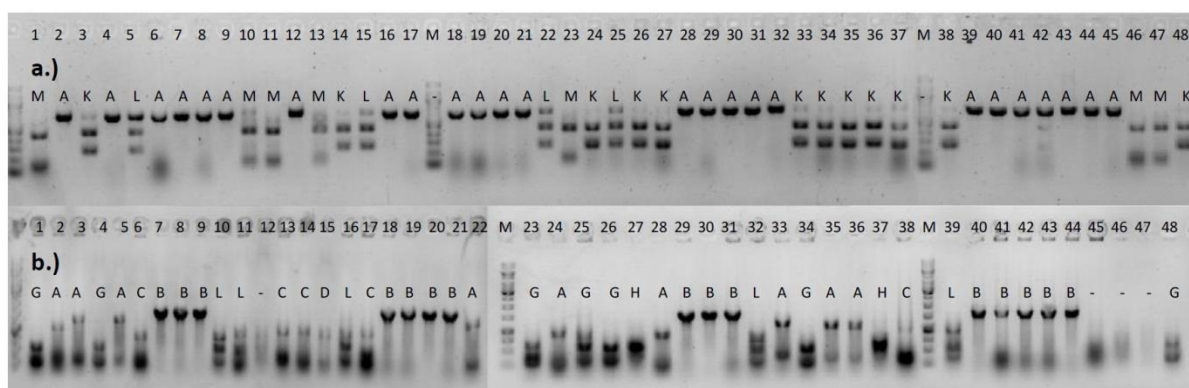


**Figure 3.13.** Example of a gel after RFLP. A) Archaea cluster and B) Bacteria cluster on the anode. For the archaea a 2% agarose gel and 100 bp marker were used, while for bacteria a 1% agarose gel and 100 bp marker were used.

Based on this pattern, each distinguishable sequence was named differently with letters. One representative clone was selected and sent for sequencing to Eurofins Genomics (Ebersberg) to reveal the corresponding organism. Moreover, at the end of the experiment electrode biofilms were analyzed in terms of presence of exoelectrogens on the surface.

#### 2.4.1. Archaeal community

Examination of the methanogenic populations revealed similar composition in all BECs that were dominated by microorganisms most similar to *Methanoculleus bourgensis*, *Methanosarcina barkeri* and *Methanobrevibacter acididurans* (Figure 3.14). The clones belonging to “A” were related with a 96-100% sequence similarity to the most predominant methanogens in both systems – the hydrogenotrophic *Methanoculleus bourgensis* (61% in the OCP and 71% in the LSV). Similar organisms have been previously identified in biogas processes (Hori *et al.*, 2006; Klocke *et al.*, 2008) and have been shown to be dominant in a biogas reactor that contained high levels of ammonium and VFA (Schnürer *et al.*, 1999). According to the fact, that the biogas reactor (to which sludge from this study belongs to) was initially pre-inoculated with *Methanosarcina barkeri* (“L” and “K” with a 99-100% sequence similarity), it was expected to find these archaea in the microbial community. In the current study they were presented with an abundance of 26% and 35% for OCP and LSV, respectively. This amount is much higher in comparison to Klocke *et al.* (2008), where the whole order was presented only with 18% and the genus only with 7%. The clones represented by “M” were affiliated with *Methanobrevibacter acididurans*, with a 99% sequence similarity.

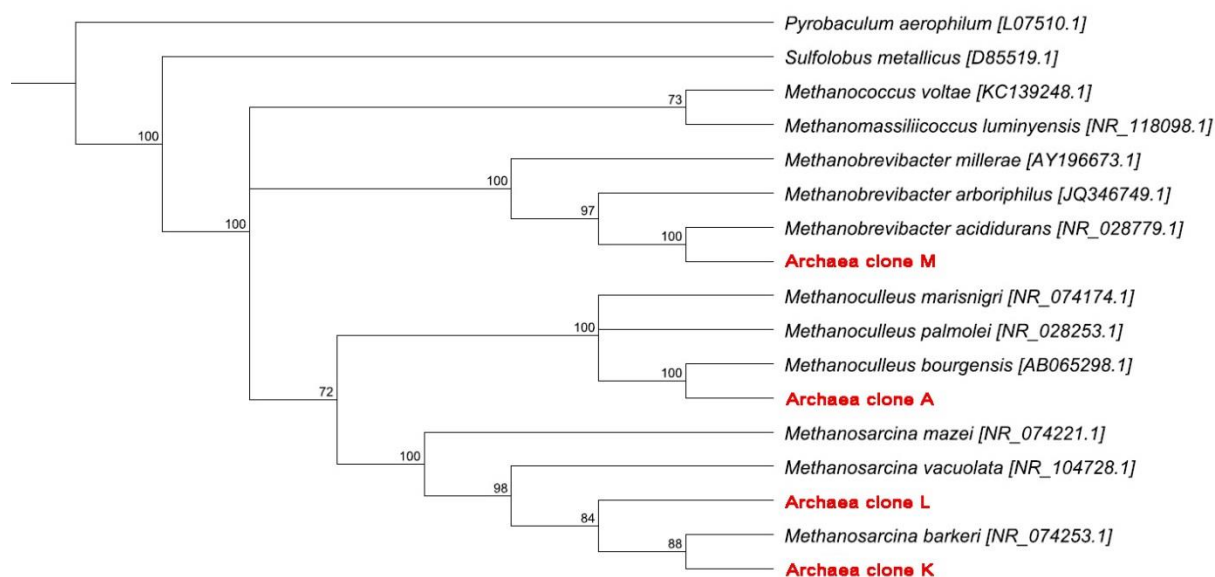


**Figure 3.14.** Phylogenetic tree (neighbour-joining) based on 16S rDNA sequences from the biomass samples from BECs for archaea clones. All bootstrap values that > 50% are shown as a percentage of 1000 repetitions. The branch length is proportional to the number of base substitutions.

These are hydrogenotrophic microorganisms, which according to Savant *et al.* (2002) metabolized neither formate nor acetate. In this study they were presented only by 3% and 4% (LSV and OCP, respectively), that was very similar to values revealed by Klocke *et al.* (2008). Such a low amount of these organisms could be due to the fact that the optimum pH value for growth is 6, whereas in our study the pH was much higher (in the range of 7.1-7.8).

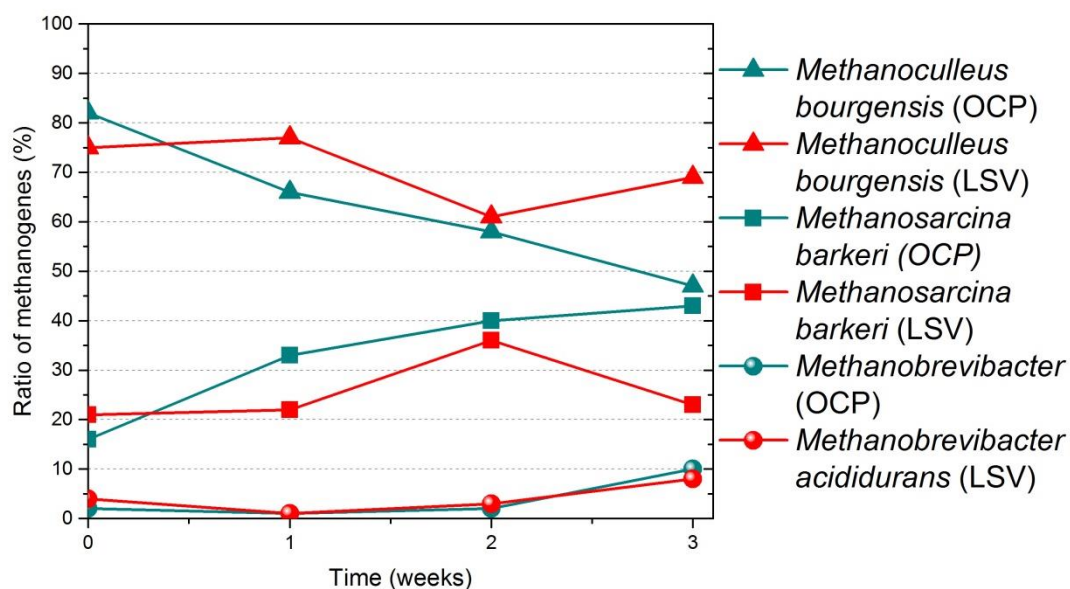


**Figure 3.15.** Proportion of methanogenic microorganisms in the BECs under open and closed systems over time.

Interestingly, the abundance of *Methanosarcina* increased by 6-10% during the first 2 weeks of the experiment in both electrochemical systems, meanwhile the abundance of *Methanoculleus* decreased by the same percentage (Figure 3.15). But at the end of the experiment *Methanosarcina* dominated the archaeal community under open circuit conditions (on 13% more, than under LSV). Meanwhile *Methanoculleus* was a major contributor under closed systems (on 28% more, than under OCP). The level of *Methanobrevibacter* was mostly stable, but a small increase (5-7%) was observed at the last week of the experiment.

Figure 3.16 shows relative proportion of the methanogens based on qPCR values, targeted on archaeal primers, and on relative quantification normalized against unit mass. Initial cell number was quantified accurately and used as unit mass. Afterwards  $C_T$  values for the initial cell number and the samples after a certain time point were then used to calculate the ratio between the two by the following equation:

$$\text{Ratio}_{(\text{sample/to})} = 2^{C_T(\text{to}) - C_T(\text{sample})}$$

Under the OCP mode amount of methanogens increased steadily over time within first 2 weeks, while developmental growth of methanogens under LSV mode was suppressed in bioelectrochemical cells. On the anode surface the amount of methanogens in both systems were detected only in minor quantities.

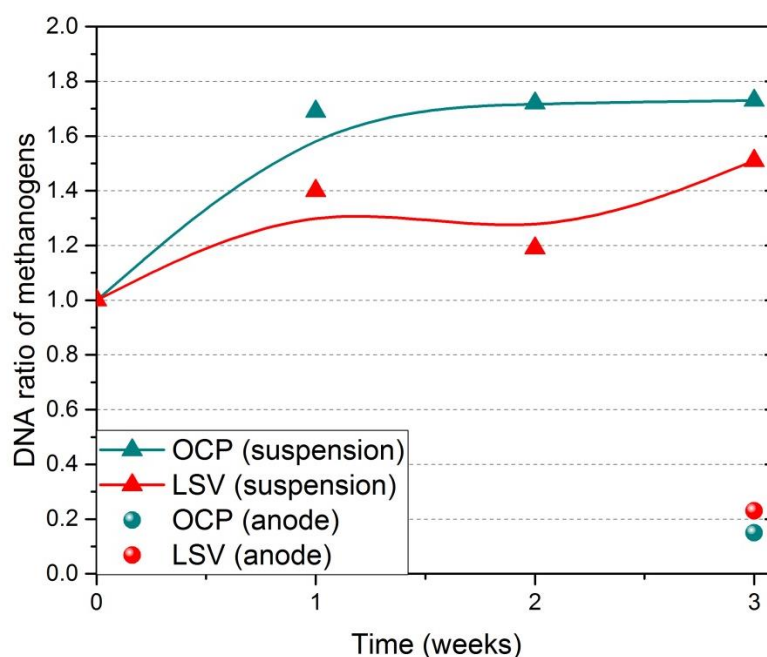


**Figure 3.16.** Proportion of methanogens based on qPCR values in planktonic phase over time and on the anode surface at the end of the experiment.

### 2.4.2. Bacterial community

The bacterial representatives of both electrochemical systems were highly diverse with a typical anaerobic digestion community with *Firmicutes* contributing as the major bacterial phylum accompanied by *Bacteroidetes* and *Spirochaetes*. They all belong to the fermentative acidogenic bacteria group. The phylogenetic tree inferred from the neighbor-joining method is shown in Figure 3.17. In the phylum *Firmicutes* (67-69% for both electrochemical systems) two different organisms were discovered: *Sedimentibacter spp.* (dominated bacteria) and *Gracilibacter spp.*.

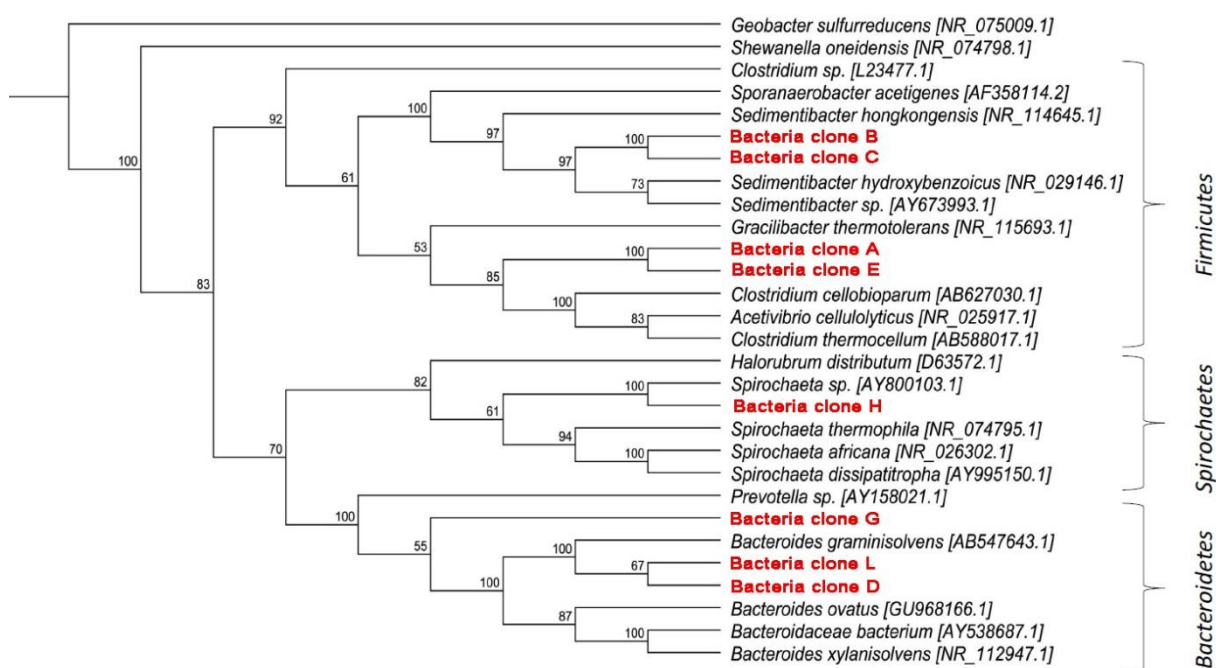


**Figure 3.17.** Phylogenetic tree (neighbour-joining) based on 16S rDNA sequences from the biomass samples from BECs for bacteria clones. All bootstrap values that > 50% are shown as a percentage of 1000 repetitions. The branch length is proportional to the number of base substitutions.

These bacteria were the second most common group that was detected also in Liu *et al.* (2009) with an abundance of 35.4%. The genus *Spirochaeta* was presented with an abundance of 11-13% that is similar to 13.2% in Liu *et al.* (2009). Figure 3.17 shows the proportion of the bacterial diversity in BECs under open and closed systems. Major differences in the growth of fermentative bacteria were not detectable in both electrochemical systems.

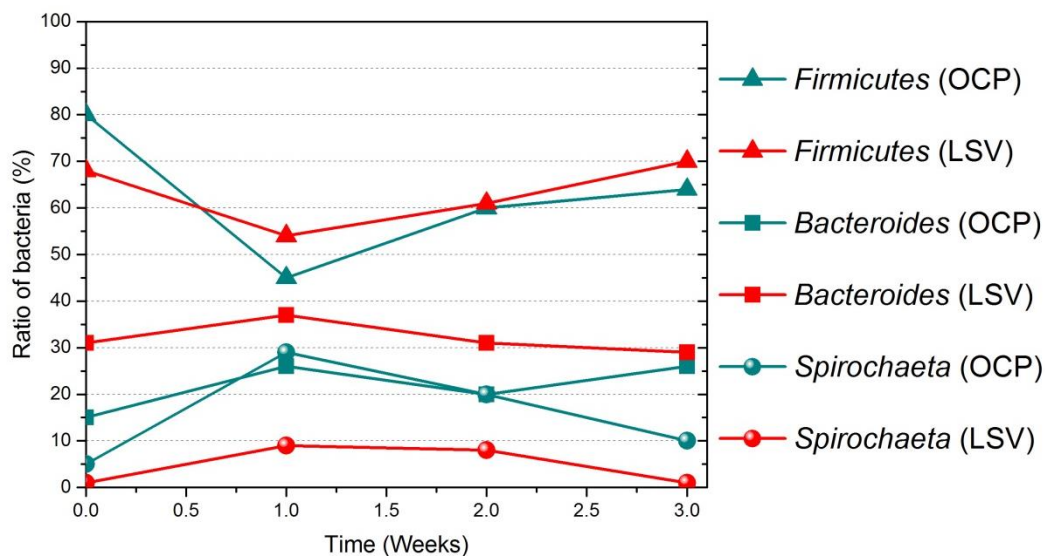


**Figure 3.18.** Proportion of bacterial microorganisms in the BECs under open and closed systems over time.

Interestingly, no potential exoelectrogenic bacteria were determined in the planktonic phase of the BECs using the RFLP technique. To isolate potential exoelectrogenic microorganisms that were presented on the anode surface, enrichments were conducted using a specific medium.

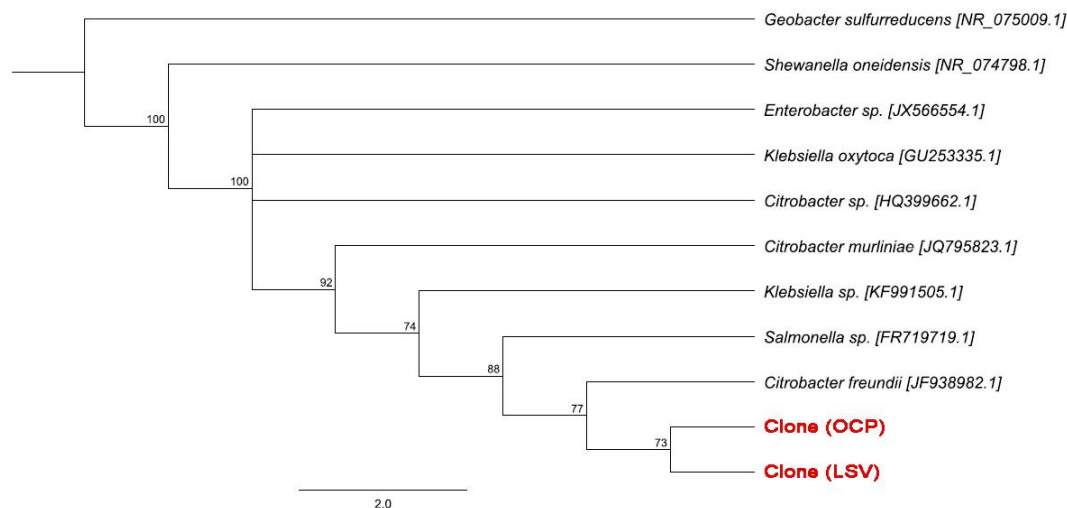


**Figure 3.17.** Phylogenetic tree (neighbour-joining) based on 16S rDNA sequences from the biomass samples from BECs for bacteria clones. All bootstrap values that > 50% are shown as a percentage of 1000 repetitions. The branch length is proportional to the number of base substitutions

Through sequencing of the isolated microorganisms *Citrobacter freundii* was identified (Figure 3.17). This organism was also found by Xu and Lui (2011) in a BEC on the anode surface.

Fluorescence *in situ* hybridization (FISH) was used to further demonstrate identification and localization of each strain in the community. Samples were taken from the planktonic phase of the BECs every week. Bacterial cells were stained in red (Cy3), archaeal cells in green (FITC). Figure 3.19 shows the development of the bacterial and archaeal community during the experimental time course in the LSV system, while figure 3.20 shows allocation of microorganisms within the community in OCP mode. Results confirmed the qPCR data that slightly more archaeal cells are present in the planktonic phase of the BECs that were run in OCP mode.

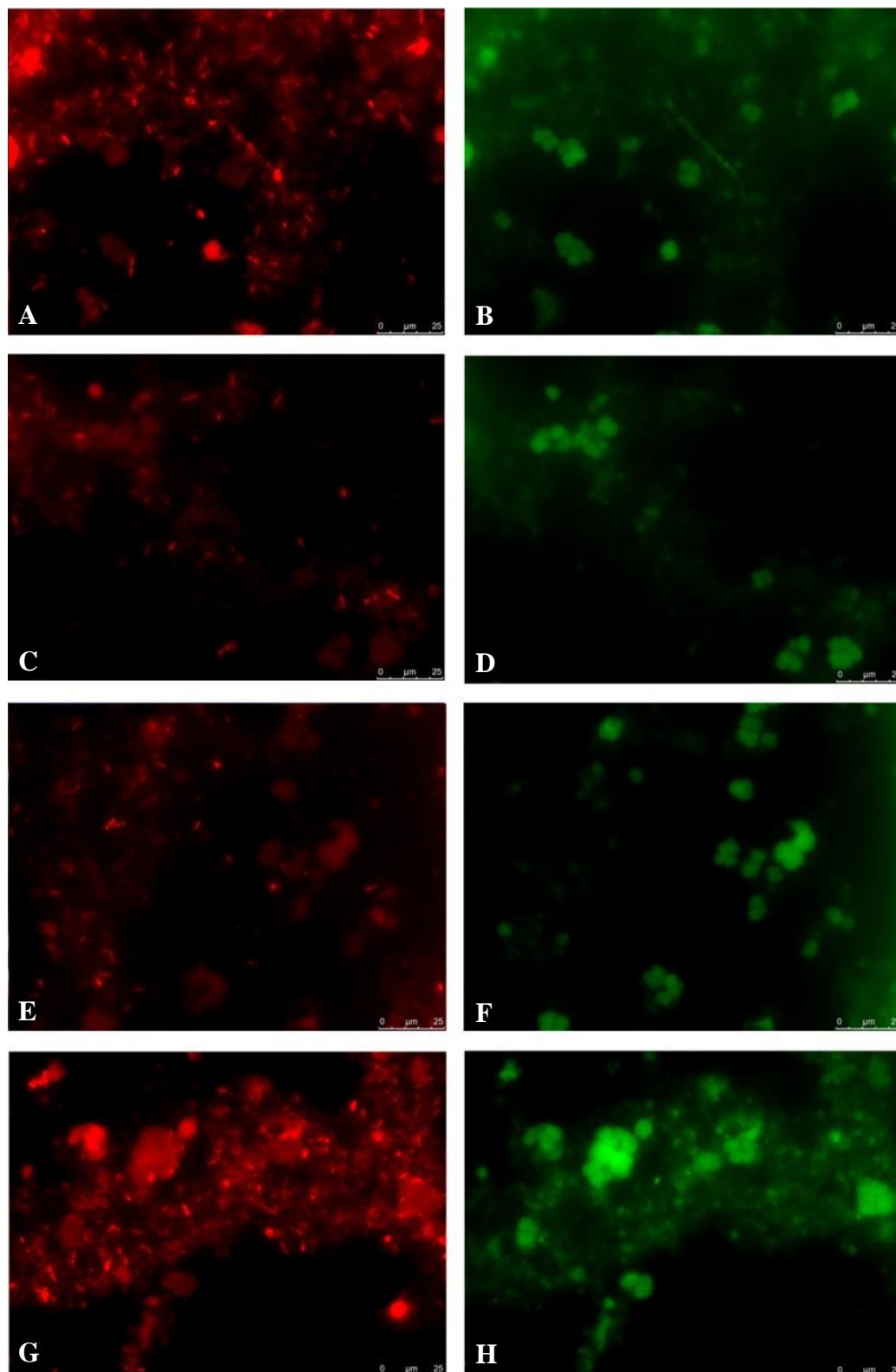


**Figure 3.19.** Fluorescent *in situ* hybridization (FISH) pictures of the planktonic microbial community in the BECs under open circuit conditions. Bacterial cells were stained in red (Cy3), archaea in green (FITC). A-B). At the initial time point of the experiment, C-D) after 1 week of the experiment, E-F) after 2 weeks of the experiment, G-H) at the end of the experiment.

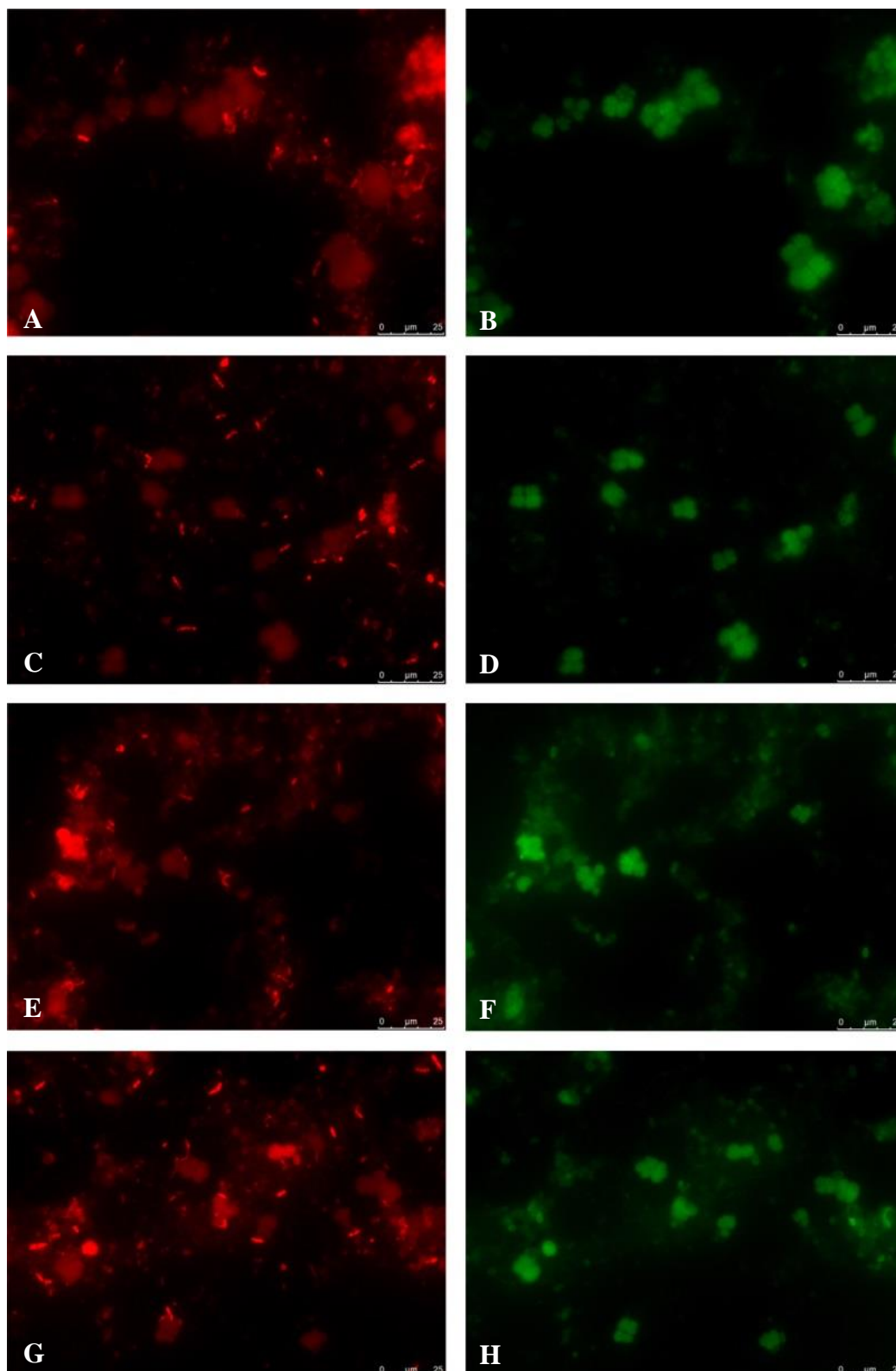


**Figure 3.20.** Fluorescent *in situ* hybridization (FISH) pictures of the planktonic microbial community in the BECs under closed circuit conditions. Bacterial cells were stained in red (Cy3), archaea in green (FITC). A-B). At the initial time point of the experiment, C-D) after 1 week of the experiment, E-F) after 2 weeks of the experiment, G-H) at the end of the experiment.

### 3. Electrical biogas system

The main goal of the third research part was to investigate the utility of BECs, supplied with pre-incubated anodes containing the previously described model exoelectrogenic biofilm, for the stable and efficient operation in an anaerobic digester for the degradation of organic waste. This research part was mainly focused on the electrochemical stability of the model biofilm on the anode surface and its effect on electricity generation and biogas production.

The model multi-species biofilms were pre-grown on the anodes within 7 days, afterwards carbonate buffered medium was exchanged with biomass (identical to that one, as described in part 2). Thereafter, BECs were operated over a time period of 14 days and showed high reproducibility in methane and current production.

#### 3.1. Assessment of process characteristics: electrochemical stability and methane production

To achieve the maximum current production rates from this system, anodes were poised to a potential of 0.04 V. Figure 3.21 (A) shows the current generation from the whole experiment, starting with the pre-incubation phase.

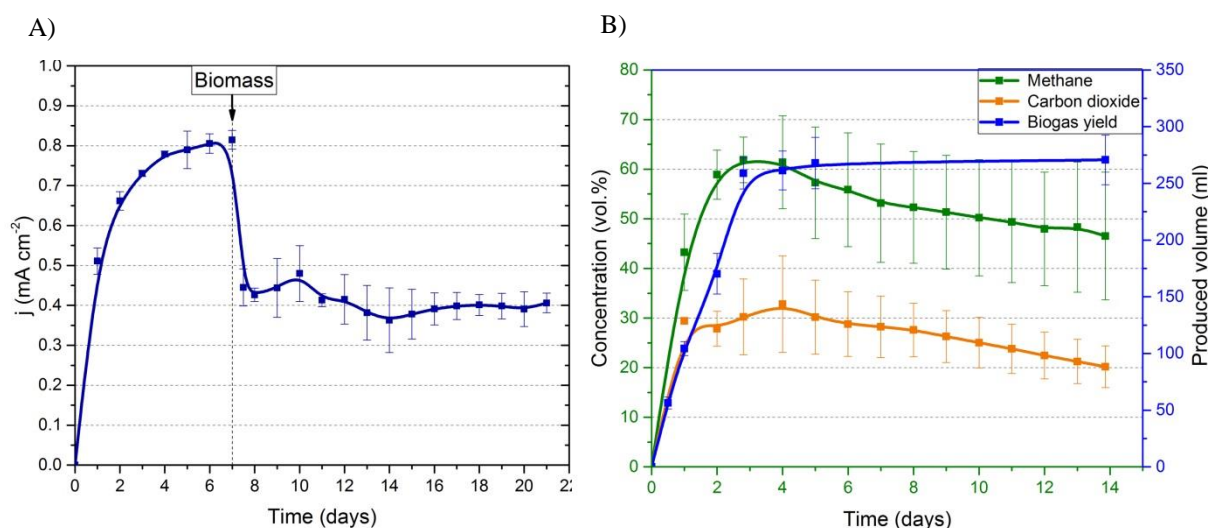


**Figure 3.21.** A) Electrochemical performance of the electrical biogas system under chronoamperometry mode (applying 0 V), representing pre-incubation period with carbonate buffered medium and the following switch to biomass. B) Headspace percentages of methane concentration, carbon dioxide concentration and biogas yield as produced volume.

Of note, due to different electrochemical setup and anode material used in this part of the research, data obtained from the pre-incubation period, such as the current production rate and

maximum values, do not 100% correspond to data from the first part. After the time point, when carbonate buffered medium was switched to biomass, current density decreased rapidly from  $0.81 \pm 0.02 \text{ mA cm}^{-2}$  to  $0.44 \pm 0.04 \text{ mA cm}^{-2}$ . Throughout the following 2 weeks of the experiment current production was relatively stable and was in the range of  $0.40 \pm 0.04 \text{ mA cm}^{-2}$ . The amount of electrical current produced during the experiment with pre-incubation with the model exoelectrogenic biofilm is approximately 300-fold higher in comparison with the experiment without pre-incubation of the anodes. Interestingly, the current output is about  $51 \pm 5\%$  of the maximum current production with carbonate buffered medium.

Gas composition in the headspace was analyzed during the whole time of the experiment in each BEC. As shown in Figure 3.21 (B) methane production increased gradually with time and reached the greatest value of  $61.4 \pm 9\%$  at 4 days of HRT, afterwards its concentration decreased. Comparatively, the carbon dioxide concentrations have shown an analogical pace of development. Within 4 days the concentration of carbon dioxide in the headspace of the BECs reached maximum values of  $33 \pm 10\%$ , but by the end of the experiment carbon dioxide was presented by only  $20 \pm 4\%$ .

The cumulative biogas yield was  $271 \pm 21 \text{ ml}$  per each reactor. Interestingly, the biogas yield was fast during the first 4 days of the experiment.

To evaluate the efficiency of the electrical biogas system, the coulomb efficiency (CE) was used as a nominal value. The total Coulombs transferred through the circuit is a measure of overall anodic activity, and it is calculated by integrating the current production over time. The CE reflects the amount of Coulombs transferred compared to the organic matter removed, evaluated on the basis of TOC data. As is indicated in Figure 3.22 CE increased steadily over time. After 14 days, the coulomb efficiency was  $64.5 \pm 11.7\%$ .

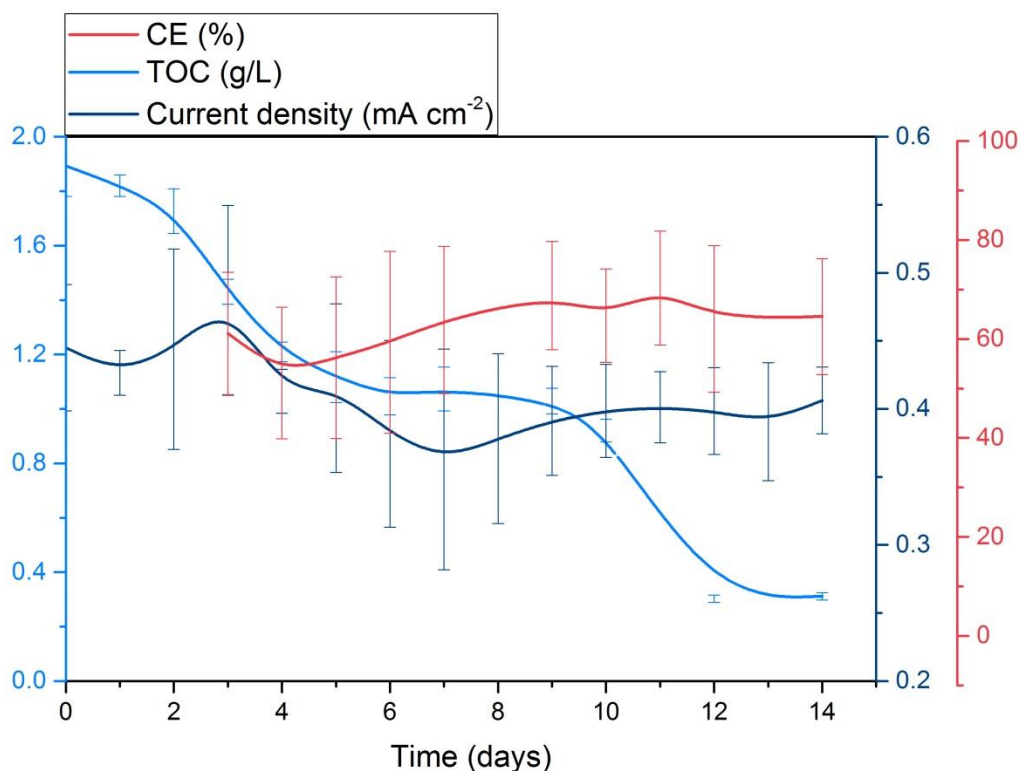


**Figure 3.22.** Process parameters of the electrical biogas reactor: the electric current density  $j$  (dark blue line), total organic carbon, TOC, (light blue line) and the obtained coulombic efficiency, CE, (red line)

### 3.2. Substrate analysis

As was previously described in section 3.2.2, substrate analysis revealed a big variety of VFA that were found in the initial phase of the experiment, but this research focuses only on the most abundant and dominant, such as acetate and propionate. Figure 3.23 (A) indicates, that the initial concentration of acetate was  $23.5 \pm 1.2$  mM and complete degradation was observed within 4 days. This is in accordance with the methane production curve shown in Figure 3.23 (B), which has reached a plateau phase at day 4 with the following depletion.

On the other side, propionate concentrations increased within the initial 2 days of the experiment, starting from  $5.1 \pm 0.3$  mM to  $10.2 \pm 0.6$  mM. Interestingly, afterwards the propionate concentration remained constant till the time point, when acetate was completely degraded. After day 5, depletion of propionate was observed. The VFA concentrations were in line with the rate of TOC degradation, as shown in Figure 3.23 (B). At the end of the experimental time  $84 \pm 0.4\%$  TOC removal was achieved. Starting from the initial time point TOC was actively degraded within 5 days, which corresponds to the acetate depletion rate. Afterwards it was in line with the propionate concentrations.

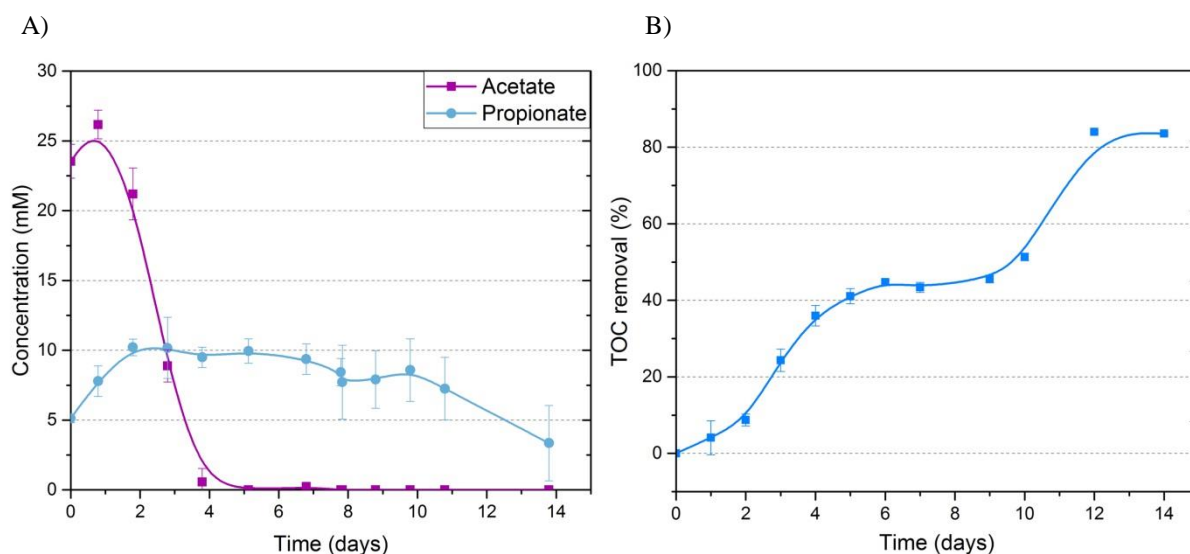


**Figure 3.23.** A) Analysis of metabolites in planktonic phase of the reactors. B) TOC removal during the experimental time.

The pH values were measured every day during the whole experimental time and were adjusted every day to 7.0-7.2 as required (Figure 3.24).

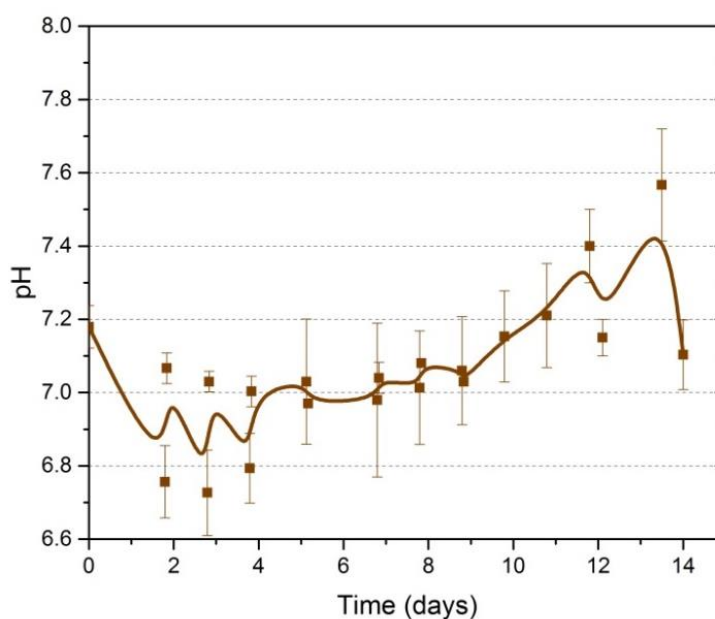


**Figure 3.24.** pH values were adjusted every day to 7.0-7.2 during the whole time of experiment. During the first 4 days of the experiment, pH values dropped dramatically to  $\text{pH } 6.74 \pm 0.14$ , but after 10 days pH started to increase to values higher than 7.2.

### 3.3. Stability of exoelectrogenic model biofilm on the anodes

In order to investigate stability of the pre-incubated model exoelectrogens on the surface of the working electrodes after 2 weeks of growth with biomass as a substrate, anodes were extracted from the reactors at the end of the experiment for the following qPCR analysis.

Figure 3.25 (A) shows the distribution of the model cells within their community in the inoculum, in the pre-incubation phase (in planktonic space of BECs and on the anode surface) and at the end of the experiment (sessile cells). The pre-incubation phase was started with cell suspensions of equal OD values, even though with a differing initial cell number, due to cell size differences. Hence, the starting inoculum was composed of  $27.3 \pm 0.4\%$  *S. oneidensis* cells,  $43.5 \pm 0.6\%$  *G.sulfurreducens* cells and  $29.2 \pm 0.2\%$  *G. metallireducens* cells. At the end of pre-incubation phase, planktonic cells of *S. oneidensis* were presented by  $72.8 \pm 2.3\%$  and *G.sulfurreducens* by  $26.3 \pm 1.4\%$ , whereas the sessile cells accounted for  $93.8 \pm 3\%$  and  $6 \pm 0.1\%$  of *G.sulfurreducens* and *S. oneidensis*, respectively. *G. metallireducens* cells were detected in the planktonic and sessile phase only in minor quantities.

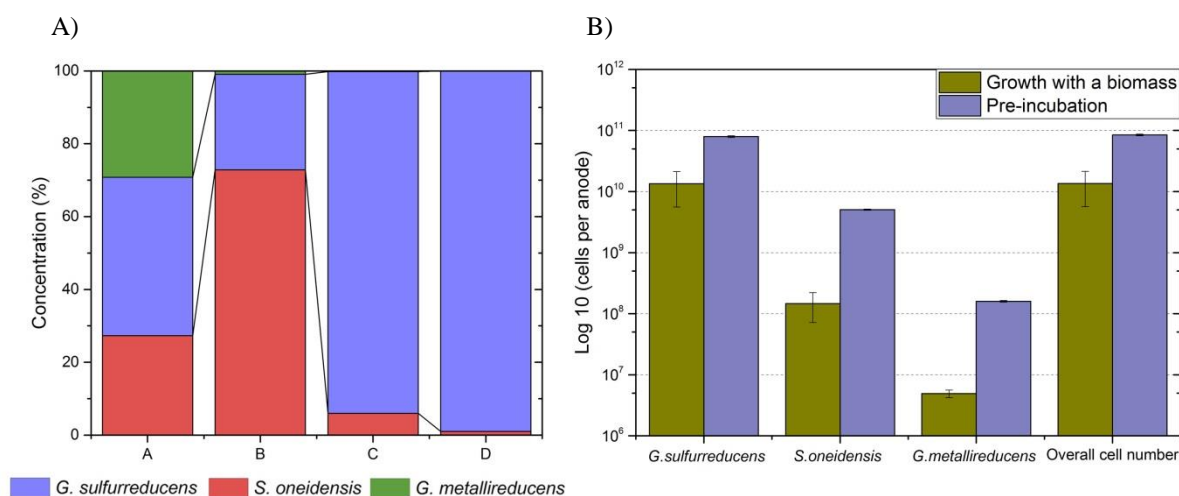


**Figure 3.25.** Quantitative analysis of the model exoelectrogenic microorganisms. A) Allocation of the model exoelectrogens: (A) allocation of model strains in the inoculum; (B) allocation of model strains in the planktonic phase of the reactor at the end of the pre-incubation phase; (C) allocation of model strains at the surface of working electrode at the end of pre-incubation phase; (D) allocation of model strains at the surface of working electrode at the end of experimental growth with biomass as a substrate for 14 days. B) Cell number of the model exoelectrogens after pre-incubation with a carbonate buffered medium for 7 days and after growth with biomass as a substrate for 14 days.

Figure 3.25 (B) shows the obtained results, where the overall cell number at the end of pre-incubation phase is compared with the overall cell number at the end of experimental growth with biomass for 14 days. After growth with biomass the amount of sessile model cells

decreased from  $8.45 \times 10^{10} \pm 2.61 \times 10^9$  to  $1.43 \times 10^{10} \pm 6.74 \times 10^9$ . Consequently, model cells that still remained on the anodes were accounted for  $17 \pm 7\%$ . Among the model strains, the dominance of *G. sulfurreducens* was even more pronounced because it constituted 98.9% of all model cells. However, none of the three strains was detected in the planktonic part of the bioelectrochemical systems.

## Discussion

Microbial fuel cells (MFCs) are devices which convert organic waste streams to electricity through the metabolic processes of microorganisms acting as a bioelectrochemical catalyst. Numerous studies have confirmed that MFCs are potentially applicable to wastewater treatment and energy conservation (Logan, 2009; Logan *et al.*, 2006). Also recently many studies have been carried out to expand the application of BESs by coupling microbial electrochemical technology with anaerobic digestion (AD) and have introduced such system as a highly stable in comparison with the conventional AD (Tartakovsky *et al.*, 2011; Zamalloa *et al.*, 2013; De Vrieze *et al.*, 2014). In order to increase the efficiency of electricity and biogas production it is necessary to understand and steer the microbial community on electrode surface. In the current study, first aim was to investigate microbe-microbe and microbe electrode interactions using the model exoelectrogenic biofilm, consisting *G. sulfurreducens*, *S. oneidensis* and *G. metallireducens*. Thereafter to check into thoroughly whether the electrodes installed inside of the AD reactor influencing the methane formation and electricity production. And finally it was a goal to use pre-incubated electrodes with the model exoelectrogenic biofilm as a tool to increase electricity production and stability of the system.

### 1. Model exoelectrogenic biofilm

In the first part of the current study it was an aim to characterize development and stability of the model exoelectrogenic biofilm in terms of electrochemical and transcriptome approach. Previously some studies have already investigated metabolic and extracellular electron transfer (EET) interactions within co-culture conditions in MFCs. Rosenbaum *et al.* (2011) studied synergistic relationships between homolactic acid fermenter *Lactococcus lactis* and well-known exoelectrogenic bacteria *Shewanella oneidensis* during the cyclic voltammetry tests. Venkataraman *et al.* (2011) revealed a mutually-beneficial relationship during co-culture growth of fermenter *Enterobacter aerogenes* and electrode-respiring bacteria *Pseudomonas aeruginosa*. Differences between Gram-negative and Gram-positive bacteria in terms of the biofilms development and current denervation and moreover their co-culture growth were investigated by Read *et al.* (2010). Generally, Gram-positive bacteria on their own make limited current in comparison to the Gram-negative (Marshall *et al.*, 2009) and developed thinner biofilms (Read *et al.*, 2010). Consequently there are possible synergistic

scenarios that could lead to accelerated electron transfer in mixed species anode communities (Nevin *et al.*, 2008).

Current study is the first one that describe the resilience, dynamics of biofilm formation and the molecular responses within a model gram-negative exoelectrogenic community, consisting of the mostly widespread and well-known bacteria, such as *Shewanella oneidensis*, *Geobacter sulfurreducens*, and *Geobacter metallireducens*. More recently, it has been shown with a variety of substrates that high power generation is usually associated with a large proportion of bacteria most similar to various *Geobacter spp.* (Kiely *et al.*, 2011), where *G. sulfurreducens* was usually the predominant microbe (Caccavo *et al.*, 1994). *G. metallireducens* is an environmentally relevant anaerobic microorganism. It is known to degrade aromatic pollutants in the groundwaters including toluene and it is also able to use easily degradable substrates present in the environment, e.g. propionate and acetate (Lovley *et al.*, 1993). *S. oneidensis* is proposed to employ all known mechanisms for microbial extracellular respiration: (1) direct electron transfer with outer membrane redox-proteins (Kim *et al.*, 1999; Myers and Myers, 2003), possibly with help of conductive appendages (Gorby *et al.*, 2006); (2) mediated electron transfer with microbially produced soluble redox-compounds (Marsili *et al.*, 2008; von Canstein *et al.*, 2008). Thus all these three strains represent important model organisms for the functional investigation within the biofilm in BESs.

### **1.1. Characterization the developmental growth of a model multi-species anode biofilm**

Examination the composition of a controlled model microbial community on anode surfaces was investigated over 7 days experimental time. Starting from the first day *G. sulfurreducens* have demonstrated dominance of the sessile community. That was expected, as the strategy of *G. sulfurreducens* cells for electron transfer to insoluble electron acceptors relies solely on a direct interaction which is mediated by conductive pili as well as *c*-type cytochromes on the surface of the cells as well as within the extracellular matrix (Liu *et al.*, 2012). Although that *S. oneidensis* and *G. metallireducens* were presented in fewer quantitative proportions, all three strains were grown actively on the anode surface during the whole experimental time, indicating about effective synergistic relationship within biofilm community. Quantitative analysis of suspension from BECs revealed the dominance of *S. oneidensis* cells. There is a strong probability that *S. oneidensis* thrives in the planktonic phase due to its ability to endogenously secreting flavin molecules and use them as electron shuttles (Marsili *et al.*, 2008). The reduced shuttles could either be re-oxidized at the surface of the anode itself or at

the biofilm covering the anode. Although the fact, that *G. sulfurreducens* is also capable to secrete and utilize riboflavin as a regulator for intracellular redox homeostasis to promote extracellular electron transfer (EET) (Okamoto *et al.*, 2014), in the current study there were detected none evidence of usage self-secreted flavins during a pure culturing growth of *G. sulfurreducens* cells (section 4.1.3). On another hand, it is possible that under co-culture conditions planktonic fraction of *G. sulfurreducens* cells could show a cheater-like strategy by using flavins produced by *S. oneidensis* as a way to transfer respiratory electrons away from the cell.

Initial studies with *G. sulfurreducens* found that cells attached to the anode surface, which responsible for the power production, formed a virtual monolayer on the anode (Bond and Lovley, 2003). However, subsequent studies revealed, that biomass accumulation on the anodes corresponded in direct proportion to the current level (Reguera *et al.*, 2006). Current results from FISH data demonstrated, that *G. sulfurreducens* cells have established thick biofilm on the carbon cloth fibers, by using pili as electrical conduits (Reguera *et al.*, 2005).

Stable and robust model multi-species biofilm was established within first two days of experiment, that indicates that BESs achieved also stable rates of carbon oxidation. The current density per anode surface reported here for the model multi-species biofilm ( $0.62 \text{ mA cm}^{-2}$ ) is 2-fold more in comparison to the  $0.32 \text{ mA cm}^{-2}$  reported to be the highest of a mixed microbial community from anaerobic digester sludge produced in a similar continuous flow and air-cathode BECs (Cheng *et al.*, 2006).

## **1.2. Influence of different redox potentials on current generation and stability of the biofilm on the anode surface**

It is known that the growth rate of microorganisms is positively proportional to the energy gained for its growth (Aelterman *et al.*, 2008). Therefore the essential role of anode potential lies in regulation of energy obtained for bacterial growth (Schröder, 2007). The lower the anode potential, the less Gibbs free energy per electron transferred that the microorganisms theoretically gain. At higher anode potentials the bacteria will be able to grow and reproduce faster per electron transferred. As a result, higher biomass densities can be sustained causing a potential current increase but also an increased competition for the available electrode surface and substrate.

Whereas in previous part development of a biofilm formation was investigated under constant applied potential of 0.04V, in a second set of the experiments the stability of the model multi-species biofilm was analyzed under varying electrochemical process parameters. In nature,

redox potentials of extracellular terminal electron acceptors metal oxide species are ranging between +1.1 and -0.4 V (Pierre *et al.*, 2002). Exoelectrogenic microorganisms utilizing a specific substrate are able to gain more energy per transferred electron, when reducing an electron acceptor with a more positive redox potential (Bosch *et al.*, 2014). This is in line with results from the current research, where model multi-species biofilm were capable to generate more currents under positive range of applied potentials. It is interesting to note, that under tested positive potentials (0.04, 0.24 and 0.44 V) electrical outputs were on the same level, indicating that the model biofilm reached its maximum rate of electron transfer under this driving force. Meanwhile negative range of applying potentials could provide a possibility to steer an exoelectrogenic activity of the model biofilm.

It seems as if working electrode potentials above -0.06 V sustained not only the maximum rate of electron transfer, but also the highest biomass production rates. In fact a recent study showed faster growth rates of *G. sulfurreducens* in MFCs with anodes poised to 0.4 and 0 V in comparison to -0.16 V (Wei *et al.*, 2010). Thus, biomass formation had to be considered as constant under positive applied working electrode potentials. We could assume, that the model exoelectrogenic biofilm cannot change the number of transferred protons per electron respired under such conditions, even if more energy was available with electrons respired at higher redox potential differences. While *S. oneidensis* as well as *G. sulfurreducens* responded similarly to the different potentials, there was not observed such a clear trend for *G. metallireducens*. It is possible that under the chosen conditions, growth of *G. metallireducens* is limited by the substrate oxidation rate rather than the electron transfer to the anode surface. Still, our findings showed that the model multi-species biofilm was able to grow at a large potential range. A constant biomass formation is maintained even at low available energies. This versatility suits to an ecology which implies the dissimilatory reduction of soluble, poorly soluble or insoluble electron acceptors with a large range of redox potentials, and it enables model multi-species biofilm to maintain at least a minimum of metabolic activity on almost all kinds of ferric iron and other metal oxide electron acceptors. Linear voltammetry experiment was used to investigate the possibility of steering exoelectrogenic activity of the model multi-species biofilm via applying negative range of potentials (below 0.04 V). Even when grown at potentials of -0.08 V, use of the same transfer scheme caused the model biofilm to operate at about half maximal velocity. This potential is in line with typical midpoint potentials of outer membrane cytochromes as well as with flavins, which are released by *S. oneidensis* and can be used as electron transfer shuttles (Meitl *et al.*, 2009). Thus, the model multi-species biofilm showed ability to tune its outer

membrane interface to take advantage of available energy. The consortium showed good stability at lower potentials for more than 9 days and did not slow their overall rate of electron transfer. Such ability to control current production of exoelectrogenic bacteria could offer promising solutions for applied processes. For instance, preliminary results suggest that it is possible to use an applied potential as a way to accelerate carbon oxidation in a biogas reactor.

### 1.3. Variations of the central metabolism as a result of co-cultivation

In order to gain insight into metabolic changes in the individual strains during the solitary growth versus growth in co-culture, transcriptomes and metatranscriptomes data were analyzed.

To date it is known, that pure cultures have generally produced substantially lower current densities than mixed cultures (Nevin *et al.*, 2008). When pure cultures are unable to produce as much current as in co-culture conditions, then appear an important ecological question of whether the multi-species microbial interactions are required for the highest current densities. Hence, as was observed for *G. sulfurreducens*, co-cultivation seems to positively affect the substrate oxidation and electron transfer processes, as the central metabolism of *G. sulfurreducens* was upregulated under co-culture conditions. There are a number of cytochrome genes that show induced expression including *omcB* and *omcE*. Both cytochromes were shown to be involved in the electron transfer to the cell surface of *G. sulfurreducens* (Nevin *et al.*, 2009). Moreover, expression of the small triheme cytochrome PpcA was increased. PpcA is localized in the periplasm and evidence was provided that it is involved in the transport of respiratory electrons from the cytoplasmic to the outer membrane (Lloyd *et al.*, 2003). In agreement with the upregulation of cytochromes is the increased transcription of pili genes, including *pilA*, which is required for high density current production (Reguera *et al.*, 2006). The hypothesis of increased electron transfer as a result of co-cultivation is nicely corroborated by the upregulation of genes coding for central reactions involved in the oxidation of acetate within the citric acid cycle as well as the NADH dehydrogenase Nuo (average upregulation of *nuo* genes: 2.65 fold). The reason for this general response might be the downregulation of the hydrogen dependent growth transcriptional regulator HgtR. HgtR has been shown to repress genes involved in biosynthesis and energy generation (Ueki *et al.*, 2010). An upregulation of HgtR under conditions of growth in pure culture might be explainable as it has been shown that electron acceptor limitation results in hydrogen production by *G. sulfurreducens* (Cord-Ruwisch *et al.*,

1998). Hence, the presence of the other strains might contribute to higher electron transfer rates, possibly due to the presence of organic molecules like flavins released by *S. oneidensis* cells. Still, although HgtR is downregulated under co-cultivation conditions, the typical uptake hydrogenase HybAB (Coppi *et al.*, 2004) of *G. sulfurreducens* is strongly upregulated (9.1- and 14.3-fold, respectively). One explanation could be that *G. sulfurreducens* under mixed species conditions enters a state in which it uses both hydrogen and acetate as electron donors. The use of hydrogen might also allow for a higher percentage of acetate that can be fed into gluconeogenesis. At least two genes of gluconeogenesis were discovered to be upregulated under mixed species conditions (*eno*: 2.4-fold upregulated; *pgk*: 2.5-fold upregulated). Hydrogen might be produced by *S. oneidensis* as will be shown later. Interestingly, genes necessary for nitrogen fixation show a strong decrease in transcription as a result of co-cultivation. This might indicate that, although the medium contains 3.7 mM ammonium, the cells face a nitrogen limitation within the anode biofilm. It is of interest to note that both *Geobacter* strains showed a downregulation of *cydA* and *cydB* as a result of co-cultivation. The encoded cytochrome bd-ubiquinol oxidase was discussed as a mechanism to cope with oxidative stress (Giuffre *et al.*, 2014). *G. sulfurreducens* was originally considered to be a strict anaerob (Caccavo *et al.*, 2004), but it is now well established that it can grow under low dissolved oxygen conditions (10% or less) and it is inactivated (Lin *et al.*, 2004) or killed at higher concentrations (Nevin *et al.*, 2011). A contamination with trace amounts of oxygen is possible with regard to the polycarbonate based reactors used. The presence of *S. oneidensis* in the biofilm and its capacity for aerobic growth would help to decrease the amount of oxygen at the anode surface. Thereby it could be hypothesized, that oxygen leakage into a reactor was the reason that the amount of current generated by multi-species biofilm is larger than that generated by a pure culture of *G. sulfurreducens*.

*G. metallireducens* showed another interesting adaptation to growth with *G. sulfurreducens* and *S. oneidensis* which is an upregulation of the *prp*-operon. The *prp*-genes encode the necessary proteins for propionate oxidation (Aklujkar *et al.*, 2009). Gmet\_1125 protein could be a succinyl:propionate CoA-transferase that, together with the other three products of the operon, would convert propionate (via propionyl-CoA) and oxaloacetate to pyruvate and succinate (Figure 3.8, see section 3.1.4.2.). *G. metallireducens* can grow with acetate and propionate. These cells apparently do not adapt their metabolism for acetate as a carbon source but rather specialize on propionate, for which there is no competitor in the community. Propionate is a challenging substrate under anoxic conditions, since its oxidation involves an energy-dependent activation to propionyl-CoA and an ATP-dependent oxidation of succinate

to fumarate if electron acceptors are used which reduction is menaquinone dependent (Muller *et al.*, 2010). This might also explain the rather slow growth of *G. metallireducens*.

*S. oneidensis* cells also show distinct responses to growth in a mixed-culture biofilm. In *S. oneidensis* 80% of membrane-bound *c*-type heme is localized to the outer membrane that indicates on their direct role for *c*-type cytochrome in metal reduction (Heidelberg *et al.*, 2002). *MtrABC*, *OmcA* and *CymA* as well as their associated proteins have a key role in extracellular transfer from *S. oneidensis* to carbon electrodes in MFCs (Fredrickson *et al.*, 2008). In the current study we could observe an upregulation of the Mtr pathway, which is necessary for electron transport through the outer membrane and on to an extracellular electron acceptor (*mtrABC* and *omcA* showed a 2.3-fold average upregulation). Furthermore, protein-coding genes involved in lactate transport and oxidation were also upregulated. Hence, as was observed for *G. sulfurreducens*, co-cultivation seems to positively affect the substrate oxidation and electron transfer processes. Interestingly, *S. oneidensis* also responded to co-cultivation with the upregulation of a hydrogenase. Meshulam-Simon (2007) investigated hydrogen metabolism in *S. oneidensis* and observed that Hya-activity under tested conditions accounted for over 75% of the hydrogen produced by *S. oneidensis*. Hydrogen formation was, at least to some extent, dependent on reverse electron transfer because the addition of the protonophor CCCP resulted in decreased hydrogen production. It was speculated that in this case proton reduction could occur via NADH as electron donor that could be produced either by a conversion of pyruvate to acetyl-CoA and NADH by pyruvate dehydrogenase or indirectly via formate resulting from pyruvate formate lyase catalyzed conversion of pyruvate to acetyl-CoA and formate. The latter is corroborated by the upregulation of the *pflA* and *pflB* genes as well as by a gene cluster encoding a typical respiratory formate dehydrogenase (SO\_4509 – SO\_4511). Along these lines, it is interesting to note that *S. oneidensis* does not seem to use oxidative phosphorylation as way of producing energy under anoxic conditions. Hunt and colleagues (2010) deleted the ATP synthase of the organisms and observed only minor growth defects. Hence, the developed proton gradient would at least partly be available for reverse electron-transfer reactions.

There are a number of gene clusters that are upregulated in cells grown in the absence of *G. sulfurreducens* and *G. metallireducens*. Very prominent are genes that are involved in the degradation of amino acids (*liuA-F*, 9.8-fold upregulation). The medium contains casitone and therefore is a source of amino acids. Currently, we can only speculate that this distinct regulatory response is due to the pool of available amino acids being lower if three organisms

simultaneously thrive in the same reactor and try to avoid using the catabolic electron source for the formation of anabolic building blocks.

## **2. Coupling bioelectrochemical system and anaerobic digestion**

The primary aim of the current research was to define the possibility to control the performance of anaerobic digester, in terms of methane production and current generation, through the installation of bioelectrochemical cells directly into digester. Some recent studies have revealed that bioelectrochemical systems could stabilize methane fermentation and increased carbon utilization rate (Sasaki *et al.*, 2010; Batlle-Vilanova *et al.*, 2015; Bo *et al.*, 2014; Clauwaert *et al.*, 2008), by using a modification of BES defined as microbial electrolysis cell (MEC), which has been conceived to store electrical energy as biofuel (hydrogen). In addition, the potentiality of a coupled AD-MFC system has also been preliminary shown, highlighting the possibility of removing the sulphide generated in AD via oxidation by controlling the anodic potential of the MFC (Rabaey *et al.*, 2006) and also accelerated total ammonia nitrogen and COD removal (Kim *et al.*, 2015). Therefore, deeper knowledge of the systems would lead to the optimization of BES, by defining the optimal structural and biological properties according to their specific application.

Thus in the second part of the thesis it was an aim to investigate the influence of installed and poised to a certain potential electrodes on methane formation and yield, substrate degradation rate as well as on electric energy production. Development of proportional growth and identification of bacterial and archaeal microorganisms, occurred in AD, were characterised through the sequences technique and qPCR based analysis. And additionally it was an aim to characterize the electrical biogas system with anodes, which were pre-incubated with the model multi-species biofilm, studied in the first part of the current thesis.

### **2.1. Evaluation of the electrical biogas system in terms of methane production and current generation**

According to the results obtained in the present study, the methane formation rate was directly depended on the applied potentials at the working electrodes. The lower quantity of methane that was detected during the LSV mode confirmed that methane production was affected by the electrodes poised to certain potentials. This is in line with the experiment with the pre-incubated anodes, where the methane formation rate did not reach the same values, as under

open circuit conditions. Of note, in the current study it was also observed, that the relative proportion of the methanogens, based on qPCR analysis, was at least slightly suppressed by the active working electrode.

A recent study by Kaur *et al.* (2014) revealed for the first time that methanogenesis can be inhibited in BECs, when they are operated on regimes characterized by different time periods of open and closed circuit operational mode. Kaur and colleagues have used BECs enriched with acetate, propionate and butyrate for the open circuit and closed circuit mode (1k $\Omega$ ). In all reactors, operated under open circuit conditions the methane production was detected at higher percentage than under closed mode, indicating that methanogens enriched predominantly in open systems rather than in closed systems. But generally, in all those experiments maximum value of methane formation reached only 3-8% under open conditions, that is in comparison with the current study extremely low. This could be due to the differences in the chosen inoculum and operating conditions.

Another previous study by Sasaki *et al.* (2010) characterized two types of BECs: with cathodic and anodic reactions in comparison with the control reactor (without applied potential). Anodic reactions under applied potentials of 0 V and -0.3 V demonstrated no big differences in comparison to the control reactor in terms of methane content, COD removal efficiency and gas production rate were higher under -0.3 V, but lower under 0V in comparison with the control. Such results could indicate that under applied potential of -0.3 V electron transfer by exoelectrogenic microorganism was slowed down, resulting in more active methane formation. Moreover it suggests that differences in redox potential could have affected the bacterial community. Interestingly, enhanced methanogenesis and COD degradation rate were achieved in the experiments under cathodic reactions. Moreover control of the electrical potential at the working electrode through a cathodic reaction was shown as a stabilizer for the methane production. This is in contrast to Vrieze *et al.* (2014), who have investigated a molasses fermenting coupled BEC and AD system in terms of stabilization effect. They revealed that the main effect behind the stabilization of BECs in AD appears to lie in biomass retention, rather than bioelectrochemical interaction with the electrode. Koch *et al.* reported, that coupling BECs with AD demonstrated constant methane yield, while current was also generated, that allowed up to 27% increase in total yield. This is also the only study, where silage was used as a sole carbon and energy source, as in the present research. But results are in contrast with the current study, where it was shown, that energy gain through the system is going either for methane formation or for both processes thereby there will be a decrease of methane production in comparison with the control systems. Ishii *et al.* (2008)

have demonstrated that BECs, inoculated with rice paddy field soil, supplemented with crystalline cellulose, showed suppression of methanogenesis under closed circuit conditions (510  $\Omega$ ), but meanwhile were able to produce electrical current of 6-10  $\mu\text{A cm}^{-2}$ .

All experiments in current study also indicate that methane was actively produced only at the time point, when acetate was presented in the reactors in abundance, while subsequently methane production proceeded at a relatively slow rate or even decreased. This is in line to Ishii *et al.* (2008), where it was also mentioned, that methane was produced only when acetate was presented. That was quite expected, because the BECs comprised a parallel way for VFA oxidation. As was already previously observed, VFA degradation was more rapid in the reactors under applied potential conditions than under open circuit operations (Kaur *et al.*, 2013). In the present study a very fast substrate turnover took place also under applied potential conditions. That is in line with our hypothesis, that substrate was used for both processes, methane production and current generation. Influence of applied potentials on substrate degradation rate was nicely demonstrated by linear sweep experiment. Where under the potentials below -0.15 V, cells stopped to produce electrons, thus substrate turnover was also slowed down, until the more positive values of applied potentials were achieved. In this manner such results show that applied potentials affected VFA-consumption with subsequent competition between methanogens and exoelectrogens, by this means they have influence on methanogenesis. Our hypothesis is in line with a previous study by Ishii (2008), where it was suggested that electrogenesis has a suppression impact on methanogenesis.

Hao *et al.* (2013) previously reported that the high initial acetate concentration resulting in the accumulation of VFA would (> 50 mM) inhibit the activity of acetoclastic methanogenesis during the starting phase. Our results indicate that the electrodes might compensate the low rate of methanogenesis. The propionate degradation was expected to be closely related with population dynamics of the microorganisms in the reactors because propionate-degrading bacteria are syntrophic and dependent on hydrogen consumers such as hydrogenotrophic methanogens. Some other researchers (Griffin *et al.*, 1998; Stroot *et al.*, 2001) also revealed, that even when acetate is consumed gradually, propionate often persists throughout reactor operation, as in the current study.

The oxidation-reduction potential in BESs under open circuit conditions was near the oxidation-reduction potential reported for other methanogenic reactors (Satoh *et al.*, 2007). Generally, the described coupling system for methane production and current generation shows very promising results in terms of electric current, that was produced in the experiment with the pre-incubated anodes with the model multi-species biofilm. Moreover, we found that

electricity production by the natural exoelectrogenic community was detected only in low quantities under LSV mode ( $0.91 \mu\text{A} \pm 0.16 \mu\text{A cm}^{-2}$ ), which is more than 480-fold lower in comparison with the current produced by the model biofilm pre-incubated on the anode surface. Pre-incubated model multi-species biofilms have generated a very stable level of current during the whole experimental time. Additionally, the pre-incubation demonstrated to lead to high cell stability of the model microorganisms on the anode surface over time, pointing to the ability of the model biofilm to thrive in these conditions by using biomass as a carbon and energy source.

#### 4.2.2. Methane yield and electron balances

Considering, that all electrons of the oxidation of the total organic carbon source in the OCP mode would be used for methane formation, 21.5 mmol of  $\text{CH}_4$  could be expected in the conducted experiment. In our experiment we could achieved methane yields of  $9 \text{ mmol g}^{-1}$  TOC, representing a methane yield of 86.4%. This is in accordance with literature values (Gülzow *et al.*, 2008). For the LSV experiment, however, the total methane efficiency was 63%. Meanwhile our theoretical expectation of the total concentration of methane achieved in the experiment with pre-incubated anodes under tested conditions was about 16.5 mmol. At the end of the experiment we have demonstrated only a production of  $3.5 \text{ mmol g}^{-1}$  TOC, thus we could achieved a methane efficiency of 44%. This lower methane yield in comparison with the OCP mode could be due to the fact that organic carbon was converted into  $\text{CO}_2$  and electric energy. In this manner it is interesting, that, whereas for LSV mode the electric current production was negligible due to the unstability of the system during the sweep voltammetry, for the experiment with the pre-incubation the electric current production had a significant contribution to the whole performance efficiency.

With the decrease of the TOC content in the BECs, the consumption of carbon was quantified. Moreover usage of the potentiostats allowed to calculate the amount of electrons that were released from the system as electrical energy. Hence, the coulombic efficiency of the individual BECs could be quantified.

In detail, the total charge transfer [Q] per batch was calculated as integrated value of current over time (1):

$$(1) \quad Q_{\text{recovered}} = \int I dt$$

Thus electric charge of 8,191 C was generated on average per reactor. Knowing that 1 C is equivalent to the charge of  $6.242 \times 10^{18}$  electrons and that Avogadro constant, that represent amount of atoms given by one mol, is  $6.022 \times 10^{23} \text{ mol}^{-1}$ , we could calculate the amount of electrons released. Thus 85 mmol of electrons were transferred in the system. Considering that 4 moles of electrons were needed to produce 1 mole of methane from the total organic carbon source, our calculation is in line with our previous hypothesis, that electrons under such tested conditions were consumed for both processes, current generation and methane formation.

Total theoretical electric charge of the system could be calculated according the Faraday's law (2):

$$(2) \quad Q_{\text{in substrate}} = \frac{F \cdot \bar{e} \cdot \Delta \text{TOC} \cdot V}{M [\text{C}]},$$

where F is a Faraday's constant (96,485 C),  $\bar{e}$  is the number of electrons exchanged per mole of carbon (4 mol  $\bar{e} \text{ mol}^{-1}$ ),  $\Delta \text{TOC}$  is the consumption of the carbon, V is the volume of liquid in the anode compartment, M is the molar weight of carbon. In this manner a total electric charge of 12,792 C could be generated per reactor for the amount of oxidated total organic carbon, equaling to 8,040 C  $\text{g}^{-1}$  TOC. Coulombic efficiency was stable over time and was about 64%. That in combination with the methane yield shows total energy yield of 108%. This exceeded 100% value could be explained by the unshielded counter electrode, which was used in the current study.

## 2.3. Analysis of microbial community structure

To analyze the microbial community structure and function, samples from the planktonic phase of the reactor were taken regularly and the electrodes biofilms at the end of the experiments.

### 2.3.1. Archaeal community

The VFA,  $\text{CO}_2$  and  $\text{H}_2$  generated by the acetogens are the substrates of methanogenesis carried out by special archaea (Thauer *et al.*, 2008; Deppenmeier *et al.*, 2008). The hydrogenotrophic archaea can reduce  $\text{CO}_2$  to  $\text{CH}_4$  using  $\text{H}_2$  as an electron donor. While  $\text{H}_2$  is the main electron donor for methanogenesis, many hydrogenotrophic methanogens can also use formate, ethanol, or some secondary alcohols as electron donors (Sarmiento *et al.*, 2011).

The maintenance of the methanogenic activity was largely independent of archaeal community composition.

Examination of the methanogenic populations revealed similar abundances in both systems, with open and closed circuit. Species of the genus *Methanoculleus* has been previously identified in biogas processes (Hori *et al.*, 2006; Klocke *et al.*, 2008; Kröber *et al.*, 2009) and has been shown to be dominant in a biogas reactor that contained high levels of ammonium and VFA (Schnürer *et al.*, 1999). *Methanoculleus bourgensis* utilizes H<sub>2</sub>/CO<sub>2</sub> or formate for growth (Maestrojuan *et al.*, 1990). Thus *Methanoculleus* is an important partner organism during the syntrophic acetate oxidation under mesophilic conditions. Species of genus *Methanosarcina* are also common in biogas processes (McHugh *et al.*, 2004). *Methanosarcina barkeri* belongs to order *Methanosarcinales*, which can utilize not only acetate, but also H<sub>2</sub>/CO<sub>2</sub>, methanol, mono- and dimethyl-amine (Stantscheff *et al.*, 2014). Hence, the *Methanosarcina* population identified here is responsible for the acetoclastic methanogenesis in the bioreactors.

Interestingly, that at the end of the experiment the abundance of *Methanoculleus* was higher under closed circuit system, meanwhile the abundance of *Methanosarcina* conversely has increased under open system. Hydrogen production in BESs leads to the predominance of hydrogenotrophic methanogens despite the high concentrations of acetate and other substrates. The present study demonstrated that the main methane production mechanism of the studied BES was hydrogen mediated. Hydrogenotrophic methanogens, such as *Methanoculleus* drove methanogenesis phase. This suggests that facultative anaerobes and exoelectrogens are largely able to outcompete acetoclastic methanogens for organic substrates in these systems.

### **2.3.1. Bacterial community**

The first step in the anaerobic degradation of complex organic substrates involves the breakdown of large molecules by hydrolysis (Lynd *et al.*, 2002). Certain communities of bacteria are capable of the efficient hydrolysis of plant biomass rich in lignocellulose. Most of these bacteria belong to the phylum of the *Firmicutes*. As expected, the overwhelming majority of the identified abundant species were members of the *Firmicutes* and, more precisely, the class of the *Clostridia*. This species can hydrolyze cellulose quite efficiently by means of its extracellular cellulases, reduce sulfate and can produce acetate, lactate and propionate, but cannot produce hydrogen (Zverlov and Schwarz, 2008).

The *Bacteroides-Prevotella* group consists mainly of species derived from human fecal and oral sources as well as other samples from mammalian organs such as the rumen (Holdeman *et al.*, 1984). The strain utilizes xylan as well as various sugars including arabinose, xylose, glucose, mannose, cellobiose, raffinose, starch and pectin. The strain produces acetate, propionate and succinate from saccharides in the presence of hemin. According to Nishiyama *et al.* (2009) hemin was required for growth of this strain.

*Spirochaeta* includes anaerobic and facultatively anaerobic spirochetes that are indigenous to aquatic environments such as the mud and water of ponds and marshes. These spirochetes occur in nature as free-living forms. That means their existence does not depend on physical associations with other organisms (Leschine *et al.*, 2006). In contrast to flagella of other bacteria, the periplasmic flagella of *Spirochetes* are permanently wound around the cell body and are entirely endocellular.

Generally, population of fermentative bacteria in both systems remained similar, indicating that electrodes poised to potentials did not influence on their developmental process.

Exoelectrogenic bacteria *Citrobacter* utilize a wide variety of substrate, such as citrate, acetate, glucose, sucrose, glycerol and lactose (Xu and Liu, 2011). They can grow not only with oxygen as an electron acceptor but also with a variety of electron accepters such as Fe(III) in the absence of oxygen (George *et al.*, 2005). It can be found in many environments such as water, wastewater and soil. Several *Citrobacter spp.* have been studied as important bioremediation bacterium for heavy metal removals, sulfate reduction, phenol degradation and chlorophenol degradation (Qiu *et al.*, 2009). *Citrobacter* species have also been found on the anodic biofilm of a diesel-degrading MFC (Morris *et al.*, 2009). The highest amount of electricity produced by *Citrobacter* was about  $205 \text{ m Am}^{-2}$ , which in comparison with the current density in this study ( $9 \text{ mA m}^{-2}$ ) was significantly higher. This could be due to the fact that in this study there were grown not with a special medium, but with the real biomass.

## 2.4. Perspectives

The present research was aimed at determining the possibility to steer the process of biogas production in AD, by coupling it to a bioelectrochemical cell. The outcomes of the project achievable on lab-scale will outline the features of the system to be taken into consideration when implementing AD-BES on pilot- and real-scale. A successfully integrated system, described in this study increased electrical outputs, substrate degradation rate and give us a possibility to steer the activity of exoelectrogens via applied potentials at the working electrodes. Regarding the energy efficiency, the oxidative conditions of the anode could be

used to carry out profitable reactions to increasing the overall energy efficiency and the value of the process.

## References

- Aelterman P, Freguia S, Keller J, Rabaey K, and Verstraete W. 2008. The anode potential regulates the bacterial activity in microbial fuel cells. *Communications in agricultural and applied biological sciences* 73(1):85-89.
- Aklujkar M, Krushkal J, DiBartolo G, Lapidus A, Land ML, and Lovley DR. 2009. The genome sequence of *Geobacter metallireducens*: features of metabolism, physiology and regulation common and dissimilar to *Geobacter sulfurreducens*. *BMC Microbiol* 9:109.
- Al Seadi T. 2008. *Biogas Handbook*. (University of Southern Denmark Esbjerg).
- Amann R, and Fuchs BM. 2008. Single-cell identification in microbial communities by improved fluorescence in situ hybridization techniques. *Nat Rev Microbiol* 6(5):339-348.
- Anders S, and Huber W. 2010. Differential expression analysis for sequence count data. *Genome biology* 11(10):R106.
- Angenent LT, Karim K, Al-Dahhan MH, Wrenn BA, and Domiguez-Espinosa R. 2004. Production of bioenergy and biochemicals from industrial and agricultural wastewater. *Trends Biotechnol* 22(9):477-485.
- Balashova VV, and Zavarzin GA. 1979. [Anaerobic reduction of ferric iron by hydrogen bacteria]. *Mikrobiologiya* 48(5):773-778.
- Balch WE, and Wolfe RS. 1976a. New Approach to the Cultivation of Methanogenic Bacteria Growth of *Methanobacterium ruminantium* in a Pressurized Atmosphere. *Appl Environ Microbiol* 32:781-791.
- Balch WE, and Wolfe RS. 1976b. New Approach to the Cultivation of Methanogenic Bacteria Growth of *Methanobacterium ruminantium* in a Pressurized Atmosphere. *Appl Environ Microbiol* 32(6):781-791.
- Batlle-Vilanova P, Puig S, Gonzalez-Olmos R, Vilajeliu-Pons A, Balaguer MD, and Colprim J. 2015. Deciphering the electron transfer mechanisms for biogas upgrading to biomethane within a mixed culture biocathode. *RSC Adv* 5(64):52243-52251.
- Bauer C, Korthals M, Gronauer A, and Lebuhn M. 2008. Methanogens in biogas production from renewable resources--a novel molecular population analysis approach. *Water science and technology : a journal of the International Association on Water Pollution Research* 58(7):1433-1439.
- Bo T, Zhu X, Zhang L, Tao Y, He X, Li D, and Yan Z. 2014. A new upgraded biogas production process: Coupling microbial electrolysis cell and anaerobic digestion in single-chamber, barrel-shape stainless steel reactor. *Electrochemistry Communications* 45:67-70.

- Bond DR, and Lovley DR. 2003. Electricity production by *Geobacter sulfurreducens* attached to electrodes. *Appl Environ Microbiol* 69(3):1548-1555.
- Bosch J, Lee KY, Hong SF, Harnisch F, Schroder U, and Meckenstock RU. 2014. Metabolic efficiency of *Geobacter sulfurreducens* growing on anodes with different redox potentials. *Curr Microbiol* 68(6):763-768.
- Braun R. 1982. *Biogas — Methangärung organischer Abfallstoffe*. (Springer Vienna).
- Breuer M, Rosso KM, Blumberger J, and Butt JN. 2015. Multi-haem cytochromes in *Shewanella oneidensis* MR-1: structures, functions and opportunities. *J R Soc Interface* 12(102):20141117.
- Brutinel ED, and Gralnick JA. 2012. Shuttling happens: soluble flavin mediators of extracellular electron transfer in *Shewanella*. *Appl Microbiol Biotechnol* 93(1):41-48.
- Butler JE, Young ND, and Lovley DR. 2010. Evolution of electron transfer out of the cell: comparative genomics of six *Geobacter* genomes. *BMC genomics* 11:40.
- Caccavo F, Jr., Lonergan DJ, Lovley DR, Davis M, Stolz JF, and McInerney MJ. 1994. *Geobacter sulfurreducens* sp. nov., a hydrogen- and acetate-oxidizing dissimilatory metal-reducing microorganism. *Appl Environ Microbiol* 60(10):3752-3759.
- Chang IS, Jang JK, Gil GC, Kim M, Kim HJ, Cho BW, and Kim BH. 2004. Continuous determination of biochemical oxygen demand using microbial fuel cell type biosensor. *Biosens Bioelectron* 19(6):607-613.
- Chang IS, Moon H, Jang JK, and Kim BH. 2005. Improvement of a microbial fuel cell performance as a BOD sensor using respiratory inhibitors. *Biosens Bioelectron* 20(9):1856-1859.
- Chaudhuri SK, and Lovley DR. 2003. Electricity generation by direct oxidation of glucose in mediatorless microbial fuel cells. *Nature biotechnology* 21(10):1229-1232.
- Cheng S, Liu H, and Logan BE. 2006. Increased performance of single-chamber microbial fuel cells using an improved cathode structure. *Electrochemistry Communications* 8(3):489-494.
- Chiao M, Lam K, Su Y, and Lin L. 2002. A miniaturized microbial fuel cell. *Technical digest of solid state sensors and actuators workshop*. Hilton Head Island:59-60.
- Clauwaert P, Aelterman P, Pham TH, De Schampelaire L, Carballa M, Rabaey K, and Verstraete W. 2008. Minimizing losses in bio-electrochemical systems: the road to applications. *Appl Microbiol Biotechnol* 79(6):901-913.
- Coppi MV, Leang C, Sandler SJ, and Lovley DR. 2001. Development of a genetic system for *Geobacter sulfurreducens*. *Appl Environ Microbiol* 67(7):3180-3187.
- Coppi MV, O'Neil RA, and Lovley DR. 2004. Identification of an Uptake Hydrogenase Required for Hydrogen-Dependent Reduction of Fe(III) and Other Electron Acceptors by *Geobacter sulfurreducens*. *Journal of Bacteriology* 186(10):3022-3028.

- Cord-Ruwisch R, Lovley D, and Schink B. 1998. Growth of *Geobacter sulfurreducens* with acetate in syntrophic cooperation with hydrogen-oxidizing anaerobic partners. *Appl Environ Microbiol* 64 (6):2232-2236.
- Cruz-Garcia C, Murray AE, Klappenbach JA, Stewart V, and Tiedje JM. 2007. Respiratory nitrate ammonification by *Shewanella oneidensis* MR-1. *J Bacteriol* 189(2):656-662.
- Czaran T, and Hoekstra RF. 2009. Microbial communication, cooperation and cheating: quorum sensing drives the evolution of cooperation in bacteria. *PLoS One* 4(8):e6655.
- Davis F, and Higson SP. 2007. Biofuel cells--recent advances and applications. *Biosens Bioelectron* 22(7):1224-1235.
- De Vrieze J, Gildemyn S, Arends JB, Vanwonterghem I, Verbeken K, Boon N, Verstraete W, Tyson GW, Hennebel T, and Rabaey K. 2014. Biomass retention on electrodes rather than electrical current enhances stability in anaerobic digestion. *Water research* 54:211-221.
- Demirel B, Neumann L, and Scherer P. 2008. Microbial Community Dynamics of a Continuous Mesophilic Anaerobic Biogas Digester Fed with Sugar Beet Silage. *Engineering in Life Sciences* 8(4):390-398.
- Deppenmeier U, and Muller V. 2008. Life close to the thermodynamic limit: how methanogenic archaea conserve energy. *Results and problems in cell differentiation* 45:123-152.
- Dolch K, Danzer J, Kabbeck T, Bierer B, Erben J, Forster AH, Maisch J, Nick P, Kerzenmacher S, and Gescher J. 2014. Characterization of microbial current production as a function of microbe-electrode-interaction. *Bioresour Technol* 157:284-292.
- Dolch K, Wuske J, and Gescher J. 2016. Genomic Barcode-Based Analysis of Exoelectrogens in Wastewater Biofilms Grown on Anode Surfaces. *J Microbiol Biotechnol* 26(3):511-520.
- Dunny GM, Brickman TJ, and Dworkin M. 2008. Multicellular behavior in bacteria: communication, cooperation, competition and cheating. *BioEssays : news and reviews in molecular, cellular and developmental biology* 30(4):296-298.
- Feist AM, Nagarajan H, Rotaru AE, Tremblay PL, Zhang T, Nevin KP, Lovley DR, and Zengler K. 2014. Constraint-based modeling of carbon fixation and the energetics of electron transfer in *Geobacter metallireducens*. *PLoS computational biology* 10(4):e1003575.
- Fonseca BM, Paquete CM, Neto SE, Pacheco I, Soares CM, and Louro RO. 2013. Mind the gap: cytochrome interactions reveal electron pathways across the periplasm of *Shewanella oneidensis* MR-1. *Biochem J* 449(1):101-108.
- Fredrickson JK, Romine MF, Beliaev AS, Auchtung JM, Driscoll ME, Gardner TS, Neelson KH, Osterman AL, Pinchuk G, Reed JL et al. . 2008. Towards environmental systems biology of *Shewanella*. *Nat Rev Micro* 6(8):592-603.

- Freguia S, Rabaey K, Yuan Z, and Keller J. 2008. Syntrophic processes drive the conversion of glucose in microbial fuel cell anodes. *Environmental science & technology* 42(21):7937-7943.
- George MG. 2005. *Bergey's manual of systematic bacteriology, The Proteobacteria: Part B the Gammaproteobacteria*. 2.
- Gil G-C, Chang I-S, Kim BH, Kim M, Jang J-K, Park HS, and Kim HJ. 2003. Operational parameters affecting the performance of a mediator-less microbial fuel cell. *Biosensors and Bioelectronics* 18(4):327-334.
- Giuffrè A, Borisov VB, Arese M, Sarti P, and Forte E. 2014. Cytochrome bd oxidase and bacterial tolerance to oxidative and nitrosative stress. *Biochim Biophys Acta* 1837(7):1178-1187.
- Gorby YA, Yanina S, McLean JS, Rosso KM, Moyles D, Dohnalkova A, Beveridge TJ, Chang IS, Kim BH, Kim KS et al. . 2006. Electrically conductive bacterial nanowires produced by *Shewanella oneidensis* strain MR-1 and other microorganisms. *Proc Natl Acad Sci U S A* 103(30):11358-11363.
- Griffin M, McMahan K, Mackie R, and Raskin L. 1998. *Methanogenic Population Dynamics during Start-Up of Anaerobic Digesters Treating Municipal Solid Waste and Biosolids*. John Wiley & Sons.
- Gülzow. 2010. *Guide to biogas: from production to use*. (Fachagentur Nachwachsende Rohstoffe ).
- Gülzow. 2013. *Fachagentur Nachwachsende Rohstoffe e. V.*
- Gussow D, and Clackson T. 1989. Direct clone characterization from plaques and colonies by the polymerase chain reaction. *Nucleic Acids Res* 17(10):4000.
- Hao L, Lu F, Li L, Wu Q, Shao L, and He P. 2013. Self-adaption of methane-producing communities to pH disturbance at different acetate concentrations by shifting pathways and population interaction. *Bioresour Technol* 140:319-327.
- Harnisch F, and Schroder U. 2010. From MFC to MXC: chemical and biological cathodes and their potential for microbial bioelectrochemical systems. *Chemical Society Reviews* 39(11):4433-4448.
- Hau HH, and Gralnick JA. 2007. Ecology and biotechnology of the genus *Shewanella*. *Annual review of microbiology* 61:237-258.
- Heidelberg JF, Paulsen IT, Nelson KE, Gaidos EJ, Nelson WC, Read TD, Eisen JA, Seshadri R, Ward N, Methe B et al. . 2002. Genome sequence of the dissimilatory metal ion-reducing bacterium *Shewanella oneidensis*. *Nature biotechnology* 20(11):1118-1123.
- Holdeman L, and Johnson J. 1982. Description of *Bacteroides loescheii* sp. nov. and Emendation of the Descriptions of *Bacteroides melaninogenicus* (Oliver and Wherry) Roy and Kelly 1939 and *Bacteroides denticola* Shah and Collins 1981. *International journal of systematic bacteriology* 32(4):399-409.

- Holmes DE, Bond DR, and Lovley DR. 2004. Electron Transfer by *Desulfobulbus propionicus* to Fe(III) and Graphite Electrodes. *Applied and Environmental Microbiology* 70(2):1234-1237.
- Holmes DE, Chaudhuri SK, Nevin KP, Mehta T, Methe BA, Liu A, Ward JE, Woodard TL, Webster J, and Lovley DR. 2006. Microarray and genetic analysis of electron transfer to electrodes in *Geobacter sulfurreducens*. *Environ Microbiol* 8(10):1805-1815.
- Hori T, Haruta S, Ueno Y, Ishii M, and Igarashi Y. 2006. Dynamic transition of a methanogenic population in response to the concentration of volatile fatty acids in a thermophilic anaerobic digester. *Appl Environ Microbiol* 72(2):1623-1630.
- Hunt KA, Flynn JM, Naranjo B, Shikhare ID, and Gralnick JA. 2010. Substrate-level phosphorylation is the primary source of energy conservation during anaerobic respiration of *Shewanella oneidensis* strain MR-1. *J Bacteriol* 192(13):3345-3351.
- Ieropoulos I, Melhuish C, and Greenman J. 2003. Artificial Metabolism: Towards True Energetic Autonomy in Artificial Life. (*ECAL*):792-799.
- Ishii S, Hotta Y, and Watanabe K. 2008. Methanogenesis versus electrogenesis: morphological and phylogenetic comparisons of microbial communities. *Biosci Biotechnol Biochem* 72(2):286-294.
- Ishii S, Suzuki S, Norden-Krichmar TM, Phan T, Wanger G, Nealson KH, Sekiguchi Y, Gorby YA, and Bretschger O. 2014. Microbial population and functional dynamics associated with surface potential and carbon metabolism. *Isme j* 8(5):963-978.
- Ishii S, Suzuki S, Norden-Krichmar TM, Wu A, Yamanaka Y, Nealson KH, and Bretschger O. 2013. Identifying the microbial communities and operational conditions for optimized wastewater treatment in microbial fuel cells. *Water research* 47(19):7120-7130.
- Jang JK, Pham TH, Chang IS, Kang KH, Moon H, Cho KS, and Kim BH. 2004. Construction and operation of a novel mediator- and membrane-less microbial fuel cell. *Process Biochemistry* 39(8):1007-1012.
- Jia J, Tang Y, Liu B, Wu D, Ren N, and Xing D. 2013. Electricity generation from food wastes and microbial community structure in microbial fuel cells. *Bioresour Technol* 144:94-99.
- Jiao Y, and Newman DK. 2007. The *pio* operon is essential for phototrophic Fe(II) oxidation in *Rhodospseudomonas palustris* TIE-1. *J Bacteriol* 189(5):1765-1773.
- Kaltschmitt M, Merten D, Fröhlich M, and Nill M. 2003. *Energiegewinnung aus Biomasse*.
- Kappler A, and Straub KL. 2005. Geomicrobiological cycling of iron. *Reviews in Mineralogy and Geochemistry* 59:85-108.
- Kaur A, Boghani HC, Michie I, Dinsdale RM, Guwy AJ, and Premier GC. 2014. Inhibition of methane production in microbial fuel cells: operating strategies which select electrogens over methanogens. *Bioresour Technol* 173:75-81.

- Kaur A, Kim JR, Michie I, Dinsdale RM, Guwy AJ, Premier GC, and Sustainable Environment Research C. 2013. Microbial fuel cell type biosensor for specific volatile fatty acids using acclimated bacterial communities. *Biosens Bioelectron* 47:50-55.
- Kerisit S, Rosso KM, Dupuis M, and Valiev M. 2007. Molecular Computational Investigation of Electron-Transfer Kinetics Across Cytochrome-Iron Oxide Interfaces. *J Phys Chem* 111:11363-11375.
- Kiely PD, Regan JM, and Logan BE. 2011. The electric picnic: synergistic requirements for exoelectrogenic microbial communities. *Curr Opin Biotechnol* 22(3):378-385.
- Kim BC, Ikeda T, Park HS, Kim HJ, Hyun MS, Kano K, Takagi K, and Tatsumi H. 1999. Electrochemical activity of an Fe(III)-reducing bacterium, *Shewanella putrefaciens* IR-1, in the presence of alternative electron acceptors. *Biotechnology Techniques* 13:475-478.
- Kim BH, Chang IS, Gil GC, Park HS, and Kim HJ. 2003. Novel BOD (biological oxygen demand) sensor using mediator-less microbial fuel cell. *Biotechnology letters* 25(7):541-545.
- Kim JR, Jung SH, Regan JM, and Logan BE. 2007. Electricity generation and microbial community analysis of alcohol powered microbial fuel cells. *Bioresour Technol* 98(13):2568-2577.
- Kim JR, Min B, and Logan BE. 2005. Evaluation of procedures to acclimate a microbial fuel cell for electricity production. *Appl Microbiol Biotechnol* 68(1):23-30.
- Kim T, An J, Jang JK, and Chang IS. 2015. Coupling of anaerobic digester and microbial fuel cell for COD removal and ammonia recovery. *Bioresour Technol* 195:217-222.
- Kipf E, Koch J, Geiger B, Erben J, Richter K, Gescher J, Zengerle R, and Kerzenmacher S. 2013. Systematic screening of carbon-based anode materials for microbial fuel cells with *Shewanella oneidensis* MR-1. *Bioresour Technol* 146:386-392.
- Klocke M, Nettmann E, Bergmann I, Mundt K, Souidi K, Mumme J, and Linke B. 2008. Characterization of the methanogenic Archaea within two-phase biogas reactor systems operated with plant biomass. *Systematic and applied microbiology* 31(3):190-205.
- Kloke A, Rubenwolf S, Bucking C, Gescher J, Kerzenmacher S, Zengerle R, and von Stetten F. 2010. A versatile miniature bioreactor and its application to bioelectrochemistry studies. *Biosens Bioelectron* 25(12):2559-2565.
- Kotloski NJ, and Gralnick JA. 2013. Flavin Electron Shuttles Dominate Extracellular Electron Transfer by *Shewanella oneidensis*. *mBio* 4(1).
- Kraemer SM, Butler A, Borer P, and Cervini-Silva J. 2005. Siderophores and the dissolution of iron-bearing minerals in marine systems. *Reviews in Mineralogy and Geochemistry* 59:53-84.
- Krober M, Bekel T, Diaz NN, Goesmann A, Jaenicke S, Krause L, Miller D, Runte KJ, Viehöver P, Puhler A et al. . 2009. Phylogenetic characterization of a biogas plant microbial community

- integrating clone library 16S-rDNA sequences and metagenome sequence data obtained by 454-pyrosequencing. *Journal of biotechnology* 142(1):38-49.
- Langmead B, and Salzberg SL. 2012. Fast gapped-read alignment with Bowtie 2. *Nature methods* 9(4):357-359.
- Leang C, Qian X, Mester T, and Lovley DR. 2010. Alignment of the c-type cytochrome OmcS along pili of *Geobacter sulfurreducens*. *Appl Environ Microbiol* 76(12):4080-4084.
- Lebuhn M, Bauer C, and Gronauer A. 2008. Probleme der Biogasproduktion aus nachwachsenden Rohstoffen im Langzeitbetrieb und molekularbiologische Analytik. *VDLUFA-Schriftenreihe* 64:118-125.
- Leschine S, Paster BJ, and Canale-Parola E. 2006. Free-Living Saccharolytic Spirochetes: The Genus *Spirochaeta*. 195-210.
- Lies DP, Hernandez ME, Kappler A, Mielke RE, Gralnick JA, and Newman DK. 2005. *Shewanella oneidensis* MR-1 uses overlapping pathways for iron reduction at a distance and by direct contact under conditions relevant for Biofilms. *Appl Environ Microbiol* 71(8):4414-4426.
- Lin WC, Coppi MV, and Lovley DR. 2004. *Geobacter sulfurreducens* can grow with oxygen as a terminal electron acceptor. *Appl Environ Microbiol* 70(4):2525-2528.
- Liu FH, Wang SB, Zhang JS, Zhang J, Yan X, Zhou HK, Zhao GP, and Zhou ZH. 2009. The structure of the bacterial and archaeal community in a biogas digester as revealed by denaturing gradient gel electrophoresis and 16S rDNA sequencing analysis. *Journal of applied microbiology* 106(3):952-966.
- Liu H, Cheng S, and Logan BE. 2005. Power generation in fed-batch microbial fuel cells as a function of ionic strength, temperature, and reactor configuration. *Environmental science & technology* 39(14):5488-5493.
- Liu H, Cheng S, and Logan BE. 2005a. Production of electricity from acetate or butyrate using a single-chamber microbial fuel cell. *Environmental science & technology* 39:652-658.
- Liu H, Grot S, and Logan BE. 2005b. Electrochemically assisted microbial production of hydrogen from acetate. *Environmental science & technology* 39(11):4317-4320.
- Liu H, and Logan BE. 2004. Electricity generation using an air-cathode single chamber microbial fuel cell in the presence and absence of a proton exchange membrane. *Environmental science & technology* 38(14):4040-4046.
- Liu Y, and Bond DR. 2012. Long-distance electron transfer by *G. sulfurreducens* biofilms results in accumulation of reduced c-type cytochromes. *ChemSusChem* 5(6):1047-1053.
- Lloyd JR, Leang C, and Hodges Myerson AL. 2003. Biochemical and genetic characterization of PpcA, a periplasmic c-type cytochrome in *Geobacter sulfurreducens*. *Biochemical Journal* 369(Pt. 1):153-161.

- Logan B. 2008. Microbial fuel cells. (John Wiley & Sons, Inc.).
- Logan BE. 2009. Exoelectrogenic bacteria that power microbial fuel cells. *Nat Rev Microbiol* 7(5):375-381.
- Logan BE, and Regan JM. 2006. Electricity-producing bacterial communities in microbial fuel cells. *Trends in microbiology* 14(12):512-518.
- Love MI, Huber W, and Anders S. 2014. Moderated estimation of fold change and dispersion for RNA-seq data with DESeq2. *Genome biology* 15(12):550.
- Lovley DR. 2006. Bug juice: harvesting electricity with microorganisms. *Nat Rev Microbiol* 4(7):497-508.
- Lovley DR. 2008. The microbe electric: conversion of organic matter to electricity. *Curr Opin Biotechnol* 19(6):564-571.
- Lovley DR, Giovannoni SJ, White DC, Champine JE, Phillips EJ, Gorby YA, and Goodwin S. 1993. *Geobacter metallireducens* gen. nov. sp. nov., a microorganism capable of coupling the complete oxidation of organic compounds to the reduction of iron and other metals. *Archives of microbiology* 159(4):336-344.
- Lovley DR, Holmes DE, and Nevin KP. 2004. Dissimilatory Fe(III) and Mn(IV) reduction. *Advances in microbial physiology* 49:219-286.
- Lovley DR, and Phillips EJ. 1987. Competitive mechanisms for inhibition of sulfate reduction and methane production in the zone of ferric iron reduction in sediments. *Appl Environ Microbiol* 53(11):2636-2641.
- Lovley DR, and Phillips EJ. 1989. Requirement for a Microbial Consortium To Completely Oxidize Glucose in Fe(III)-Reducing Sediments. *Appl Environ Microbiol* 55(12):3234-3236.
- Lynd LR, Weimer PJ, van Zyl WH, and Pretorius IS. 2002. Microbial Cellulose Utilization: Fundamentals and Biotechnology. *Microbiology and Molecular Biology Reviews* 66(3):506-577.
- Maestrojuan G, Xun L, and Zhang L. 1990. Transfer of *Methanogenium bourgense*, *Methanogenium marisnigri*, *Methanogenium olentangyi*, and *Methanogenium thermophilicum* to the Genus *Methanoculleus* gen. nov., Emendation of *Methanoculleus marisnigri* and *Methanogenium*, and Description of New Strains of *Methanoculleus bourgense* and *Methanoculleus marisnigri*. *International journal of systematic bacteriology*.
- Malvankar NS, Vargas M, Nevin KP, Franks AE, Leang C, Kim BC, Inoue K, Mester T, Covalla SF, Johnson JP et al. . 2011. Tunable metallic-like conductivity in microbial nanowire networks. *Nature nanotechnology* 6(9):573-579.

- Marshall CW, and May HD. 2009. Electrochemical evidence of direct electrode reduction by a thermophilic Gram-positive bacterium, *Thermincola ferriacetica*. *Energy & Environmental Science* 2(6):699-705.
- Marsili E, Baron DB, Shikhare ID, Coursolle D, Gralnick JA, and Bond DR. 2008. *Shewanella* secretes flavins that mediate extracellular electron transfer. *Proc Natl Acad Sci U S A* 105(10):3968-3973.
- McHugh S, Carton M, Collins G, and O'Flaherty V. 2004. Reactor performance and microbial community dynamics during anaerobic biological treatment of wastewaters at 16-37 degrees C. *FEMS Microbiol Ecol* 48(3):369-378.
- McLean JS, Wanger G, Gorby YA, Wainstein M, McQuaid J, Ishii SI, Bretschger O, Beyenal H, and Neilson KH. 2010. Quantification of electron transfer rates to a solid phase electron acceptor through the stages of biofilm formation from single cells to multicellular communities. *Environmental science & technology* 44(7):2721-2727.
- Mehta T, Coppi MV, Childers SE, and Lovley DR. 2005. Outer membrane c-type cytochromes required for Fe(III) and Mn(IV) oxide reduction in *Geobacter sulfurreducens*. *Appl Environ Microbiol* 71(12):8634-8641.
- Meitl LA, Eggleston CM, Colberg PJS, Khare N, Reardon CL, and Shi L. 2009. Electrochemical interaction of *Shewanella oneidensis* MR-1 and its outer membrane cytochromes OmcA and MtrC with hematite electrodes. *Geochimica et Cosmochimica Acta* 73(18):5292-5307.
- Meshulam-Simon G, Behrens S, Choo AD, and Spormann AM. 2007. Hydrogen metabolism in *Shewanella oneidensis* MR-1. *Appl Environ Microbiol* 73(4):1153-1165.
- Min B, Kim J, Oh S, Regan JM, and Logan BE. 2005. Electricity generation from swine wastewater using microbial fuel cells. *Water research* 39(20):4961-4968.
- Mohanakrishna G, Venkata Mohan S, and Sarma PN. 2010. Bio-electrochemical treatment of distillery wastewater in microbial fuel cell facilitating decolorization and desalination along with power generation. *Journal of hazardous materials* 177(1-3):487-494.
- Moon H, Chang IS, Jang JK, and Kim BH. 2005. Residence time distribution in microbial fuel cell and its influence on COD removal with electricity generation. *Biochemical Engineering Journal* 27(1):59-65.
- Moon H, Chang IS, and Kim BH. 2006. Continuous electricity production from artificial wastewater using a mediator-less microbial fuel cell. *Bioresource Technology* 97(4):621-627.
- Morris JM, Jin S, Crimi B, and Pruden A. 2009. Microbial fuel cell in enhancing anaerobic biodegradation of diesel. *Chemical Engineering Journal* 146(2):161-167.

- Muller N, Worm P, Schink B, Stams AJ, and Plugge CM. 2010. Syntrophic butyrate and propionate oxidation processes: from genomes to reaction mechanisms. *Environ Microbiol Rep* 2(4):489-499.
- Myers CR, and Myers JM. 2003. Cell surface exposure of the outer membrane cytochromes of *Shewanella oneidensis* MR-1. *Letters in applied microbiology* 37(3):254-258.
- Nalinga Y, and Legonda I. 2015. Experimental investigation on biogas production from anaerobic co-digestion international *Journal of Innovative research in technology and science* 4(2).
- Nealson KH, Belz A, and McKee B. 2002. Breathing metals as a way of life: geobiology in action. *Antonie van Leeuwenhoek* 81(1-4):215-222.
- Nevin KP, Kim BC, Glaven RH, Johnson JP, Woodard TL, Methe BA, Didonato RJ, Covalla SF, Franks AE, Liu A et al. . 2009. Anode biofilm transcriptomics reveals outer surface components essential for high density current production in *Geobacter sulfurreducens* fuel cells. *PLoS One* 4(5):e5628.
- Nevin KP, and Lovley DR. 2002. Mechanisms for Fe(III) Oxide Reduction in Sedimentary Environments. *Geomicrobiology Journal* 19(2):141-159.
- Nevin KP, Richter H, Covalla SF, Johnson JP, Woodard TL, Orloff AL, Jia H, Zhang M, and Lovley DR. 2008. Power output and columbic efficiencies from biofilms of *Geobacter sulfurreducens* comparable to mixed community microbial fuel cells. *Environ Microbiol* 10(10):2505-2514.
- Nevin KP, Zhang P, Franks AE, Woodard TL, and Lovley DR. 2011. Anaerobes unleashed: Aerobic fuel cells of *Geobacter sulfurreducens*. *Journal of Power Sources* 196(18):7514-7518.
- Nielsen LP, Risgaard-Petersen N, Fossing H, Christensen PB, and Sayama M. 2010. Electric currents couple spatially separated biogeochemical processes in marine sediment. *Nature* 463(7284):1071-1074.
- Niessen J, Schröder U, and Scholz F. 2004. Exploiting complex carbohydrates for microbial electricity generation – a bacterial fuel cell operating on starch. *Electrochemistry Communications* 6(9):955-958.
- Nishiyama A, Komitova M, Suzuki R, and Zhu X. 2009. Polydendrocytes (NG2 cells): multifunctional cells with lineage plasticity. *Nature reviews Neuroscience* 10(1):9-22.
- Oh S, and Logan BE. 2005a. Hydrogen and electricity production from a food processing wastewater using fermentation and microbial fuel cell technologies. *Water research* 39(19):4673-4682.
- Oh S, Min B, and Logan B. 2004. Cathode Performance as a Factor in Electricity Generation in Microbial Fuel Cells. *Environmental science & technology*(38):4900-4904.
- Oh SE, and Logan BE. 2005b. Hydrogen and electricity production from a food processing wastewater using fermentation and microbial fuel cell technologies. *Water research* 39(19):4673-4682.

- Okamoto A, Kalathil S, Deng X, Hashimoto K, Nakamura R, and Neilson KH. 2014. Cell-secreted flavins bound to membrane cytochromes dictate electron transfer reactions to surfaces with diverse charge and pH. *Sci Rep* 4:5628.
- Paquete CM, and Louro RO. 2010. Molecular details of multielectron transfer: the case of multiheme cytochromes from metal respiring organisms. *Dalton Trans* 39(18):4259-4266.
- Park D, and Zeikus G. 2000. Electricity Generation in Microbial Fuel Cells Using Neutral Red as an Electronophore. *Appl Environ Microbiol* 66(4):1292–1297.
- Park DH, and Zeikus JG. 2003. Improved fuel cell and electrode designs for producing electricity from microbial degradation. *Biotechnology and bioengineering* 81(3):348-355.
- Pierre JL, Fontecave M, and Crichton RR. 2002. Chemistry for an essential biological process: the reduction of ferric iron. *Biometals : an international journal on the role of metal ions in biology, biochemistry, and medicine* 15(4):341-346.
- Pirbadian S, Barchinger SE, Leung KM, Byun HS, Jangir Y, Bouhenni RA, Reed SB, Romine MF, Saffarini DA, Shi L et al. . 2014. *Shewanella oneidensis* MR-1 nanowires are outer membrane and periplasmic extensions of the extracellular electron transport components. *Proc Natl Acad Sci U S A* 111(35):12883-12888.
- Potter MC. 1911. Electrical effects accompanying the decomposition of organic compounds. *Proc R Soc London*(84):260-276.
- Qian X, Mester T, Morgado L, Arakawa T, Sharma ML, Inoue K, Joseph C, Salueiro CA, Maroney MJ, and Lovley DR. 2011. Biochemical characterization of purified OmcS, a c-type cytochrome required for insoluble Fe(III) reduction in *Geobacter sulfurreducens*. *Biochim Biophys Acta* 1807(4):404-412.
- Qiu X, Wu P, Zhang H, Li M, and Yan Z. 2009. Isolation and characterization of *Arthrobacter* sp. HY2 capable of degrading a high concentration of p-nitrophenol. *Bioresour Technol* 100(21):5243-5248.
- Rabaey K, Boon N, Siciliano SD, Verhaege M, and Verstraete W. 2004. Biofuel cells select for microbial consortia that self-mediate electron transfer. *Appl Environ Microbiol* 70(9):5373-5382.
- Rabaey K, Van de Sompel K, Maignien L, Boon N, Aelterman P, Clauwaert P, De Schampelaire L, The Pham H, Vermeulen J, Verhaege M et al. . 2006. Microbial Fuel Cells for Sulfide. *Environmental science & technology*(40):5218-5224.
- Rabaey K, and Verstraete W. 2005. Microbial fuel cells: novel biotechnology for energy generation. *Trends Biotechnol* 23(6):291-298.
- Read ST, Dutta P, Bond PL, Keller J, and Rabaey K. 2010. Initial development and structure of biofilms on microbial fuel cell anodes. *BMC Microbiology* 10(1):1-10.

- Reguera G, McCarthy KD, Mehta T, Nicoll JS, Tuominen MT, and Lovley DR. 2005. Extracellular electron transfer via microbial nanowires. *Nature* 435(7045):1098-1101.
- Reguera G, Nevin KP, Nicoll JS, Covalla SF, Woodard TL, and Lovley DR. 2006. Biofilm and nanowire production leads to increased current in *Geobacter sulfurreducens* fuel cells. *Appl Environ Microbiol* 72(11):7345-7348.
- Reguera G, Pollina RB, Nicoll JS, and Lovley DR. 2007. Possible nonconductive role of *Geobacter sulfurreducens* pilus nanowires in biofilm formation. *J Bacteriol* 189(5):2125-2127.
- Rodney MD. 2002. Biofilms: Microbial Life on Surfaces. *Emerging Infectious Disease journal* 8(9):881.
- Rosenbaum M, Schröder U, and Scholz F. 2006. Investigation of the electrocatalytic oxidation of formate and ethanol at platinum black under microbial fuel cell conditions. *Journal of Solid State Electrochemistry* 10(10):872-878.
- Rosenbaum MA, Bar HY, Beg QK, Segre D, Booth J, Cotta MA, and Angenent LT. 2011. *Shewanella oneidensis* in a lactate-fed pure-culture and a glucose-fed co-culture with *Lactococcus lactis* with an electrode as electron acceptor. *Bioresour Technol* 102(3):2623-2628.
- Rosso KM, Zachara JM, Fredrickson JK, Gorby YA, and Smith SC. 2003. Nonlocal bacterial electron transfer to hematite surfaces. *Geochimica et Cosmochimica Acta* 67(5):1081-1087.
- Russell MJ. 2002. Chemiosmotic coupling and transition element clusters in the onset of life and photosynthesis. *Geochemical News* 113:6-12.
- Saitou N, and Nei M. 1987. The neighbor-joining method: a new method for reconstructing phylogenetic trees. *Molecular biology and evolution* 4(4):406-425.
- Sambrook J, Fritsch EF, Maniatis T, and Russell DW. 1989. *Molecular cloning*. Cold Spring Harbor Laboratory Press, Cold Spring Harbor, NY.
- Santos TC, Silva MA, Morgado L, Dantas JM, and Salgueiro CA. 2015. Diving into the redox properties of *Geobacter sulfurreducens* cytochromes: a model for extracellular electron transfer. *Dalton Trans* 44(20):9335-9344.
- Sarmiento F, Leigh JA, and Whitman WB. 2011. Genetic systems for hydrogenotrophic methanogens. *Methods Enzymol* 494:43-73.
- Sasaki K, Sasaki D, Morita M, Hirano S, Matsumoto N, Ohmura N, and Igarashi Y. 2010. Bioelectrochemical system stabilizes methane fermentation from garbage slurry. *Bioresour Technol* 101(10):3415-3422.
- Satoh H, Miura Y, Tsushima I, and Okabe S. 2007. Layered structure of bacterial and archaeal communities and their in situ activities in anaerobic granules. *Appl Environ Microbiol* 73(22):7300-7307.
- Schechter M, Schechter A, Rozenfeld S, Efrat E, and Cahan R. 2014. *Anode Biofilm*.
- Schlegel HG, and Fuchs G. 2007. *Allgemeine Mikrobiologie*. Thieme.

- Schnurer A, and Nordberg A. 2008. Ammonia, a selective agent for methane production by syntrophic acetate oxidation at mesophilic temperature. *Water science and technology : a journal of the International Association on Water Pollution Research* 57(5):735-740.
- Schnürer A, Zellner G, and Svensson BH. 1999. Mesophilic syntrophic acetate oxidation during methane formation in biogas reactors. *FEMS Microbiology Ecology* 29(3):249-261.
- Schroder U. 2007. Anodic electron transfer mechanisms in microbial fuel cells and their energy efficiency. *Phys Chem Chem Phys* 9(21):2619-2629.
- Schroder U, Niessen J, and Scholz F. 2003. A generation of microbial fuel cells with current outputs boosted by more than one order of magnitude. *Angewandte Chemie (International ed in English)* 42(25):2880-2883.
- Schuetz B, Schicklberger M, Kuermann J, Spormann AM, and Gescher J. 2009. Periplasmic electron transfer via the c-type cytochromes MtrA and FccA of *Shewanella oneidensis* MR-1. *Appl Environ Microbiol* 75(24):7789-7796.
- Schwalb C, Chapman SK, and Reid GA. 2002. The membrane-bound tetrahaem c-type cytochrome CymA interacts directly with the soluble fumarate reductase in *Shewanella*. *Biochemical Society transactions* 30(4):658-662.
- Schwalb C, Chapman SK, and Reid GA. 2003. The tetraheme cytochrome CymA is required for anaerobic respiration with dimethyl sulfoxide and nitrite in *Shewanella oneidensis*. *Biochemistry* 42(31):9491-9497.
- Scott JH, and Nealson KH. 1994. A biochemical study of the intermediary carbon metabolism of *Shewanella putrefaciens*. *J Bacteriol* 176(11):3408-3411.
- Serres MH, and Riley M. 2006. Genomic analysis of carbon source metabolism of *Shewanella oneidensis* MR-1: Predictions versus experiments. *J Bacteriol* 188(13):4601-4609.
- Shirodkar S, Reed S, Romine M, and Saffarini D. 2011. The octahaem SirA catalyses dissimilatory sulfite reduction in *Shewanella oneidensis* MR-1. *Environ Microbiol* 13(1):108-115.
- Shukla AK, Suresh P, Berchmans S, and Rahjendran A. 2004. Biological fuel cells and their applications. *Curr Science* 87:455-468.
- Sisler FD. 1962. Electrical energy from microbial processes. *J Wash Acad Sci* 52:182-187.
- Smith JA, Tremblay PL, Shrestha PM, Snoeyenbos-West OL, Franks AE, Nevin KP, and Lovley DR. 2014. Going wireless: Fe(III) oxide reduction without pili by *Geobacter sulfurreducens* strain JS-1. *Appl Environ Microbiol* 80(14):4331-4340.
- Stantscheff R, Kuever J, Rabenstein A, Seyfarth K, Droge S, and König H. 2014. Isolation and differentiation of methanogenic Archaea from mesophilic corn-fed on-farm biogas plants with special emphasis on the genus *Methanobacterium*. *Appl Microbiol Biotechnol* 98(12):5719-5735.

- Stern. 2004. Economic Growth and Energy. *Encyclopedia of Energy* 2.
- Straub KL, Benz M, and Schink B. 2001. Iron metabolism in anoxic environments at near neutral pH. *FEMS Microbiol Ecol* 34(3):181-186.
- Stroot PG, McMahon KD, Mackie RI, and Raskin L. 2001. Anaerobic codigestion of municipal solid waste and biosolids under various mixing conditions--I. Digester performance. *Water research* 35(7):1804-1816.
- Strycharz-Glaven SM, Snider RM, Guiseppi-Elie A, and Tender LM. 2011. On the electrical conductivity of microbial nanowires and biofilms. *Energy & Environmental Science* 4(11):4366-4379.
- Sturm-Richter K. 2014. Etablierung und Intensivierung von Mikroben-Anoden-Interaktionen in synthetischen und natürlichen exoelektrogenen Stämmen.
- Sturm-Richter K, Golitsch F, Sturm G, Kipf E, Dittrich A, Beblawy S, Kerzenmacher S, and Gescher J. 2015. Unbalanced fermentation of glycerol in *Escherichia coli* via heterologous production of an electron transport chain and electrode interaction in microbial electrochemical cells. *Bioresour Technol* 186:89-96.
- Summers ZM, Ueki T, Ismail W, Haveman SA, and Lovley DR. 2012. Laboratory evolution of *Geobacter sulfurreducens* for enhanced growth on lactate via a single-base-pair substitution in a transcriptional regulator. *Isme j* 6(5):975-983.
- Suzuki S, Karube I, and Matsunaga T. 1978. Application of a biochemical fuel cell to wastewater. *Biotechnol Bioeng Symp* 8:501-511.
- Tartakovsky B, and Guiot SR. 2006. A comparison of air and hydrogen peroxide oxygenated microbial fuel cell reactors. *Biotechnology progress* 22(1):241-246.
- Tartakovsky B, Mehta P, Bourque JS, and Guiot SR. 2011. Electrolysis-enhanced anaerobic digestion of wastewater. *Bioresour Technol* 102(10):5685-5691.
- Thamdrup B, Rossello-Mora R, and Amann R. 2000. Microbial manganese and sulfate reduction in Black Sea shelf sediments. *Appl Environ Microbiol* 66(7):2888-2897.
- Thauer RK, Kaster AK, Seedorf H, Buckel W, and Hedderich R. 2008. Methanogenic archaea: ecologically relevant differences in energy conservation. *Nat Rev Microbiol* 6(8):579-591.
- Tremblay PL, Aklujkar M, Leang C, Nevin KP, and Lovley D. 2012. A genetic system for *Geobacter metallireducens*: role of the flagellin and pilin in the reduction of Fe(III) oxide. *Environ Microbiol Rep* 4(1):82-88.
- Ueki T, and Lovley DR. 2010. Genome-wide gene regulation of biosynthesis and energy generation by a novel transcriptional repressor in *Geobacter* species. *Nucleic Acids Res* 38(3):810-821.
- Vargas M, Kashefi K, Blunt-Harris EL, and Lovley DR. 1998. Microbiological evidence for Fe(III) reduction on early Earth. *Nature* 395(6697):65-67.

- Venkataraman A, Rosenbaum MA, Perkins SD, Werner JJ, and Angenent LT. 2011. Metabolite-based mutualism between *Pseudomonas aeruginosa* PA14 and *Enterobacter aerogenes* enhances current generation in bioelectrochemical systems. *Energy & Environmental Science* 4(11):4550.
- Venkateswaran K, Moser DP, Dollhopf ME, Lies DP, Saffarini DA, MacGregor BJ, Ringelberg DB, White DC, Nishijima M, Sano H et al. . 1999. Polyphasic taxonomy of the genus *Shewanella* and description of *Shewanella oneidensis* sp. nov. *International journal of systematic bacteriology* 49 Pt 2:705-724.
- Verstraete W, Morgan-Sagastume F, Aiyuk S, Waweru M, Rabaey K, and Lissens G. 2005. Anaerobic digestion as a core technology in sustainable management of organic matter. *Water science and technology : a journal of the International Association on Water Pollution Research* 52(1-2):59-66.
- von Canstein H, Ogawa J, Shimizu S, and Lloyd JR. 2008. Secretion of flavins by *Shewanella* species and their role in extracellular electron transfer. *Appl Environ Microbiol* 74(3):615-623.
- Wagner RC, Call DF, and Logan BE. 2010. Optimal potential set anode potentials vary in Bioelectrochemical systems. *Environmental science & technology* 44:6036-6041.
- Wandrey C, and Aivasidis A. 1983. Continuous Anaerobic Digestion with *Methanosarcina barkeri*.
- Wei J, Liang P, Cao X, and Huang X. 2010. A new insight into potential regulation on growth and power generation of *Geobacter sulfurreducens* in microbial fuel cells based on energy viewpoint. *Environmental science & technology* 44(8):3187-3191.
- Weiland P. 2010. Biogas production: current state and perspectives. *Appl Microbiol Biotechnol* 85(4):849-860.
- Wilkinson S. 2000. "Gastrobots"—Benefits and Challenges of Microbial Fuel Cells in Food Powered Robot Applications. *Autonomous Robots* 9:99-111.
- Xiao B, Yang F, and Liu J. 2013. Evaluation of electricity production from alkaline pretreated sludge using two-chamber microbial fuel cell. *Journal of hazardous materials* 254-255:57-63.
- Xu S, and Liu H. 2011. New exoelectrogen *Citrobacter* sp. SX-1 isolated from a microbial fuel cell. *Journal of applied microbiology* 111(5):1108-1115.
- Zacharoff L, Chan CH, and Bond DR. 2016. Reduction of low potential electron acceptors requires the CbcL inner membrane cytochrome of *Geobacter sulfurreducens*. *Bioelectrochemistry* 107:7-13.
- Zamalloa C, Arends JB, Boon N, and Verstraete W. 2013. Performance of a lab-scale bio-electrochemical assisted septic tank for the anaerobic treatment of black water. *N Biotechnol* 30(5):573-580.

- Zhao F, Slade RCT, and Varcoe JR. 2009. Techniques for the study and development of microbial fuel cells: an electrochemical perspective. *Chemical Society Reviews* 38(7):1926-1939.
- Zuo Y, Maness PC, and Logan BE. Electricity production from steam-exploded corn stover biomass. *Energy Fuel* 20:1716-1721.
- Zverlov VV, and Schwarz WH. 2008. Bacterial cellulose hydrolysis in anaerobic environmental subsystems--*Clostridium thermocellum* and *Clostridium stercorarium*, thermophilic plant-fiber degraders. *Ann N Y Acad Sci* 1125:298-307.
2006. Real-Time PCR Applications Guide. Bio-Rad Laboratories.

## Appendix

Supplementary Table 1. *G. sulfurreducens* gene expression.

ID	name	product	GsA_mixA	
			log2fc	padj
GSU0003	gyrB	DNA gyrase subunit B	-1,353	0,005
GSU0004	gyrA	DNA gyrase subunit A	-1,870	0,000
GSU0007	0	sensor histidine kinase; HAMP and PAS domain-containing	-1,497	0,007
GSU0008	0	response receiver sensor histidine kinase; PAS domain-containing	-1,565	0,041
GSU0009	fgrK	sensor histidine kinase of FgrL; PAS domain-containing	-2,162	0,008
GSU0010	fgrL	flagellar biogenesis master response receiver sensor histidine kinase; PAS and GAF domain-containing	-1,868	0,010
GSU0012	hemY	protoporphyrinogen oxidase	1,315	0,000
GSU0013	0	MarR family winged helix-turn-helix transcriptional regulator	1,945	0,000
GSU0014	0	DnaJ-like molecular chaperone	-1,807	0,000
GSU0018	0	GntR family transcriptional regulator	2,154	0,000
GSU0020	yrdA	hypothetical protein	-1,792	0,000
GSU0023	0	lipoprotein	-1,863	0,000
GSU0024	0	peptidoglycan-binding outer membrane lipoprotein Pal; OmpA family	-1,532	0,000
GSU0030	hemN	oxygen-independent coproporphyrinogen III oxidase	1,920	0,000
GSU0033	dnaK	molecular chaperone DnaK	-1,776	0,000
GSU0034	dnaJ	chaperone protein DnaJ	-2,822	0,000
GSU0037	serS	seryl-tRNA ligase	2,174	0,000
GSU0041	lexA-1	LexA family transcriptional repressor	3,789	0,000
GSU0042	0	hypothetical protein	4,138	0,000
GSU0043	0	DNA polymerase IV	4,574	0,000
GSU0050	0	HIRAN domain-containing protein	1,486	0,000
GSU0053	csb1	CRISPR-associated protein Csb1	-1,246	0,046
GSU0054	csb2	CRISPR-associated protein Csb2	-1,519	0,004
GSU0055	0	toxin; RelE family	3,922	0,000
GSU0057	cas1-1/cas4	CRISPR-associated geneuclease Cas4 and endodeoxyribonuclease Cas1	-1,594	0,006
GSU0061	0	hypothetical protein	1,301	0,012
GSU0062	0	TraD protein	2,420	0,003
GSU0065	tadA	tRNA (adenosine-34) deaminase	1,517	0,000
GSU0066	0	peroxiredoxin-like 2 family protein; selenocysteine-containing	-1,088	0,039
GSU0069	0	oxidoreductase; iron-sulfur cluster-binding subunit	-2,568	0,000
GSU0071	0	hypothetical protein	-3,409	0,000
GSU0073	0	outer membrane protein	-1,190	0,000

GSU0075	0	SDR_a2 family oxidoreductase	-1,090	0,014
GSU0076	0	hypothetical protein	-1,225	0,030
GSU0077	0	hypothetical protein	-3,414	0,000
GSU0078	0	PilZ domain-containing protein	-2,383	0,000
GSU0081	0	hypothetical protein	-1,755	0,000
GSU0084	0	hypothetical protein	-2,284	0,000
GSU0085	hdrF	heterodisulfide oxidoreductase; NAD(P)H oxidoreductase subunit F	-1,592	0,046
GSU0088	hdrD	heterodisulfide oxidoreductase; iron-sulfur cluster-binding subunit D	-2,480	0,003
GSU0090	hdrA	heterodisulfide oxidoreductase; FAD-binding and iron-sulfur cluster-binding subunit A	-1,215	0,002
GSU0094	dnaX	DNA polymerase III subunits gamma and tau	1,214	0,001
GSU0096	recR	recombination protein RecR	1,384	0,000
GSU0103	0	sensor histidine kinase	-1,744	0,000
GSU0107	0	ParB-like nuclease domain-containing protein	-1,050	0,011
GSU0108	atpX	ATP synthase F0; B' subunit	1,210	0,000
GSU0114	atpC	FOF1 ATP synthase subunit epsilon	-1,582	0,000
GSU0115	pdxA	4-hydroxythreonine-4-phosphate dehydrogenase	1,713	0,000
GSU0127	ttcA	tRNA 2-thiocytidine biosynthesis protein TtcA	1,268	0,020
GSU0128	priA	primosomal protein N'; ATP-dependent helicase	3,551	0,000
GSU0129	def-1	polypeptide formylmethionine deformylase	3,304	0,000
GSU0130	fmt	methionyl-tRNA formyltransferase	2,686	0,000
GSU0131	0	hypothetical protein	2,216	0,000
GSU0134	0	ribonuclease Z	1,207	0,038
GSU0138	prfC	peptide chain release factor 3	1,178	0,000
GSU0139	0	hypothetical protein	1,964	0,001
GSU0143	cinA	molybdopterin-binding domain nicotinamide nucleotide amidohydrolyase	-1,267	0,010
GSU0144	0	sensor histidine kinase; PAS and GAF domain-containing	-1,572	0,000
GSU0148	alaS	alanyl-tRNA ligase	-1,409	0,006
GSU0153	argG	argininosuccinate synthase	-1,396	0,000
GSU0155	0	hypothetical protein	-2,309	0,001
GSU0158	lysA	diaminopimelate decarboxylase	1,718	0,000
GSU0164	0	hypothetical protein	1,875	0,001
GSU0165	0	hypothetical protein	1,038	0,005
GSU0169	0	ABC transporter ATP-binding protein	1,833	0,000
GSU0170	0	hypothetical protein	2,311	0,019
GSU0173	0	cupin	-1,041	0,002
GSU0178	hxlR	helix-turn-helix transcriptional regulator HxlR	4,283	0,000
GSU0179	0	flavodoxin	3,027	0,000
GSU0180	0	hypothetical protein	3,748	0,000
GSU0182	0	lipoprotein	-1,029	0,004
GSU0183	0	peptidoglycan L,D-transpeptidase lipoprotein; YkuD family; SPOR domain-containing	2,110	0,000

GSU0185	0	hypothetical protein	-1,465	0,000
GSU0186	0	hypothetical protein	-2,015	0,000
GSU0191	0	cold shock DNA/RNA-binding protein	1,742	0,000
GSU0192	0	hypothetical protein	1,365	0,000
GSU0194	0	ADP-ribosylglycohydrolase-like protein	1,282	0,009
GSU0195	0	flavin and coenzyme A sequestration protein dodecin	-1,840	0,001
GSU0200	0	aerobic-type carbon monoxide dehydrogenase; small subunit-like protein	-2,731	0,000
GSU0201	0	aerobic-type carbon monoxide dehydrogenase; large subunit-like protein	-3,282	0,000
GSU0202	0	dehydrogenase molybdenum cofactor insertion protein	-2,731	0,000
GSU0203	0	MobA-related glycosyltransferase	-2,575	0,000
GSU0208	0	hypothetical protein	1,468	0,000
GSU0209	0	hypothetical protein	3,631	0,000
GSU0217	0	nitroreductase-like family 3 protein	-1,580	0,002
GSU0231	0	hypothetical protein	-2,226	0,000
GSU0233	0	hypothetical protein	1,590	0,006
GSU0244	0	radical SAM domain-containing iron-sulfur cluster-binding oxidoreductase	1,214	0,000
GSU0245	0	undecaprenyl-phosphate glycosyltransferase	2,583	0,000
GSU0246	0	polysaccharide deacetylase	3,570	0,000
GSU0250	0	hypothetical protein	1,365	0,001
GSU0251	0	hypothetical protein	1,179	0,047
GSU0267	0	GntR family transcriptional regulator	2,503	0,000
GSU0268	0	hypothetical protein	1,587	0,000
GSU0269	0	hypothetical protein	2,489	0,014
GSU0270	glmS	glucosamine--fructose-6-phosphate aminotransferase	-1,202	0,001
GSU0283	0	sensor histidine kinase	2,828	0,000
GSU0284	0	TraR/DksA family zinc finger transcriptional regulator	1,065	0,000
GSU0290	fabH-1	3-oxoacyl-ACP synthase	2,804	0,000
GSU0292	0	hypothetical protein	2,483	0,001
GSU0294	0	metal-dependent phosphohydrolase; HDOD domain-containing	1,565	0,023
GSU0304	pepN	aminopeptidase N	1,864	0,000
GSU0306	hypF	hydrogenase maturation protein HypF	1,137	0,002
GSU0313	0	DnaJ domain-containing protein	2,697	0,000
GSU0318	0	M48 family peptidase	3,381	0,000
GSU0327	gspF	type II secretion system inner membrane protein GspF	-1,647	0,003
GSU0328	gspE	type II secretion system ATPase GspE	-1,364	0,002
GSU0330	gspC	type II secretion system protein GspC serine protease	1,218	0,000
GSU0331	degP	periplasmic trypsin-like serine protease DegP	-1,565	0,000
GSU0332	pepA	multifunctional aminopeptidase A	-1,964	0,000
GSU0341	nuoD	NADH dehydrogenase I subunit D	-1,076	0,004
GSU0354	0	hypothetical protein	1,264	0,001
GSU0356	0	sensor histidine kinase response regulator	-1,288	0,039

GSU0357	0	cytochrome c nitrite reductase	-2,195	0,000
GSU0358	0	periplasmic nitrate reductase; iron-sulfur cluster-binding subunit	-1,679	0,044
GSU0359	0	sigma-54-dependent sensor transcriptional regulator; PAS domain-containing	1,628	0,000
GSU0362	0	hypothetical protein	1,523	0,005
GSU0363	dinG	ATP-dependent DNA helicase DinG	2,451	0,000
GSU0364	ppcB	cytochrome c	1,206	0,000
GSU0367	yhcC-1	radical SAM domain-containing iron-sulfur cluster-binding oxidoreductase	2,213	0,000
GSU0372	0	sigma-54-dependent transcriptional response regulator	-1,866	0,000
GSU0377	gcvP1	glycine dehydrogenase subunit 1	-1,866	0,007
GSU0378	gcvP2	glycine dehydrogenase subunit 2	-1,423	0,030
GSU0379	lplA	lipoate--protein ligase A	-2,453	0,007
GSU0380	lipA	lipoyl synthase	-3,142	0,000
GSU0383	0	FKBP-type peptidylprolyl cis-trans isomerase	-1,364	0,000
GSU0416	fliK	flagellar hook-length control protein FliK	1,865	0,044
GSU0428	tssJ	type VI secretion system outer membrane lipoprotein TssJ	2,145	0,005
GSU0429	tssK	type VI secretion system protein TssK	2,417	0,004
GSU0434	0	thiamin biosynthesis protein ThiI-related adenine nucleotide alpha hydrolase superfamily protein	1,868	0,000
GSU0437	0	UbiD family decarboxylase	2,509	0,000
GSU0438	0	lipoprotein	3,150	0,000
GSU0439	0	prenyltransferase	1,530	0,015
GSU0446	rsmE	16S ribosomal RNA methyltransferase RsmE	-1,573	0,016
GSU0448	0	zinc-dependent amidohydrolase	1,992	0,000
GSU0451	0	winged-helix transcriptional response regulator	-1,124	0,017
GSU0459	0	3-oxoacyl-(ACP) synthase-like protein	1,098	0,011
GSU0460	fabF-1	3-oxoacyl-(acyl carrier protein) synthase II	1,659	0,000
GSU0466	macA	cytochrome c peroxidase	-2,720	0,000
GSU0470	0	sigma-54-dependent transcriptional response regulator	1,051	0,002
GSU0471	0	sensor histidine kinase	1,210	0,000
GSU0472	0	SRPBCC domain-containing protein	-3,647	0,000
GSU0473	0	transcriptional regulator	-1,250	0,042
GSU0475	0	sensor histidine kinase; PAS domain-containing	1,524	0,000
GSU0477	0	HAD superfamily hydrolase	-1,852	0,000
GSU0478	0	ferritin-like domain-containing protein	-2,827	0,000
GSU0479	aspA	aspartate ammonia-lyase	-2,068	0,000
GSU0480	0	thioredoxin/NifU-like domain-containing protein	-2,162	0,000
GSU0481	0	hypothetical protein	-2,235	0,000
GSU0486	tdcB	threonine dehydratase	-1,289	0,026
GSU0487	dmeF	cobalt/zinc/iron/cadmium/nickel efflux protein	1,130	0,042
GSU0490	ato-1	succinyl:acetate coenzyme A transferase	-1,264	0,000

GSU0491	rhIE-1	ATP-dependent RNA helicase RhIE	2,617	0,000
GSU0492	xerC	site-specific recombinase XerC	1,827	0,000
GSU0496	0	RND family efflux pump membrane fusion protein	3,668	0,000
GSU0498	0	hypothetical protein	2,273	0,001
GSU0508	yceG	hypothetical protein	-1,654	0,003
GSU0510	sfrB	NADPH oxidoreductase subunit beta	-1,211	0,003
GSU0514	0	IclR family transcriptional regulator	1,939	0,000
GSU0515	usp-1	universal stress protein Usp	-1,225	0,027
GSU0531	dapF	diaminopimelate epimerase	1,191	0,037
GSU0534	iscR-1	helix-turn-helix iron-sulfur cluster-binding transcriptional regulator IscR	3,158	0,000
GSU0535	cysK	cysteine synthase A	3,180	0,000
GSU0538	hspA-1	ATP-independent chaperone	-3,846	0,000
GSU0539	0	hypothetical protein	-5,544	0,000
GSU0542	0	diguanylate cyclase	2,381	0,000
GSU0543	0	outer membrane lipoprotein; Slp family	-1,064	0,027
GSU0544	0	SAM-dependent methyltransferase	-2,039	0,000
GSU0548	0	radical SAM domain-containing iron-sulfur cluster-binding oxidoreductase	4,423	0,000
GSU0572	0	hydrolase; cyclic phosphodiesterase-like domain-containing	-1,888	0,011
GSU0574	0	hypothetical protein	3,051	0,000
GSU0581	0	cold shock DNA/RNA-binding protein	-1,202	0,041
GSU0583	mcp64H-1	methyl-accepting chemotaxis sensory transducer; class 40 24H	-3,822	0,000
GSU0588	thiG	thiazole synthase	1,741	0,000
GSU0589	thiS	thiamin biosynthesis sulfur carrier protein	2,904	0,000
GSU0590	0	hypothetical protein	-2,341	0,000
GSU0591	0	cytochrome c	-2,234	0,000
GSU0592	omcQ	lipoprotein cytochrome c	-1,057	0,008
GSU0596	0	response receiver	1,065	0,000
GSU0598	0	sigma-54-dependent transcriptional response regulator	1,508	0,000
GSU0602	0	hypothetical protein	-1,770	0,002
GSU0605	thiE/thiD	4-amino-5-hydroxymethyl-2-methylpyrimidine-phosphate kinase and thiamin monophosphate synthase	2,384	0,000
GSU0612	ppcA	cytochrome c	-3,412	0,000
GSU0618	omcE	cytochrome c	-1,733	0,000
GSU0621	0	hypothetical protein	1,946	0,003
GSU0625	0	transcriptional regulator	2,769	0,000
GSU0640	0	hypothetical protein	2,125	0,000
GSU0642	ffh	signal recognition particle protein	1,327	0,000
GSU0645	rimM	16S rRNA processing protein RimM	1,090	0,000
GSU0649	rnhB	ribonuclease HII	1,508	0,006
GSU0655	rpoH	RNA polymerase sigma-32 factor RpoH	1,332	0,000

GSU0658	clpB	ATP-dependent chaperone ClpB	-2,569	0,000
GSU0665	rpsF	30S ribosomal protein S6	1,841	0,000
GSU0667	0	hypothetical protein	1,917	0,000
GSU0670	omcX	lipoprotein cytochrome c	-1,242	0,000
GSU0672	0	cytidylate kinase-like domain-containing protein	-3,811	0,000
GSU0673	0	hypothetical protein	-4,441	0,000
GSU0674	hcp	hybrid cluster protein	-1,141	0,000
GSU0675	0	hypothetical protein	3,067	0,000
GSU0676	0	lipoprotein	2,069	0,010
GSU0677	0	ABC transporter membrane protein	3,816	0,000
GSU0678	0	ABC transporter ATP-binding protein	1,654	0,042
GSU0680	0	hypothetical protein	-2,641	0,000
GSU0681	0	sensor histidine kinase	-1,291	0,006
GSU0685	hpnH	diploptene adenosyltransferase and reductase	-2,156	0,000
GSU0693	0	sensor histidine kinase; PAS; PAS and PAS domain-containing	3,342	0,000
GSU0700	0	response receiver sensor protein serine/threonine phosphatase; PP2C family; PAS and PAS domain-containing	-4,208	0,000
GSU0709	0	hypothetical protein	-3,543	0,000
GSU0710	0	hypothetical protein	-3,566	0,000
GSU0711	0	endonuclease/geneuclease/phosphatase family protein	-3,747	0,000
GSU0712	0	hypothetical protein	-3,661	0,000
GSU0713	0	hypothetical protein	-3,398	0,000
GSU0714	0	hypothetical protein	-3,750	0,000
GSU0715	0	hypothetical protein	-3,263	0,000
GSU0716	0	C14 family peptidase	-2,893	0,000
GSU0718	0	sensor histidine kinase response receiver; PAS domain-containing	-2,426	0,000
GSU0719	0	hypothetical protein	-2,524	0,000
GSU0720	0	desulfoferrodoxin	-1,785	0,000
GSU0721	rpoE	RNA polymerase factor sigma-70	3,931	0,000
GSU0722	0	hypothetical protein	3,101	0,000
GSU0723	0	hypothetical protein	1,623	0,000
GSU0725	0	hypothetical protein	4,189	0,000
GSU0726	cheD64H	protein glutamine deamidase and protein glutamate methylesterase CheD associated with MCPs of classes 40H and 40 24H	1,963	0,000
GSU0727	0	lipoprotein	1,424	0,000
GSU0729	0	iron-sulfur cluster-binding oxidoreductase	1,783	0,047
GSU0733	mreB-2	rod shape-determining protein MreB	1,483	0,019
GSU0734	ehrA-2	Ech-hydrogenase-related complex; NuoL-like integral membrane lipoprotein subunit	2,102	0,000
GSU0735	0	MerR family transcriptional regulator	2,426	0,000
GSU0736	0	toxin; MazF family	1,126	0,001

GSU0737	0	antitoxin	1,964	0,000
GSU0739	ehrA-1	Ech-hydrogenase-related complex; NuoL-like integral membrane subunit	1,871	0,000
GSU0742	ehrD	Ech-hydrogenase-related complex; HyfF-like integral membrane subunit	-1,114	0,005
GSU0743	ehrL	Ech-hydrogenase-related complex large subunit	-1,558	0,000
GSU0745	ehrS	Ech-hydrogenase-related complex small subunit	-1,326	0,010
GSU0746	0	cytochrome p460; 1 heme-binding site	-3,828	0,000
GSU0757	0	lipoprotein	2,564	0,000
GSU0767	0	outer membrane channel protein	-2,163	0,000
GSU0768	0	AzIC family protein	-2,475	0,000
GSU0769	rarD	RarD protein; DMT superfamily transporter	1,541	0,000
GSU0770	0	TetR family transcriptional regulator	3,889	0,000
GSU0771	0	NADPH:quinone oxidoreductase family protein	2,540	0,000
GSU0772	0	flavodoxin	1,517	0,016
GSU0776	0	sigma-54-dependent transcriptional response regulator	1,772	0,000
GSU0782	hybS	periplasmically oriented; membrane-bound [NiFe]-hydrogenase small subunit	-1,119	0,000
GSU0783	hybA	hydrogenase 2 protein HybA	-3,183	0,000
GSU0784	hybB	hydrogenase 2 b cytochrome subunit	-3,840	0,000
GSU0785	hybL	periplasmically oriented; membrane-bound [NiFe]-hydrogenase large subunit	-4,648	0,000
GSU0786	hybP	periplasmically oriented; membrane-bound [NiFe]-hydrogenase maturation protease	-5,936	0,000
GSU0787	hybT	twin-arginine translocation pathway protein; TatA/TatE family	-6,065	0,000
GSU0788	0	hypothetical protein	-5,373	0,000
GSU0794	0	FAD-dependent pyridine nucleotide-disulfide oxidoreductase family protein	1,769	0,014
GSU0801	0	hypothetical protein	-2,140	0,031
GSU0802	0	short chain dehydrogenase	-3,499	0,000
GSU0803	ppsA	phosphoenolpyruvate synthase	-4,364	0,000
GSU0804	wrbA	NAD(P)H:quinone oxidoreductase	-3,484	0,000
GSU0807	citX	apo-citrate lyase 2'-(5"-triphosphoribosyl)-3'-dephospho-coenzyme A transferase	1,194	0,005
GSU0809	0	carbonic anhydrase	-1,764	0,006
GSU0810	0	peptidoglycan-binding outer membrane protein	-4,083	0,000
GSU0813	0	organic solvent tolerance ABC transporter substrate-binding protein	-2,296	0,000
GSU0815	0	ABC transporter substrate-binding lipoprotein	-1,439	0,005
GSU0816	0	organic solvent tolerance ABC transporter ATP-binding protein	-1,184	0,015
GSU0822	0	sensor histidine kinase; Cache_1; HAMP and PAS domain-containing	1,909	0,000

GSU0826	0	hypothetical protein	1,058	0,028
GSU0827	0	hypothetical protein	3,762	0,000
GSU0828	0	RND family efflux pump outer membrane protein	3,422	0,000
GSU0849	scdA	iron-sulfur cluster repair protein ScdA	-2,546	0,000
GSU0855	0	TerC family membrane protein	2,097	0,000
GSU0856	htpX-1	membrane-bound zinc-dependent protease HtpX	3,684	0,000
GSU0858	0	periplasmic energy transduction protein	1,337	0,002
GSU0861	0	5,10-methylenetetrahydrofolate reductase-associated protein	1,474	0,010
GSU0863	0	regulatory protein; CxxC_CxxC_SSSS domain-containing	2,323	0,000
GSU0867	0	menaquinone biosynthesis methyltransferase	1,369	0,007
GSU0868	0	diadenylate cyclase; YbbR and YbbR domain-containing	1,871	0,000
GSU0869	0	hypothetical protein	1,300	0,000
GSU0874	0	hypothetical protein	1,713	0,000
GSU0883	0	ligand-gated TonB-dependent outer membrane channel	-1,190	0,006
GSU0885	0	BioD and DRTGG domain-containing protein	-1,386	0,000
GSU0893	prx-1	peroxiredoxin; typical 2-Cys subfamily	-2,164	0,000
GSU0894	0	cyclophilin type peptidyl-prolyl cis-trans isomerase	-1,492	0,000
GSU0896	tldD	zinc protease TldD modulator of DNA gyrase	-1,351	0,001
GSU0897	0	protein 3-oxoalanine-generating enzyme family protein	1,306	0,000
GSU0898	recQ	ATP-dependent DNA helicase RecQ	1,179	0,004
GSU0905	0	hypothetical protein	3,981	0,000
GSU0914	rhIE-2	ATP-dependent RNA helicase RhIE	2,317	0,000
GSU0915	0	hypothetical protein	-3,167	0,000
GSU0917	0	hypothetical protein	1,519	0,006
GSU0919	0	hypothetical protein	-3,487	0,000
GSU0921	0	ribonuclease; Rne/Rng family	1,191	0,000
GSU0926	0	ABC transporter substrate-binding lipoprotein	-1,446	0,005
GSU0927	0	zinc-dependent peptidase	-1,523	0,000
GSU0936	0	glutamine-dependent amidotransferase; class I	3,091	0,000
GSU0937	nifV	trans-homoaconitate synthase	6,046	0,000
GSU0938	0	hypothetical protein	6,238	0,000
GSU0940	amtB	ammonium transporter	5,102	0,000
GSU0941	gnfK	nitrogen fixation transcript antitermination sensor histidine kinase	3,216	0,000
GSU0942	hisN	histidinol-phosphate phosphatase	2,611	0,000
GSU0943	0	PilZ domain-containing protein	1,804	0,005
GSU0945	metC-2	cystathionine gamma-synthase/beta-lyase	2,574	0,005
GSU0951	0	TetR family transcriptional regulator	2,755	0,001
GSU0954	0	transposase; Y1_Tnp domain-containing	-2,135	0,007
GSU0964	0	hypothetical protein	2,216	0,000
GSU0966	0	hypothetical protein	1,981	0,000
GSU0967	0	hypothetical protein	1,936	0,000

GSU0968	0	hypothetical protein	-2,757	0,000
GSU0973	0	hypothetical protein	-2,353	0,000
GSU0974	0	hypothetical protein	-1,590	0,000
GSU0975	0	phage tail sheath protein	-1,864	0,000
GSU0976	0	phage tail tube protein gp19	-1,621	0,005
GSU0977	0	hypothetical protein	-1,606	0,018
GSU0979	0	phage tail tube protein gp19	-1,493	0,001
GSU0980	0	hypothetical protein	-2,023	0,000
GSU0981	0	hypothetical protein	-4,262	0,000
GSU0982	0	phage protein D	-1,775	0,000
GSU0983	0	phage tail spike protein	-2,452	0,000
GSU0986	0	phage baseplate outer wedge protein (acidic lysozyme)	-2,357	0,001
GSU0987	0	hypothetical protein	-1,921	0,000
GSU0988	0	hypothetical protein	-1,803	0,000
GSU0989	0	NHL repeat domain-containing protein	-2,147	0,000
GSU0990	0	hypothetical protein	-1,257	0,005
GSU0991	0	ExpC-like family glycosyltransferase	-1,667	0,006
GSU0992	0	hypothetical protein	-1,735	0,000
GSU0994	fumB	fumarate hydratase	-1,020	0,001
GSU0996	0	SAP domain-containing protein	-3,535	0,000
GSU1001	0	hypothetical protein	2,756	0,000
GSU1004	gnfL	nitrogen fixation master sensor histidine kinase; PAS domain-containing	1,944	0,000
GSU1006	0	hypothetical protein	1,586	0,001
GSU1007	0	sensor cyclic diguanylate phosphodiesterase; GAF and GAF domain-containing	-3,545	0,000
GSU1010	0	lytic transglycosylase; SLT; LysM and LysM domain-containing	2,239	0,000
GSU1013	0	peptidoglycan-binding lipoprotein; OmpA family	-1,103	0,001
GSU1018	0	hypothetical protein	-2,830	0,000
GSU1024	ppcD	cytochrome c	-2,909	0,000
GSU1028	aguA	agmatine deiminase	1,745	0,000
GSU1037	0	response receiver-modulated diguanylate cyclase/phosphodiesterase	-1,870	0,046
GSU1038	0	response receiver histidine kinase	-1,757	0,001
GSU1039	0	sigma-54-dependent sensor transcriptional response regulator	-1,942	0,001
GSU1046	0	hypothetical protein	-1,531	0,030
GSU1050	0	sensor histidine kinase	1,671	0,032
GSU1055	0	hypothetical protein	1,511	0,007
GSU1057	0	hypothetical protein	1,168	0,003
GSU1059	sucD	succinyl-CoA synthetase subunit alpha	-1,624	0,000
GSU1060	0	hypothetical protein	3,521	0,000
GSU1067	0	nucleotidyltransferase	1,396	0,002
GSU1072	0	IclR family transcriptional regulator	1,703	0,029

GSU1080	0	hypothetical protein	3,432	0,000
GSU1081	0	hypothetical protein	4,384	0,000
GSU1082	0	hypothetical protein	4,130	0,000
GSU1083	0	hypothetical protein	5,340	0,000
GSU1084	0	hypothetical protein	4,830	0,000
GSU1085	0	hypothetical protein	5,261	0,000
GSU1086	0	hypothetical protein	4,971	0,000
GSU1087	0	phasin superfamily protein	-1,373	0,005
GSU1090	0	response receiver	-1,122	0,001
GSU1102	phoB	winged-helix phosphate transcriptional response regulator	1,556	0,000
GSU1106	gltA	type I citrate synthase	-1,011	0,001
GSU1110	ndk	multifunctional nucleoside diphosphate kinase/apurimidine endonuclease/3'-phosphodiesterase	1,059	0,000
GSU1111	rlmN	ribosomal RNA large subunit methyltransferase N	4,080	0,000
GSU1112	mtaP	methylthioadenosine phosphorylase	2,878	0,000
GSU1114	0	lipoprotein	2,228	0,000
GSU1116	0	GAF domain-containing protein	1,256	0,000
GSU1118	usp-2	universal stress protein Usp	-1,880	0,000
GSU1119	0	response receiver histidine kinase	-1,154	0,010
GSU1124	coaBC	phosphopantothencysteine decarboxylase and phosphopantothenate--cysteine ligase	-1,808	0,000
GSU1125	0	hypothetical protein	2,221	0,000
GSU1134	zapA	cell division protein ZapA	2,186	0,000
GSU1135	0	hypothetical protein	2,597	0,000
GSU1136	0	5-formyltetrahydrofolate cyclo-ligase	3,354	0,000
GSU1140	mcp34H-3	methyl-accepting chemotaxis sensory transducer; class 34H	4,785	0,000
GSU1141	mcp34H-10	methyl-accepting chemotaxis sensory transducer; class 34H	3,982	0,000
GSU1142	cheW34H-1	scaffold protein CheW associated with MCPs of class 34H	3,239	0,000
GSU1143	cheR34H	protein glutamate methyltransferase CheR associated with MCPs of class 34H	1,945	0,026
GSU1145	cheB34H	protein glutamate methylesterase CheB associated with MCPs of class 34H; response receiver domain-containing	3,270	0,000
GSU1146	0	lipoprotein	1,296	0,004
GSU1153	0	outer membrane lipoprotein	-2,830	0,000
GSU1154	0	surface repeat protein	-2,629	0,000
GSU1158	sodA	superoxide dismutase; iron/manganese-containing	-1,420	0,000
GSU1160	0	hypothetical protein	-1,785	0,000
GSU1165	ptsP	GAF domain phosphoenolpyruvate--protein phosphotransferase PtsP	1,689	0,000
GSU1167	0	hypothetical protein	-4,822	0,000

GSU1168	0	SCP-like extracellular lipoprotein	-1,531	0,000
GSU1171	yyaL	thioredoxin domain-containing protein YyaL	-1,740	0,005
GSU1177	frdA	succinate dehydrogenase flavoprotein subunit	-1,129	0,000
GSU1178	frdB	succinate dehydrogenase/fumarate reductase iron-sulfur subunit	-1,260	0,000
GSU1180	ftsH-1	cell division ATP-dependent zinc protease FtsH	-1,097	0,020
GSU1182	malQ	4-alpha-glucanotransferase	-1,410	0,047
GSU1183	metY-1	O-acetyl-L-homoserine sulfhydrylase	3,841	0,000
GSU1185	0	adenosine kinase	-2,206	0,000
GSU1189	0	M48 family peptidase	1,413	0,049
GSU1190	selU	tRNA 2-selenouridine synthase	1,091	0,048
GSU1198	serA	D-3-phosphoglycerate dehydrogenase	1,177	0,000
GSU1199	0	nuclease	3,149	0,000
GSU1209	0	hypothetical protein	-2,840	0,000
GSU1212	0	hypothetical protein	-3,376	0,000
GSU1213	0	hypothetical protein	-2,114	0,000
GSU1221	0	ammonium transporter	4,791	0,000
GSU1231	0	response receiver-related domain-containing protein	1,938	0,000
GSU1233	0	manganese/nickel-dependent phosphodiesterase; YfcE family	1,285	0,000
GSU1235	0	archaeal-type glutamate synthase subunit	-2,541	0,000
GSU1236	0	glutamine amidotransferase	-1,177	0,046
GSU1237	0	FAD-dependent pyridine nucleotide-disulfide oxidoreductase family protein	-1,510	0,005
GSU1239	0	glutamate synthase	1,039	0,001
GSU1251	0	lipoprotein	2,755	0,000
GSU1258	0	NosL family protein	1,726	0,000
GSU1263	yhbY	RNA-binding protein YhbY	1,026	0,017
GSU1264	0	histidine phosphotransfer domain-containing protein	2,801	0,000
GSU1265	0	sensor histidine kinase response regulator	1,137	0,000
GSU1266	lepA	GTP-binding protein LepA	1,294	0,000
GSU1268	0	LysR family transcriptional regulator	1,748	0,000
GSU1269	0	hypothetical protein	1,635	0,027
GSU1270	pyrR	bifunctional pyrimidine regulatory protein PyrR/uracil phosphoribosyltransferase	2,500	0,000
GSU1271	pyrB	aspartate carbamoyltransferase catalytic subunit	2,484	0,000
GSU1273	carA	carbamoyl phosphate synthase small subunit	1,305	0,007
GSU1276	carB	carbamyl-phosphate synthase; large subunit lipoprotein; glutamine-dependent	2,788	0,000
GSU1277	greA	transcription elongation factor GreA	2,863	0,000
GSU1278	0	hypothetical protein	1,704	0,000
GSU1279	nikMN	nickel ABC transporter membrane protein NikMN	2,813	0,000
GSU1280	nikQ	nickel ABC transporter membrane protein NikQ	2,410	0,002
GSU1281	nikO	nickel ABC transporter ATP-binding protein	1,722	0,046

GSU1285	0	sensor histidine kinase response regulator; PAS and PAS domain-containing	1,552	0,047
GSU1292	0	sensor histidine kinase; PAS domain-containing	1,374	0,001
GSU1293	0	LuxR family transcriptional regulator	1,694	0,000
GSU1294	mcp34H-7	methyl-accepting chemotaxis sensory transducer; class 34H	2,354	0,000
GSU1303	mcp34H-11	methyl-accepting chemotaxis sensory transducer; class 34H	-2,418	0,000
GSU1306	0	phosphotransferase; PolIIIAC domain-containing	-2,530	0,000
GSU1307	ftn	nonheme ferritin	-2,975	0,000
GSU1309	0	hypothetical protein	2,094	0,000
GSU1314	0	hypothetical protein	1,448	0,049
GSU1316	0	response regulator sensor; GAF domain-containing	2,643	0,000
GSU1317	ispB	octaprenyl diphosphate synthase	1,662	0,000
GSU1318	0	hypothetical protein	1,827	0,001
GSU1330	0	RND family metal ion efflux pump outer membrane protein	2,141	0,000
GSU1333	0	hypothetical protein	-2,692	0,000
GSU1337	0	lipoprotein	1,301	0,000
GSU1339	0	hypothetical protein	5,878	0,000
GSU1341	0	ABC transporter ATP-binding protein	3,940	0,000
GSU1343	0	amidohydrolase	-4,156	0,000
GSU1344	0	amidohydrolase	-5,327	0,000
GSU1345	0	Rrf2 family winged helix-turn-helix transcriptional regulator	2,702	0,000
GSU1346	cysP	sulfate ABC transporter substrate-binding protein	4,538	0,000
GSU1347	cysU	sulfate ABC transporter membrane protein CysU	4,324	0,000
GSU1348	cysW	sulfate ABC transporter membrane protein CysW	3,120	0,007
GSU1354	0	toxin; RelE family	2,174	0,012
GSU1359	0	helicase	-1,976	0,009
GSU1370	0	oxidoreductase; aldo/keto reductase family	-2,352	0,000
GSU1377	0	enoyl-CoA hydratase/isomerase	-1,729	0,001
GSU1379	fur	ferric uptake regulation protein Fur	1,242	0,000
GSU1380	feoB-1	ferrous iron transport protein B	1,628	0,000
GSU1382	ideR	iron/manganese-dependent transcriptional regulator	-2,050	0,002
GSU1390	0	antitoxin; XRE family	2,626	0,011
GSU1391	0	toxin; Fic family	2,041	0,028
GSU1395	0	hypothetical protein	1,202	0,001
GSU1396	0	hypothetical protein	-1,962	0,031
GSU1398	0	SCO family protein	-1,016	0,004
GSU1399	corA-1	magnesium transport protein CorA	-2,647	0,008
GSU1401	dnaE	DNA polymerase III subunit alpha	4,243	0,000
GSU1404	0	radical SAM domain-containing iron-sulfur cluster-binding oxidoreductase	-1,526	0,000
GSU1415	0	response regulator	-2,421	0,000
GSU1416	0	iron-sulfur cluster-binding flavodoxin	-3,045	0,000

GSU1424	0	hypothetical protein	-1,184	0,049
GSU1425	lgt	prolipoprotein diacylglyceryl transferase	1,891	0,000
GSU1426	rsbW	anti-sigma factor; protein serine/threonine kinase	1,803	0,000
GSU1427	rsbV	anti-anti-sigma factor	1,210	0,000
GSU1429	0	sodium/solute symporter serine/threonine phosphatase domain-containing protein	-1,132	0,006
GSU1442	0	carbonic anhydrase	-1,175	0,006
GSU1446	0	radical SAM domain-containing iron-sulfur cluster-binding oxidoreductase	1,532	0,000
GSU1447	0	hypothetical protein	-2,955	0,000
GSU1448	0	metal-dependent phosphoesterase; PHP family	-1,827	0,000
GSU1452	0	TrmA family RNA methyltransferase	1,846	0,000
GSU1461	pyrF	orotidine 5'-phosphate decarboxylase	-1,426	0,016
GSU1480	0	RND family multidrug resistance efflux pump inner membrane protein EmrB	-2,094	0,000
GSU1484	0	lytic transglycosylase domain-containing protein	1,083	0,005
GSU1486	tatC	twin-arginine translocation pathway protein TatC	1,089	0,007
GSU1492	pilT-4	twitching motility pilus retraction protein	-1,185	0,027
GSU1496	pilA-N	hypothetical protein	-1,382	0,000
GSU1497	pilA-C	hypothetical protein	-1,949	0,000
GSU1509	0	glycosyltransferase	1,106	0,038
GSU1510.1	0	glycosyltransferase	1,598	0,010
GSU1515	thrS	threonyl-tRNA ligase	1,340	0,000
GSU1519	pheS	phenylalanyl-tRNA ligase subunit alpha	1,171	0,002
GSU1523	surE	5'(3')-nucleotidase/polyphosphatase	2,911	0,000
GSU1528	0	ABC transporter substrate-binding protein	1,713	0,000
GSU1529	0	sensor histidine kinase response regulator; PAS domain-containing	1,153	0,018
GSU1532	0	hypothetical protein	2,445	0,000
GSU1533	recC	exodeoxyribonuclease V subunit gamma	1,274	0,001
GSU1535	recD	exodeoxyribonuclease V subunit alpha	-1,756	0,030
GSU1537	exeA	peptidoglycan-binding ATPase	1,086	0,013
GSU1538	0	cytochrome c	-1,541	0,000
GSU1542	0	antitoxin; XRE family	3,535	0,000
GSU1555	0	sensor histidine kinase response regulator; 5TM; PAS; PAS; GAF and PAS domain-containing	1,234	0,002
GSU1557	0	mechanosensitive ion channel family protein	-2,974	0,000
GSU1558	0	hypothetical protein	-4,334	0,000
GSU1560	0	radical SAM domain-containing iron-sulfur cluster-binding oxidoreductase	-2,569	0,000
GSU1564	0	Glu/Leu/Phe/Val dehydrogenase	-1,308	0,017
GSU1567	htpX-2	membrane-bound zinc-dependent protease HtpX	5,233	0,000
GSU1568	0	hypothetical protein	2,579	0,016
GSU1569	0	transcriptional repressor	2,333	0,016
GSU1570	0	TerC family membrane protein	3,375	0,000

GSU1580	0	peptidoglycan L,D-transpeptidase	1,314	0,004
GSU1585	0	hypothetical protein	2,863	0,000
GSU1586	nusA	transcription elongation factor NusA	3,085	0,000
GSU1587	ylxRQ	RNA-binding protein YlxRQ	3,003	0,000
GSU1588	infB	translation initiation factor IF-2	1,698	0,000
GSU1592	rpsO	30S ribosomal protein S15	1,022	0,000
GSU1593	pnp	polynucleotide phosphorylase/polyadenylase	1,017	0,000
GSU1595	dut	deoxyuridine 5'-triphosphate nucleotidohydrolase	-2,426	0,000
GSU1596	yrdC	tRNA (N6-threonylcarbamyl-A37) modification ATPase	-1,862	0,002
GSU1597	0	hypothetical protein	-1,781	0,000
GSU1604	acpP-2	acyl carrier protein	-1,063	0,001
GSU1605	fabF-2	3-oxoacyl-(acyl carrier protein) synthase II	-1,328	0,000
GSU1606	rpiB	ribose-5-phosphate isomerase B	-1,009	0,034
GSU1608	0	hypothetical protein	-1,433	0,012
GSU1610	0	RND family efflux pump membrane fusion lipoprotein	-1,030	0,006
GSU1613	0	endonuclease III family protein	-1,675	0,005
GSU1614	0	Rossmann fold nucleotide-binding protein	-2,436	0,000
GSU1615	0	redox-active membrane protein	-2,358	0,000
GSU1616	0	DNA polymerase IV	5,165	0,000
GSU1617	lexA-2	LexA family transcriptional repressor	6,334	0,000
GSU1621	0	hypothetical protein	1,670	0,000
GSU1624	glcF-2	D-lactate/glycolate dehydrogenase; iron-sulfur cluster-binding protein	-1,725	0,021
GSU1630	0	sensor histidine kinase; HAMP and PAS domain-containing	1,433	0,000
GSU1631	0	metal-dependent hydrolase	1,127	0,000
GSU1637	pyrE	orotate phosphoribosyltransferase	-2,809	0,000
GSU1640	cydA	cytochrome bd menaquinol oxidase; subunit I	2,611	0,000
GSU1641	cydB	cytochrome bd menaquinol oxidase; subunit II	2,441	0,000
GSU1642	0	ferritin-like domain-containing protein	-3,481	0,000
GSU1646	0	lipoprotein	1,214	0,001
GSU1647	0	hypothetical protein	-1,033	0,000
GSU1648	0	cytochrome c	-2,007	0,014
GSU1658	0	response receiver-modulated diguanylate cyclase	1,371	0,000
GSU1661	0	hypothetical protein	-4,436	0,000
GSU1662	0	hypothetical protein	-2,708	0,000
GSU1669	0	hypothetical protein	-1,944	0,000
GSU1670	0	lipoprotein	-2,332	0,000
GSU1673	0	hypothetical protein	1,509	0,002
GSU1676	0	hypothetical protein	1,836	0,000
GSU1677	0	acyl-(acyl carrier protein) ligase; acyl carrier; [acyl-glycerolphosphate acyltransferase fusion protein	1,956	0,000
GSU1681	0	BioD and DRTGG domain-containing protein	-1,735	0,000
GSU1682	0	lipoprotein	4,088	0,000
GSU1684	0	hypothetical protein	-3,032	0,000

GSU1685	0	metal-dependent phosphohydrolase; HDc domain-containing	1,712	0,022
GSU1686	0	deoxycytidylate deaminase	1,061	0,019
GSU1697	0	transglutaminase/protease-like membrane protein	-1,550	0,032
GSU1699	0	hypothetical protein	1,308	0,000
GSU1705	panB	3-methyl-2-oxobutanoate hydroxymethyltransferase	3,079	0,000
GSU1706	panC	pantoate--beta-alanine ligase	1,290	0,004
GSU1708	0	metal-dependent hydrolase; subgroup D	-1,365	0,006
GSU1709	smpB	SsrA-binding protein	1,582	0,000
GSU1710	0	integrase family protein	1,752	0,000
GSU1711	0	integrative genetic element Gsu5; resolvase	4,107	0,000
GSU1716	apr	adenosine-5'-phosphosulfate reductase; glutathione-dependent	7,132	0,000
GSU1717	cysD	sulfate adenylyltransferase subunit 2	4,676	0,000
GSU1718	cysN	sulfate adenylyltransferase; subunit 1	2,751	0,001
GSU1721	queE	7-cyano-7-deazaguanine synthase	1,629	0,000
GSU1723	0	mechanosensitive ion channel family protein	-1,955	0,000
GSU1726	0	hypothetical protein	-2,623	0,000
GSU1727	0	TraR/DksA family zinc finger transcriptional regulator	-1,708	0,001
GSU1728	0	radical SAM domain-containing iron-sulfur cluster-binding oxidoreductase	-2,450	0,000
GSU1733	livH	branched-chain amino acid ABC transporter membrane protein	-2,187	0,018
GSU1734	livK-1	branched-chain amino acid ABC transporter substrate-binding protein	-1,093	0,039
GSU1735	livK-2	branched-chain amino acid ABC transporter substrate-binding protein	-1,134	0,028
GSU1741	gppA-1	pppGpp 5'-phosphohydrolase and exopolyphosphatase	-1,665	0,044
GSU1748	0	TrmA family RNA methyltransferase	1,188	0,001
GSU1749	0	hypothetical protein	1,416	0,011
GSU1750	infA	translation initiation factor IF-1	1,582	0,000
GSU1752	efp-2	elongation factor P	2,408	0,000
GSU1753	genX	translation elongation factor P-lysine lysyltransferase	2,991	0,000
GSU1761	pgcA	lipoprotein cytochrome c	1,098	0,003
GSU1767	xseA	exodeoxyribonuclease VII large subunit	1,440	0,000
GSU1768	0	ParA family protein	1,632	0,000
GSU1770	0	hypothetical protein	1,999	0,000
GSU1773	0	zinc metalloendopeptidase M23 domain-containing protein	2,098	0,000
GSU1777	pulG	type II secretion system pseudopilin PulG	-2,515	0,002
GSU1778	pulQ	type II secretion system secretin lipoprotein PulQ	-1,033	0,002
GSU1784	pulF	type II secretion system inner membrane protein PulF	1,302	0,000
GSU1786	0	cytochrome c	-1,691	0,028
GSU1788	0	NHL repeat domain-containing protein	2,138	0,000

GSU1789	0	GDP-mannose--undecaprenyl-phosphate mannosyltransferase	2,479	0,000
GSU1791	clpX	ATP-dependent protease ATP-binding subunit ClpX	2,411	0,000
GSU1792	clpP	ATP-dependent Clp protease proteolytic subunit	2,153	0,000
GSU1793	tig	trigger factor	2,431	0,000
GSU1800	yjeE	nucleoid maintenance ATPase YjeE	-2,278	0,027
GSU1809	ftsH-2	cell division ATP-dependent zinc protease FtsH	1,130	0,000
GSU1810	0	tRNA(Ile) lysidine-34 synthase	4,372	0,000
GSU1817	0	outer membrane lipoprotein; Slp family	-2,298	0,000
GSU1820	glnD	nitrogen regulatory protein P-II uridylyltransferase; GlnD	-1,128	0,014
GSU1822	mutS-1	DNA mismatch repair protein MutS	2,093	0,000
GSU1826	0	lytic transglycosylase domain-containing protein	1,258	0,000
GSU1830	0	MEMO-like protein	-2,265	0,000
GSU1833	trpS	tryptophanyl-tRNA ligase	1,996	0,000
GSU1834	0	protease; S2P-M50-like family 1	3,214	0,000
GSU1835	glnA	glutamine synthetase; type I	2,773	0,000
GSU1836	glnB	nitrogen regulatory protein P-II	2,961	0,000
GSU1837	0	zinc metalloendopeptidase	2,487	0,000
GSU1840	0	membrane-associated phosphatase; PAP2_like_5 family	-2,146	0,000
GSU1844	0	IPT/TIG domain-containing protein	2,822	0,000
GSU1852	0	hypothetical protein	1,316	0,032
GSU1853	0	hypothetical protein	1,338	0,028
GSU1858	0	IPT/TIG domain-containing protein	2,662	0,000
GSU1867	0	lipoprotein	2,620	0,000
GSU1868	0	cysteine desulfurase	1,824	0,000
GSU1869	0	lipoprotein	1,657	0,011
GSU1870	0	sensor diguanylate cyclase; GAF domain-containing	2,970	0,000
GSU1875	ahcY	S-adenosyl-L-homocysteine hydrolase	1,164	0,000
GSU1876	0	hypothetical protein	1,150	0,001
GSU1877	0	oxidoreductase; 2-nitropropane dioxygenase family	3,261	0,000
GSU1883	0	phosphotransferase system; mannose-type; protein IIA	-2,090	0,024
GSU1884	0	glmZ(sRNA)-inactivating NTPase	-1,565	0,006
GSU1885	hprK	HPr kinase/phosphorylase	-1,730	0,000
GSU1886	raiA	ribosomal subunit interface-associated sigma-54 modulation protein RaiA	-2,689	0,000
GSU1888	lptB	lipopolysaccharide ABC transporter ATP-binding protein	1,155	0,001
GSU1890	lptC	lipopolysaccharide ABC transporter periplasmic protein LptC	1,648	0,000
GSU1895	pyrG	CTP synthetase	1,174	0,000
GSU1896	kdsB	3-deoxy-manno-octulosonate cytidyltransferase	2,634	0,000
GSU1904	0	Rossmann fold nucleotide-binding protein	1,561	0,001
GSU1907	pssA	CDP-diacylglycerol--serine O-phosphatidyltransferase	-1,482	0,029
GSU1909	ilvC	ketol-acid reductoisomerase	-1,248	0,006

GSU1915	dxr	1-deoxy-D-xylulose 5-phosphate reductoisomerase	2,144	0,000
GSU1916	cdsA	phosphatidate cytidyltransferase	3,534	0,000
GSU1917	uppS	undecaprenyl pyrophosphate synthase	2,974	0,000
GSU1922	lptF	lipopolysaccharide ABC transporter membrane protein LptF	2,604	0,000
GSU1923	lptG	lipopolysaccharide ABC transporter membrane protein LptG	1,789	0,000
GSU1930	0	GTP-binding domain-containing protein	-1,531	0,029
GSU1931	0	hypothetical protein	-1,764	0,044
GSU1933	fusA-1	elongation factor G	-1,693	0,000
GSU1937	0	nucleotide cyclase	1,034	0,001
GSU1939	0	sensor histidine kinase cyclic nucleotide phosphodiesterase	2,127	0,000
GSU1942	capL	UDP-N-acetyl-D-galactosamine 6-dehydrogenase	1,533	0,000
GSU1943	0	PEP motif-containing protein exosortase substrate	1,351	0,000
GSU1944	0	PEP motif-containing protein exosortase substrate	2,436	0,000
GSU1950	0	adenyltransferase	-1,269	0,013
GSU1953	asnB	asparagine synthetase	-1,028	0,047
GSU1959	0	exopolysaccharide biosynthesis protein	-2,286	0,002
GSU1961	0	glycosyltransferase	-1,663	0,009
GSU1962	0	glycosyltransferase	-1,700	0,013
GSU1963	0	undecaprenyl-diphospho-oligosaccharide flippase	-1,215	0,038
GSU1964	0	hypothetical protein	-2,182	0,005
GSU1965	0	polysaccharide pyruvyl transferase-related domain-containing protein	-2,616	0,000
GSU1966	0	hypothetical protein	-4,022	0,000
GSU1968	0	nucleotidyltransferase	-2,578	0,000
GSU1969	0	hypothetical protein	-1,813	0,000
GSU1970	neuB	N-acetylneuraminate synthase	-1,893	0,000
GSU1971	0	hypothetical protein	-2,088	0,004
GSU1972	0	N-acetylneuraminate cytidyltransferase	-2,187	0,001
GSU1973	0	acyltransferase	-2,347	0,014
GSU1974	0	aminotransferase; AHBA_syn family	-2,330	0,000
GSU1975	0	NAD-dependent nucleoside diphosphate-sugar epimerase/dehydratase	-2,386	0,000
GSU1976	0	YqgM-like family glycosyltransferase	-2,875	0,000
GSU1977	0	CESA-like subfamily glycosyltransferase	-2,411	0,000
GSU1979	epsH	exopolysaccharide synthesis membrane protein H (exosortase)	-2,407	0,000
GSU1980	0	polysaccharide deacetylase	-1,688	0,000
GSU1981	0	hypothetical protein	-2,310	0,000
GSU1982	0	ATPase	-3,147	0,000
GSU1983	0	protein tyrosine kinase	-2,556	0,000
GSU1984	0	polysaccharide chain length determinant protein	-2,772	0,000
GSU1985	0	periplasmic polysaccharide biosynthesis/export protein	-1,629	0,000

GSU1986	0	undecaprenyl-phosphate glycosylphosphotransferase	-2,004	0,000
GSU1987	0	lipoprotein	-1,552	0,000
GSU1989	0	sigma-54-dependent transcriptional response regulator	-2,080	0,000
GSU1996	0	cytochrome c	1,132	0,001
GSU1998	0	hypothetical protein	1,351	0,001
GSU1999	hfq	RNA-binding protein Hfq	-1,473	0,000
GSU2005	0	branched-chain amino acid ABC transporter substrate-binding protein	-4,291	0,000
GSU2006	0	branched-chain amino acid ABC transporter membrane protein	-2,585	0,007
GSU2007	0	branched-chain amino acid ABC transporter membrane protein	-2,106	0,015
GSU2008	0	branched-chain amino acid ABC transporter ATP-binding protein	-2,622	0,012
GSU2009	0	branched-chain amino acid ABC transporter ATP-binding protein	-3,425	0,001
GSU2010	0	hypothetical protein	-3,049	0,001
GSU2011	nifS-1	nitrogen fixation iron-sulfur cluster assembly cysteine desulfurase NifS	-1,344	0,000
GSU2014	0	hypothetical protein	1,738	0,000
GSU2015	0	NUDIX hydrolase	3,280	0,000
GSU2016	0	sensor diguanylate cyclase/phosphodiesterase; PAS domain-containing	-1,162	0,008
GSU2018	gcvH-2	glycine cleavage system lipoyl carrier protein GcvH	-1,460	0,005
GSU2020	accB	acetyl-CoA carboxylase; biotin carboxyl carrier protein	1,285	0,005
GSU2021	0	prolidase family protein	1,604	0,000
GSU2025	aroB	3-dehydroquinate synthase	2,238	0,000
GSU2027	aroC	chorismate synthase	-1,765	0,001
GSU2028	pilQ	type IV pilus secretin lipoprotein PilQ	-1,581	0,000
GSU2029	pilP	type IV pilus assembly lipoprotein PilP	-1,564	0,001
GSU2030	pilO	type IV pilus biogenesis protein PilO	-1,241	0,008
GSU2032	pilM	type IV pilus biogenesis ATPase PilM	-1,272	0,000
GSU2034	pilX-2	type IV pilus minor pilin PilX	-2,297	0,000
GSU2035	pilW-2	type IV pilus minor pilin PilW	-1,299	0,000
GSU2036	pilV-2	type IV pilus minor pilin PilV	-2,275	0,000
GSU2037	fimU	type IV pilus minor pilin FimU	-1,368	0,008
GSU2038	pilY1-2	type IV pilus assembly protein PilY	-1,675	0,000
GSU2053	iorA-2	indolepyruvate:ferredoxin oxidoreductase subunit alpha	2,123	0,000
GSU2060	0	zinc protease PmbA	-1,895	0,001
GSU2063	0	metal-dependent phosphohydrolase; HDOD domain-containing	-1,759	0,005
GSU2067	rarA	recombination factor protein RarA	-1,597	0,028
GSU2069	0	HAD superfamily hydrolase	1,740	0,003
GSU2071	rnhA	ribonuclease H	1,630	0,024

GSU2072	0	[acyl-]glycerolphosphate acyltransferase	2,342	0,000
GSU2077	0	hypothetical protein	1,312	0,000
GSU2078	rodA	cell shape-determining protein RodA	1,550	0,030
GSU2082	0	nucleoside diphosphate-sugar dehydratase	1,479	0,028
GSU2083	rmlA	glucose-1-phosphate thymidyltransferase	1,326	0,000
GSU2094	0	response receiver-modulated cyclic diguanylate phosphodiesterase	2,746	0,023
GSU2098	cooS	carbon monoxide dehydrogenase; catalytic subunit	2,916	0,000
GSU2105	0	hypothetical protein	-1,351	0,035
GSU2110	0	hypothetical protein	1,417	0,004
GSU2137	0	RND family efflux pump outer membrane protein	2,297	0,015
GSU2147	0	heavy metal-translocating P-type ATPase	1,463	0,000
GSU2148	0	hypothetical protein	2,980	0,000
GSU2149	0	ArsR family transcriptional regulator	3,070	0,000
GSU2175	0	TrfA family protein	2,194	0,001
GSU2183	0	Fic family protein	2,326	0,000
GSU2184	ccaC	cytidine-specific tRNA nucleotidyltransferase	2,368	0,000
GSU2185	0	FlgM family protein	1,819	0,000
GSU2189	0	sensor histidine kinase	1,886	0,000
GSU2190	0	aldolase domain-containing protein	-1,172	0,007
GSU2193	0	ferritin-like domain-containing protein	-2,590	0,000
GSU2195	guaB	inosine-5'-monophosphate dehydrogenase	1,851	0,000
GSU2198	miaB	(dimethylallyl)adenosine tRNA methylthiotransferase	1,197	0,000
GSU2213	0	GAF domain-containing protein	-1,702	0,036
GSU2214	cheB40H	protein glutamate methyltransferase CheB associated with MCPs of class 40H; response receiver domain-containing	-1,969	0,022
GSU2217	cheY40H-3	response receiver CheY associated with MCPs of class 40H	-2,035	0,007
GSU2219	cheY40H-2	response receiver CheY associated with MCPs of class 40H	-1,902	0,003
GSU2226	era	GTPase Era	1,041	0,032
GSU2227	0	radical SAM domain-containing iron-sulfur cluster-binding oxidoreductase	3,127	0,000
GSU2228	rnc	ribonuclease III	2,875	0,000
GSU2229	tmk-1	thymidylate kinase	1,441	0,003
GSU2230	holB	DNA polymerase III subunit delta'	1,956	0,000
GSU2233	0	hypothetical protein	1,976	0,005
GSU2235	0	endoribonuclease L-PSP	1,588	0,024
GSU2236	relA	GTP/GDP 3'-pyrophosphokinase and (p)ppGpp 3'-pyrophosphohydrolase	2,946	0,000
GSU2237	rpoZ	DNA-directed RNA polymerase subunit omega	1,709	0,000
GSU2238	gmk	guanylate kinase	3,332	0,000
GSU2251	0	hypothetical protein	-2,574	0,011
GSU2256	0	ADP-heptose--lipopolysaccharide heptosyltransferase	2,232	0,000
GSU2261	lpxB	lipid-A-disaccharide synthase	-1,806	0,035

GSU2264	lpxA-1	UDP-N-acetylglucosamine acyltransferase	-1,710	0,013
GSU2269	loID	ABC transporter ATP-binding protein	2,730	0,000
GSU2270	loE	lipoprotein release ABC transporter membrane protein	1,867	0,000
GSU2272	0	lipoprotein	-1,217	0,028
GSU2276	0	hypothetical protein	-1,254	0,012
GSU2278	prfB	peptide chain release factor 2	-1,759	0,000
GSU2285	0	membrane-associated metal-dependent phosphohydrolase; HDc domain-containing	2,118	0,000
GSU2286	eno	enolase	-1,286	0,000
GSU2287	0	response regulator	1,625	0,000
GSU2288	0	sensor histidine kinase; HAMP domain-containing	1,859	0,000
GSU2289	0	nicotinate phosphoribosyltransferase	1,872	0,000
GSU2292	ald	alanine dehydrogenase	-1,425	0,014
GSU2294	omcM	cytochrome c	1,593	0,000
GSU2296	0	metal-dependent phosphohydrolase; HDOD domain-containing	1,954	0,000
GSU2297	0	sensor histidine kinase; Cache_1; HAMP and PAS domain-containing	1,465	0,030
GSU2301	0	hypothetical protein	4,090	0,000
GSU2302	0	HAD superfamily hydrolase	4,184	0,000
GSU2303	0	sodium/proton antiporter family protein	4,657	0,000
GSU2304	0	hypothetical protein	3,963	0,000
GSU2305	0	peptidoglycan-binding outer membrane lipoprotein Pal; OmpA family	1,848	0,004
GSU2307	can-2	carbonic anhydrase	1,811	0,029
GSU2313	0	response receiver-modulated diguanylate cyclase	-2,868	0,002
GSU2318	0	cyclopropane-fatty-acyl-phospholipid synthase	-1,349	0,020
GSU2319	0	hypothetical protein	-2,411	0,000
GSU2323	0	hypothetical protein	-2,762	0,001
GSU2329	0	cyclopropane-fatty-acyl-phospholipid synthase	-2,414	0,013
GSU2338	mrpG	monovalent cation/H antiporter subunit G	-2,713	0,001
GSU2352	aplC	sodium/solute symporter family protein	-2,268	0,042
GSU2355	0	hypothetical protein	1,863	0,001
GSU2361	treS	trehalose/maltose transglucosylase and maltokinase	-1,465	0,008
GSU2379	trpB2	tryptophan synthase subunit beta	-1,323	0,004
GSU2383	trpE	anthranilate synthase; catalytic subunit	1,776	0,000
GSU2390	htpG	heat shock protein 90	-2,320	0,000
GSU2403	0	hypothetical protein	1,374	0,001
GSU2404	0	pentapeptide repeat-containing protein	-2,055	0,000
GSU2405	0	hypothetical protein	-2,456	0,023
GSU2406	0	DnaJ domain-containing protein	-3,404	0,000
GSU2408	0	ATP-independent chaperone	-5,632	0,000
GSU2409	0	ATP-independent chaperone	-2,505	0,000
GSU2410	hspA-2	ATP-independent chaperone	-1,868	0,002
GSU2413	0	ABC transporter ATP-binding protein	1,686	0,001

GSU2424	0	hypothetical protein	1,888	0,000
GSU2425	metY-2	O-acetyl-L-homoserine sulfhydrylase	1,157	0,001
GSU2430	0	hypothetical protein	-1,829	0,004
GSU2431	nfeD	membrane-bound serine protease NfeD; long form	-2,224	0,000
GSU2433	0	ATP-dependent protease	-1,118	0,001
GSU2435	aceF	branched-chain alpha-keto acid dehydrogenase E2 subunit	-2,225	0,000
GSU2436	pdhB	pyruvate dehydrogenase E1 component subunit beta	-3,144	0,000
GSU2437	0	hypothetical protein	-1,885	0,000
GSU2438	0	antitoxin; Phd family	1,440	0,041
GSU2439	0	toxin; RelE family	1,881	0,044
GSU2441	0	SAM-dependent methyltransferase	-2,818	0,003
GSU2444	0	periplasmic substrate-binding histidine kinase	-2,741	0,000
GSU2445	0	aconitate hydratase	-2,979	0,000
GSU2446	lpdA-1	dihydrolipoamide dehydrogenase	-3,013	0,000
GSU2447	0	hypothetical protein	-2,162	0,001
GSU2448	sucB	2-oxoglutarate dehydrogenase; E2 protein; dihydrolipoamide succinyltransferase	-3,227	0,000
GSU2449	sucA	2-oxoglutarate dehydrogenase E1 component	-2,331	0,000
GSU2452	copA	copper-translocating P-type ATPase	-1,584	0,003
GSU2458	0	transpeptidase	1,398	0,000
GSU2461	0	hypothetical protein	-2,532	0,000
GSU2462	metX	homoserine O-acetyltransferase	1,846	0,000
GSU2465	0	metal-dependent hydrolase	1,960	0,008
GSU2468	0	hypothetical protein	1,312	0,021
GSU2471	0	RNA-directed DNA polymerase and maturase; group II intron origin	3,884	0,000
GSU2472	0	toxin; PIN family	5,910	0,000
GSU2473	0	antitoxin; AbrB family	4,895	0,000
GSU2475	0	sensor sigma-54-dependent transcriptional regulator	1,698	0,000
GSU2480	kdpA	potassium-transporting ATPase subunit A	-1,539	0,001
GSU2481	kdpB	potassium-transporting ATPase; B subunit	-2,444	0,000
GSU2483	kdpD	osmosensitive potassium channel sensor histidine kinase KdpD; KdpD and USP_OKCHK domain-containing	-1,976	0,002
GSU2484	kdpE	winged-helix transcriptional response regulator KdpE	-1,776	0,042
GSU2485	0	Kup system potassium transporter	1,160	0,004
GSU2486	0	hypothetical protein	-2,012	0,004
GSU2487	cpkA	amino acid kinase	-2,316	0,004
GSU2489	0	magnesium-dependent deoxyribonuclease	1,558	0,002
GSU2490	0	major facilitator superfamily membrane protein	2,735	0,000
GSU2491	0	major facilitator superfamily membrane protein	1,155	0,006
GSU2507	0	sensor histidine kinase; Cache_1 and HAMP domain-containing	2,511	0,000
GSU2519	yjiM	(R)-2-hydroxyacyl-CoA dehydratase YjiM	2,388	0,000

GSU2520	yjiL	(R)-2-hydroxyacyl-CoA dehydratase-radicalizing ATPase YjiL	3,101	0,000
GSU2521	yedF	selenium metabolism protein YedF	2,792	0,000
GSU2523	0	LysR family transcriptional regulator	1,952	0,000
GSU2524	0	sigma-54-dependent transcriptional response regulator	1,867	0,004
GSU2529	fusA-2	elongation factor G	1,160	0,004
GSU2536	0	dienelactone hydrolase family protein	-2,857	0,000
GSU2545	maf	Maf-like protein	-1,967	0,014
GSU2546	0	hypothetical protein	-2,218	0,000
GSU2551	0	LysM domain-containing protein	-1,527	0,000
GSU2561	0	hypothetical protein	-2,425	0,001
GSU2571	iscR-2	helix-turn-helix iron-sulfur cluster-binding transcriptional regulator IscR	1,791	0,001
GSU2572	cysE-1	serine O-acetyltransferase	1,059	0,001
GSU2576	0	metal-dependent phosphohydrolase; HDOD domain-containing	1,556	0,035
GSU2583	0	amidohydrolase	-3,572	0,000
GSU2596	0	lipoprotein	-2,611	0,001
GSU2608	pheA	chorismate mutase and prephenate dehydratase	1,115	0,003
GSU2609	0	PilB/PulE/GspE family ATPase	-1,695	0,034
GSU2612	0	rubrerythrin	-2,026	0,032
GSU2615	0	hypothetical protein	-2,129	0,000
GSU2616	secF	preprotein translocase subunit SecF	-1,062	0,009
GSU2622	0	sensor cyclic diguanylate phosphodiesterase; HAMP and GAF domain-containing heme-binding site	-1,812	0,003
GSU2633	0	lipoprotein	-3,346	0,000
GSU2641	0	PATAN domain GTPase-activating protein	-2,720	0,000
GSU2649	0	amino acid ABC transporter substrate-binding protein	-2,339	0,000
GSU2650	0	amino acid ABC transporter membrane protein	-2,025	0,000
GSU2651	0	amino acid ABC transporter ATP-binding protein	-2,419	0,022
GSU2656	bkdF	branched-chain alpha-keto acid dehydrogenase E2 subunit	-1,623	0,018
GSU2665	0	RND family efflux pump membrane fusion lipoprotein	1,792	0,000
GSU2666	0	TetR family transcriptional regulator	1,373	0,001
GSU2669	0	sensor histidine kinase	-1,091	0,008
GSU2672	0	lipoprotein	1,968	0,048
GSU2675	0	C1 family peptidase domain-containing protein	-2,122	0,000
GSU2678	0	ATP-independent chaperone	-1,921	0,000
GSU2686	rbbA	ribosome-associated ATPase and membrane protein RbbA	-1,950	0,026
GSU2687	0	RND family efflux pump membrane fusion protein	-2,901	0,001
GSU2692	0	periplasmic solute-binding protein	-1,340	0,012
GSU2696	acrB	RND family efflux pump inner membrane protein	1,578	0,001
GSU2697	acrA	RND family efflux pump membrane fusion lipoprotein	3,942	0,000
GSU2698	0	TetR family transcriptional regulator	3,900	0,000

GSU2701	tupB	tungstate ABC transporter membrane protein	1,289	0,018
GSU2707	ackA	acetate kinase A/propionate kinase 2	1,243	0,003
GSU2713	0	hypothetical protein	1,029	0,003
GSU2714	0	metal-dependent hydrolase	2,584	0,000
GSU2719	hoxS	bidirectional NAD-reducing hydrogenase; small subunit	-1,305	0,046
GSU2721	hoxF	bidirectional NAD-reducing hydrogenase; diaphorase subunit	-1,992	0,001
GSU2723	yedY	TMAO/DMSO reductase	-2,314	0,010
GSU2724	0	cytochrome c	-2,399	0,000
GSU2725	0	lipoprotein cytochrome c	-2,605	0,001
GSU2726	0	hypothetical protein	-2,267	0,000
GSU2728	0	hypothetical protein	1,561	0,000
GSU2731	omcC	lipoprotein cytochrome c	-1,870	0,000
GSU2737	omcB	lipoprotein cytochrome c	-1,177	0,000
GSU2742	0	hypothetical protein	-1,495	0,000
GSU2743	0	cytochrome c; 1 heme-binding site	-1,100	0,007
GSU2747	0	hypothetical protein	-4,272	0,000
GSU2750	0	hypothetical protein	1,363	0,000
GSU2751	dcuB	anaerobic C4-dicarboxylate transporter	2,092	0,000
GSU2753	0	sigma-54-dependent transcriptional response regulator	-2,793	0,000
GSU2755	0	periplasmic substrate-binding histidine kinase	-1,474	0,005
GSU2767	dhc1	cytochrome c	-2,453	0,010
GSU2769	0	metal-dependent hydrolase	2,168	0,008
GSU2770	0	lipoprotein	-1,884	0,001
GSU2780	0	hypothetical protein	5,801	0,000
GSU2781	0	RND family efflux pump membrane fusion protein	-1,291	0,025
GSU2787	0	LysR family transcriptional regulator	2,007	0,000
GSU2789	0	sensor histidine kinase; PAS; PAS and PAS domain-containing	1,435	0,001
GSU2791	0	hypothetical protein	-2,325	0,000
GSU2792	0	SAM-dependent methyltransferase	-3,044	0,000
GSU2793	0	hypothetical protein	-4,420	0,000
GSU2794	mscL	large-conductance mechanosensitive channel	-2,112	0,000
GSU2800	draG	ADP-ribosyl-(nitrogenase)-activating glycohydrolase	2,383	0,012
GSU2805	nifX	nitrogenase molybdenum-iron cofactor biosynthesis protein NifX	3,270	0,002
GSU2806	nifEN	bifunctional nitrogenase molybdenum-cofactor biosynthesis protein NifE/NifN	5,807	0,000
GSU2811	0	cytochrome c	-1,029	0,001
GSU2812	0	glutaredoxin family protein	-1,363	0,020
GSU2814	0	rubrerythrin	-1,643	0,000
GSU2815	0	sensor histidine kinase; PAS; PAS; PAS and PAS domain-containing	1,016	0,033
GSU2817	0	LysR family transcriptional regulator	1,267	0,036
GSU2819	nifK	nitrogenase molybdenum-iron protein subunit beta	4,307	0,000

GSU2820	nifD	nitrogenase molybdenum-iron protein subunit alpha	5,932	0,000
GSU2821	nifH	nitrogenase iron protein	5,791	0,000
GSU2822	gnfR	nitrogen fixation transcript antitermination response regulator; ANTAR domain-containing	5,461	0,000
GSU2823	ybhG	RND family efflux pump membrane fusion protein	-1,578	0,000
GSU2825	ybhS	ABC transporter membrane protein	-1,908	0,013
GSU2827	0	hypothetical protein	-1,885	0,002
GSU2829	0	deoxyribodipyrimidine photo-lyase	-1,599	0,000
GSU2835	map	methionine aminopeptidase	1,364	0,000
GSU2836	adk	adenylate kinase	1,543	0,000
GSU2837	secY	preprotein translocase subunit SecY	1,344	0,000
GSU2838	rplO	50S ribosomal protein L15	-1,551	0,000
GSU2839	rpmD	50S ribosomal protein L30	-1,646	0,010
GSU2840	rpsE	30S ribosomal protein S5	-1,004	0,006
GSU2841	rplR	50S ribosomal protein L18	-1,218	0,001
GSU2842	rplF	50S ribosomal protein L6	-1,958	0,000
GSU2843	rpsH	30S ribosomal protein S8	-1,943	0,000
GSU2846	rplX	50S ribosomal protein L24	-1,630	0,000
GSU2850	rplP	50S ribosomal protein L16	-1,711	0,000
GSU2852	rplV	50S ribosomal protein L22	-1,809	0,001
GSU2853	rpsS	30S ribosomal protein S19	-1,245	0,003
GSU2858	rpsJ	30S ribosomal protein S10	1,443	0,000
GSU2860	fusA-3	elongation factor G	1,925	0,000
GSU2861	rpsG	30S ribosomal protein S7	2,220	0,000
GSU2863	rpoB	DNA-directed RNA polymerase subunit beta	-1,138	0,000
GSU2864	rplL	50S ribosomal protein L7/L12	-1,400	0,000
GSU2873	0	radical SAM domain-containing iron-sulfur cluster-binding oxidoreductase	2,313	0,000
GSU2874	argC	N-acetyl-gamma-glutamyl-phosphate reductase	2,490	0,000
GSU2877	truA	tRNA pseudouridine synthase A	1,932	0,002
GSU2878	asd	aspartate-semialdehyde dehydrogenase	1,436	0,000
GSU2879	leuB	3-isopropylmalate dehydrogenase	2,166	0,000
GSU2882	omcG	cytochrome c	-2,249	0,000
GSU2883	omcH	cytochrome c	-2,045	0,011
GSU2884	omcA	cytochrome c	-1,277	0,020
GSU2895	0	hypothetical protein	-2,294	0,030
GSU2896	0	ankyrin	-1,863	0,007
GSU2898	omcN	lipoprotein cytochrome c	-1,801	0,000
GSU2899	0	lipoprotein cytochrome c	-1,117	0,044
GSU2912	omcO	cytochrome c	-2,188	0,000
GSU2915	0	sigma-54-dependent transcriptional response regulator	1,092	0,000
GSU2916	0	sensor histidine kinase; HAMP domain-containing heme-binding site	-1,646	0,001
GSU2917	tklG	type II secretion system pseudopilin TklG	-1,165	0,033

GSU2922	0	germane superfamily protein	1,087	0,025
GSU2923	murl	glutamate racemase	1,165	0,013
GSU2924	0	hypothetical protein	2,697	0,000
GSU2925	0	(R)-2-hydroxyacyl-CoA dehydratase	1,889	0,000
GSU2926	0	(R)-2-hydroxyacyl-CoA dehydratase-radicalizing ATPase	1,226	0,012
GSU2933	0	cytochrome b/b6 complex; iron-sulfur cluster-binding subunit	-3,794	0,000
GSU2934	0	cytochrome c	-1,593	0,000
GSU2935	0	lipoprotein cytochrome c	1,379	0,000
GSU2946	czcR	winged-helix heavy metal transcriptional response regulator	1,806	0,005
GSU2952	0	ArsR family transcriptional regulator	2,373	0,000
GSU2960	modC	molybdate ABC transporter ATP-binding protein	2,176	0,000
GSU2961	modB	molybdate ABC transporter permease	1,242	0,028
GSU2962	modA	molybdate ABC transporter substrate-binding protein	2,916	0,000
GSU2963	modD	ModD protein	3,896	0,000
GSU2964	modE	molybdate transport regulatory protein ModE	-1,476	0,000
GSU2967	0	ferritin-like domain-containing protein	-1,258	0,000
GSU2979	folk	2-amino-4-hydroxy-6- hydroxymethylidihydropteridine pyrophosphokinase	1,037	0,001
GSU2991	0	sensor histidine kinase; HAMP domain-containing	-1,013	0,024
GSU3002	cbiQ	cobalt ABC transporter membrane protein CbiQ	1,554	0,013
GSU3009	cobT	nicotinate-nucleotide--dimethylbenzimidazole phosphoribosyltransferase	1,065	0,024
GSU3010	cobU	adenosylcobinamide kinase and adenosylcobinamide phosphate guanylyltransferase	2,246	0,002
GSU3014	0	metal-dependent phosphohydrolase; HDOD domain-containing	2,216	0,002
GSU3015	flaG	flagellar protein FlaG	-2,687	0,000
GSU3029	0	2-acylglycerophosphoethanolamine acyltransferase	2,199	0,007
GSU3057	nfnA	dihydropyrimidine dehydrogenase subunit A	2,366	0,001
GSU3060	0	TetR family transcriptional regulator	2,107	0,043
GSU3062	0	radical SAM domain-containing iron-sulfur cluster-binding oxidoreductase	1,660	0,000
GSU3063	ftsZ	cell division protein FtsZ	-1,327	0,000
GSU3064	ftsA	cell division protein FtsA	-3,068	0,000
GSU3065	ftsQ	cell division protein FtsQ	-1,329	0,012
GSU3066	ddl	D-alanine--D-alanine ligase	-1,632	0,000
GSU3067	murB	UDP-N-acetylenolpyruvoylglucosamine reductase	-1,821	0,002
GSU3068	murC	UDP-N-acetylmuramate--L-alanine ligase	-1,219	0,009
GSU3069	murG	undecaprenyldiphospho-muramoylpentapeptide beta-N-acetylglucosaminyltransferase	-1,398	0,001
GSU3070	ftsW	cell division protein FtsW	-1,550	0,000
GSU3071	murD	UDP-N-acetylmuramylalanine--D-glutamate ligase	-2,614	0,000
GSU3076	ftsL	cell division septum formation protein FtsL	1,108	0,003

GSU3077	rsmH	16S rRNA m(4)C1402 methyltransferase	1,271	0,000
GSU3078	mraZ	cell division protein MraZ	1,673	0,000
GSU3085	yqfO	dimetal-binding protein YqfO	2,004	0,000
GSU3087	srtN	NAD-dependent protein deacetylase; Sir2 family	2,142	0,000
GSU3088	0	misacylated tRNA(Pro) deacylase; YbaK/ProX family	2,358	0,000
GSU3089	rpoD	RNA polymerase sigma-70 factor RpoD	1,407	0,000
GSU3090	dnaG	DNA primase	2,540	0,000
GSU3091	0	membrane protein implicated in colicin V production	2,248	0,000
GSU3092	yqeY	hypothetical protein	2,822	0,000
GSU3096	hisA	1-(5-phosphoribosyl)-5-[(5-phosphoribosylamino)methylideneamino] imidazole-4-carboxamide isomerase	-1,675	0,024
GSU3103	hemK	N5-glutamine S-adenosyl-L-methionine-dependent methyltransferase	2,063	0,000
GSU3104	prfA	peptide chain release factor 1	1,067	0,000
GSU3105	0	hypothetical protein	2,828	0,000
GSU3106	thyX	FAD-dependent thymidylate synthase	3,590	0,000
GSU3116	0	[acyl-]glycerolphosphate acyltransferase	1,818	0,000
GSU3125	mtd	mannitol dehydrogenase	1,610	0,045
GSU3126	0	oxidoreductase; aldo/keto reductase family	2,538	0,000
GSU3127	0	AraC family transcriptional regulator	1,484	0,000
GSU3129	norM	sodium-driven efflux pump; MatE and MatE domain-containing	1,227	0,025
GSU3130	0	lipoprotein	-1,534	0,001
GSU3132	hup	histone-like protein	-1,378	0,000
GSU3143	0	FKBP-type peptidylprolyl cis-trans isomerase	2,334	0,025
GSU3146	moaA	pyranopterin triphosphate synthase	1,792	0,000
GSU3148	0	sensor histidine kinase; GAF domain-containing	1,265	0,002
GSU3151	0	hypothetical protein	-1,803	0,036
GSU3162	ltaA	L-allo-threonine aldolase; stereospecific	-1,722	0,007
GSU3165	tssL	type VI secretion system inner membrane protein TssL	1,917	0,016
GSU3187	frx-6	ferredoxin	-1,681	0,016
GSU3188	0	rubredoxin	-1,374	0,026
GSU3189	0	hypothetical protein	1,149	0,004
GSU3202	0	outer membrane lipoprotein carrier/sorting protein LolA	-1,028	0,034
GSU3205	rimO	30S ribosomal protein S12 methylthiotransferase	-1,619	0,002
GSU3206	0	TraR/DksA family zinc finger transcriptional regulator	-1,773	0,000
GSU3213	obgE	GTPase CgtA	1,491	0,000
GSU3214	0	cytochrome c	-2,532	0,000
GSU3240	0	radical SAM domain-containing iron-sulfur cluster-binding oxidoreductase	2,452	0,000
GSU3243	0	hypothetical protein	-1,656	0,000
GSU3251	0	hypothetical protein	-3,396	0,000
GSU3252	0	sensor histidine kinase; GAF domain-containing	-1,449	0,000
GSU3253	0	response regulator	-2,605	0,000

GSU3254	0	mannose-1-phosphate guanylyltransferase/mannose-6-phosphate isomerase-like protein	-3,521	0,000
GSU3255	0	glycoside hydrolase	-3,788	0,000
GSU3256	galT	UDP-glucose--galactose-1-phosphate uridylyltransferase	-2,956	0,000
GSU3257	glgA-2	glycogen synthase	-2,781	0,000
GSU3261	0	response regulator	2,152	0,000
GSU3262	uvrB	excinuclease ABC subunit B	1,604	0,000
GSU3271	0	outer membrane channel; OprB family	1,890	0,008
GSU3273	0	hypothetical protein	5,357	0,000
GSU3274	0	cytochrome c; 1 heme-binding site	1,534	0,000
GSU3277	0	LysM domain-containing protein	-2,073	0,001
GSU3280	0	thioredoxin-like protein disulfide reductase	2,109	0,000
GSU3281	trxA	thioredoxin	2,063	0,000
GSU3283	0	ResC/HemX-like cytochrome c biogenesis membrane protein	1,482	0,001
GSU3285	hemC	porphobilinogen deaminase	-1,549	0,000
GSU3289	0	ferritin-like domain-containing protein	-2,812	0,000
GSU3292	0	Fur family transcriptional regulator	1,560	0,000
GSU3293	0	ferritin-like domain-containing protein	1,374	0,000
GSU3295	0	hypothetical protein	1,160	0,000
GSU3300	0	biotin-dependent acyl-CoA carboxylase; biotin carboxylase subunit	-1,205	0,002
GSU3301	tmk-2	thymidylate kinase	-1,231	0,040
GSU3304	ompJ	outer membrane channel OmpJ	-1,633	0,000
GSU3305	0	hypothetical protein	-1,865	0,000
GSU3308	purA	adenylosuccinate synthetase	-1,460	0,000
GSU3309	0	ATPase	-1,239	0,029
GSU3311	0	heme-binding sensor globin domain-containing protein	2,599	0,000
GSU3319	ppiA	cytosolic peptidylprolyl cis-trans isomerase; cyclophilin A-like protein	1,358	0,000
GSU3320	0	SAM-dependent methyltransferase	1,568	0,014
GSU3321	0	phosphoglucomutase/phosphomannomutase family protein	1,118	0,014
GSU3322	corA-2	magnesium transport protein CorA	1,001	0,036
GSU3326	0	hypothetical protein	1,062	0,025
GSU3330	0	NADH-dependent flavin oxidoreductase; Oye family	-1,342	0,000
GSU3333	aroG-1	3-deoxy-7-phosphoheptulonate synthase	1,698	0,000
GSU3336	0	hypothetical protein	1,484	0,029
GSU3340	groEL	chaperonin GroEL	-1,479	0,000
GSU3341	prkA	protein serine/threonine kinase PrkA	-1,765	0,000
GSU3342	0	hypothetical protein	-3,019	0,000
GSU3343	0	SpoVR-like family protein	-3,264	0,000
GSU3344	0	AAA ATPase	-2,997	0,000
GSU3345	0	hypothetical protein	-2,607	0,002
GSU3347	0	U32 family peptidase	1,836	0,000

GSU3349	0	cyclase/hydrolase	-2,395	0,000
GSU3350	0	sensor histidine kinase response receiver diguanylate cyclase	-3,553	0,000
GSU3351	0	hypothetical protein	-4,754	0,000
GSU3356	0	diguanylate cyclase; HAMP domain-containing	1,024	0,009
GSU3359	0	hypothetical protein	1,949	0,000
GSU3364	hgtR	hydrogen-dependent growth transcriptional repressor	2,661	0,000
GSU3365	cysS	cysteinyl-tRNA ligase	-1,633	0,000
GSU3368	ispD	2-C-methyl-D-erythritol 4-phosphate cytidylyltransferase	1,264	0,007
GSU3373	rsmB	16S rRNA (5-methyl-C967)-methyltransferase	2,775	0,000
GSU3378	glnE	glutamate--ammonia ligase adenylyltransferase	-1,238	0,021
GSU3379	mtnA	S-methyl-5-thio-alpha-D-ribose-1-phosphate isomerase	-1,351	0,020
GSU3388	0	hypothetical protein	1,190	0,000
GSU3392	0	branched-chain amino acid ABC transporter ATP-binding protein	-1,656	0,010
GSU3394	0	branched-chain amino acid ABC transporter membrane protein	1,262	0,000
GSU3395	putA	proline dehydrogenase and Delta-1-pyrroline-5-carboxylate dehydrogenase	1,539	0,000
GSU3396	0	GntR family transcriptional regulator	2,322	0,000
GSU3397	0	hypothetical protein	3,175	0,000
GSU3398	0	RND family efflux pump outer membrane protein	2,225	0,023
GSU3399	0	RND family efflux pump membrane fusion lipoprotein	3,435	0,001
GSU3401	0	branched-chain amino acid ABC transporter substrate-binding lipoprotein	-1,602	0,000
GSU3402	0	hypothetical protein	-1,586	0,001
GSU3403	0	outer membrane channel OmpJ-like protein	-1,636	0,000
GSU3404	0	amino acid ABC transporter ATP-binding protein	-1,562	0,000
GSU3407	0	hypothetical protein	2,862	0,000
GSU3409	0	hypothetical protein	1,498	0,000
GSU3414	0	hypothetical protein	1,431	0,006
GSU3415	0	radical SAM domain-containing iron-sulfur cluster-binding oxidoreductase	1,470	0,000
GSU3429	nuoN-2	NADH dehydrogenase I subunit N	-1,147	0,044
GSU3435	0	ankyrin	-2,317	0,000
GSU3436	nuoH-2	NADH:ubiquinone oxidoreductase subunit H	-1,622	0,000
GSU3437	0	sensor histidine kinase; PAS and GAF domain-containing	-2,321	0,000
GSU3439	nuoG-2	NADH dehydrogenase subunit G	-1,292	0,003
GSU3441	nuoF-2	NADH dehydrogenase I subunit F	-1,547	0,003
GSU3442	0	hypothetical protein	-3,005	0,001
GSU3443	nuoE-2	NADH dehydrogenase subunit E	-2,095	0,034
GSU3444	nuoBCD	trifunctional NADH dehydrogenase I subunit B/C/D	-1,063	0,001
GSU3446	trx-3	thioredoxin family protein; selenocysteine-containing	-1,877	0,001

GSU3447	prx-4	peroxiredoxin; 1-Cys subfamily	-2,950	0,000
GSU3448	0	acetate kinase-like protein	-2,165	0,000
GSU3449	frx-4	ferredoxin	-1,662	0,009
GSU3454	0	radical SAM domain-containing iron-sulfur cluster-binding oxidoreductase	1,937	0,000
GSU3457	0	amino acid-binding ACT domain-containing regulatory protein	-1,057	0,009
GSU3459	0	hypothetical protein	-3,363	0,000
GSU3460	0	AmsE-like family glycosyltransferase	-3,089	0,000
GSU3461	0	acyl-CoA thioesterase	-3,082	0,000
GSU3462	0	lipoprotein	-2,702	0,000
GSU3466	yidC	preprotein translocase subunit YidC	1,234	0,003
GSU3467	0	hypothetical protein	2,150	0,007
GSU3473	0	hypothetical protein	-2,827	0,000
GSU3474	0	hypothetical protein	-1,713	0,016
GSU3477	0	hypothetical protein	4,241	0,000
GSU3478	0	hypothetical protein	-2,085	0,000
GSU3484	0	ABC transporter ATP-binding protein	2,756	0,000
GSU3485	0	ABC transporter membrane protein	1,876	0,000
GSU3486	0	hypothetical protein	2,401	0,000
GSU3495	0	hypothetical protein	3,072	0,000
GSU3506	0	hypothetical protein	1,087	0,000
GSU3509	0	hypothetical protein	2,499	0,000
GSU3513	0	hypothetical protein	-2,005	0,035
GSU3518	0	sensor histidine kinase	4,143	0,000
GSU3520	0	hypothetical protein	-1,193	0,000
GSU3524	0	lipoprotein	-1,528	0,000
GSU3533	0	toxin; RelE family	4,058	0,000
GSU3545	0	hypothetical protein	2,060	0,000
GSU3546	0	hypothetical protein	1,492	0,019
GSU3549	0	hypothetical protein	-1,348	0,044
GSU3560	0	hypothetical protein	2,046	0,000
GSU3567	0	hypothetical protein	-1,716	0,005
GSU3583	0	hypothetical protein	-2,137	0,000
GSU3586	0	YVTN family beta-propeller domain-containing protein	-1,861	0,000
GSU3601	0	hypothetical protein	-2,657	0,000
GSU3603	0	hypothetical protein	-3,501	0,000
GSU3608	ybhF-N	ABC transporter ATP-binding protein	-3,361	0,000
GSU3609	ybhF-C	ABC transporter ATP-binding protein	-3,031	0,000
GSU3612	rpsL	30S ribosomal protein S12	1,525	0,000
GSU3624	0	rubredoxin	2,669	0,000
GSU3628	pgk	phosphoglycerate kinase	-1,304	0,000
GSU3629	0	hypothetical protein	-1,966	0,000

Supplementary Table 2. *G. metallireducens* gene expression.

ID	gene name		GmA_mixA	
			log2fc	padj
Gmet_0244	0	hypothetical protein	1,953	0,009
Gmet_0294	nrfA-1	cytochrome c nitrite and sulfite reductase; catalytic subunit lipoprotein	2,201	0,006
Gmet_0329	narG-1	nitrate reductase Z subunit alpha	1,326	0,030
Gmet_0392	yqeY	hypothetical protein	-1,307	0,000
Gmet_1123	prpD	2-methylcitrate dehydratase	-1,786	0,009
Gmet_1124	0	type I citrate synthase	-1,440	0,018
Gmet_1125	0	succinyl:acetate coenzyme A transferase	-1,525	0,010
Gmet_1293	0	oxidoreductase; 2-nitropropane dioxygenase family	-1,130	0,009
Gmet_1380	dsbA	disulfide bond formation oxidoreductase DsbA	2,647	0,015
Gmet_1929	cydB	cytochrome bd menaquinol oxidase; subunit II	1,762	0,050
Gmet_1930	cydA	cytochrome bd menaquinol oxidase; subunit I	2,209	0,000
Gmet_2058	0	thiolase	1,572	0,001
Gmet_2059	0	short-chain dehydrogenase/reductase family oxidoreductase	1,391	0,009
Gmet_2069	sucC-2	succinyl-CoA synthetase subunit beta	1,473	0,001
Gmet_2075	bamM	glutaryl-CoA dehydrogenase	1,344	0,004
Gmet_2150	bamR	cyclohexa-1;5-dienecarbonyl-CoA hydratase	1,346	0,015
Gmet_2152	0	electron transfer flavoprotein subunit alpha	1,162	0,005
Gmet_2153	0	electron transfer flavoprotein subunit beta	1,345	0,000
Gmet_2742	0	hypothetical protein	-1,588	0,001
Gmet_2921	0	hypothetical protein	1,707	0,005
Gmet_2971	0	radical SAM domain-containing iron-sulfur cluster-binding oxidoreductase	-1,429	0,006
Gmet_3038	0	RND family efflux pump membrane fusion protein	-1,004	0,041
Gmet_3186	prx-2	peroxiredoxin; typical 2-Cys subfamily	2,270	0,000

Supplementary Table 2. *S. oneidensis* gene expression.

ID	gene_name	product	SoA_mixA	
			log2fc	padj
SO_0017		bifunctional TolB-family protein/amidohydrolase	2,970	0,000
SO_0019	tusA	tRNA 2-thiouridine synthesizing protein TusA	-1,793	0,014
SO_0020	fadA	aerobic fatty oxidation complex 3-ketoacyl-CoA thiolase beta subunit FadA	1,221	0,004
SO_0021	fadB	aerobic fatty oxidation complex 3-hydroxyacyl-CoA epimerase alpha subunit FadB	1,179	0,010
SO_0027	hemG	oxygen-independent protoporphyrinogen oxidase HemG	-1,105	0,034
SO_0052	secB	protein export chaperone SecB	1,082	0,001
SO_0075	icfE	long-chain-fatty-acid--CoA ligase IcfE	-2,527	0,000
SO_0097	hutU	urocanate hydratase HutU	1,234	0,027
SO_0098	hutH	histidine ammonia-lyase HutH	1,851	0,001
SO_0112		inhibitor of invertebrate-type lysozyme PliI-like family	2,411	0,000
SO_0130	prtV	extracellular metalloprotease PrtV	2,137	0,000
SO_0154		inner membrane protein of unknown function DUF893	-1,566	0,012
SO_0160		aminobenzoyl-glutamate transporter AbgT family	1,396	0,036
SO_0162	pckA	phosphoenolpyruvate carboxykinase PckA	1,692	0,000
SO_0183		acteyltransferase GNAT family	1,702	0,031
SO_0198	fabR	transcriptional repressor of fatty acid biosynthesis FabR	-1,518	0,000
SO_0208		RNA-binding protein	1,275	0,010
SO_0224	rpoB	DNA-directed RNA polymerase beta subunit RpoB	1,056	0,001
SO_0225	rpoC	DNA-directed RNA polymerase beta' subunit RpoC	1,850	0,000
SO_0229	tufA	translation elongation factor Tu TufA	1,463	0,000
SO_0234	rplB	50S ribosomal protein L2 RplB	1,145	0,002
SO_0235	rpsS	30S ribosomal protein S19 RpsS	1,342	0,001
SO_0236	rplV	50S ribosomal protein L22 RplV	1,369	0,000
SO_0237	rpsC	30S ribosomal protein S3 RpsC	1,903	0,000
SO_0238	rplP	50S ribosomal protein L16 RplP	1,943	0,000
SO_0239	rpmC	50S ribosomal protein L29 RpmC	1,536	0,000
SO_0240	rpsQ	30S ribosomal protein S17 RpsQ	1,711	0,000
SO_0246	rplF	50S ribosomal protein L6 RplF	1,079	0,008
SO_0247	rplR	50S ribosomal protein L18 RplR	1,618	0,000
SO_0248	rpsE	30S ribosomal protein S5 RpsE	1,468	0,000
SO_0249	rpmD	50S ribosomal protein L30 RpmD	1,172	0,018
SO_0250	rplO	50S ribosomal protein L15 RplO	1,577	0,000
SO_0251	secY	preprotein translocase subunit SecY	1,851	0,000
SO_0252	rpmJ	50S ribosomal protein L36 RpmJ	1,574	0,000
SO_0254	rpsK	30S ribosomal protein S11 RpsK	1,169	0,004
SO_0255	rpsD	30S ribosomal protein S4 RpsD	1,247	0,000
SO_0256	rpoA	DNA-directed RNA polymerase alpha subunit RpoA	1,363	0,000
SO_0257	rplQ	50S ribosomal protein L17 RplQ	1,701	0,000

SO_0265	ccmI	apo-cytochrome c chaperone CcmI	-1,226	0,004
SO_0278	argG	argininosuccinate synthase ArgG	2,245	0,000
SO_0279	argH	argininosuccinate lyase ArgH	3,132	0,000
SO_0296		10 TMS drug/metabolite efflux pump (DME) family	-1,883	0,007
SO_0306		outer membrane protein COG4775 family	1,526	0,040
SO_0309		membrane protein MAPEG superfamily	1,487	0,035
SO_0311	ygiQ	uncharacterized radical SAM protein YgiQ	-1,274	0,000
SO_0313	potE	putrescine:ornithine antiporter PotE	-1,921	0,004
SO_0314	speF	ornithine decarboxylase SpeF	-2,293	0,000
SO_0321		putative periplasmic protein of unknown function	1,759	0,002
SO_0342	prpF	2-methyl aconitate cis-trans isomerase PrpF	2,393	0,000
SO_0343	acnD	2-methyl citrate dehydratase Fe-S dependent AcnD	3,169	0,000
SO_0344	prpC	2-methylcitrate synthase PrpC	2,698	0,000
SO_0345	prpB	2-methylisocitrate lyase PrpB	1,941	0,000
SO_0346	prpR	methylcitrate-responsive transcriptional regulator of methylisocitrate utilization PrpR	1,179	0,003
SO_0355		AMP-dependent synthetase and ligase family protein	2,381	0,000
SO_0363		nucleoside-diphosphate-sugar pyrophosphorylase	-1,081	0,015
SO_0393	fis	global transcriptional activator Fis	-1,955	0,000
SO_0394	dusB	tRNA-dihydrouridine synthase DusB	-1,683	0,000
SO_0404		zinc dependent metalloprotease domain lipoprotein	1,655	0,000
SO_0412	yacF	protein of unknown function DUF1342 YacF	1,206	0,031
SO_0417	pilA	type IV pilin protein PilA	1,097	0,000
SO_0423	pdhR	transcriptional repressor of pyruvate metabolism PdhR	-1,641	0,000
SO_0429	pepO	cell surface zinc endopeptidase PepO	2,457	0,000
SO_0432	acnB	aconitate hydratase AcnB	1,165	0,000
SO_0435	hemE	uroporphyrinogen decarboxylase HemE	-1,163	0,001
SO_0439		hypothetical protein	-3,753	0,000
SO_0443	zntR	zinc and cadmium (II) responsive transcriptional activator ZntR	-1,831	0,000
SO_0450		transporter MFS superfamily	-2,270	0,000
SO_0452	trxC	thioredoxin 2 TrxC	1,461	0,008
SO_0455		alpha-ketoglutarate uptake system bifunctional large and small subunit permease component	1,598	0,008
SO_0456		alpha-ketoglutarate uptake system substrate-binding component	1,185	0,036
SO_0458		hypothetical protein	-2,096	0,000
SO_0487	nosF	ABC-type copper transport system ATPase component NosF	-1,623	0,018
SO_0488	nosY	ABC-type copper transport system permease component NosY	-1,480	0,027
SO_0490		transmembrane transcriptional regulator CadC family	-1,264	0,027
SO_0514		protein of unknown function DUF3478	-1,312	0,003
SO_0519		heavy metal efflux pump MFP component CzcB family	2,031	0,001
SO_0520		heavy metal efflux pump permease component CzcA family	2,091	0,000
SO_0521		monooxygenase domain protein	1,129	0,040

SO_0522	mscL	large conductance mechanosensitive ion channel protein MscL	1,103	0,038
SO_0552		predicted periplasmic protein	1,129	0,011
SO_0554		periplasmic protein of unknown function DUF3016	1,330	0,001
SO_0555		bifunctional diguanylate cyclase/phosphodiesterase	-2,020	0,005
SO_0563		membrane protein	2,478	0,000
SO_0576		predicted ATPase PhoH family	1,027	0,011
SO_0578	arcS	periplasmic metalloprotease	1,202	0,005
SO_0581		Zn-binding protein	-2,537	0,000
SO_0582	tpmT	thiopurine S-methyltransferase TpmT	-2,036	0,000
SO_0595		hypothetical protein	-1,395	0,003
SO_0598	yjeF	hydroxyethylthiazole kinase-related protein YjeF	-1,542	0,000
SO_0599	yjeE	ATPase YjeE	-1,032	0,036
SO_0609	petB	ubiquinol-cytochrome c reductase cytochrome b subunit PetB	1,196	0,003
SO_0613	pabA	para-aminobenzoate synthase glutamine amidotransferase subunit PabA	-2,206	0,001
SO_0614		peptidase S9 family	1,825	0,000
SO_0617	argD	bifunctional acetylorbithine aminotransferase/succinyl-diaminopimelate aminotransferase/succinylornithine transaminase ArgD	1,989	0,000
SO_0618	astA	arginine N-succinyltransferase AstA	2,442	0,000
SO_0619	astD	succinylglutamic semialdehyde dehydrogenase AstD	2,023	0,000
SO_0620		putative hydrolase involved in arginine and ornithine metabolism	2,349	0,000
SO_0623		hypothetical protein	1,162	0,027
SO_0632	hrpB	ATP-dependent helicase HrpB	-1,062	0,030
SO_0668	gpF	Mu phage minor capsid protein GpF	-2,684	0,000
SO_0697	cutA	divalent cation tolerance protein CutA	-1,116	0,041
SO_0702		multidrug and toxin efflux protein MATE family	-1,791	0,001
SO_0720		predicted periplasmic protein	1,570	0,032
SO_0727		protein of unknown function DUF134	-2,258	0,004
SO_0728		hypothetical protein	-1,515	0,016
SO_0741	ggtB	gamma-glutamyltransferase GgtB	2,166	0,000
SO_0743	fbpB	ABC-type Fe <sup>3</sup> uptake system permease component FbpB	2,009	0,005
SO_0744	fbpA	ABC-type Fe <sup>3</sup> uptake system substrate-binding component FbpA	2,974	0,000
SO_0746		glutathione S-transferase family protein	1,374	0,014
SO_0752		hypothetical protein	-1,262	0,000
SO_0753		hypothetical protein	2,030	0,000
SO_0762		isochorismate hydrolase family protein	2,308	0,001
SO_0783		superfamily I DNA and RNA helicase	1,061	0,008
SO_0798		TonB-dependent receptor	-1,682	0,017
SO_0807		predicted phosphoribosyltransferase	-1,518	0,001
SO_0808		protein of unknown function DUF3622	-1,160	0,006
SO_0809	azu	periplasmic azurin Azu	2,901	0,000

SO_0826		protein of unknown function DUF342	1,626	0,004
SO_0830	phoA	periplasmic alkaline phosphatase PhoA	1,019	0,017
SO_0831	gshB	ATP-dependent glutathione synthetase GshB	1,158	0,006
SO_0837	blaA	class D carbapenem-hydrolyzing beta-lactamase BlaA	1,623	0,000
SO_0844		hypothetical protein	-5,522	0,000
SO_0846	napH	quinol dehydrogenase ferredoxin subunit NapH	-1,545	0,035
SO_0847	napG	periplasmic nitrate reductase ferredoxin component NapG	-1,642	0,013
SO_0848	napA	periplasmic nitrate reductase molybdopterin-binding subunit NapA	-1,600	0,000
SO_0858	glyP	Na( )-linked D-alanine glycine transporter GlyP	2,124	0,001
SO_0862	serA	D-3-phosphoglycerate dehydrogenase SerA	1,248	0,002
SO_0871	folK	2-amino-4-hydroxy-6- hydroxymethyldihydropteridine pyrophosphokinase FolK	-1,059	0,044
SO_0872	pcnB	polyA polymerase PcnB	-1,265	0,000
SO_0873	yadB	glutamyl-Q-tRNA-Asp synthetase YadB	-1,157	0,032
SO_0881		predicted TAT leader-containing periplasmic protein	1,832	0,000
SO_0882		oxidoreductase GMC family	1,556	0,001
SO_0883	gfaA	glutathione-dependent formaldehyde-activating enzyme GfaA	2,139	0,003
SO_0900		oxidoreductase aldo/keto reductase family	1,932	0,000
SO_0902	nqrA	Na-translocating NADH-quinone reductase subunit A NqrA	-1,527	0,004
SO_0906	nqrE	Na-translocating NADH-quinone reductase subunit E NqrE	-1,787	0,011
SO_0912		hypothetical protein	1,652	0,045
SO_0918	aaiD	acyl-homoserine lactone acylase AaiD	2,350	0,000
SO_0919	sdaC	serine uptake transporter SdaC	-2,464	0,000
SO_0922		dicarboxylate:amino acid:cation symporter DAACS family	-1,996	0,000
SO_0931	e4pd	D-erythrose-4-phosphate dehydrogenase E4pd	-1,026	0,005
SO_0933	fba	fructose-bisphosphate aldolase class II Calvin cycle subtype Fba	1,193	0,000
SO_0935	nhaD	sodium:proton antiporter NhaD	-2,706	0,000
SO_0940		transmembrane transcriptional regulator	-1,739	0,018
SO_0944		radical SAM protein TatD family-associated	-2,870	0,000
SO_0946		RND superfamily efflux pump MFP component	1,944	0,018
SO_0956	ahpF	alkyl hydroperoxide reductase flavoprotein component AhpF	-1,442	0,003
SO_0958	ahpC	alkyl hydroperoxide reductase peroxiredoxin component AhpC	-1,431	0,002
SO_0959		periplasmic leucyl metal-dependent aminopeptidase	1,071	0,032
SO_0970	fccA	periplasmic fumarate reductase FccA	-1,546	0,002
SO_0974		putative cytoplasmic protein	-1,278	0,012
SO_0975		disulphide interchange protein DsbD family	-2,050	0,000
SO_0980	rumB	23S rRNA (uracil747-C5)-methyltransferase RumB	-1,954	0,000
SO_0988		molybdopterin-binding oxidoreductase	-1,243	0,030

SO_1013	nuoJ	NADH-ubiquinone oxidoreductase subunit J NuoJ	1,385	0,020
SO_1015	nuoH	NADH-ubiquinone oxidoreductase subunit H NuoH	1,516	0,009
SO_1016	nuoG	NADH-ubiquinone oxidoreductase subunit G NuoG	1,172	0,027
SO_1017	nuoF	NADH-ubiquinone oxidoreductase subunit F NuoF	1,126	0,027
SO_1030	metH	B12-dependent 5-methyltetrahydrofolate-- homocysteine methyltransferase MetH	1,432	0,009
SO_1047	lrgA	inner membrane protein LrgA	-4,463	0,000
SO_1048	lrgB	inner membrane protein LrgB	-4,892	0,000
SO_1049		acteyltransferase GNAT family	-1,475	0,024
SO_1052	pitB	metal ion-phosphate:proton symporter PitB	-1,540	0,004
SO_1056		methyl accepting sensory transducer with Cache_1 small molecule binding domain	1,099	0,023
SO_1060		TIGR02722 family lipoprotein	1,295	0,000
SO_1066	exeM	extracellular endonuclease ExeM	-1,138	0,035
SO_1075		dipeptidyl peptidase S46 family	3,269	0,000
SO_1094		hypothetical protein	2,829	0,000
SO_1095	metY	O-acetylhomoserine (thiol)-lyase MetY	1,680	0,006
SO_1104	nqrB	Na-translocating NADH-quinone reductase subunit B NqrB	1,016	0,006
SO_1105	nqrC	Na-translocating NADH-quinone reductase subunit C NqrC	1,204	0,000
SO_1106	nqrD	Na-translocating NADH-quinone reductase subunit D NqrD	1,652	0,000
SO_1108	nqrF	Na-translocating NADH-quinone reductase subunit F NqrF	1,659	0,000
SO_1114	dinB	DNA polymerase IV DinB	-1,697	0,000
SO_1144		chemotaxis signal transduction system methyl accepting sensory transducer	1,583	0,005
SO_1150	rpiA	ribose 5-phosphate isomerase RpiA	-1,027	0,009
SO_1158	dpsA	DNA-binding ferritin-like protein (oxidative damage protectant) DpsA	-1,653	0,003
SO_1165	rlpA	septal ring lipoprotein RlpA	1,393	0,012
SO_1181	miaB	tRNA-N(6)-(isopentenyl)adenosine-37 thiotransferase enzyme MiaB	-1,251	0,000
SO_1187		hypothetical protein	-1,182	0,030
SO_1191	greA	transcription elongation factor GreA	-1,018	0,004
SO_1192		predicted extracytoplasmic protein	-1,443	0,001
SO_1193	secD	preprotein translocase subunit SecD	-1,287	0,015
SO_1200	tpiA	triosephosphate isomeraseTpiA	-1,174	0,000
SO_1205	rbfA	ribosome-binding factor A RbfA	1,269	0,039
SO_1207	rpsO	30S ribosomal protein S15 RpsO	-1,231	0,000
SO_1208		bifunctional diguanylate cyclase/phosphodiesterase	1,097	0,015
SO_1210	nlpl	globular tetratricopeptide repeat containing lipoprotein Nlpl	1,034	0,002
SO_1217	deoC	deoxyribose-phosphate aldolase DeoC	-1,025	0,014
SO_1218	deoA	thymidine phosphorylase DeoA	-1,128	0,004
SO_1225		c-di-GMP-binding protein	1,081	0,035

SO_1236		purine transporter AzgA family	-1,689	0,001
SO_1250		SCP-2 sterol transfer family protein	-1,982	0,000
SO_1251		ferredoxin 4Fe-4S	-1,511	0,038
SO_1252	yegQ	peptidase U32 family YegQ	-1,817	0,000
SO_1258		adenylosuccinate synthetase	-2,183	0,000
SO_1265	puuR	putrescine degradation gene regulator PuuR	-1,331	0,000
SO_1270	potF	ABC-type putrescine uptake system substrate-binding component PotF	1,223	0,001
SO_1271	potG	ABC-type putrescine uptake system ATPase component PotG	2,012	0,000
SO_1274	puuB	gamma-glutamylputrescine oxidoreductase PuuB	-1,185	0,003
SO_1288	rpsU	30S ribosomal protein S21 RpsU	-1,252	0,002
SO_1289	ygiD	essential endopeptidase YgiD	-1,210	0,000
SO_1300	hemL	glutamate-1-semialdehyde-21-aminomutase HemL	-1,265	0,000
SO_1301	pyrB	aspartate carbamoyltransferase PyrB	-1,169	0,003
SO_1324	gltD	NADPH-dependent glutamate synthase small subunit GltD	2,621	0,000
SO_1325	gltB	NADPH-dependent glutamate synthase large subunit GltB	1,846	0,000
SO_1328	oxyR	transcriptional regulator of oxidative stress OxyR	-1,495	0,001
SO_1329	cyaC	adenylate cyclase CyaC	-1,663	0,000
SO_1337		predicted periplasmic protein	1,121	0,042
SO_1376		integral membrane protein of unknown function DUF1449	1,278	0,035
SO_1377		putative negative regulator of univalent cation permeability	2,282	0,000
SO_1381		alkyl hydroperoxide reductase/ thiol specific antioxidant family protein	-1,411	0,033
SO_1383		ATP-dependent RNA helicase DEAD box family	-1,305	0,002
SO_1388	ampP	aminopeptidase P AmpP	1,448	0,001
SO_1410		periplasmic RmlC-type Cupin domain family protein	-1,668	0,006
SO_1427	dmsE	periplasmic decaheme cytochrome c DmsE	-1,768	0,001
SO_1428	dmsF	extracellular dimethyl sulfoxide/manganese oxide reductase outer membrane translocase DmsF	-2,001	0,001
SO_1429	dmsA	extracellular dimethyl sulfoxide/manganese oxide reductase molybdopterin-binding subunit DmsA	-1,482	0,002
SO_1430	dmsB	extracellular dimethyl sulfoxide/manganese oxide reductase ferredoxin subunit DmsB	-1,125	0,030
SO_1431	dmsG	extracellular dimethyl sulfoxide/manganese oxide reductase chaperone DmsG	-1,627	0,018
SO_1441		putative cytoplasmic protein	1,546	0,003
SO_1460	hsdS	type I restriction-modification system restriction endonuclease DNA specificity subunit HsdS	1,411	0,000
SO_1461		serine/threonine protein kinase	1,275	0,000
SO_1462		cytoplasmic protein in type I restriction-modification system locus	1,075	0,008
SO_1471	intA	CP4-57-like prophage integrase IntA	1,269	0,007

SO_1474	yfjG	lipid binding/transport family protein YfjG	-1,206	0,016
SO_1475	yfjF	UPF0125 family protein YfjF	-1,597	0,011
SO_1483	aceB	malate synthase A AceB	3,066	0,000
SO_1484	aceA	isocitrate lyase AceA	2,973	0,000
SO_1505		proton:peptide symporter POT family	1,331	0,009
SO_1506		Na( )-coupled multidrug efflux pump VmrA-like protein	-1,058	0,019
SO_1518	lldG	L-lactate dehydrogenase complex protein LldG	-1,570	0,023
SO_1519	lldF	L-lactate dehydrogenase iron-sulfur cluster-binding protein LldF	-1,855	0,021
SO_1520	lldE	L-lactate dehydrogenase complex protein LldE	-2,702	0,000
SO_1522		lactate transport protein LctP family	-2,063	0,000
SO_1531	thil	thiazole biosynthesis/tRNA modification proteinThil	-1,013	0,000
SO_1532		predicted periplasmic protein	-3,183	0,000
SO_1550		putative lysine decarboxylase with DUF3412 domain	1,114	0,008
SO_1560	pstS	ABC-type phosphate uptake system substrate-binding component PstS	-1,565	0,000
SO_1589		hypothetical protein	1,369	0,004
SO_1599	pfaC	multi-domain beta-ketoacyl synthase PfaC	2,263	0,000
SO_1600	pfaB	omega-3 polyunsaturated fatty acid synthase PfaB	2,221	0,001
SO_1602	pfaA	omega-3 polyunsaturated fatty acid synthase subunit PfaA	2,407	0,000
SO_1604	pfaE	4'-phosphopantetheinyl transferase PfaE	-1,050	0,040
SO_1605		lipoprotein	2,327	0,000
SO_1606		alkyl sulfatase	2,358	0,005
SO_1616	tnpA	ISSod4 transposase TnpA_ISSod4	2,191	0,000
SO_1648		cold shock protein Csp family	1,443	0,001
SO_1659		surface localized decaheme cytochrome c lipoprotein	-1,345	0,000
SO_1666	phhA	phenylalanine-4-hydroxylase PhhA	2,614	0,000
SO_1667	phhB	pterin-4-alpha-carbinolamine dehydratase PhhB	2,441	0,000
SO_1669	tyrR	Sigma54-dependent transcriptional activator of amino acid degradation TyrR	1,359	0,001
SO_1670	fahA	fumarylacetoacetate hydrolase FahA	2,252	0,000
SO_1671	maiA	maleylacetoacetate isomerase MaiA	1,537	0,024
SO_1673	ompW	outer membrane protein OmpW	-1,142	0,018
SO_1677	ivdA	3-ketoacyl-CoA thiolase IvdA	2,962	0,000
SO_1678	ivdB	methylmalonate-semialdehyde dehydrogenase IvdB	2,992	0,000
SO_1679	ivdC	2-methylbutanoyl-CoA dehydrogenase IvdC	2,679	0,000
SO_1680	ivdD	enoyl-CoA hydratase IvdD	2,649	0,000
SO_1681	ivdE	3-hydroxyisobutyryl-CoA hydrolase IvdE	2,721	0,000
SO_1682	ivdF	3-hydroxyisobutyrate dehydrogenase IvdF	1,941	0,001
SO_1689	copA	Cu <sup>2+</sup> -exporting ATPase CopA	2,530	0,000
SO_1691	blc	lipocalin family lipoprotein Blc	1,751	0,021
SO_1699		transmembrane transcriptional regulator	1,772	0,010
SO_1712		transcriptional regulator	-1,672	0,000
SO_1713		putative lipoprotein	1,618	0,000
SO_1723	pstC	ABC-type high affinity phosphate uptake system permease component PstC	-2,045	0,000

SO_1747		tellurium ion resistance family protein	1,231	0,032
SO_1769		glutamate decarboxylase	-1,182	0,002
SO_1770	garK	glycerate kinase GarK	3,540	0,000
SO_1771	grtP	D-glycerate transporter GrtP	4,097	0,000
SO_1776	mtrB	extracellular iron oxide respiratory system outer membrane component MtrB	-1,061	0,013
SO_1777	mtrA	extracellular iron oxide respiratory system periplasmic decaheme cytochrome c component MtrA	-1,131	0,031
SO_1778	mtrC	extracellular iron oxide respiratory system surface decaheme cytochrome c component MtrC	-1,350	0,002
SO_1779	omcA	extracellular iron oxide respiratory system surface decaheme cytochrome c component OmcA	-1,195	0,012
SO_1783	feoA	ferrous iron transport protein A FeoA	-1,026	0,016
SO_1806	pspF	Sigma 54-dependent transcriptional activator of phage shock response PspF	1,416	0,009
SO_1819	dinG	ATP-dependent helicase DinG	-1,430	0,000
SO_1822		TonB-dependent receptor	2,330	0,000
SO_1824		TonB2 energy transduction system periplasmic component	1,561	0,000
SO_1825	ttpC	TonB2 energy transduction system inner membrane component TtpC	2,188	0,000
SO_1826	exbB	TonB2 energy transduction system inner membrane component ExbB	2,188	0,000
SO_1827	exbD	TonB2 energy transduction system membrane anchored component ExbD	2,511	0,000
SO_1828	tonB2	TonB2 mediated energy transduction system energy transducer component TonB2	1,943	0,000
SO_1829		putative Zn-dependent protease associated with TonB2 energy transduction system	2,123	0,000
SO_1839		hypothetical protein	1,636	0,019
SO_1862	pgsA	CDP-diacylglycerol--glycerol-3-phosphate 3-phosphatidyltransferase PgsA	-1,128	0,005
SO_1882		HAE1 family efflux pump permease component	1,195	0,009
SO_1891	liuG	acetyl-CoA:acetoacetate-CoA transferase beta subunit LiuG	2,234	0,000
SO_1892	liuF	acetyl-CoA:acetoacetate-CoA transferase alpha subunit LiuF	3,111	0,000
SO_1893	liuE	3-hydroxymethylglutaryl-CoA lyase LiuE	3,166	0,000
SO_1894	liuD	methylcrotonyl-CoA carboxylase biotin-binding subunit LiuD	3,288	0,000
SO_1895	liuC	methylglutaconyl-CoA hydratase LiuC	3,305	0,000
SO_1896	liuB	methylcrotonyl-CoA carboxylase carboxyl transferase subunit LiuB	3,713	0,000
SO_1897	liuA	isovaleryl-CoA dehydrogenase LiuA	3,382	0,000
SO_1898	liuR	transcriptional repressor of branched chain amino acid degradation LiuR	3,089	0,000
SO_1900	prpE	propionyl-CoA synthetase PrpE	2,319	0,000

SO_1902	gnd	6-phosphogluconate dehydrogenase decarboxylating Gnd	-1,514	0,000
SO_1909		catalytic subunit of aromatic ring-opening dioxygenase	-1,120	0,022
SO_1910	menA	1;4-dihydroxy-2-naphthoate octaprenyltransferase MenA	-1,599	0,003
SO_1911		oxidoreductase short chain dehydrogenase/reductase family	-2,354	0,000
SO_1917		major facilitator superfamily transporter required for growth on DMSO MFS superfamily	-1,543	0,013
SO_1921		protein of unknown function DUF2986	-1,072	0,012
SO_1926	gltA	citrate synthase GltA	1,334	0,000
SO_1929	sdhB	succinate dehydrogenase iron-sulfur protein SdhB	1,545	0,000
SO_1930	sucA	2-oxoglutarate dehydrogenase complex dehydrogenase E1 component SucA	1,916	0,000
SO_1931	sucB	2-oxoglutarate dehydrogenase complex succinyl-CoA:dihydrolipoate S-succinyltransferase E2 component SucB	2,395	0,000
SO_1932	sucC	succinyl-CoA synthase beta subunit SucC	2,584	0,000
SO_1933	sucD	succinyl-CoA synthase alpha subunit SucD	2,681	0,000
SO_1945	phoQ	two component signal transduction system histidine kinase PhoQ	1,156	0,011
SO_1949		invasin domain protein	1,431	0,000
SO_1952	ggtA	gamma-glutamyltransferase GgtA	1,338	0,007
SO_1962	hppD	4-hydroxyphenylpyruvate dioxygenase HppD	4,056	0,000
SO_1963	hmgA	homogentisate 1;2-dioxygenase HmgA	3,124	0,000
SO_1965	hmgR	homogentisate-responsive transcriptional repressor of homogentisate degradation HmgR	1,106	0,033
SO_1971		AMP-dependent synthetase and ligase family protein	1,699	0,001
SO_1986		RNA polymerase sigma factor ECF family 11	-1,382	0,000
SO_2005		dksA-type zinc finger protein	-2,775	0,000
SO_2017		heat shock response protein	1,020	0,014
SO_2019	hemH	ferrochelataze HemH	-1,736	0,004
SO_2020	gsk	inosine-guanosine kinase Gsk	-1,484	0,001
SO_2049		diguanylate cyclase	1,745	0,011
SO_2090	hypE	NiFe hydrogenase accessory/formation protein HypE	-2,119	0,001
SO_2093	hypB	Ni <sub>2</sub> -binding GTPase involved in regulation of NiFe hydrogenase expression and maturation HypB	-1,321	0,025
SO_2094	hypF	NiFe hydrogenase maturation protein HypF	-1,555	0,003
SO_2095	hyaE	NiFe hydrogenase assembly chaperone HyaE	-2,185	0,000
SO_2096	hyaD	NiFe hydrogenase maturation protease HyaD	-2,168	0,001
SO_2097	hyaC	periplasmic [Ni-Fe] hydrogenase cytochrome b subunit HyaC	-2,757	0,000
SO_2098	hyaB	periplasmic [Ni-Fe] hydrogenase large subunit HyaB	-2,979	0,000
SO_2099	hyaA	periplasmic [Ni-Fe] hydrogenase small subunit HyaA	-3,474	0,000
SO_2111		hypothetical protein	-2,086	0,000
SO_2112	rplY	50S ribosomal protein L25 RplY	-1,179	0,000

SO_2115	iaaA	bifunctional isoaspartyl dipeptidase / l-asparaginase IaaA	1,764	0,012
SO_2136	adhE	aldehyde-alcohol dehydrogenase AdhE	-1,876	0,000
SO_2137	ycheE	6TMS neutral amino acid transporter (NAAT) family protein YcheE	-2,122	0,000
SO_2148	recB	exodeoxyribonuclease V beta subunit RecB	1,038	0,040
SO_2178	ccpA	diheme cytochrome c5 peroxidase CcpA	-1,819	0,000
SO_2183		LD-transpeptidase ErfK/YbiS/YcfS/YnhG family	-1,166	0,006
SO_2185	ppx	exopolyphosphatase Ppx	-1,411	0,002
SO_2194	pdsO	sortase system OmpA family protein PdsO	2,138	0,001
SO_2196	srtA	sortase SrtA	1,626	0,007
SO_2203	dgkA	diacylglycerol kinase DgkA	-2,069	0,001
SO_2215	gluP	ribosomal RNA small subunit methyltransferase RsmB family	-1,068	0,009
SO_2216		bifunctional diguanylate cyclase with GAF and PAS sensory domains/signalling protein with EAL domain	1,984	0,000
SO_2223		subfamily S9C unassigned peptidase	1,505	0,000
SO_2228		CBS domain containing protein	-1,467	0,011
SO_2241		protein of unknown function DUF3334	1,544	0,000
SO_2251		enzyme of unknown function UPF0227	-1,356	0,008
SO_2260	suhB	inositol-phosphate phosphatase SuhB	-2,254	0,000
SO_2261	trmJ	tRNA (cytidine32/uridine32-2'-O)-methyltransferase TrmJ	-1,029	0,005
SO_2265	iscU	FeS cluster assembly scaffold protein IscU	1,007	0,013
SO_2266	iscA	FeS cluster assembly accessory protein IscA	1,694	0,008
SO_2270	rimK	ribosomal protein S6 glutaminyl transferase RimK	-1,086	0,011
SO_2329		Efp-associated protein of unknown function DUF2331	-1,054	0,008
SO_2332		protein of unknown function DUF2788	-1,444	0,025
SO_2339	bkdA1	3-methyl-2-oxobutanoate dehydrogenase complex E1 component alpha subunit BkdA1	1,069	0,008
SO_2340	bkdA2	3-methyl-2-oxobutanoate dehydrogenase complex E1 component beta subunit BkdA2	1,442	0,000
SO_2341	bkdB	3-methyl-2-oxobutanoate dehydrogenase complex E2 component BkdB	1,857	0,000
SO_2353		protein of unknown function DUF2987	-1,105	0,007
SO_2354	ydaO	tRNA(Cytosine32)-2-thiocytidine synthetase YdaO	-1,449	0,003
SO_2361	ccoP	Cbb3-type cytochrome c oxidase subunit III CcoP	1,717	0,000
SO_2362	ccoQ	Cbb3-type cytochrome c oxidase subunit IV CcoQ	1,826	0,005
SO_2363	ccoO	Cbb3-type cytochrome c oxidase subunit II CcoO	1,327	0,000
SO_2364	ccoN	Cbb3-type cytochrome c oxidase subunit I CcoN	1,405	0,000
SO_2387		DTW domain-containing protein	-1,781	0,001
SO_2389	emrD	multidrug efflux protein EmrD	-3,386	0,000
SO_2415	nrdA	aerobic ribonucleoside-diphosphate reductase alpha subunit NrdA	1,276	0,000
SO_2416	nrdB	aerobic ribonucleoside-diphosphate reductase beta subunit NrdB	1,618	0,000
SO_2417	yfaE	ferredoxin cofactor maintenance protein YfaE	1,501	0,007

SO_2419	fadH	NADP-dependent 24-dienoyl-CoA reductase FadH	1,338	0,005
SO_2420	sppA	signal peptide peptidase SppA	1,800	0,000
SO_2427		ArgR-regulated TonB-dependent receptor	1,159	0,001
SO_2445	thiC	thiamin biosynthesis protein ThiC	-2,339	0,000
SO_2481		sodium:proton antiporter NhaC family	-1,413	0,003
SO_2492	fadE1	acyl-CoA dehydrogenase FadE1	1,188	0,001
SO_2493	psrA	transcriptional repressor of fatty acid degradation PsrA	1,077	0,034
SO_2494		peptidase family M2	1,562	0,003
SO_2499		protein of unknown function DUF406	-1,426	0,038
SO_2500	s4P	30S ribosomal protein S4P	-1,881	0,001
SO_2507		bifunctional diguanylate cyclase/phosphodiesterase	1,211	0,006
SO_2509	rnfB	ion (H or Na )-translocating NADH:ferredoxin oxidoreductase subunit RnfB	-1,348	0,017
SO_2530	def	peptide deformylase Def	-2,415	0,000
SO_2570		DUF885 family lipoprotein	2,998	0,000
SO_2573	ycgN	UCP006173 family protein	-1,041	0,010
SO_2587	hemB	delta-aminolevulinic acid dehydratase HemB	-1,221	0,008
SO_2594		MMPL family efflux pump	1,468	0,005
SO_2595		BNR repeat protein	1,699	0,003
SO_2596		putative periplasmic protein of unknown function DUF1329	3,089	0,000
SO_2597		outer membrane protein of unknown function DUF1302	3,802	0,000
SO_2610	ycfH	TatD family deoxyribonuclease YcfH	-1,114	0,007
SO_2625	infA	translation initiation factor IF-1 InfA	-2,070	0,000
SO_2629	icd	isocitrate dehydrogenase NADP-dependent Icd	1,032	0,000
SO_2633	trmU	tRNA (5-methylaminomethyl-2-thiouridylate)-methyltransferase TrmU	-1,264	0,000
SO_2634	hflD	high frequency lysogenization protein HflD	-1,151	0,007
SO_2637		hypothetical protein	1,035	0,016
SO_2638	ldh	leucine dehydrogenase Ldh	2,100	0,000
SO_2639		hypothetical protein	1,644	0,036
SO_2647		4-hydroxybenzoyl-CoA thioesterase family protein	-1,261	0,036
SO_2654	tnpA	Mu phage transposase OrfA TnpA_MuSo2	1,777	0,026
SO_2720		lipoprotein of unknown function DUF1425	1,152	0,003
SO_2725		transcriptional regulator LuxR family	1,431	0,003
SO_2737	bioD	dethiobiotin synthase BioD	2,107	0,002
SO_2738	bioC	SAM-dependent methylase involved in biotin synthesis protein BioC	1,254	0,045
SO_2740	bioB	biotin synthase BioB	2,591	0,000
SO_2743	acs	acetyl-coenzyme A synthetase AcsA	3,890	0,000
SO_2748	tolB	TonB biopolymer transport system periplasmic component TolB	1,147	0,001
SO_2752	ybgC	TolA energy-transducing system-associated acyl-CoA thioesterase YbgC	-1,213	0,010
SO_2754	motY	smf-dependent flagellar motor protein MotY	-1,810	0,001
SO_2755	rnt	ribonuclease T Rnt	-1,286	0,012

SO_2759	upp	uracil phosphoribosyltransferase Upp	-1,840	0,000
SO_2766	nagD	peptidase M28A family	2,940	0,000
SO_2787	cspA	cold shock protein CspA	1,226	0,000
SO_2821	yechH	probable metal-binding protein YechH	-1,637	0,025
SO_2830		predicted outer membrane protein	-1,400	0,005
SO_2832		protein of unknown function DUF2810	-1,135	0,002
SO_2833	nrdG	anaerobic ribonucleoside-triphosphate reductase activating protein NrdG	-1,183	0,050
SO_2834	nrdD	anaerobic ribonucleoside-triphosphate reductase NrdD	-2,095	0,000
SO_2848		putative periplasmic protein	1,192	0,023
SO_2850		acetyltransferase GNAT family	1,357	0,007
SO_2854		hypothetical protein	1,984	0,004
SO_2856		putative nucleotidyltransferase DUF294	3,055	0,000
SO_2857		putative solute:sodium symporter large subunit	3,875	0,000
SO_2858		putative solute:sodium symporter small subunit	2,718	0,001
SO_2865	argO	L-arginine efflux transporter ArgO	-3,387	0,000
SO_2877	hda	DnaA regulatory inactivator Hda	-1,081	0,011
SO_2883		protein of unknown function DUF444	1,342	0,008
SO_2884		SpoVR family protein	1,503	0,009
SO_2899	cysZ	putative sulfate transporter CysZ	1,183	0,027
SO_2900		carbohydrate binding outer membrane protein	1,283	0,049
SO_2905		O-methyltransferase	-1,767	0,018
SO_2906		tellurite-resistance/dicarboxylate transporter (TDT) family protein	-1,725	0,005
SO_2907		ArgR-regulated TonB-dependent receptor	3,972	0,000
SO_2911	focA	bidirectional formate transporter FocA	-1,284	0,018
SO_2912	pflB	pyruvate formate-lyase PflB	-1,503	0,008
SO_2913	pflA	pyruvate formate-lyase 1 activating enzyme PflA	-1,603	0,015
SO_2923	gltS	sodium:glutamate symporter GltS	-1,435	0,003
SO_2934		extracellular lipase Pla-1/cef family	2,753	0,000
SO_2938		Lambda phage encoded lipoprotein	1,155	0,005
SO_3022	trpCF	bifunctional indole-3-glycerolphosphate synthetase/phosphoribosylanthranilate isomerase TrpCF	1,064	0,045
SO_3030	pubA	putrescine monooxygenase PubA	-2,499	0,000
SO_3054		metallo-beta-lactamase family protein	-1,320	0,001
SO_3059		Sigma54 specific transcriptional regulator Fis family	-1,814	0,000
SO_3061	topB	DNA topoisomerase III TopB	-2,073	0,000
SO_3063		cation:alanine/glycine transporter AGCS family	1,801	0,003
SO_3068	truA	tRNA pseudouridine38-40 synthase TruA	-1,093	0,003
SO_3084		bifunctional diguanylate cyclase/phosphodiesterase with PAS sensory domain	1,927	0,001
SO_3096		RNA polymerase sigma factor ECF family 28	-1,918	0,000
SO_3097		anti-sigma factor	-1,656	0,000
SO_3101		putative outer membrane protein of unknown function DUF541	2,491	0,000
SO_3103		thiophosphate efflux pump permease component	1,203	0,015

SO_3110	secF	preprotein translocase subunit SecF	1,660	0,000
SO_3119		hypothetical protein	-2,304	0,000
SO_3120	agaO	sugar oxidoreductase AgaO	2,844	0,000
SO_3121		hypothetical protein	-1,155	0,031
SO_3134	dctP	TRAP-type C4-dicarboxylate:H symport system substrate-binding component DctP	2,398	0,003
SO_3142	dcp	dipepidyl carboxypeptidase II Dcp	3,367	0,000
SO_3148		periplasmic amidohydrolase family protein	2,015	0,001
SO_3149		periplasmic amidohydrolase family protein	2,441	0,001
SO_3151	yaeB	putative methyltransferase YaeB	-1,015	0,030
SO_3159	wbfB	outer membrane protein of unknown function DUF940 WbfB	1,349	0,000
SO_3175	wbpQ	asparagine synthase glutamine-hydrolyzing WbpQ	1,122	0,000
SO_3178		polysaccharide deacetylase	1,067	0,022
SO_3179	wzy	O-antigen polymerase Wzy	1,090	0,050
SO_3180	wbni	glycosyl transferase family 2 Wbni	1,412	0,007
SO_3182	wbnH	O-antigen biosynthesis acetyltransferase WbnH	1,770	0,003
SO_3183		perosamine synthetase-related protein	1,992	0,000
SO_3184	wbqC	putative glycine transferase in O-antigen biosynthesis cluster WbqC	1,832	0,000
SO_3185		enzyme for biosynthesis of dTDP-Qui4N	1,704	0,000
SO_3186	rmlA	glucose-1-phosphate-thymidyltransferase RmlA	1,235	0,001
SO_3188	rfbB	dTDP-glucose-4;6-dehydratase RfbB	1,160	0,000
SO_3189	wbpP	UDP-GlucNAc C4 epimerase WbpP	1,661	0,000
SO_3190	wbpA	UDP-N-acetyl-d-glucosamine 6-dehydrogenase WbpA	1,163	0,000
SO_3195		proton:peptide symporter POT family	1,148	0,001
SO_3202	cheW	chemotaxis signal transduction system adaptor protein CheW	1,052	0,026
SO_3234	fliT	flagella biosynthesis chaperone for FliD FliT	-1,118	0,013
SO_3235	fliD	flagellar filament capping protein FliD	-1,174	0,000
SO_3236	flaG	uncharacterized flagella locus protein FlaG	-2,190	0,000
SO_3237	fliC	flagellin FliC	-2,627	0,000
SO_3254	flgM	flagellar biosynthesis anti-sigma factor FlgM	-1,110	0,018
SO_3325	nrfJ	periplasmic protein of unknown function NrfJ	-1,600	0,001
SO_3343		predicted lipoprotein	1,352	0,000
SO_3345	yciH	translation initiation factor protein YciH	-1,484	0,002
SO_3361		protein of unknown function DUF885	2,534	0,000
SO_3368	mutY	adenine glycosylase MutY	-1,158	0,040
SO_3370	ycel	UPF0312 family alkali-inducible periplasmic protein Ycel	1,598	0,000
SO_3377		predicted periplasmic protein	1,665	0,032
SO_3386		bifunctional protein of unknown functions DUF523 and DUF1722	-1,090	0,001
SO_3391		ATP-dependent protease family S16 unassigned peptidase	1,448	0,001
SO_3403	raiA	ribosome-associated inhibitor A RaiA	1,231	0,011

SO_3404		methyl accepting sensory transducer with PAS sensory domain	-1,269	0,034
SO_3410		hypothetical protein	1,593	0,000
SO_3411		predicted non-catalytic member of peptidase subfamily S41B	2,778	0,000
SO_3413	thrC	threonine synthase ThrC	1,520	0,000
SO_3414	thrB	homoserine kinase ThrB	1,740	0,001
SO_3415	thrA	bifunctional aspartokinase I / homoserine dehydrogenase I ThrA	1,208	0,008
SO_3420		monoheme cytochrome c'	1,207	0,001
SO_3430	recA	recombinase A RecA	-1,417	0,000
SO_3432	rpoS	RNA polymerase sigma-38 factor RpoS	1,769	0,000
SO_3441	pyrG	CTP synthase PyrG	-1,179	0,000
SO_3462	recN	DNA repair protein RecN	-2,088	0,000
SO_3489		diguanylate cyclase	1,401	0,040
SO_3503	nagP	N-acetyl glucosamine transporter NagP	2,024	0,001
SO_3509	hexB	beta-N-acetylhexosaminidase HexB	1,775	0,002
SO_3514		TonB-dependent chitooligosaccharide receptor	1,006	0,007
SO_3538	hlyU	transcriptional activator HlyU	-2,127	0,000
SO_3549		hemerythrin	-1,114	0,022
SO_3553		sulfate transporter SulP family	-1,917	0,000
SO_3563		2OG-Fe(II) oxygenase family protein	-1,506	0,002
SO_3564	dcp	dipeptidyl carboxypeptidase Dcp	1,169	0,005
SO_3565	cpdB	bifunctional 2';3'-cyclic-nucleotide 2'-phosphodiesterase/3'-nucleotidase CpdB	-1,112	0,005
SO_3586		glyoxalase family protein	1,557	0,032
SO_3641	apaH	bis(5-nucleosyl)-tetraphosphatase ApaH	1,414	0,020
SO_3642		energy taxis modulating methyl accepting sensory transducer	1,755	0,002
SO_3659		thiol:disulfide interchange protein	2,857	0,000
SO_3664	fadD	long chain fatty acid CoA ligase FadD	1,493	0,000
SO_3665		ABC-type multidrug efflux system bifunctional ATPase and permease component	2,043	0,001
SO_3681		universal stress protein family	-2,119	0,000
SO_3682		protein of unknown function DUF3478	-2,057	0,000
SO_3714		ABC-type monosaccharide transport system substrate binding component	-1,296	0,031
SO_3715	nfnB	bifunctional oxygen-insensitive NAD(P)H nitroreductase/dihydropteridine reductase NfnB	-1,200	0,002
SO_3718		thiol:disulfide interchange protein DsbA family	1,665	0,002
SO_3719		cytochrome b561	-1,734	0,012
SO_3720	hemG	oxygen-independent protoporphyrinogen oxidase HemG	-1,578	0,038
SO_3731	pIdA	hypothetical protein	-1,327	0,029
SO_3743		transcriptional regulator TetR family	1,167	0,000
SO_3769	ygiF	adenylate cyclase YgiF	1,288	0,005

SO_3774	putA	bifunctional proline dehydrogenase/delta-1-pyrroline-5-carboxylate dehydrogenase PutA	1,322	0,001
SO_3783	rhIE	ATP-dependent RNA helicase RhIE	-1,097	0,019
SO_3800		surface-associated serine protease	3,265	0,000
SO_3802		ABC-type DrugE1 family export system ATPase component	1,227	0,012
SO_3827	kdsA	2-dehydro-3-deoxyphosphooctonate aldolase KdsA	1,027	0,003
SO_3834	hemA	glutamyl-tRNA reductase HemA	-1,324	0,000
SO_3835	lolB	outer membrane lipoprotein LolB	-1,272	0,014
SO_3836	ispE	4-diphosphocytidyl-2C-methyl-D-erythritol kinase IspE	-1,195	0,006
SO_3837	prsA	ribose-phosphate pyrophosphokinase PrsA	-1,061	0,004
SO_3840		RNA polymerase sigma-70 factor ECF subfamily	-2,024	0,000
SO_3841		anti-sigma factor	-1,208	0,002
SO_3844	pepO	thermoregulated outer membrane M13 family zinc endopeptidase PepO	1,339	0,000
SO_3846	relV	(p)ppGpp synthetase RelV	1,963	0,000
SO_3888		protein of unknown function DUF1508	-1,781	0,000
SO_3891		protein of unknown function DUF3149	-2,281	0,000
SO_3901	cpdA	cyclic 3'; 5'-adenosine monophosphate phosphodiesterase CpdA	-1,610	0,000
SO_3916	alr	alanine racemase biosynthetic Alr	-1,054	0,006
SO_3920	hydA	periplasmic [Fe-Fe] hydrogenase large subunit HydA	-1,465	0,026
SO_3934	rlmB	23S rRNA (guanosine2251-2'-O)-methyltransferase RlmB	1,029	0,008
SO_3953	miaE	ABC-type phospholipid uptake (salvage) system permease component MiaE	-1,032	0,002
SO_3985	dapA	dihydrodipicolinate synthase DapA	1,318	0,039
SO_3986	lysC	lysine-sensitive aspartokinase III LysC	1,707	0,004
SO_3987		protein of unknown function DUF3293	-1,014	0,038
SO_3993		hypothetical protein	1,578	0,005
SO_3994		hypothetical protein	1,490	0,002
SO_4005		protein of unknown function DUF2220	1,842	0,029
SO_4013		TPR repeat domain protein	1,282	0,033
SO_4043	tonB	TonB mediated energy transduction system energy transducer component TonB	1,667	0,003
SO_4055	metL	bifunctional aspartokinase II/homoserine dehydrogenase methionine-sensitive MetL	1,465	0,010
SO_4068		hypothetical protein	1,371	0,035
SO_4072	rimO	ribosomal protein S12 methylthiotransferase RimO	-1,677	0,000
SO_4081	puuP	putrescine uptake protein PuuP	-1,668	0,000
SO_4082		putative microcin	-2,210	0,008
SO_4092		hydrolase carbon-nitrogen family	1,397	0,038
SO_4120	rpmE	50S ribosomal protein L31 RpmE	-1,071	0,004
SO_4133	udp	uridine phosphorylase Udp	-1,433	0,000
SO_4134		protein of unknown function DUF465	-1,321	0,021
SO_4138		putative periplasmic protein	-2,299	0,000
SO_4151		polysaccharide deacetylase	-2,066	0,000

SO_4152		SnoaL family protein	-2,549	0,001
SO_4160	fliUV	lysine-N-methylase FliUV	1,072	0,016
SO_4178	mxdC	membrane anchored protein MxdC	1,495	0,037
SO_4179	mxdB	glycosyl transferase family 2 MxdB	1,923	0,004
SO_4180	mxdA	diguanylate cyclase-like protein MxdA	1,506	0,002
SO_4193		esterase/lipase/thioesterase family protein	-1,499	0,000
SO_4196		predicted membrane protein	-1,662	0,017
SO_4202	tatA	twin arginine protein translocase system protein TatA	-1,470	0,005
SO_4204	tatC	twin arginine protein translocase system protein TatC	-1,362	0,001
SO_4226	ftsL	cell division protein FtsL	-1,151	0,035
SO_4228	mraZ	protein MraZ	-1,080	0,009
SO_4229		hypothetical protein	-2,814	0,000
SO_4241	recQ	ATP-dependent DNA helicase RecQ	-1,010	0,009
SO_4245	argA	amino-acid acetyltransferase ArgA	-1,115	0,030
SO_4252		subfamily S9C unassigned peptidase	2,078	0,000
SO_4256	rph	ribonuclease PH Rph	-1,115	0,002
SO_4281	ktrA	sodium-dependent potassium uptake system NAD binding component KtrA	1,346	0,015
SO_4283		ApbE family lipoprotein	1,595	0,017
SO_4290	pstA	ABC-type phosphate uptake system permease component PstA	-1,614	0,020
SO_4292	pstS	ABC-type phosphate uptake system substrate-binding component PstS	-1,376	0,031
SO_4320	aggA	type I protein secretion system secretin component AggA	2,089	0,000
SO_4321		Pal-like T1SS-linked outer membrane lipoprotein	2,405	0,000
SO_4322		T1SS associated periplasmic transglutaminase-like cysteine proteinase	1,830	0,000
SO_4323		bifunctional diguanylate cyclase/phosphodiesterase LasD-like protein	1,914	0,000
SO_4343	agxT	serine-pyruvate aminotransferase AgxT	1,024	0,027
SO_4349	ilvC	ketol-acid reductoisomerase IlvC	1,158	0,020
SO_4365		protein of unknown function DUF3014	1,091	0,006
SO_4374		phenylalanine/tyrosine ammonia-lyase	1,886	0,000
SO_4376		hypothetical protein	2,331	0,001
SO_4377		MMPL family efflux pump permease component	1,266	0,035
SO_4378		FAD-binding protein	1,449	0,010
SO_4380		beta-ketoacyl synthase	1,585	0,020
SO_4383	fabF	3-oxoacyl-(acyl-carrier-protein) synthase II FabF	1,613	0,006
SO_4384		hypothetical protein	2,132	0,000
SO_4391	tnpA	protein of unknown function DUF2971	1,617	0,000
SO_4404		iron-sulfur cluster-binding protein	-1,691	0,002
SO_4417	dcuB	anaerobic C4-dicarboxylate transporter DcuB	-1,796	0,018
SO_4447	modB	ABC-type molybdate uptake system permease component ModB	-1,729	0,029
SO_4448	modA	ABC-type molybdate uptake system substrate-binding component ModA	-1,257	0,046

SO_4473		autotransporter	1,508	0,000
SO_4480	exaC	NAD -dependent acetaldehyde dehydrogenase ExaC	3,650	0,000
SO_4483		cytochrome b	2,660	0,003
SO_4484	shp	monoheme cytochrome c Shp	3,118	0,000
SO_4492		protein of unknown function DUF1993	1,134	0,002
SO_4504		formate dehydrogenase associated protein of unknown function DUF3505	-2,085	0,006
SO_4505		formate dehydrogenase associated protein of unknown function DUF3506	-2,047	0,003
SO_4506		iron-sulfur cluster-binding protein	-1,114	0,027
SO_4507	fdhT	formate dehydrogenase chaperone FdhT	-2,472	0,000
SO_4508	fdhX	formate dehydrogenase accessory protein FdhX	-1,831	0,000
SO_4509	fdhA	formate dehydrogenase molybdopterin-binding subunit FdhA	-1,831	0,000
SO_4510	fdhB	formate dehydrogenase FeS subunit FdhB	-1,755	0,001
SO_4511	fdhC	formate dehydrogenase cytochrome b subunit FdhC	-1,913	0,000
SO_4512	fdhX	Fnr-inducible formate dehydrogenase accessory protein FdhX	-3,857	0,000
SO_4513	fdhA	Fnr-inducible formate dehydrogenase molybdopterin-binding subunit FdhA	-3,162	0,000
SO_4514	fdhB	Fnr-inducible formate dehydrogenase FeS subunit FdhB	-2,426	0,000
SO_4515	fdhC	Fnr-inducible formate dehydrogenase cytochrome b subunit FdhC	-2,182	0,000
SO_4537		serine peptidase family S9	3,656	0,000
SO_4538		predicted non-catalytic member of peptidase subfamily M16B	2,243	0,000
SO_4558		hypothetical protein	-1,106	0,005
SO_4571	dmsE	transcriptional regulator LysR family	2,597	0,001
SO_4591	cymA	membrane anchored tetraheme cytochrome c CymA	-1,661	0,000
SO_4593		periplasmic protein of unknown function DUF2057	2,327	0,002
SO_4596	cusF	copper efflux pump periplasmic metallochaperone CusF	1,699	0,002
SO_4597	cusB	copper/silver efflux pump MFP component CusB	1,968	0,001
SO_4598	cusA	copper/silver efflux pump permease component CusA	2,363	0,000
SO_4603	lexA	bifunctional transcriptional repressor of SOS-response/self-cleaving protease LexA	-1,358	0,000
SO_4604	sulA	UV induced cell division inhibitor SulA	-1,281	0,000
SO_4645		putative bifunctional autotransporter / extracellular effector	1,489	0,001
SO_4649		histidine-rich protein of unknown function DUF3300	1,120	0,013
SO_4680		CDP-glycerol glycerophosphotransferase family protein	1,085	0,019
SO_4688		glycosyl transferase family 2	-1,036	0,018
SO_4700		outer membrane porin	-1,732	0,013
SO_4716		acteyltransferase GNAT family	-1,664	0,001
SO_4728	yihI	GAP-like protein YihI	-1,496	0,000
SO_4730	hemN	coproporphyrinogen III oxidase oxygen-independent HemN	-1,442	0,006

SO_4731	add	adenosine deaminase Add	-1,006	0,006
SO_4732		lipoprotein of unknown function DUF885	1,696	0,002
SO_4740		predicted membrane protein of unknown function DUF2061	-3,208	0,000
SO_4742	glmR	glucosamine-6-phosphate sensitive transcriptional repressor of lipopolysaccharide biosynthesis GlmR	-1,052	0,001
SO_4746	atpC	ATP synthase F1 epsilon subunit AtpC	1,361	0,002
SO_4747	atpD	ATP synthase F1 beta subunit AtpD	2,079	0,000
SO_4748	atpG	ATP synthase F1 gamma subunit AtpG	1,788	0,000
SO_4749	atpA	ATP synthase F1 alpha subunit AtpA	1,901	0,000
SO_4750	atpH	ATP synthase F1 delta subunit AtpH	1,204	0,000
SO_4751	atpF	ATP synthase F0 B subunit AtpF	1,035	0,000
SO_4752	atpE	ATP synthase F0 C subunit AtpE	1,281	0,006
SO_4753	atpB	ATP synthase F0 A subunit AtpB	1,238	0,000
SO_4761		protein of unknown function DUF2618	-3,861	0,000
SO_4778	sdhD	succinate dehydrogenase membrane anchor subunit SdhD	1,025	0,046
SO_4799	wbnJ	O-antigen biosynthesis acetyltransferase WbnJ	1,459	0,029
SO_4811		periplasmic peptidase family M16B	3,397	0,000
SO_4823		integral membrane protein	2,387	0,000
SO_A0003		type II restriction endonuclease; putative	1,399	0,001
SO_A0012	,rulB	SOS mutagenesis protein RulB	-2,201	0,000
SO_A0013	,rulA	SOS mutagenesis protein RulA	-1,940	0,000
SO_A0048		prolyl oligopeptidase family protein	2,364	0,000
SO_A0049		toxin secretion ABC transporter; ATP-binding subunit/permease protein; putative	3,019	0,000
SO_A0050		toxin secretion; membrane fusion protein	4,211	0,000
SO_A0056		hypothetical protein	1,317	0,044
SO_A0058		hypothetical protein	-1,117	0,002
SO_A0060		acetyltransferase	-1,286	0,001
SO_A0080		hypothetical protein	1,071	0,026
SO_A0122		hypothetical protein	1,226	0,024
SO_A0132		hypothetical protein	1,743	0,004
SO_A0149		hypothetical protein	1,794	0,005
SO_A0153		CzcA family heavy metal efflux protein	2,202	0,000
SO_A0154		heavy metal efflux protein; putative	1,232	0,009
SO_A0155		hypothetical protein	1,273	0,023
SO_A0172		resolvase family site-specific recombinase	-1,118	0,005
SO_A0177		bacteriocin-like peptide	1,691	0,004
SO_A0178		bacteriocin-like peptide	1,865	0,001
SO_A0180		hypothetical protein	1,021	0,049

1 **Resilience, dynamics and interactions within a multi-species exoelectrogenic model**  
2 **biofilm community**

3 Anna Prokhorova<sup>a</sup>, Andreas Doetsch<sup>b</sup>, Johannes Gescher<sup>a,c,\*</sup>

4 <sup>a</sup>Institute for Applied Biosciences, Department of Applied Biology, Karlsruhe Institute of Technology,  
5 Fritz-Haber-Weg 2, 76131 Karlsruhe, Germany

6 <sup>b</sup>Institute of Functional Interfaces, Department of Interface Microbiology, Karlsruhe Institute of  
7 Technology, Hermann-von-Helmholtz-Platz 1, 76344 Eggenstein-Leopoldshafen, Germany  
8 Institute for Biological Interfaces, Karlsruhe Institute of Technology (KIT), Eggenstein-  
9 Leopoldshafen, Germany<sup>c</sup>

10

11

12 \*Corresponding author. Tel.: +49 721 608 41940; fax: +49 721 608 41941

13 *E-mail addresses:* [anna.prokhorova@kit.edu](mailto:anna.prokhorova@kit.edu) (A. Prokhorova)

14 [andreas.doetsch@kit.edu](mailto:andreas.doetsch@kit.edu) (A. Doetsch)

15 [johannes.gescher@kit.edu](mailto:johannes.gescher@kit.edu) (J. Gescher)

16

17

18 Reviewers:

19 1. Julea N. Butt (School of Biological Sciences and School of Chemistry, University of East  
20 Anglia, Norwich NR4 7TJ, UK)

21 [j.butt@uea.ac.uk](mailto:j.butt@uea.ac.uk)

22 2. Liang Shi (Pacific Northwest National Laboratory, 902 Battelle Boulevard, P.O. Box 999,  
23 Richland, WA 99352, USA)

24 [liang.shi@pnl.gov](mailto:liang.shi@pnl.gov)

25

26 3. Ricardo O. Louro (Inorganic Biochemistry and NMR Laboratory Instituto de Tecnologia  
27 Química e Biológica António Xavier, Universidade Nova de Lisboa, Oeiras, Portugal)

28 [louro@itqb.unl.pt](mailto:louro@itqb.unl.pt)

29

30

31

32

33

34

35

36

37

38 **Abstract:** Anode-associated multi-species exoelectrogenic biofilms are essential to the function of  
39 bioelectrochemical systems (BESs). The investigation of electrode-associated biofilms is critical to  
40 advance the understanding of the function of individual members within communities that thrive using  
41 an electrode as the terminal electron acceptor. This study focusses on the analysis of a model biofilm  
42 community consisting of *Shewanella oneidensis*, *Geobacter sulfurreducens* and *Geobacter*  
43 *metallireducens*. The conducted experiments revealed that the organisms build a stable biofilm on an  
44 electrode surface that is rather resilient to changes in the redox potential of the anode. The community  
45 operated at maximum electron transfer rates at electrode potentials that were higher than 0.04 V versus  
46 normal hydrogen electrode. Current densities decreased gradually with lower potentials and reached  
47 half-maximal values at -0.08 V. Transcriptomic results point towards a positive interaction of the  
48 individual strains. At least *S. oneidensis* and *G. sulfurreducens* show an upregulation of their central  
49 metabolism as a response to cultivation under mixed-species conditions. Interestingly, *G.*  
50 *sulfurreducens* was detected in the planktonic phase of the bioelectrochemical reactors only in mixed-  
51 culture experiments but not when it was grown in the absence of the other two organisms. It is  
52 possible that *G. sulfurreducens* cells used flavins which were released by *S. oneidensis* cells as  
53 electron shuttles. This would allow the organism to broaden its environmental niche.

54  
55 **Importance:** To the best of our knowledge, this is the first study describing the dynamics of biofilm  
56 formation of a model exoelectrogenic community, the resilience of the biofilm, and the molecular  
57 responses towards mixed-species conditions. The results suggest possible synergistic scenarios that  
58 could lead to accelerated electron transfer in mixed species anode communities, an unresolved  
59 phenomenon that was observed in many previous studies.

60 **Keywords:** bio-electrochemical systems, *Shewanella*, *Geobacter*, exoelectrogenic biofilm,  
61 transcriptome analysis

## 62 63 **Introduction**

64 Several microorganisms have the ability to transfer respiratory electrons to an extracellular electron  
65 acceptor. Extracellular respiration is highly relevant for a number of biogeochemical cycles because  
66 these electron transport chains were developed for the reduction of metal oxides as well as for non-  
67 membrane permeable environmental electron shuttles like humic substances (1). It is likely that the  
68 selective pressure to evolve terminal reductases that can catalyze an electron transfer to solid electron  
69 acceptors forced the microorganisms to develop rather unspecific enzymes. These enzymes can  
70 catalyze the transfer of electrons to a variety of surfaces and substances that are basically characterized  
71 by a redox potential above -200 mV versus normal hydrogen electrode (2). This lack of specificity  
72 allows the application of these microorganisms in so-called bioelectrochemical systems (BES), in  
73 which they catalyze the direct or indirect electron transfer to electrode surfaces (3). These systems  
74 have the potential to become a promising technology for generating bioenergy or recovering products

75 coupled to the elimination of organic carbon and, hence, have attracted increasing attention (4-7).  
76 Recently many studies have been carried out to expand the application of BESs and increase the  
77 efficiency of electricity production (6, 8). One strategy is to understand and steer the microbial  
78 community on electrode surfaces (9). Still, we are far away from understanding the role of individual  
79 groups of microorganisms that thrive on anode surfaces in non-axenic systems. The interactions are  
80 most likely as diverse as they are in natural environments, in which, for instance, syntrophic  
81 associations between microorganisms play a dominant role in the overall fitness of the communities  
82 (10).

83 So far, several exoelectrogenic bacteria have been identified. The predominant model organisms  
84 studied belong to the *Geobacteraceae* (11) and *Shewanellaceae* (12). However, even with these model  
85 organisms the understanding of performance of electrochemically active mixed-species biofilms is still  
86 poor due to limited knowledge of possible microbial interactions between these organisms. The  
87 respiratory activity of microbial communities on anodes can be monitored as current generation.  
88 Moreover, the anode potential can be controlled by a potentiostat (2) that enables acceleration or  
89 suppression of extracellular electron transfer rates in the biofilm community as a function of the  
90 applied surface redox potential (13, 14). It is still poorly understood how the electrode potentials affect  
91 the developmental processes in an exoelectrogenic community and how metabolic networks are  
92 established and maintained within the community. This knowledge is critical for expanding our  
93 comprehension of extracellular electron transfer processes with regard to microbe-microbe and  
94 microbe-electrode interactions.

95 Therefore, the objectives of the current study were to analyze the dynamics of biofilm formation at  
96 different stages of growth and to characterize the metabolic networks of the community through the  
97 systematic integration of electrochemical and transcriptomic analyses. The model multi-species  
98 biofilm consisted of the three well-known exoelectrogenic microorganisms: *Shewanella oneidensis*,  
99 *Geobacter sulfurreducens*, and *Geobacter metallireducens*. The three organisms have different  
100 characteristics. *S. oneidensis* is a facultative anaerobic organism. It has a rather narrow spectrum of  
101 usable electron donors and shows only a partial oxidation of the used carbon and electron sources to a  
102 mixture of acetate, formate, CO<sub>2</sub> and hydrogen as end products of its anaerobic metabolism. Several  
103 studies have found that *S. oneidensis* can release flavin molecules that can be used as endogenous  
104 electron shuttles under batch culture conditions. Hence, the organism can grow planktonically while  
105 still interacting with the electron acceptor by the use of such shuttle molecules. Nevertheless, the  
106 organism can also grow as a biofilm in direct contact with the electrode, but these biofilms are rather  
107 thin. Earlier studies concluded that the organism uses the direct contact for only 25% of the overall  
108 electron transfer in a batch system (15). *Geobacter sulfurreducens* is the most studied organism within  
109 the *Geobacteriaceae*. Several studies characterized this organism in bioelectrochemical systems  
110 because it forms biofilms which are several micrometers thick and typically shows five-fold higher  
111 current production compared to *S. oneidensis* (16). The organism is oxygen tolerant and uses acetate

112 as the preferred carbon and electron source. *G. metallireducens* has an extremely wide spectrum of  
113 growth substrates. Nevertheless, the organism is highly oxygen sensitive and current production is  
114 typically lower compared to *G. sulfurreducens* (17).

115 It was the aim of this study to analyze the dynamics on an anode-biofilm composed of the three model  
116 organisms under different bioelectrochemical conditions and to understand potential interactions  
117 between the three microorganisms. Hence, bioelectrochemical cells were operated with several  
118 different working electrode potentials and the community composition was then analyzed using  
119 quantitative PCR as well as fluorescent in situ hybridization. The physiological role of the three model  
120 organisms as well as their potential interaction were analyzed with a (meta-)transcriptomic approach.  
121 Our analysis highlights the different ecological niches of the three model organisms that allow not  
122 only parallel growth but also a synergistic interaction.

123

#### 124 **Materials and methods**

125 Chemicals and biochemicals were obtained from Allichem (Darmstadt, Germany), Carl Roth GmbH & Co. KG  
126 (Karlsruhe, Germany), Sigma-Aldrich (Munich, Germany), Bionline (Luckenwalde, Germany), New England  
127 Biolabs (Frankfurt am Main, Germany), Fluka Chemie GmbH (Steinheim, Germany) and Thermo Scientific  
128 (Karlsruhe, Germany).

129

#### 130 **Bacterial strains and growth conditions**

131 *Shewanella oneidensis* MR-1, *Geobacter sulfurreducens* PCA and *Geobacter metallireducens* GS-15 were  
132 routinely cultured anaerobically at 30 °C on a medium that was developed following Coppi and Holmes (18, 19).  
133 The growth medium contained 0.42 g/l KH<sub>2</sub>PO<sub>4</sub>, 0.22 g/l K<sub>2</sub>HPO<sub>4</sub>, 0.2 g/l NH<sub>4</sub>Cl, 0.38 g/l KCl, 0.36 g/l NaCl,  
134 0.21 g/l MgCl<sub>2</sub> 6H<sub>2</sub>O, 1.8 g/l NaHCO<sub>3</sub>, 0.5 g/l Na<sub>2</sub>CO<sub>3</sub>, 60 mg/l CaCl<sub>2</sub> 2H<sub>2</sub>O, 2 g/l casitone and was further  
135 complemented with 1.0 ml/l of selenite-tungstate solution (0.5 g/l NaOH, 3 mg/l Na<sub>2</sub>SeO<sub>3</sub>, 4 mg/l Na<sub>2</sub>WO<sub>4</sub>  
136 2H<sub>2</sub>O), 10 ml NB/l trace mineral solution (18), 10 ml/l vitamin solution (German Type Culture Collection,  
137 DSMZ, media 141), 0.2 mM sodium ascorbate, 1.0 mM cysteine, 0.2 % (w/v) yeast extract and 50 mM ferric  
138 citrate as an electron acceptor. The medium contained sodium lactate (12.5 mM), sodium acetate (6.25 mM)  
139 sodium propionate (5 mM) as electron donors. Standard anaerobic techniques were used throughout the study  
140 (20).

141 All anaerobic media were prepared in bottles capped with butyl rubber stoppers. To remove oxygen, the media  
142 were boiled for 10 minutes and flushed with a mixture of 80% N<sub>2</sub>/20% CO<sub>2</sub> for 30 min. After that, the pH was  
143 adjusted to 7.2. The optical density during anaerobic growth on ferric citrate was measured at a wavelength of  
144 655 nm to avoid an influence by ferric iron. All experiments were carried out in at least three independent  
145 replicates. Error bars represent the *standard deviation*.

146

#### 147 **Preparation and operation of BES**

148 The electrochemical setup used in this study was previously described by Kloeke (21). All experiments were  
149 carried out in a three-electrode setup. The individual chambers of the bio-electrochemical system (BES) were  
150 separated from each other by a Fumapem F-950 membrane (Quintech, Göppingen, Germany). A saturated  
151 calomel electrode (Sensortechnik Meinsberg GmbH, Ziegra-Knobelsdorf, Germany) was used as the reference

152 electrode. Throughout the study, all potentials were corrected for the corresponding values against normal  
153 hydrogen electrode (NHE). Two 2.25 cm<sup>2</sup> pieces of activated carbon cloth C-Tex 13 (MAST Carbon  
154 International Ltd., Hampshire, United Kingdom) were used as an anode and cathode, respectively. The  
155 electrodes were connected to a potentiostat (Pine Instruments, Grove City, USA) using a titanium wire. All BES  
156 experiments were carried out at 30 °C.

157 The medium for these experiments was composed as described above but did not contain a soluble electron  
158 acceptor. It contained 12.5 mM sodium lactate and 5 mM sodium propionate as electron donors. If *G.*  
159 *sulfurreducens* was cultured alone, 5 mM sodium acetate was added to the medium, since this strain cannot grow  
160 with propionate and only slowly with lactate. In contrary, acetate is produced from lactate by *S. oneidensis*  
161 which allows a constant acetate feed under co-culture conditions. In all experiments the anode chamber  
162 contained 22.5 ml of growth medium, whereas the cathode chamber and the reference electrode compartment  
163 contained 25 ml and 5 ml, respectively of medium without electron donor or acceptor. During the whole  
164 experiment, the anode chamber was flushed with a gas mixture of 80 % N<sub>2</sub>/20 % CO<sub>2</sub>, while the cathode  
165 chamber was purged with compressed air.

166 Prior to all BES experiments, the cells were washed twice in a buffer containing 0.42 g/l KH<sub>2</sub>PO<sub>4</sub>, 0.22 g/l  
167 K<sub>2</sub>HPO<sub>4</sub>, 0.2 g/l NH<sub>4</sub>Cl and 0.38 g/l KCl and were thereafter re-suspended to an OD<sub>655</sub> of 1.0 in the same buffer.  
168 The initial cell density in the BESs was set to an OD<sub>655</sub> of 0.1. The anode chamber was connected to a peristaltic  
169 pump and after the first 24 h of the experiment fresh medium was constantly pumped through the system with a  
170 flow rate of 0.14 ml/min, resulting in a hydraulic retention time of 160 min.

171

#### 172 **Extraction and quantification of genomic DNA**

173 Genomic DNA was extracted from the planktonic cells and the anode biofilm using the innuPREP Stool DNA  
174 Kit (Analytic Jena, Jena, Germany). Planktonic cells were treated as suggested by the manufacturer, while  
175 biofilm samples were additionally incubated in the lysis solution at room temperature for 10 minutes. Cell  
176 quantities were obtained by using quantitative PCR (qPCR), with specific primers for inserted barcode regions in  
177 the genome (Table 1) (22). All experiments were conducted in independent biological triplicates and three  
178 technical replicates for each biological sample. To obtain the qPCR detection limits for each strain, a standard  
179 curve based on the threshold cycle (C<sub>T</sub>) for a dilution series of DNA from pure cultures (1, 1x10<sup>-1</sup>, 2x10<sup>-2</sup>, 1x10<sup>-2</sup>  
180 <sup>2</sup>, 2x10<sup>-3</sup> and 1x10<sup>-3</sup> diluted with the DNase-free water) was constructed. The negative control samples contained  
181 DNase-free water instead of template DNA. To determine the initial concentration, cells were counted using a  
182 Neubauer hemocytometer with a 0.01 mm depth (Marienfeld, Lauda-Knigshofen, Germany).

183 The amplification was carried out using the DyNamo Flash SYBR Green qPCR Kit (Biozyme, Hessisch  
184 Oldendorf, Germany) according to the manufacturer's instructions. The optimal annealing temperature was  
185 determined by using a temperature gradient qPCR. All qPCR reactions were analyzed in a CFX96 Cyclyer (Bio-  
186 Rad, Munich, Germany). The amplification was conducted using the following program: 5 min at 95 °C for pre-  
187 denaturation and then 34 cycles of 10 seconds at 95 °C for denaturation, 30 seconds at 56 °C and then at 60 °C  
188 for annealing and extension reactions respectively. As a last step, a melting curve from 60 °C up to 95 °C was  
189 used to analyze the purity of the qPCR products. The amplified DNA samples were loaded on a 2.5% agarose-  
190 gel for verification of the expected fragment length. The C<sub>T</sub> values were automatically calculated with the Bio-  
191 Rad CFX Manager software. The standard curves were obtained by plotting the C<sub>T</sub> value against the logarithm of  
192 the concentration of each dilution of template DNA. For *Shewanella oneidensis* and *Geobacter sulfurreducens*,

193 primers described by Dolch (16) were used. For *Geobacter metallireducens*, specific primers were designed with  
194 the software tool Geneious (Biomatters, Auckland, New Zealand). All primer sequences are depicted in Table 1.

195

#### 196 **Fluorescence *in situ* hybridization (FISH)**

197 FISH was used for the simultaneous visualization, identification and localization of each strain in the multi-  
198 species biofilm community. Samples for FISH were taken from the planktonic phase and directly from the anode  
199 surface at the end of the experiment. Liquid samples were fixed with 4% formaldehyde for 1 hour at 4 °C.  
200 Afterwards, they were washed twice in PBS medium via centrifuging at 8000 rcf for 2 minutes. The samples  
201 were then stored in a 50% (v/v) ethanol solution at -20 °C. Complete anodes were fixed with the same  
202 concentration of formaldehyde for 4 hours at 4 °C. Thereafter, they were washed in PBS medium for 30 minutes  
203 and then stored at 4 °C. FISH analysis was conducted as described by Dolch (16) with the probes specified in  
204 Table 2. Images were analyzed with a Leica DM 5500 B microscope using a 63x immersion lens and a digital  
205 color camera DFC 300 FX (Leica, Wetzlar, Germany). Filter sets are listed in Table 3.

206

#### 207 **Single-nucleotide resolution RNA sequencing**

208 RNA was extracted individually from the triplicates of four experimental BES set-ups, which were inoculated  
209 either with pure cultures of *Shewanella oneidensis* MR-1, *Geobacter sulfurreducens* PCA, *Geobacter*  
210 *metallireducens* GS-15 or a mixed culture of the three strains. Prior to the extraction, all anodes with a biofilm  
211 were additionally pre-incubated in 3 ml of Bacteria Protect solution for 10 minutes at room temperature (Qiagen  
212 RNeasy Mini kit, Hilden, Germany). Total RNA was isolated from the anode-biofilms using the RNeasy kit  
213 provided by Qiagen according to the manufacturer's instructions. Residual DNA was removed with an overnight  
214 DNase I digestion at 37 °C. Further purification of RNA from DNA was conducted using the Ambion DNA-free  
215 kit (Life Technologies, Carlsbad, CA, USA). Aliquots from treated samples were subjected to PCR amplification  
216 with specific primers (Table 1) to validate the absence of genomic DNA. The Ambion MICROBExpress  
217 bacterial mRNA enrichment kit (Life Technologies) was used for rRNA depletion. Strand specific cDNA  
218 libraries were prepared from 50 ng of rRNA-depleted RNA following the TruSeq v2 RNA protocol (Illumina).  
219 The libraries were prepared using multiplex primers to allow simultaneous sequencing on a single lane, which  
220 was performed on a HiSeq1500 using SBS v3 kits (Illumina) generating paired end reads of 2 x 51 nt (*G.*  
221 *sulfurreducens* and *S. oneidensis*) or 2 x 100 nt (mixed species and *G. metallireducens* samples). Cluster  
222 detection and base calling were performed using RTAv1.13 and quality of reads was assessed with CASAVA  
223 v1.8.1 (Illumina). Sequencing yielded between 2.3 and 37.2 million read pairs that were deposited at the GEO  
224 database under the accession number GSE79750.

225

#### 226 **RNA-sequencing data analysis**

227 Sequence data were clipped for the samples with 2 x 100 nt to obtain a fixed read length of 51 nt in all samples  
228 and mapped to a database containing the merged genomes of *Geobacter metallireducens* GS-15 (NCBI GenBank  
229 accession number NC\_002939.5), *Geobacter sulfurreducens* PCA (NC\_007517.1), *Shewanella oneidensis* MR-1  
230 (NC\_004347.2) and its megaplasmid (NC\_004349.1) using *bowtie2* (23). Differential expression profiles were  
231 calculated for each species individually in pure cultures versus the mixed culture by comparing the gene  
232 expression from the mapped sequences using *HTSeq* (24) for counting and *DESeq2* (25) for differential

233 expression analysis. An adjusted P-value (P<sub>adj</sub>) of 0.05 was used as the threshold to determine statistical  
234 significance of differential gene expression.

235

### 236 **Analytical techniques**

237 Organic acids that were consumed or produced during the experiments were quantified using high-performance  
238 liquid chromatography (HPLC). Quantification of organic acids was conducted as described by Sturm-Richter  
239 (26). Cell density was determined via the Thermo Scientific GENESYS 20 spectrophotometer. The coulomb  
240 efficiency was calculated according to Kipf (27).

241

## 242 **Results and Discussion**

243

### 244 **Dynamics of a model multi-species anode biofilm formation and coulombic efficiency**

245 The overall aim of this study was to analyze the dynamics of community composition as well as of  
246 metabolic processes of a controlled microbial community on anode surfaces. In a first set of  
247 experiments the dynamics of a biofilm composed of the three model organisms *S. oneidensis*, *G.*  
248 *sulfurreducens* and *G. metallireducens* was analyzed over a time course of seven days. The three  
249 strains were added with equal OD-values to the microbial electrochemical cells, so that the final  
250 optical density was 0.1. Of note, the OD values do not correspond to the same cell numbers for the  
251 different species, due to the differences in the cell size of these strains. The anode potential was  
252 adjusted to 0 mV. The composition of anode biofilms as well as the planktonic community was  
253 analyzed in triplicates 1, 2, 4, and 7 days following inoculation using quantitative PCR. *G.*  
254 *sulfurreducens* clearly dominated the sessile community starting from the first day on (Fig. 1 A). That  
255 was expected, as the strategy of *G. sulfurreducens* cells for electron transfer to insoluble electron  
256 acceptors relies solely on a direct interaction which is mediated by conductive pili as well as *c*-type  
257 cytochromes on the surface of the cells as well as within the extracellular matrix (28). Nevertheless,  
258 neither *S. oneidensis* nor *G. metallireducens* were outcompeted from the anode during the time course  
259 of the experiment. On the contrary, active growth was observed. Results from the planktonic phase  
260 (Fig. 1 B) display a more dynamic development of the community as compared to the anode biofilm.  
261 The percentage of *S. oneidensis* cells increased within the first 4 days to 73%, while *G.*  
262 *metallireducens* cells were almost eliminated from the planktonic phase. It is very likely that *S.*  
263 *oneidensis* thrives in the planktonic phase by using endogenously produced flavin molecules as  
264 electron shuttles (29). The reduced shuttles could either be re-oxidized at the surface of the anode itself  
265 or at the biofilm covering the anode. Interestingly, we could observe planktonic *G. sulfurreducens*  
266 cells in the mixed species experiment but not in reactors that were inoculated with *G. sulfurreducens*  
267 alone (see below). Hence, it is possible that this planktonic fraction could show a cheater-like strategy  
268 by using flavins produced by *S. oneidensis* as a way to transfer respiratory electrons away from the  
269 cell.

270 FISH experiments nicely corroborated the qPCR-based results (Fig. 2). The microscopic pictures also  
271 display the different sizes of *Shewanella* compared to *Geobacter* cells that lead to a starting  
272 composition of equal OD values but different concentrations of the individual strains. After 2-3 days  
273 of cultivation, the multi-species biofilm generated stable currents that reached values between 0.60 –  
274 0.64 mA/cm<sup>2</sup>. This observation indicates that the community within the BESs achieved also stable  
275 rates of carbon oxidation. The coulombic efficiency (30) of the BES was (53 ± 6) %, which is in the  
276 range of values, published before for mixed species communities.

277

### 278 **Characterization of the biofilm stability under different electrochemical conditions**

279 In a second set of experiments the stability of the previously described multi-species biofilm was  
280 investigated under varying electrochemical process parameters. Fifteen BES setups were started at the  
281 same time under the following applied potentials: 0.44 V, 0.24 V, 0.04 V, -0.06 V and -0.16 V.  
282 Interestingly, the produced current values were highly similar during the time course of the experiment  
283 if the applied potential was in a range between 0.04 and 0.44 V (Fig. 3). Lower currents were observed  
284 only if the working electrodes were poised to potentials lower than 0.04 V.

285 The biofilm community compositions at the end of the experiments were similar under all tested  
286 conditions and comparable to the results shown in the previous section (Fig. 4). At the end of the 7  
287 days of incubation, *G. sulfurreducens* accounted for 86% – 96% of all organisms. *S. oneidensis* cells  
288 represented 4 to 12% of the community, while *G. metallireducens* was only detectable in minor  
289 quantities. In line with the measured current densities we could see a pronounced drop in cell density  
290 if potentials below 0 mV were applied. Working electrodes poised to a potential of -0.06V had more  
291 than 80% less cells compared to anodes adjusted to a potential of 0.04 V. In comparison, all anodes  
292 poised to positive values showed only minor differences in terms of overall cell number. Planktonic  
293 cells in the reactors were also quantified. Here, *S. oneidensis* (57 – 73%) and *G. sulfurreducens* (26 –  
294 43%) comprised the majority of organisms (Fig. 4). It seems as if working electrode potentials above -  
295 0.06 V sustained the maximum rate of electron transfer, which correlates to the highest biomass  
296 production rates. While *S. oneidensis* as well as *G. sulfurreducens* responded similarly to the different  
297 potentials, we could not observe such a clear trend for *G. metallireducens*. It is possible that under the  
298 chosen conditions, growth of *G. metallireducens* is limited by the substrate oxidation rate rather than  
299 the electron transfer to the anode surface.

300

### 301 **Steering metabolic activity via working electrode potentials**

302 Linear sweep voltammetry experiments were conducted to determine the minimal potential at which  
303 an exoelectrogenic multi-species biofilm is still capable to transfer respiratory electrons to the working  
304 electrode. An initial applied potential of 0.04 V was linearly decreased to the value of -0.26 V with a  
305 sweep rate of 0.75 μV s<sup>-1</sup>. Thereafter, the sweep was repeated in reverse direction until the starting  
306 potential of 0.04 V was reached. As indicated in Fig. 5, the cells stopped to produce current if the

307 applied potential was below approximately -0.2 V. Half-maximal electron transfer rates were achieved  
308 with anode potentials of -0.08 V. This potential is in line with typical mid-point potentials of outer  
309 membrane cytochromes as well as with flavins, which are released by *S. oneidensis* and can be used as  
310 electron transfer shuttles (31). Interestingly, the consortium stability does not seem to be highly  
311 affected by variations of electron transfer rates since an immediately following experiment in the other  
312 potential direction showed similar current values. This is surprising since the very low sweep rate  
313 results in an overall time course for the experiment of more than 9 days for the overall sweep from  
314 0.04 V down to -0.26 V and back up to 0.04 V. The ability to control current production of  
315 exoelectrogenic bacteria could offer promising solutions for applied processes. For instance,  
316 preliminary results suggest that it is possible to use an applied potential as a way to accelerate carbon  
317 oxidation in a biogas plant (data not shown).

318

### 319 **Transcriptome analysis**

320 Transcriptomes and metatranscriptomes were analyzed to reveal metabolic changes in the individual  
321 strains as a result of the shift from solitary to multispecies growth on anodes. Twelve BES setups were  
322 started. They contained in triplicate either single cultures of *S. oneidensis*, *G. sulfurreducens* and *G.*  
323 *metallireducens* or a mixture of all three strains. The applied working electrode potential was in all  
324 cases 0.04 V. The experiment was conducted over seven days. The medium contained lactate and  
325 propionate as carbon and electron sources. Acetate (5 mM) was additionally added only in the  
326 experiments which were solely conducted with *G. sulfurreducens*. Summers (32) could show that *G.*  
327 *sulfurreducens* wild type can grow on lactate (this is, contrary to an initial publication by Caccavo  
328 (33)). Nevertheless, growth rates were very low and increased according to Summers (32) only after a  
329 spontaneous point mutation to 8 hours. Under co-culture conditions, acetate will be produced by *S.*  
330 *oneidensis* as an end-product of lactate oxidation.

331 During solitary growth, all strains produced less current compared to co-culture conditions (0.62 mA  
332 cm<sup>-2</sup>). The highest current production in solitary growth was recorded for *G. sulfurreducens* (0.47 mA  
333 cm<sup>-2</sup>), whereas *S. oneidensis* produced only around 0.13 mA cm<sup>-2</sup> and *G. metallireducens* 0.06 mA cm<sup>-2</sup>.

335 A comparison of the transcriptomes from solitary and co-culture growth revealed that 1124 of the  
336 3,430 protein-coding genes of *G. sulfurreducens* showed log<sub>2</sub>fold changes higher than +/-1 with  
337 corresponding padJ values below 0.05. Of the total 4,214 genes of *S. oneidensis*, 677 followed the  
338 above-described characteristics, while in *G. metallireducens* only 23 genes could be detected as  
339 differentially expressed (Tab. S1). The reason for this rather low amount of detectable candidate genes  
340 might be due to a reduced experimental sensitivity caused by the limited growth of the *G.*  
341 *metallireducens* cells compared to the other two strains and its subsequently reduced representation in  
342 the mixed species transcriptomic data.

343

**344 Variations of the central metabolism as a result of co-cultivation**

345 As mentioned above, there is a multitude of differential gene expression in *G. sulfurreducens* cells  
346 grown in the absence or presence of *S. oneidensis* and *G. metallireducens*. This study focuses on the  
347 central metabolic changes that are results of co-cultivation. Generally, it seems as if the central  
348 metabolism of *G. sulfurreducens* is generally upregulated under co-culture conditions. There are a  
349 number of cytochrome genes that show induced expression including *omcB* and *omcE*. Both  
350 cytochromes were shown to be involved in the electron transfer to the cell surface of *G.*  
351 *sulfurreducens* (34). Moreover, expression of the small triheme cytochrome PpcA was increased.  
352 PpcA is localized in the periplasm and evidence was provided that it is involved in the transport of  
353 respiratory electrons from the cytoplasmic to the outer membrane (35). In agreement with the  
354 upregulation of cytochromes is the increased transcription of pili genes, including *pilA*, which is  
355 required for high density current production (36). The hypothesis of increased electron transfer as a  
356 result of co-cultivation is nicely corroborated by the upregulation of genes coding for central reactions  
357 involved in the oxidation of acetate within the citric acid cycle as well as the NADH dehydrogenase  
358 Nuo (average upregulation of *nuo* genes: 2.65 fold). The reason for this general response might be the  
359 downregulation of the hydrogen dependent growth transcriptional regulator HgtR. HgtR has been  
360 shown to repress genes involved in biosynthesis and energy generation (37). An upregulation of HgtR  
361 under conditions of growth in pure culture might be explainable as it has been shown that electron  
362 acceptor limitation results in hydrogen production by *G. sulfurreducens* (38). Hence, the presence of  
363 the other strains might contribute to higher electron transfer rates, possibly due to the presence of  
364 organic molecules like flavins released by *S. oneidensis* cells. Still, although HgtR is downregulated  
365 under co-cultivation conditions, the typical uptake hydrogenase HybAB (39) of *G. sulfurreducens* is  
366 strongly upregulated (9.1- and 14.3-fold, respectively). One explanation could be that *G.*  
367 *sulfurreducens* under mixed species conditions enters a state in which it uses both hydrogen and  
368 acetate as electron donors. The use of hydrogen might also allow for a higher percentage of acetate  
369 that can be fed into gluconeogenesis. At least two genes of gluconeogenesis were discovered to be  
370 upregulated under mixed species conditions (*eno*: 2.4-fold upregulated; *pgk*: 2.5-fold upregulated).  
371 Hydrogen might be produced by *S. oneidensis* as will be shown later. Interestingly, genes necessary  
372 for nitrogen fixation show a strong decrease in transcription as a result of co-cultivation. This might  
373 indicate that, although the medium contains 3.7 mM ammonium, the cells face a nitrogen limitation  
374 within the anode biofilm. It is of interest to note that both *Geobacter* strains showed a downregulation  
375 of *cydA* and *cydB* as a result of co-cultivation. The encoded cytochrome bd-ubiquinol oxidase was  
376 discussed as a mechanism to cope with oxidative stress (40). A contamination with trace amounts of  
377 oxygen is possible with regard to the polycarbonate based reactors used. The presence of *S. oneidensis*  
378 in the biofilm and its capacity for aerobic growth would help to decrease the amount of oxygen at the  
379 anode surface. *G. metallireducens* showed another interesting adaptation to growth with *G.*  
380 *sulfurreducens* and *S. oneidensis* which is an upregulation of the *prp*-operon. The *prp*-genes encode

381 the necessary proteins for propionate oxidation (41). *G. metallireducens* can grow with acetate and  
382 propionate. These cells apparently do not adapt their metabolism for acetate as a carbon source but  
383 rather specialize on propionate, for which there is no competitor in the community. Propionate is a  
384 challenging substrate under anoxic conditions, since its oxidation involves an energy-dependent  
385 activation to propionyl-CoA and an ATP-dependent oxidation of succinate to fumarate if electron  
386 acceptors are used which reduction is menaquinone dependent (42). This might also explain the rather  
387 slow growth of *G. metallireducens*.

388 *S. oneidensis* cells also show distinct responses to growth in a mixed-culture biofilm. We could  
389 observe an upregulation of the Mtr pathway, which is necessary for electron transport through the  
390 outer membrane and on to an extracellular electron acceptor (*mtrABC* and *omcA* showed a 2.3-fold  
391 average upregulation). Furthermore, protein-coding genes involved in lactate transport and oxidation  
392 were also upregulated (SO\_1518 – 1522 > 3-fold). Hence, as was observed for *G. sulfurreducens*, co-  
393 cultivation seems to positively affect the substrate oxidation and electron transfer processes.  
394 Interestingly, *S. oneidensis* also responded to co-cultivation with the upregulation of a hydrogenase  
395 (*hypBEF* > 2.5-fold, *hyaABCD* > 4.5-fold). Meshulam-Simon (43) investigated hydrogen metabolism  
396 in *S. oneidensis* and observed that Hya-activity accounted for over 75% of the hydrogen produced by  
397 *S. oneidensis*. Hydrogen formation was, at least to some extent, dependent on reverse electron transfer  
398 because the addition of the protonophor CCCP resulted in decreased hydrogen production. It was  
399 speculated that in this case proton reduction could occur via NADH as electron donor that could be  
400 produced either by a conversion of pyruvate to acetyl-CoA and NADH by pyruvate dehydrogenase or  
401 indirectly via formate resulting from pyruvate formate lyase catalyzed conversion of pyruvate to  
402 acetyl-CoA and formate. The latter is corroborated by the upregulation of the *pflA* and *pflB* genes as  
403 well as by a gene cluster encoding a typical respiratory formate dehydrogenase (SO\_4509 –  
404 SO\_4511). Along these lines, it is interesting to note that *S. oneidensis* does not seem to use oxidative  
405 phosphorylation as way of producing energy under anoxic conditions. Hunt and colleagues (44)  
406 deleted the ATP synthase of the organisms and observed only minor growth defects. Hence, the  
407 developed proton gradient would at least partly be available for reverse electron-transfer reactions.  
408 There are a number of gene clusters that are upregulated in cells grown in the absence of *G.*  
409 *sulfurreducens* and *G. metallireducens*. Very prominent are genes that are involved in the degradation  
410 of amino acids (*liuA-F*, 9.8-fold upregulation). The medium contains casitone and therefore is a source  
411 of amino acids. Currently, we can only speculate that this distinct regulatory response is due to the  
412 pool of available amino acids being lower if three organisms simultaneously thrive in the same reactor  
413 and try to avoid using the catabolic electron source for the formation of anabolic building blocks.

414

## 415 **Conclusions**

416 In this study the interaction of three exoelectrogenic strains within BESs was analyzed for the first  
417 time. The biofilms formed on the anode surface seem to be highly stable and could be steered in their

418 metabolic activity by the anode potential. Although *G. metallireducens* plays a minor role in terms of  
419 cell size, it appears to occupy a stable ecological niche, which is likely characterized by the organism's  
420 ability to use propionate as electron donor. The interaction of *G. sulfurreducens* and *S. oneidensis* is  
421 nicely displayed by the presence of *G. sulfurreducens* cells in the planktonic phase only in the  
422 presence of *S. oneidensis*. This observation is similar to cheater-like behavior that may occur once  
423 extracellular products can be shared as a 'public good', like it was described for extracellular signals in  
424 quorum sensing studies (45, 46). Transcriptomic analysis revealed that the interaction with other  
425 exoelectrogenic strains generally led to an upregulation of the central metabolism of the organisms,  
426 thus supporting a hypothesis of synergistic interaction. The results presented in this manuscript at least  
427 partially explain the observation reported multiple times in the literature, that multispecies biofilms  
428 tend to be more efficient in current production compared to single cultures.

429

430

### 431 **Acknowledgements**

432 This research was supported by the German Ministry of Education and Research (BMBF)  
433 (03SF0424A).

434

435

436

437

438

439

440

441

442

443

444

445

446

447

448

449

450

451

452

453

454 *Table 1: Sequences of primers for qPCR (Dolch et al., 2016)*

455

Probe	Sequence (5' – 3')	Amplicon size (bp)
S. oneidensis for	GACTGTACTTGGCATTGG	18
S. oneidensis rev	GATCCATTAGCACAGACTTA	20
G. sulfurreducens for	CGGTTCTATCGACCTACC	18
G. sulfurreducens rev	CTGCTTGATGAACGAGAG	18
G. metallireducens for	CCGTGCTCTGTATGATAC	18
G. metallireducens rev	CAGGATTTCTCGAATTTCTC	20

456

457

458 *Table 2: Fluorescently labeled oligonucleotide probes and helper oligonucleotides for FISH*  
459 *experiment*

460

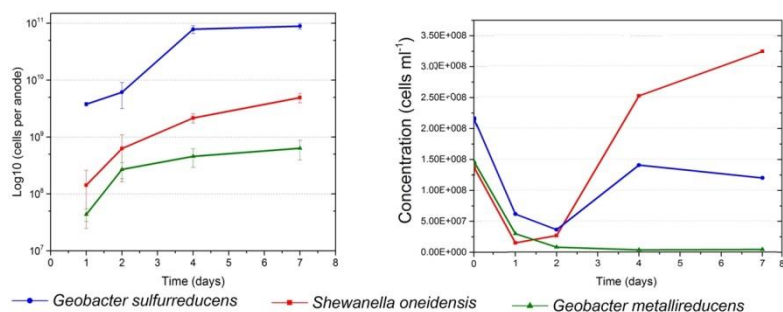
Probe	Sequence (5' {3'})	Specification	Reference
SHEW227	AGCTAATCCCACCTAGGTWCATC	<i>Shewanella spp.</i>	Hugget et al. (2008)
GEO1	AGAATCCAAGGACTCCGT	<i>G. metallireducens</i>	Summers et al. (2010)
HGEO1-1	GAAGGTCCCCCCTTTTCCCGC	Helpers for GEO1	
HGEO1-2	GGGCTTATCCGGTATTAGCACC	Helpers for GEO1	
GEO2	AGAATCCAAGGACTCCGT	<i>G. sulfurreducens</i>	Richter et al. (2007)
HGEO2-1	GTCCCCCCTTTTCCCGCAAGA	Helpers for GEO2	
HGEO2-2	CTAATGGTACGCGGACTCATCC	Helpers for GEO2	

461

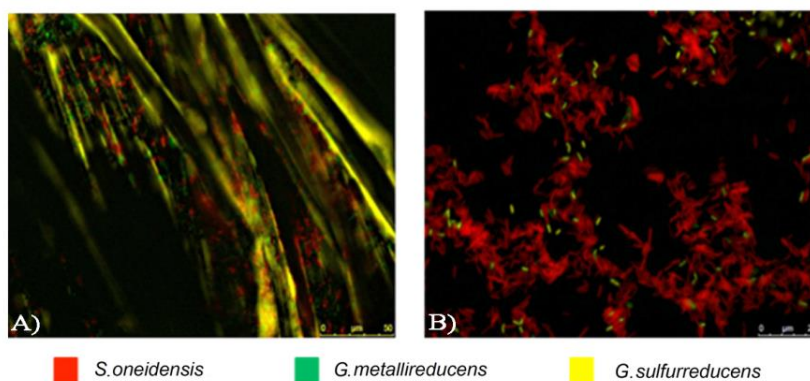
462 *Table 3: Specification of the filters for FISH experiment that were used in the Leica DM 5500*463 *B microscope*

464

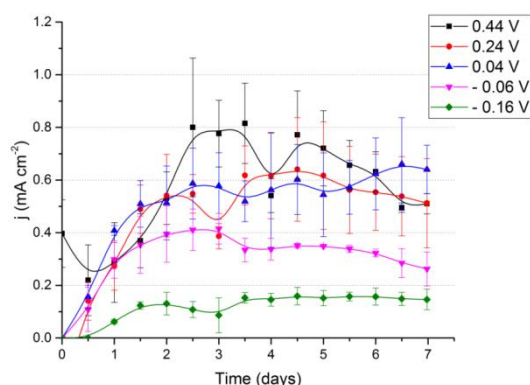
Filter cube	Fluor dye	Excitation range	Excitation filter	Suppression filter
A4	DAPI	UV	BP 360/40	BP 470/40
I3	FITC	Blue	BP 450/490	LP 515
Y3	CY3	Green	BP 545/30	BP 610/75
Y5	CY5	Red	BP 640/30	BP 690/50



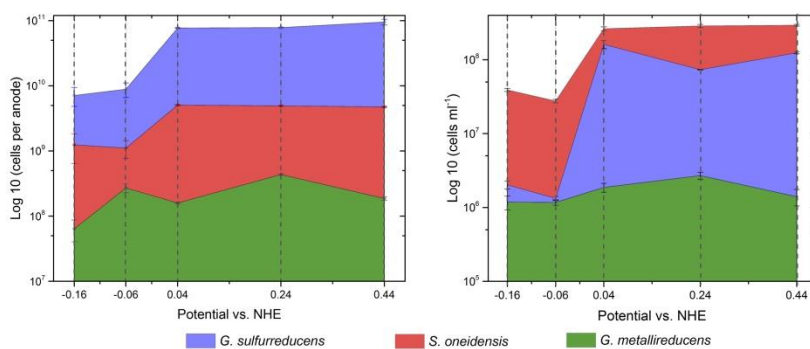
465  
 466 **Fig. 1.** Growth of the model exoelectrogenic biofilm A) directly on the anode surface and B) in the planktonic  
 467 phase in a time course of 7 days. The analyses were conducted at different time point following inoculation with  
 468 an initial inoculum that consisted of equal fractions of the three barcoded strains. Cell numbers were quantified  
 469 using a qPCR analysis.  
 470



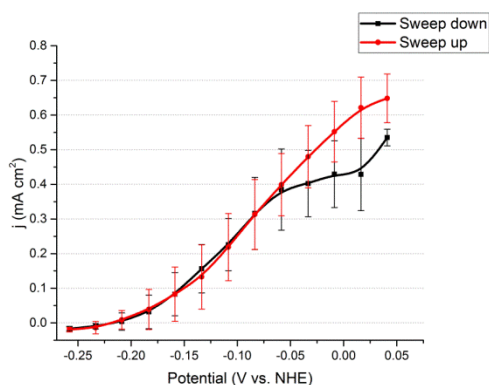
471  
 472 **Fig. 2.** Fluorescent *in situ* hybridization (FISH) pictures of the exoelectrogenic community. A) Cells on the  
 473 anode surface, B) cells in the planktonic phase after 1 week of the experiment. *Geobacter sulfurreducens* was  
 474 stained in yellow (Cy5), *Geobacter metallireducens* in green (FITC) and *Shewanella oneidensis* in red (Cy3).  
 475



476  
 477 **Fig. 3.** Stability of the model exoelectrogenic biofilm under different applied potentials (versus NHE). Under  
 478 positive applied potentials (0.04 – 0.44 V) current density  $j$  was roughly identical and was in the range of 0.5 –  
 479 0.7 mA cm<sup>-2</sup>. The negative range of applied potentials lead to a limitation of electron transfer.  
 480



481  
 482 **Fig. 4.** Quantitative analysis of the cells on the anode surface (A) and in the planktonic phase (B) under different  
 483 applied potentials. *Geobacter sulfurreducens* clearly dominated in this model exoelectrogenic biofilm. Under  
 484 applied negative potentials decreased amounts of cells were detected throughout all three strains.  
 485



486  
 487 **Fig. 5.** Stability and activity of the model exoelectrogenic biofilm during a linear sweep voltammetry  
 488 experiment. The applied potentials ranged from +0.05 mV to -0.25 mV against NHE. The experiment was started  
 489 at 0.05 mV. After reaching -0.25 mV the sweep was reversed back to 0.05 mV. The limiting potential, at which  
 490 cells stopped to produce electrons was detected below approximately -0.2 V. Generally, the exoelectrogenic  
 491 consortium was not affected by applying negative potentials regarding its overall capabilities, since a directly  
 492 following experiment in the other potential direction showed similar results.

493

494

## References

495

496 1. **Nielsen LP, Risgaard-Petersen N, Fossing H, Christensen PB, Sayama M.** 2010. Electric  
 497 currents couple spatially separated biogeochemical processes in marine sediment. *Nature*  
 498 **463**:1071-1074.

499 2. **Wagner RC, Call DF, Logan BE.** 2010. Optimal potential set anode potentials vary in  
 500 Bioelectrochemical systems. *Environ Sci Technol* **44**:6036-6041.

501 3. **Harnisch F, Schroder U.** 2010. From MFC to MXC: chemical and biological cathodes and  
 502 their potential for microbial bioelectrochemical systems. *Chemical Society Reviews* **39**:4433-  
 503 4448.

504 4. **Liu H, Logan BE.** 2004. Electricity generation using an air-cathode single chamber microbial  
 505 fuel cell in the presence and absence of a proton exchange membrane. *Environ Sci Technol*  
 506 **38**:4040-4046.

507 5. **Lovley DR.** 2006. Bug juice: harvesting electricity with microorganisms. *Nat Rev Microbiol*  
 508 **4**:497-508.

- 509 6. **Zhao F, Slade RCT, Varcoe JR.** 2009. Techniques for the study and development of  
510 microbial fuel cells: an electrochemical perspective. *Chemical Society Reviews* **38**:1926-  
511 1939.
- 512 7. **Jia J, Tang Y, Liu B, Wu D, Ren N, Xing D.** 2013. Electricity generation from food wastes  
513 and microbial community structure in microbial fuel cells. *Bioresour Technol* **144**:94-99.
- 514 8. **Xiao B, Yang F, Liu J.** 2013. Evaluation of electricity production from alkaline pretreated  
515 sludge using two-chamber microbial fuel cell. *J Hazard Mater* **254-255**:57-63.
- 516 9. **Ishii S, Suzuki S, Norden-Krichmar TM, Phan T, Wanger G, Neilson KH, Sekiguchi Y,  
517 Gorby YA, Bretschger O.** 2014. Microbial population and functional dynamics associated  
518 with surface potential and carbon metabolism. *Isme j* **8**:963-978.
- 519 10. **Freguia S, Rabaey K, Yuan Z, Keller J.** 2008. Syntrophic processes drive the conversion of  
520 glucose in microbial fuel cell anodes. *Environ Sci Technol* **42**:7937-7943.
- 521 11. **Lovley DR.** 2008. The microbe electric: conversion of organic matter to electricity. *Curr Opin  
522 Biotechnol* **19**:564-571.
- 523 12. **Serres MH, Riley M.** 2006. Genomic analysis of carbon source metabolism of *Shewanella  
524 oneidensis* MR-1: Predictions versus experiments. *J Bacteriol* **188**:4601-4609.
- 525 13. **Aelterman P, Freguia S, Keller J, Rabaey K, Verstraete W.** 2008. The anode potential  
526 regulates the bacterial activity in microbial fuel cells. *Commun Agric Appl Biol Sci* **73**:85-89.
- 527 14. **Ishii S, Suzuki S, Norden-Krichmar TM, Wu A, Yamanaka Y, Neilson KH, Bretschger  
528 O.** 2013. Identifying the microbial communities and operational conditions for optimized  
529 wastewater treatment in microbial fuel cells. *Water Res* **47**:7120-7130.
- 530 15. **Kotloski NJ, Gralnick JA.** 2013. Flavin Electron Shuttles Dominate Extracellular Electron  
531 Transfer by *Shewanella oneidensis*. *mBio* **4**.
- 532 16. **Dolch K, Danzer J, Kabbeck T, Bierer B, Erben J, Forster AH, Maisch J, Nick P,  
533 Kerzenmacher S, Gescher J.** 2014. Characterization of microbial current production as a  
534 function of microbe-electrode-interaction. *Bioresour Technol* **157**:284-292.
- 535 17. **Lovley DR, Giovannoni SJ, White DC, Champine JE, Phillips EJ, Gorby YA, Goodwin  
536 S.** 1993. *Geobacter metallireducens* gen. nov. sp. nov., a microorganism capable of coupling  
537 the complete oxidation of organic compounds to the reduction of iron and other metals. *Arch  
538 Microbiol* **159**:336-344.
- 539 18. **Coppi MV, Leang C, Sandler SJ, Lovley DR.** 2001. Development of a genetic system for  
540 *Geobacter sulfurreducens*. *Appl Environ Microbiol* **67**:3180-3187.
- 541 19. **Holmes DE, Bond DR, Lovley DR.** 2004. Electron Transfer by *Desulfobulbus propionicus* to  
542 Fe(III) and Graphite Electrodes. *Applied and Environmental Microbiology* **70**:1234-1237.
- 543 20. **Balch WE, Wolfe RS.** 1976. New Approach to the Cultivation of Methanogenic Bacteria  
544 Growth of *Methanobacterium ruminantium* in a Pressurized Atmosphere. *Appl Environ  
545 Microbiol* **32**:781-791.
- 546 21. **Kloke A, Rubenwolf S, Bucking C, Gescher J, Kerzenmacher S, Zengerle R, von Stetten  
547 F.** 2010. A versatile miniature bioreactor and its application to bioelectrochemistry studies.  
548 *Biosens Bioelectron* **25**:2559-2565.
- 549 22. **Dolch K, Wuske J, Gescher J.** 2016. Genomic Barcode-Based Analysis of Exoelectrogens in  
550 Wastewater Biofilms Grown on Anode Surfaces. *J Microbiol Biotechnol* **26**:511-520.
- 551 23. **Langmead B, Salzberg SL.** 2012. Fast gapped-read alignment with Bowtie 2. *Nat Methods*  
552 **9**:357-359.
- 553 24. **Anders S, Huber W.** 2010. Differential expression analysis for sequence count data. *Genome  
554 Biol* **11**:R106.
- 555 25. **Love MI, Huber W, Anders S.** 2014. Moderated estimation of fold change and dispersion for  
556 RNA-seq data with DESeq2. *Genome Biol* **15**:550.
- 557 26. **Sturm-Richter K, Golitsch F, Sturm G, Kipf E, Dittrich A, Beblawy S, Kerzenmacher S,  
558 Gescher J.** 2015. Unbalanced fermentation of glycerol in *Escherichia coli* via heterologous  
559 production of an electron transport chain and electrode interaction in microbial  
560 electrochemical cells. *Bioresour Technol* **186**:89-96.

- 561 27. **Kipf E, Koch J, Geiger B, Erben J, Richter K, Gescher J, Zengerle R, Kerzenmacher S.** 2013. Systematic screening of carbon-based anode materials for microbial fuel cells with *Shewanella oneidensis* MR-1. *Bioresour Technol* **146**:386-392.
- 562
- 563
- 564 28. **Liu Y, Bond DR.** 2012. Long-distance electron transfer by *G. sulfurreducens* biofilms results in accumulation of reduced c-type cytochromes. *ChemSusChem* **5**:1047-1053.
- 565
- 566 29. **Marsili E, Baron DB, Shikhare ID, Coursolle D, Gralnick JA, Bond DR.** 2008. *Shewanella* secretes flavins that mediate extracellular electron transfer. *Proc Natl Acad Sci U S A* **105**:3968-3973.
- 567
- 568
- 569 30. **Logan B.** 2008. Microbial fuel cells.
- 570 31. **Brutinel ED, Gralnick JA.** 2012. Shuttling happens: soluble flavin mediators of extracellular electron transfer in *Shewanella*. *Appl Microbiol Biotechnol* **93**:41-48.
- 571
- 572 32. **Summers ZM, Ueki T, Ismail W, Haveman SA, Lovley DR.** 2012. Laboratory evolution of *Geobacter sulfurreducens* for enhanced growth on lactate via a single-base-pair substitution in a transcriptional regulator. *Isme j* **6**:975-983.
- 573
- 574
- 575 33. **Caccavo F, Jr., Lonergan DJ, Lovley DR, Davis M, Stolz JF, McInerney MJ.** 1994. *Geobacter sulfurreducens* sp. nov., a hydrogen- and acetate-oxidizing dissimilatory metal-reducing microorganism. *Appl Environ Microbiol* **60**:3752-3759.
- 576
- 577
- 578 34. **Nevin KP, Kim BC, Glaven RH, Johnson JP, Woodard TL, Methe BA, Didonato RJ, Covalla SF, Franks AE, Liu A, Lovley DR.** 2009. Anode biofilm transcriptomics reveals outer surface components essential for high density current production in *Geobacter sulfurreducens* fuel cells. *PLoS One* **4**:e5628.
- 579
- 580
- 581
- 582 35. **Lloyd JR, Leang C, Hodges Myerson AL.** 2003. Biochemical and genetic characterization of PpcA, a periplasmic c-type cytochrome in *Geobacter sulfurreducens*. *Biochemical Journal* **369**:153-161.
- 583
- 584
- 585 36. **Reguera G, Nevin KP, Nicoll JS, Covalla SF, Woodard TL, Lovley DR.** 2006. Biofilm and nanowire production leads to increased current in *Geobacter sulfurreducens* fuel cells. *Appl Environ Microbiol* **72**:7345-7348.
- 586
- 587
- 588 37. **Ueki T, Lovley DR.** 2010. Genome-wide gene regulation of biosynthesis and energy generation by a novel transcriptional repressor in *Geobacter* species. *Nucleic Acids Res* **38**:810-821.
- 589
- 590
- 591 38. **Cord-Ruwisch R, Lovley D, Schink B.** 1998. Growth of *geobacter sulfurreducens* with acetate in syntrophic cooperation with hydrogen-oxidizing anaerobic partners. *Appl Environ Microbiol* **64** 2232-2236.
- 592
- 593
- 594 39. **Coppi MV, O'Neil RA, Lovley DR.** 2004. Identification of an Uptake Hydrogenase Required for Hydrogen-Dependent Reduction of Fe(III) and Other Electron Acceptors by *Geobacter sulfurreducens*. *Journal of Bacteriology* **186**:3022-3028.
- 595
- 596
- 597 40. **Giuffre A, Borisov VB, Arese M, Sarti P, Forte E.** 2014. Cytochrome bd oxidase and bacterial tolerance to oxidative and nitrosative stress. *Biochim Biophys Acta* **1837**:1178-1187.
- 598
- 599 41. **Aklujkar M, Krushkal J, DiBartolo G, Lapidus A, Land ML, Lovley DR.** 2009. The genome sequence of *Geobacter metallireducens*: features of metabolism, physiology and regulation common and dissimilar to *Geobacter sulfurreducens*. *BMC Microbiol* **9**:109.
- 600
- 601
- 602 42. **Muller N, Worm P, Schink B, Stams AJ, Plugge CM.** 2010. Syntrophic butyrate and propionate oxidation processes: from genomes to reaction mechanisms. *Environ Microbiol Rep* **2**:489-499.
- 603
- 604
- 605 43. **Meshulam-Simon G, Behrens S, Choo AD, Spormann AM.** 2007. Hydrogen metabolism in *Shewanella oneidensis* MR-1. *Appl Environ Microbiol* **73**:1153-1165.
- 606
- 607 44. **Hunt KA, Flynn JM, Naranjo B, Shikhare ID, Gralnick JA.** 2010. Substrate-level phosphorylation is the primary source of energy conservation during anaerobic respiration of *Shewanella oneidensis* strain MR-1. *J Bacteriol* **192**:3345-3351.
- 608
- 609
- 610 45. **Dunny GM, Brickman TJ, Dworkin M.** 2008. Multicellular behavior in bacteria: communication, cooperation, competition and cheating. *Bioessays* **30**:296-298.
- 611
- 612 46. **Czaran T, Hoekstra RF.** 2009. Microbial communication, cooperation and cheating: quorum sensing drives the evolution of cooperation in bacteria. *PLoS One* **4**:e6655.
- 613
- 614
- 615



## The performance of microbial anodes in municipal wastewater: Pre-grown multispecies biofilm vs. natural inocula



Joana Madjarov<sup>a,1</sup>, Anna Prokhorova<sup>b,1</sup>, Thorsten Messinger<sup>a</sup>, Johannes Gescher<sup>b,c</sup>, Sven Kerzenmacher<sup>a,\*</sup>

<sup>a</sup> Laboratory for MEMS Applications, IMTEK – Department of Microsystems Engineering, University of Freiburg, Georges-Koehler-Allee 103, 79110 Freiburg, Germany

<sup>b</sup> Institute for Applied Biosciences, Department of Applied Biology, Karlsruhe Institute of Technology, Fritz-Haber-Weg 2, 76131 Karlsruhe, Germany

<sup>c</sup> Institute for Biological Interfaces, Karlsruhe Institute of Technology, Hermann-von-Helmholtz-Platz 1, D-76344 Eggenstein-Leopoldshafen, Germany

### HIGHLIGHTS

- Comparison of inoculation strategies for continuously operated microbial anodes.
- Inoculation with sludge or plain municipal wastewater yielded similar results.
- Also a pre-grown biofilm of exoelectrogens did not yield higher currents.
- 99% of the pre-grown biofilm was detached after 20 days of operation with wastewater.

### ARTICLE INFO

#### Article history:

Received 13 July 2016

Received in revised form 31 August 2016

Accepted 1 September 2016

Available online 4 September 2016

#### Keywords:

Microbial fuel cell  
Anode  
Wastewater  
Inoculation  
Geobacter  
Shewanella  
Pregrown biofilm  
Microbial community

### ABSTRACT

In this study, different inoculation strategies for continuously operated microbial anodes are analyzed and compared. After 20 days of operation with municipal wastewater anodes pre-incubated with a biofilm of the exoelectrogenic species *Geobacter* and *Shewanella* showed current densities of  $(65 \pm 8) \mu\text{A}/\text{cm}^2$ . This is comparable to the current densities of non-inoculated anodes and anodes inoculated with sewage sludge. Analysis of the barcoded pre-grown multispecies biofilms reveal that 99% of the original biofilm was detached after 20 days of operation with municipal wastewater. This is in contrast to previous experiments where a pre-grown biofilm of exoelectrogens was operated in batch mode. To implement pre-grown biofilms in continuous systems it will thus be necessary to reveal a window of process parameters in which typical exoelectrogenic microorganisms including model organisms can be kept and/or enriched on anodes.

© 2016 Published by Elsevier Ltd.

### 1. Introduction

The established treatment process for domestic wastewater involves active aeration to achieve oxidation of the organic carbon fraction to  $\text{CO}_2$  by aerobic bacteria, which consumes considerable amounts of electricity. To aerate domestic wastewater approx. 18–26 kWh per year and inhabitant can be estimated, from which only approximately 35% of the overall oxygen demand are required for the elimination of ammonia (by a nitrification/denitrification step) (Sperling, 2007).

Microbial fuel cells are considered to be a promising alternative to reduce the energy demand of wastewater treatment since they

enable elimination of organic carbon while generating useful electricity from its chemical energy content (Oh et al., 2010).

Calculations based on a 45 L pilot microbial fuel cell operated with municipal wastewater have shown that an electricity production of 2.91 kW per year and inhabitant can be achieved with the microbial fuel cell. Overall, total energy savings of 23% can be expected, including the savings for aeration and sludge treatment as well as the reduced biogas energy production (Hiegemann et al., 2016).

Key components of microbial fuel cells are the electroactive bacteria that oxidize organic matter and transfer the respiratory electrons to the anode of the fuel cell, which acts as a solid phase electron acceptor. From the anode, the electrons flow as an electrical current through an external load circuit to the cathode where oxygen is reduced. Commonly, microbial fuel cell anodes intended for practical application in wastewater treatment are inoculated

\* Corresponding author.

E-mail address: [kerzenma@imtek.uni-freiburg.de](mailto:kerzenma@imtek.uni-freiburg.de) (S. Kerzenmacher).

<sup>1</sup> Both authors contributed equally.

e.g. with sludge from a conventional treatment plant or an acclimated consortium of operating fuel cells (Wang et al., 2010).

In literature, a number of studies using fed-batch systems and synthetic media containing acetate or glucose (Liu et al., 2008; Jiang et al., 2010; Vázquez-Larios et al., 2011; Yu et al., 2014) report that in the most cases, inoculation highly affects the performance. It is shown, that specialized exoelectrogenic consortia or single strains, like *Geobacter sulfurreducens* (Jiang et al., 2010) or a sulphate reducing inoculum (Vázquez-Larios et al., 2011) show better performances than wastewater and soil or aerobic sludge and a methanogenic consortium, respectively. (Yu et al., 2014) in contrast show, that inoculating microbial fuel cells with activated sludge or anaerobic sludge do not lead to significantly different power outputs.

Only few studies are available that compare different inoculation strategies in realistic environments with real and unsterile wastewater. (Dolch et al., 2016) could show that a model biofilm composed of the exoelectrogenic model organisms *Shewanella oneidensis*, *G. sulfurreducens* and *G. metallireducens* shows surprising resilience even in non-axenic systems. More than 50% of the anode community was comprised by organisms of the initial inoculum even after 14 days of operation. Still, this and most other studies analyze batch or fed-batch systems (Liu and Li, 2007; Mathuriya, 2013). Consequently, the continuous outflow of slow growing organisms is not considered. The only study in a continuously fed reactor is (Ismail and Jaeel, 2013), but even here, the dimensions are chosen so that the hydraulic retention time results in 383 h (ca. 16 days, calculation based on the reactor dimensions indicated in the paper).

The aim of the present study was to analyze the impact of different inoculation strategies on bioelectrochemical systems that were continuously fed with domestic wastewater as carbon and energy source at a realistic hydraulic retention time.

Our results revealed that inoculation strategies have under the here described conditions—if at all—only a minor impact on the performance of the bioelectrochemical systems.

## 2. Materials and methods

### 2.1. Experiment design

An overview of the different inoculation strategies investigated in this work is given in Fig. 1. In a first run of experiments, a multispecies model biofilm with *Geobacter sulfurreducens*, *Geobacter metallireducens* and *Shewanella oneidensis* was pre-incubated on the anode surface under anoxic conditions with carbonate buffered medium containing lactate (12.5 mM) and propionate (5 mM). After one week of operation, the grown multispecies biofilm was analyzed with qPCR and FISH to reveal its composition.

In a second run of experiments the inflow was changed to wastewater after one week of preincubation with the model biofilm community. As a control, parallel experiments were conducted without preincubation with exoelectrogenic model organisms.

In run 3 (see Fig. 1) reactors inoculated with sludge were compared with non-inoculated reactors. To inoculate the anodes (anode chamber volume: 25 ml) 1 ml of sludge was used. The inoculation sludge was a mixture of activated sludge and anaerobic sludge in the volume ratio 1:4 from the same municipal treatment plant. After inoculation, the cells were run without flow for 24 h before starting the pump.

The inflow in run 2 and 3 was real municipal wastewater of the “Verbandskläranlage Untere Elz” in Teningen, sampled after the sand trap. The wastewater was collected weekly and stored at 4 °C (the different batches are marked in the results). The

wastewater showed very low COD concentrations with a maximum of 97.5 mg/l COD during the time the experiments were carried out, due to dilution with rain water. To achieve a municipal wastewater with higher carbon content, the water was complemented with 0.323 g/l peptone (from soybean, Carl Roth, Germany) and 0.226 g/l meat extract (Carl Roth, Germany) to COD concentrations of (715 ± 38) mg/l COD. The complementation was conducted right before connecting a new wastewater subbatch to the experimental setup.

### 2.2. Growth of a synthetic multispecies biofilms

*Shewanella oneidensis* MR-1, *Geobacter sulfurreducens* PCA and *Geobacter metallireducens* GS-15 were routinely cultured anaerobically at 30 °C in a medium that was developed according to (Dolch et al., 2014) as blueprint. All three strains were genetically modified to contain a genomic barcode for qPCR based quantification (Dolch et al., 2016). The growth medium contained 0.42 g/l  $\text{KH}_2\text{PO}_4$ , 0.22 g/l  $\text{K}_2\text{HPO}_4$ , 0.2 g/l  $\text{NH}_4\text{Cl}$ , 0.38 g/l KCl, 0.36 g/l NaCl, 0.21 g/l  $\text{MgCl}_2 \cdot 6\text{H}_2\text{O}$ , 1.8 g/l  $\text{NaHCO}_3$ , 0.5 g/l  $\text{Na}_2\text{CO}_3$ , 60 mg/l  $\text{CaCl}_2 \cdot 2\text{H}_2\text{O}$ , 2 g/l casitone, and 1.0 ml/l of selenite-tungstate solution (0.5 g/l NaOH, 3 mg/l  $\text{Na}_2\text{SeO}_3$ , 4 mg/l  $\text{Na}_2\text{WO}_4 \cdot 2\text{H}_2\text{O}$ ). The medium was further supplemented with 10 ml/l NB trace mineral solution (Coppi et al., 2001), 10 ml/l vitamin solution (German Type Culture Collection, DSMZ, media 141), 0.2 mM sodium ascorbate, 1.0 mM cysteine, 0.2% (w/v) yeast extract and 50 mM ferric citrate as electron acceptor. Sodium lactate (12.5 mM), sodium acetate (6.25 mM) and sodium propionate (5 mM) were used as electron donors. Medium pH was adjusted to 7.2. The optical density during anaerobic growth on ferric citrate was measured at a wavelength of 655 nm. The addition of ferric citrate was omitted in the bioelectrochemical cell experiments. Here, the working electrode served as sole electron acceptor.

### 2.3. Continuous flow reactors

The experiments were conducted in two chambered microbial fuel cells made from polycarbonate as described elsewhere (Dolch et al., 2014). Both, anode and cathode compartment have a volume of ca. 45 ml each and were filled with 25 ml. A proton exchange membrane (Fumapem F-950, 50  $\mu\text{m}$ , FumaTech, Germany) was used to separate the anode compartment from the counter electrode as well as the reference electrode compartment. Activated carbon cloth (CTex13; MAST Carbon, UK) with a geometric size of 2.25  $\text{cm}^2$  exposed to the anolyte and catholyte was used as material for the working and counter electrode. The electrodes were connected to a potentiostat (1470E, Solartron Analytical, Farnborough, UK) using platinum wires (0.1 mm; Chempur, Germany).

The synthetic medium was stored in a sterile container without cooling while wastewater was held at 4 °C. In both cases the storage tank was continuously sparged with nitrogen to ensure anaerobic conditions. The container was connected in parallel to the inflow of all anode chambers using viton tubings (LEZ-VIT 70, Lézaud, Germany). The anode compartments were fed using a peristaltic pump (Reglo Digital, Ismatec, Germany) with Fluran tubes (HCA, F-5500-A, Ismatec, Germany) with an inner diameter of 0.51 mm. The HRT was between 3 and 4 h (flow rate of 0.22–0.17 ml/min). Before introduction into the anode chamber the feed flow was acclimated to 30 °C.

All parallel experiments were fed from the same tank with wastewater to eliminate the effect of fluctuations in the wastewater composition. The wastewater was renewed weekly. The cathode compartment was filled with medium once and not exchanged during the operation.

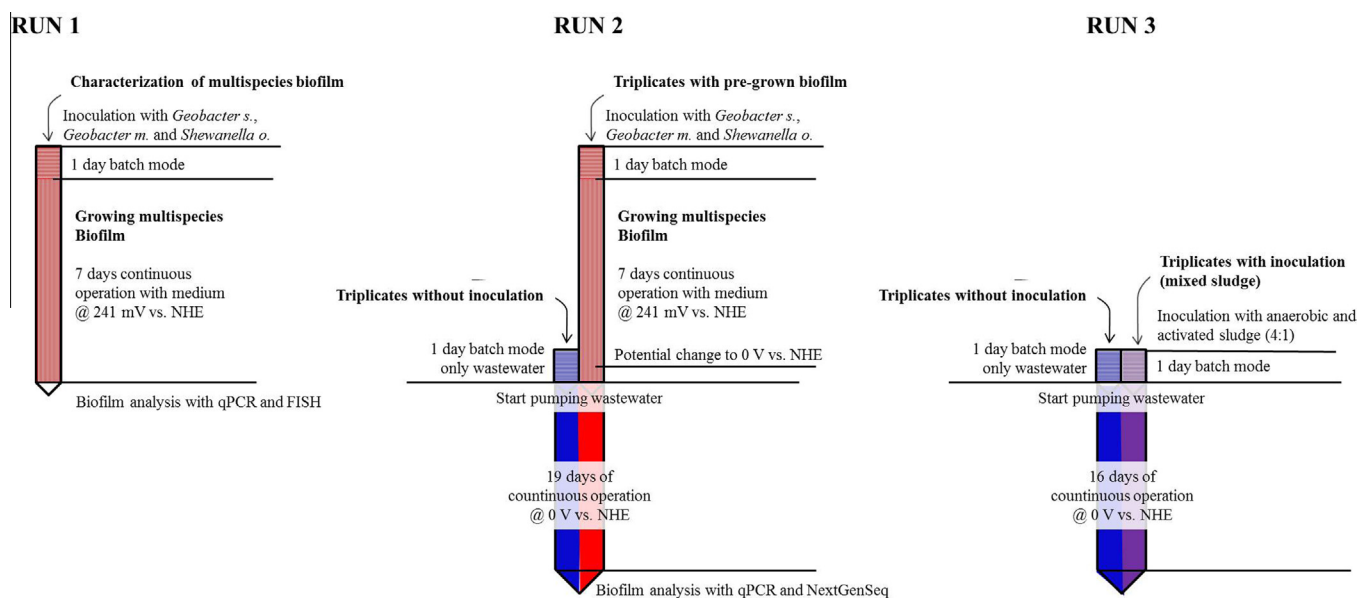


**Fig. 1.** Overview of experimental Runs: Run 1 for the characterization of a synthetic multispecies biofilm. Run 2 for the comparison of a pre-grown synthetic multispecies biofilm with anodes that are not inoculated and run with plain wastewater. Run 3 for the comparison of inoculation with sewage sludge and plain wastewater.

All experiments were performed in triplicates at 30 °C and the anode chamber was purged with a nitrogen/carbon dioxide mixture containing 0.3% carbon dioxide. To keep the pH constant at  $7.0 \pm 0.5$  the carbon dioxide flow was slightly in- or decreased. The cathode compartment was purged with air.

#### 2.4. Electrochemical characterization

All experiments were carried out in a three electrode setup and chronoamperometry was performed with the anode as a working electrode. The activated carbon cloth cathode was used as counter electrode. Except the pre-growth of the multispecies biofilm, all experiments were carried out at 0 V vs. NHE as working electrode potential. Previous experiments revealed high current densities with mixed cultures and synthetic wastewater around this value compared to more negative potentials (Fig. S1).

The model exoelectrogenic biofilm was pre-incubated for 7 days at 241 mV vs. NHE. Before switching to real wastewater on day 7, the potential was slowly lowered to 0 V vs. NHE at a scan rate of 0.0335 mV/s (Fig. 1). Since wastewater has a comparably low conductivity, uncompensated resistance in the experimental setup may falsify the actual potential at the working electrode (anode). To quantify this error the wastewater conductivity in the anode compartments was analyzed to an average of 1056  $\mu\text{S}/\text{cm}$  (run 1) and 1159  $\mu\text{S}/\text{cm}$  (run 2). This corresponds to an average uncompensated resistance of 600 Ohms as determined by numerical simulation according to the used reactor geometry and the position of the electrodes (reference, working and counter electrode) using an averaged conductivity of 1100  $\mu\text{S}/\text{cm}$ . At the maximum current densities of 82  $\mu\text{A}/\text{cm}^2$  this uncompensated resistance corresponds to a maximum error in anode potential of  $-122$  mV. We assume that this deviation has no effect on the overall conclusion.

#### 2.5. Fluorescent in situ hybridization (FISH)

Preincubated anodes were microscopically analyzed using FISH. Whole anodes were fixed with 4% formaldehyde for 4 h at 4 °C. Thereafter, they were washed in PBS medium for 30 min and afterwards stored in 50% v/v PBS-ethanol solution at 4 °C. Fluorescently labeled oligonucleotide probes with the concentration 50 ng/ $\mu\text{l}$

were used in this study according to the protocol described by (Dolch et al., 2014) (Table S1).

In this study a Leica DM 5500 B microscope with a 63x immersion lens and a digital color camera DFC 300 FX (Leica, Wetzlar, Germany) was used. Filter sets that were used are listed in Table S2.

#### 2.6. Extraction and quantification of genomic DNA

Genomic DNA was extracted directly from the anode surface at the end of the experiments using the innuPREP Stool DNA Kit (Analytic Jena, Jena, Germany). Prior to the extraction all anodes were additionally incubated in the lysis solution at room temperature for 10 min. Quantification of each strain on the anode surface was analyzed by qPCR. Therefore, genetically modified exoelectrogenic model organisms were used, that contain individual genomic barcodes in their sequence (Dolch et al., 2016). Such barcodes not only enable to quantify the organisms but also to distinguish them from phylogenetically related organisms that are part of the native exoelectrogenic community in wastewater. Quantitative PCR was conducted according to (Dolch et al., 2016) with the primers listed in Table S3.

#### 2.7. Next generation sequencing (NGS)

In this study Amplicon sequencing was used to assess the phylogenetic diversity of the anode community in run 2. The experiment was conducted according to (Majzlan et al., 2014). All amplicons were designed according to the same pattern that includes the 454 sequencing primer, library key and unique multiplex identifier (MID) sequences necessary for identification during the data analysis (Tables S4 and S5).

#### 2.8. Analytical techniques

Cell density was determined via the Thermo Scientific GENESYS 20 spectrophotometer. Samples for pH measurement were taken directly from the anode compartment and measured with an InoLab 720 (WTW, Germany) daily. For conductivity measurements the samples were taken from the outflow. By stopping the time while sampling, the flow rate was determined. Samples were

regularly taken for quantification of total organic carbon (TOC) using a multi N/C 2100S (Analytik Jena, Jena, Germany). TOC degradation rates were calculated for the time between day 4 and 14, during which the current generation in all experiments was relatively stable. The reported median values include all measured data points of every single experiment in this time frame. As can be seen from Figs. S4 and S5 in the Supplementary material, the deviations between the three cells of one triplicate are relatively high.

### 3. Results and discussion

#### 3.1. Characterization of biofilm formation on the anode surface after 7 days of incubation (Run 1)

It was the aim of this study to analyze different inoculation strategies for microbial electrochemical cells. One of the inoculation strategies included the formation of a tailored biofilm consisting of three exoelectrogenic model organisms. These model organisms were genetically modified to contain specific barcode sequences that allow to quantify the cells but also to distinguish them from phylogenetically similar organisms in non-axenic environments.

In run 1 the synthetic biofilm was grown over the time course of one week with carbonate buffered medium and then analyzed with regard to its composition. Anodes poised to a potential of 241 mV vs. NHE were used as sole electron acceptors. The three strains were added to the anode compartment in identical  $OD_{655}$  values, leading to a final OD of 0.1. At the end of the experiment a macroscopically visible biofilm completely coated the fibers of the activated carbon cloth anodes. Fig. 2A shows the results from qPCR based quantification. *Geobacter sulfurreducens* cells clearly dominated the anode surface. However, neither *Shewanella oneidensis* nor *Geobacter metallireducens* were completely outcompeted from the anode surface. At the end of the one week experiment the percentage of *Geobacter sulfurreducens* cells was  $(93.3 \pm 0.8)\%$ , while *Shewanella oneidensis* and *Geobacter metallireducens* comprised only  $(5.92 \pm 0.9)\%$  and  $(0.77 \pm 0.2)\%$ , respectively of the community. Fluorescence *in situ* hybridization (FISH) experiments were conducted in parallel to corroborate the qPCR-based results (Fig. 2B). These pictures also reveal the qPCR detected dominance of *G. sulfurreducens* cells on the anode surface.

#### 3.2. Comparison of the electrical performance and the survival of the model exoelectrogenic biofilm using real wastewater as medium (Run 2)

So far, the composition of a synthetic exoelectrogenic biofilm was analyzed after seven days of growth under axenic conditions in carbonate buffered medium. In the following experiment, it was sought for the effect of preincubation on electron transfer performance if wastewater was used as carbon and electron source. Therefore, the carbonate buffered medium was exchanged by a continuous flow of wastewater after the seven day preincubation period. As control another triplicate was started without preincubation. Hence, the natural wastewater community was the only source of potential exoelectrogenic microorganisms. After 20 days of operation with wastewater, DNA was isolated from the anode biofilms and the residual amount of barcode containing cells was analyzed. Similar to the results described above, *Geobacter sulfurreducens* comprised the majority of barcode containing organisms with  $(91.75 \pm 2.5)\%$ . *S. oneidensis* and *G. metallireducens* accounted only for  $(3.01 \pm 0.8)\%$  and  $(5.24 \pm 1.9)\%$  of the barcode containing community (Fig. 3A). Despite the fact that the ratio of the cells remained almost unchanged, the total amount of barcoded

organisms decreased to 1% compared to the end of the 7 days preincubation period in the first run of experiments (Fig. 3B).

Current densities of the pre-incubated anodes with the model exoelectrogenic biofilm during the growth in a carbonate buffered medium reached  $> 400 \mu\text{A}/\text{cm}^2$  after two days and stabilized at  $(407 \pm 21) \mu\text{A}/\text{cm}^2$  during the first 7 days (see Supplementary Fig. S2). When the influent was changed to wastewater after that period, current values decreased immediately. At the end of the experiment after 20 days, the pre-incubated anodes showed insignificantly lower current densities of  $65 \pm 8 \mu\text{A}/\text{cm}^2$  compared to the anodes that have not been inoculated  $81 \pm 7 \mu\text{A}/\text{cm}^2$  (see Fig. 4).

Between day 14 and 16, the wastewater in the storage tank (wastewater batch B3) had changed to lower pH and high COD values (possibly by the degradation of particulate matter), leading to a drastic drop of current. After changing to a fresh batch of wastewater, the anodes recovered. For this reason, the values of those days were not taken in consideration in all averaged data. The TOC degradation reached values of  $(18 \pm 4)\%$  with the preincubated biofilm, and  $(19 \pm 7)\%$  in the reference experiment with plain wastewater (expressed as: median  $\pm$  median absolute deviation, see also complete data in Fig. S4).

The microbial diversity of anodes was analyzed to detect potential differences in community composition that could be a result of preincubation. The phylotypes in the communities were classified as operational taxonomic units (OTUs, grouped using  $> 79\%$  cut-off value). The results are summarized in Fig. 5.

The individual biofilms of the two triplicates were composed of a diverse microbial community and comparison of the triplicates revealed an overall quite similar picture. Organisms belonging to the orders *Bacteroidales*, *Clostridiales*, *Desulfuromonadales*, *Desulfobivibrionales*, *Cloacamonales* and *Synergistales* dominated the biofilm. Minor differences were observed in the relative abundance of *Bacteroidales* (26.3% vs. 26.7%), *Clostridiales* (14.5% vs. 16.8%), *Cloacamonales* (4.0% vs. 3.8%) if biofilms from preincubated anodes were compared to anode communities without preincubation period. The most prominent difference was that members of the *Synergistales* showed an abundance of 10% on anodes without compared to 4.3% in MFCs with preincubation. Interestingly, *Shewanella spp.* (order *Alteromonadales*) were found only in MFCs with pre-incubated anodes and here with an abundance of 1%.

*Geobacteraceae* (order *Desulfuromonadales*) phylotypes were with 6% relatively abundant in both anode triplicates. Still, the strain diversity of the *Geobacter* communities varied according to an existing or non-existing preincubation period (Fig. S3). Biofilms from anodes with pre-incubation contained mostly *G. sulfurreducens* and *G. metallireducens* cells in a concentration of 36% and 44% of the *Geobacteraceae*, respectively. In comparison, the non-preincubated biofilms comprised a *Geobacteraceae* community composed of 77% *G. sulfurreducens* and 7% *G. metallireducens*.

#### 3.3. Comparison of the electrical performance of anodes inoculated with sewage sludge and plain wastewater (Run 3)

The third run of experiments showed very similar current densities of  $(64 \pm 2) \mu\text{A}/\text{cm}^2$  for the anodes that had not been inoculated and  $(61 \pm 6) \mu\text{A}/\text{cm}^2$  for the anodes inoculated with sewage sludge (evaluated on day 14). After those 14 days of operation, the influence of the flow rate was tested by decreasing or increasing the flow rate, to establish HRTs of 6.6 and 1.7 h, respectively. Still, no significant difference in current production was detectable due to these variations of HRT (Fig. 6).

In this experimental run, the TOC degradation between day 4 and 14 is higher than in run 2 and reaches values of  $(24 \pm 6)\%$  for the triplicates run with plain wastewater, and  $(36 \pm 11)\%$  in the anode compartments inoculated with sewage sludge (expressed

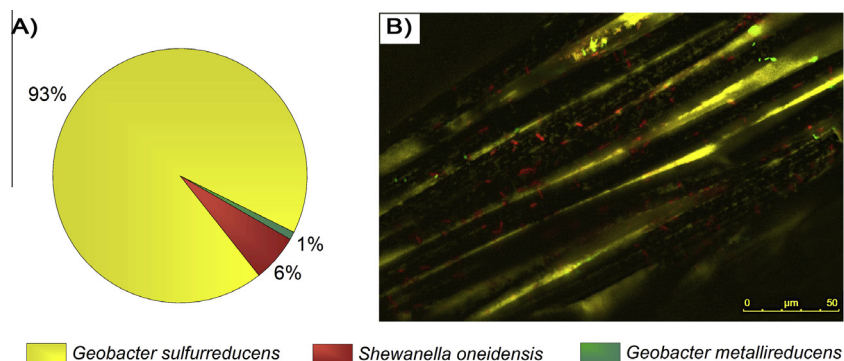


**Fig. 2.** A) Quantitative analysis of the pre-incubated anodes with the model exoelectrogenic strains after 7 days of incubation in the carbonate buffered medium. B) Fluorescent *in situ* hybridization (FISH) pictures of the exoelectrogenic community after 1 week of the experiment. *Geobacter sulfurreducens* was stained in yellow (Cy5), *Geobacter metallireducens* in green (FITC) and *Shewanella oneidensis* in red (Cy3). (For interpretation of the references to color in this figure legend, the reader is referred to the web version of this article.)

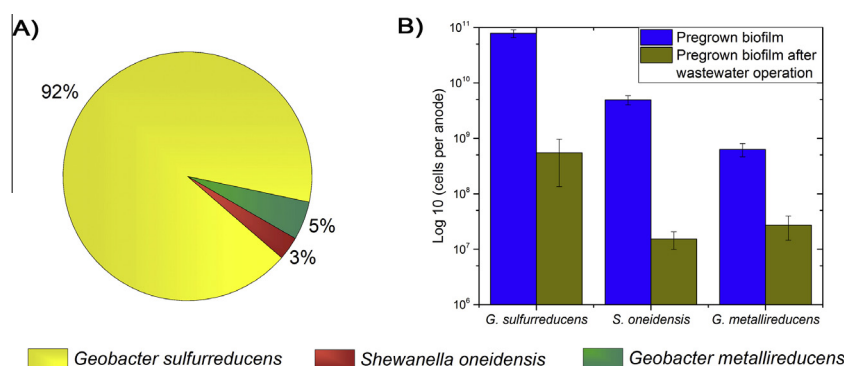


**Fig. 3.** Quantitative analysis of the retention of the barcoded exoelectrogenic community after 14 days of continuous growth with waste water as medium: A) ratio of the model exoelectrogenic cells on the anode, B) quantitative comparison before and after the 20 day period.

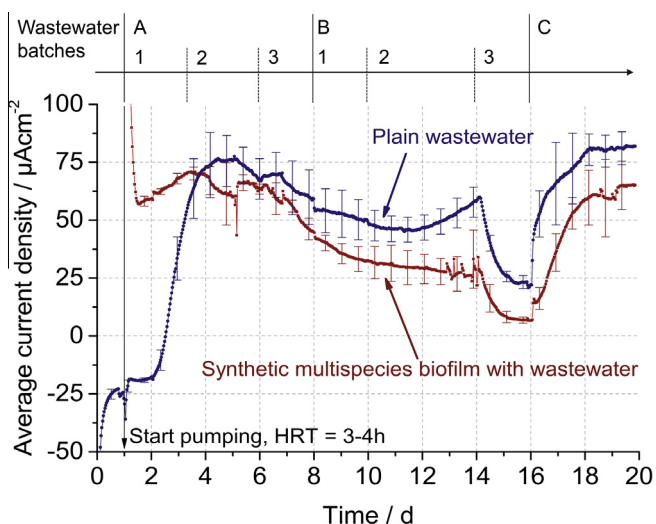


**Fig. 4.** Run 2: Comparison of current densities achieved with anodes with a pregrown multispecies biofilm and without any inoculation. Chronoamperometry at 0V vs. NHE, bars represent the sample standard deviation. The switch to real wastewater for the precultured cells was conducted at day 1. Data of the preculturing is not shown in this graph, but available in the [Supplementary data](#).

as median ± median absolute deviation). Here, the inoculation with sewage sludge predictably leads to higher TOC degradation through the insertion of biomass. When comparing the plain wastewater experiments of run 2 and run 3 it becomes apparent, that the slightly higher TOC degradation rates in run 3 must be

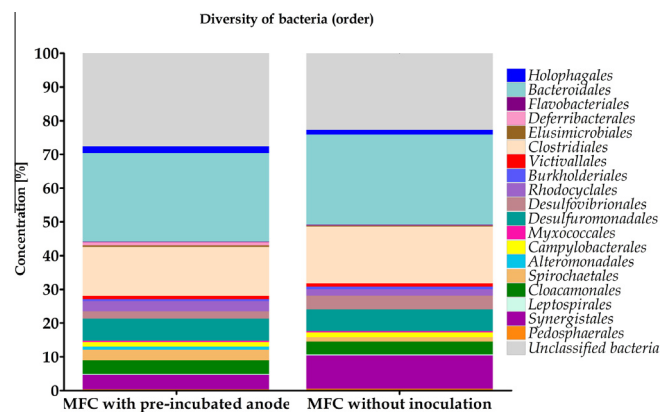


**Fig. 5.** Relative abundance and comparison profiles of bacterial 16S rRNA OTUs identified in MFCs with pre-incubated anodes and without inoculation after 20 days of running with a wastewater.

related to the composition of the different wastewater batches used in these experiments.

### 3.4. Overview of the achieved results and discussion

Regarding the averaged current densities over a period of 9 days (day 5–14) all experimental runs and all inoculation strategies yield anode performances which were in the same range (Table 1). This is in contrast to previous studies, in which a decisive influence of inoculation on anode performance has been demonstrated (Liu

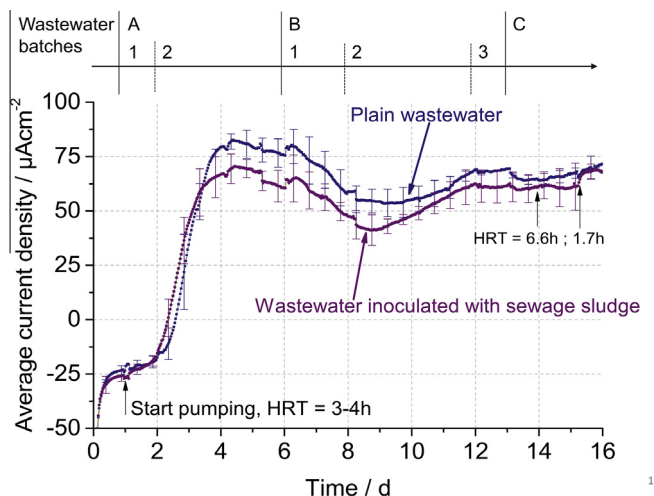


**Fig. 6.** Run 3: Comparison of current densities achieved without any inoculation and inoculated with sewage sludge. Chronoamperometry at 0 V vs. NHE bars represent the sample standard deviation.

and Li, 2007; Liu et al., 2008; Vázquez-Larios et al., 2011; Juang, 2012; Miceli et al., 2012; Commault et al., 2015). Here it has to be considered, that these studies were performed with a sterile synthetic wastewater containing acetate, butyrate, or glucose. Furthermore, most of these studies were conducted in batch or fed-batch systems. With this operation mode, the bacterial composition is obviously highly defined and conserved on the basis of the initial inoculum. In contrast, by feeding real wastewater as described in this study, new bacteria are constantly flushed into the system during the whole time course of the experiment and bacteria of a pre-grown biofilm or the inoculum can be flushed out. Nevertheless, not all studies performed with synthetic media show the same effect of inoculation. For instance, (Yu et al., 2014) found that also in a fed-batch system inoculation with anaerobic or aerobic sludge does not significantly affect power generation.

Microbial community development studies using unsterile real wastewater as used in this study are rare. Similar to our findings, different inoculum types (*Rhodospirillum rubrum* and activated sludge) do not result in significantly different power densities when using real wastewater from a glutamate plant (Liu and Li, 2007). In contrast, (Mathuriya, 2013) shows different inoculation strategies in fed-batch MFCs using real tannery wastewater. The results show improved current production of cells inoculated with a mixed microflora of isolates compared to plain wastewater. Unfortunately, the experiments were conducted only in single determination. Hence, it is difficult to draw decisive conclusions from this study.

The only study (Ismail and Jaeeel, 2013), that uses real municipal wastewater in a continuous flow experiment reports a maximum

power density of 270 mW/m<sup>2</sup> with *Bacillus subtilis* while activated sludge yields a maximum of half the power (120 mW/m<sup>2</sup>). However, since the HRT in this system was 383 h (~16 d) it has to be considered as a batch system.

To our best knowledge our work is the first study investigating a pre-grown biofilm in a continuous system using real wastewater.

qPCR of the experiments with barcoded pre-grown multispecies biofilms reveal, that 99% of the original biofilm was detached after 20 days of operation with municipal wastewater. Here, the operation mode in a continuously fed system might be the reason for the detachment and out-washing of the pre-grown biofilm. The HRT of our experiments with 3–4 h is chosen in a very low range to reproduce a realistic alternative compared to a system with activated sludge treatment. A rough estimation based on the COD data of our experiments reveals, that the dimensions of an activated sludge sewage treatment would require a HRT of 7.6 h for a typical volumetric loading rate of 1 kgBOD/m<sup>3</sup>d (Mudrack and Kunst, 1986), if a COD/BOD ratio of 2.25 (Henze, 2002) is assumed. The low TOC degradation rates of 19% for the experiment with pure wastewater and 18% in the experiments with the pre-grown biofilm can be explained by the high volumetric load in our experiments which comes to 2.2 kg BOD/m<sup>3</sup>d.

Furthermore, these TOC degradation rates are in a range where they will not impede nitrogen removal via the nitrification/denitrification route that requires a carbon source. Additionally, the surface to volume ratio of 9 m<sup>2</sup>/m<sup>3</sup> in our system is not optimized but of importance for holding immobilized and current producing biomass in the MFC.

It was of interest to observe that the retention of biomass from a preincubation phase on the anode surface was so much lower compared to a previous study using the same strains but under fed-batch conditions (Dolch et al., 2016). The here described system was designed in a way that allowed a constant oversupply of organic carbon to the anode compartment. From this supply of organic carbon on average around 20% were eliminated. Exoelectrogenic organisms are in most cases dependent on the activity of fermentative microbes that degrade biomass to a typical spectrum of organic acids. The continuous flow, the high volume to anode surface ratio in the reactor and the low carbon elimination rate might lead to conditions that were not selective enough for anode assisted carbon elimination. This hypothesis is corroborated by the relatively low amount of  $\delta$ -proteobacteria within the anode community. Ishii et al. conducted a study, in which bioelectrochemical systems were fed in a repeated-batch process with municipal waste water. At a potential of +100 mV against standard hydrogen electrode, the anode community consisted to at least 40% of members of the  $\delta$ -proteobacteria (Ishii et al., 2013). Most of the sequences that could be assigned to the level of the genus belonged to members of the Desulfobacteraceae, Desulfobulbaceae, Desulfomadaeaceae and Geobacteraceae. At least for members of the Desulfobulbaceae and certainly for members of the Geobacteraceae it was shown that they are able to conduct a direct extracellular

**Table 1**  
Averaged current densities between days 5 and 14 of operation with continuously fed wastewater. Results are taken from chronoamperometry at 0 V vs. NHE and given as mean value  $\pm$  sample standard deviation.

Inoculation strategy	Normalized current density based on			
	Geometric area A/m <sup>2</sup>	BET area $\mu$ A/m <sup>2</sup>	Electrode volume A/m <sup>3</sup>	Chamber volume A/m <sup>3</sup>
Pre-grown multispecies biofilm	0.42 $\pm$ 0.04	3.2 $\pm$ 0.3	(8.3 $\pm$ 0.9)·10 <sup>2</sup>	3.7 $\pm$ 0.4
Inoculated with sewage sludge	0.56 $\pm$ 0.05	4.2 $\pm$ 0.4	(11 $\pm$ 1.1)·10 <sup>2</sup>	5.0 $\pm$ 0.5
Plain wastewater (Run 1)	0.56 $\pm$ 0.07	4.2 $\pm$ 0.6	(11 $\pm$ 1.5)·10 <sup>2</sup>	5.0 $\pm$ 0.7
Plain wastewater (Run 2)	0.65 $\pm$ 0.04	4.9 $\pm$ 0.3	(13 $\pm$ 0.8)·10 <sup>2</sup>	5.8 $\pm$ 0.4
Multispecies biofilm with medium*	4.07 $\pm$ 0.21	31 $\pm$ 1.6	(81 $\pm$ 4.1)·10 <sup>2</sup>	37 $\pm$ 1.9

\* The values are taken after 6 days of operation with medium at 0.241 V vs. NHE.

electron transfer (Holmes et al., 2003; Pfeffer et al., 2012). It seems possible that related organisms have similar physiological capabilities. In contrary only 10.1% and 11.6%, respectively of the communities in this study could be assigned to the  $\delta$ -proteobacteria.

#### 4. Conclusion

Our results show that the inoculation of microbial anodes operated continuously at an HRT of 3–4 h does not significantly affect current production, at least under the here described experimental conditions. In contrast to previous batch experiments, a pre-grown biofilm of exoelectrogens species did not yield higher current densities than a non-inoculated anode. After 20 days of operation with municipal wastewater 99% of the pre-grown biofilm was detached. To implement pre-grown biofilms in continuous systems it is required to reveal in which window of process parameters typical exoelectrogenic microorganisms including model organisms can be kept and/or enriched on anodes.

#### Acknowledgements

Financial support by the Baden-Württemberg Stiftung under the program “Umwelttechnologieforschung” is gratefully acknowledged.

#### Appendix A. Supplementary data

Supplementary data associated with this article can be found, in the online version, at <http://dx.doi.org/10.1016/j.biortech.2016.09.004>.

#### References

- Commaut, A.S., Barrière, F., Lapinsonnière, L., Lear, G., Bouvier, S., Weld, R.J., 2015. Influence of inoculum and anode surface properties on the selection of Geobacter-dominated biofilms. *Bioresour. Technol.* 195, 265–272.
- Coppi, M.V., Leang, C., Sandler, S.J., Lovley, D.R., 2001. Development of a genetic system for geobacter sulfurreducens. *App. Environ. Microbiol.* 67, 3180–3187.
- Dolch, K., Danzer, J., Kabbeck, T., Bierer, B., Erben, J., Förster, A.H., Maisch, J., Nick, P., Kerzenmacher, S., Gescher, J., 2014. Characterization of microbial current production as a function of microbe–electrode–interaction. *Bioresour. Technol.* 157, 284–292.
- Dolch, K., Wuske, J., Gescher, J., 2016. Genomic barcode based analysis of exoelectrogens in wastewater biofilms grown on anode surfaces. *J. Microbiol. Biotechnol.* 26, 511–520.
- Hiegemann, H., Herzer, D., Nettmann, E., Lübken, M., Schulte, P., Schmelz, K.-G., Gredigk-Hoffmann, S., Wichern, M., 2016. An integrated 45 L pilot microbial fuel cell system at a full-scale wastewater treatment plant. *Bioresour. Technol.* 218, 115–122.
- Henze, M., 2002. *Wastewater Treatment: Biological and Chemical Processes*. Springer, Berlin, New York, p. 430.
- Holmes, D.E., Bond, D.R., Lovley, D.R., 2003. Electron transfer by desulfobulbus propionicus to Fe(III) and graphite electrodes. *Appl. Environ. Microbiol.* 70, 1234–1237.
- Ishii, S., Suzuki, S., Norden-Krichmar, T.M., Wu, A., Yamanaka, Y., Neelson, K.H., Bretschger, O., 2013. Identifying the microbial communities and operational conditions for optimized wastewater treatment in microbial fuel cells. *Water Res.* 47, 7120–7130.
- Ismail, Z.Z., Jael, A.J., 2013. Sustainable power generation in continuous flow microbial fuel cell treating actual wastewater: influence of biocatalyst type on electricity production. *Sci. World J.*, 713515.
- Jiang, D.Q., Li, B.K., Jia, W.Z., Lei, Y., 2010. Effect of inoculum types on bacterial adhesion and power production in microbial fuel cells. *Appl. Biochem. Biotechnol.* 160, 182–196.
- Juang, D.-F., 2012. Organic removal efficiencies and power production capabilities of microbial fuel cells with pure cultures and mixed culture. *APCBEE Proc.* 1, 2–7.
- Liu, Z., Li, H., Liu, J., Su, Z., 2008. Effects of inoculation strategy and cultivation approach on the performance of microbial fuel cell using marine sediment as bio-matrix. *J. Appl. Microbiol.* 104, 1163–1170.
- Liu, Z.-D., Li, H.-R., 2007. Effects of bio- and abio-factors on electricity production in a mediatorless microbial fuel cell. *Biochem. Eng. J.* 36, 209–214.
- Majzlan, J., Plasil, J., Skoda, R., Gescher, J., Kogler, F., Rusznyak, A., Kusel, K., Neu, T.R., Mangold, S., Rothe, J., 2014. Arsenic-rich acid mine water with extreme arsenic concentration: mineralogy, geochemistry, microbiology, and environmental implications. *Environ. Sci. Technol.* 48, 13685–13693.
- Mathuriya, A.S., 2013. Inoculum selection to enhance performance of a microbial fuel cell for electricity generation during wastewater treatment. *Environ. Technol.* 34, 1957–1964.
- Miceli, J.F., Parameswaran, P., Kang, D.W., Krajmalnik-Brown, R., Torres, C.I., 2012. Enrichment and analysis of anode-respiring bacteria from diverse anaerobic inocula. *Environ. Sci. Technol.* 46, 10349–10355.
- Mudrack, K., Kunst, S., 1986. *Biology of sewage treatment and water pollution control*. In: Horwood, E. (Ed.). Halsted Press, Chichester; New York.
- Oh, S.T., Kim, J.R., Premier, G.C., Lee, T.H., Kim, C., Sloan, W.T., 2010. Sustainable wastewater treatment: How might microbial fuel cells contribute. *Biotechnol. Adv.* 28, 871–881.
- Pfeffer, C., Larsen, S., Song, J., Dong, M., Besenbacher, F., Meyer, R.L., Kjeldsen, K.U., Schreiber, L., Gorby, Y.A., El-Naggar, M.Y., Leung, K.M., Schramm, A., Risgaard-Petersen, N., Nielsen, L.P., 2012. Filamentous bacteria transport electrons over centimetre distances. *Nature* 491, 218–221.
- Sperling, M.V., 2007. *Activated Sludge and Aerobic Biofilm Reactors*. IWA Publishing, London.
- Vázquez-Larios, A.L., Solorza-Feria, O., Vázquez-Huerta, G., Esparza-García, F., Rinderknecht-Seijas, N., Poggi-Varaldo, H.M., 2011. Effects of architectural changes and inoculum type on internal resistance of a microbial fuel cell designed for the treatment of leachates from the dark hydrogenogenic fermentation of organic solid wastes. *Int. J. Hydrogen Energy* 36, 6199–6209.
- Wang, A., Sun, D., Ren, N., Liu, C., Liu, W., Logan, B.E., Wu, W.M., 2010. A rapid selection strategy for an anodophilic consortium for microbial fuel cells. *Bioresour. Technol.* 101, 5733–5735.
- Yu, J., Park, Y., Lee, T., 2014. Effect of separator and inoculum type on electricity generation and microbial community in single-chamber microbial fuel cells. *Bioprocess Biosyst. Eng.* 37, 667–675.